# UNIVERSITÀ DEGLI STUDI DI TRIESTE

## XXX CICLO DEL DOTTORATO DI RICERCA IN
## SCIENZE DELLA TERRA E MECCANICA DEI FLUIDI

# THE ROLE OF PLANKTON SIZE IN COMMUNITY STRUCTURE, BIODIVERSITY AND BIOGEOCHEMICAL FLUXES: A MODELING APPROACH

Settore scientifico-disciplinare: GEO/12 OCEANOGRAFIA E FISICA DELL'ATMOSFERA


DOTTORANDO
**MARCO DE PASQUALE**

COORDINATORE
**PROF. PIERPAOLO OMARI**

SUPERVISORE DI TESI
**DR. STEFANO SALON**

CO-SUPERVISORE DI TESI
**DR. COSIMO SOLIDORO**


**ANNO ACCADEMICO 2016/2017**

# The role of plankton size in community structure, biodiversity and biogeochemical fluxes: a modeling approach

Author:

**Marco De Pasquale**

OGS - Istituto Nazionale di Oceanografia e di Geofisica Sperimentale, Ecology and Computational Hydrodynamics in Oceanography (ECHO) group, Via Beirut 2-4, 34151, Trieste (TS), Italy

E-mail: mdepasquale@inogs.it

Supervisor:

**Stefano Salon**

OGS - Istituto Nazionale di Oceanografia e di Geofisica Sperimentale, Ecology and Computational Hydrodynamics in Oceanography (ECHO) group, Via Beirut 2-4, 34151, Trieste (TS), Italy

Co-supervisor:

**Cosimo Solidoro**

OGS - Istituto Nazionale di Oceanografia e di Geofisica Sperimentale, Ecology and Computational Hydrodynamics in Oceanography (ECHO) group, Via Beirut 2-4, 34151, Trieste (TS), Italy

The research reported in this work was supported by OGS and CINECA under HPC-TRES (Line A2) program award number 2014-01

# The role of plankton size in community structure, biodiversity and biogeochemical fluxes: a modeling approach

KEYWORDS: Phytoplankton, Zooplankton, Size, Export, Biogeochemistry

**Abstract**

A new N-P-Z (nutrient-phytoplankton-zooplankton) model is presented, named SPLAS (Sea PLAnkton Simulator). SPLAS is a size-structure model, based on two simple assumptions: 1) fundamental plankton physiological traits scale with organism size, and 2) grazing by zooplankton is structured by an optimal predator-prey length ratio. The model is based on empirical allometric relationships used to parameterize major plankton characteristics. 70 size-classes are defined for phytoplankton, in the range 1-200 μm, and there are 70 matching size-classes for zooplankton, in the range 2-1000 μm. Here phytoplankton are considered uptaking Nitrogen, and growing according to external N concentration and internal cellular quota. Zooplankton feed on phytoplankton through a size-based preference. No mixotrophy is considered.

This work expands and improves the work done by Banas (2011) where a mechanistical model with size-resolution was presented, and it gave good results consistent with observations.

Remaining simple in the formulation, SPLAS is able to mimic general pattern of plankton size distribution and diversity, at least in a 0-D sense, and to reproduce bottom-up and top-down interactions.

Results from 10 years of integration show an emergent pattern of plankton size-structure consistent with theoretical and model prediction made, for example, by Ward et al. (2013), where the observed size structure was justified in terms of basic interactions between nutrient (bottom-up) and grazing (top-down) control.

Then, SPLAS has been extended to a 1-D representation with explicit turbulent diffusion mechanism and a detritus pool collecting organic matter. The 1-D setup has been used to discuss the importance of light in this framework. With the inclusion of light (PAR) in phytoplankton growth rate the model represents also a Deep Biological Maximum (DBM) in phytoplankton biomass depth profile, and depth-dependence in phytoplankton growth rate triggers a non-homogeneous size-structure in depth that was not possible to obtain and describe in the 0-D setup nor in the 1-D setup without light (homogeneous plankton size-spectrum in depth).

SPLAS reproduces also depth variations in the maximum biomass (DBM) with varying extinction constant for light and multiple maxima when phytoplankton self-shading is introduced.

In the 1-D framework we also studied depth-varying diffusivities to analyze their impact on our modeled phytoplankton biomass profile.

Lastly, we tried to use SPLAS 1-D to estimate biogeochemical fluxes, for instance Carbon export, obtaining about 68 mgC $m^{-2}$ $day^{-1}$with our 1-D model. Our estimate of Carbon export is meant to be a starting point for future developments, rather than a real valid estimate, even if it is quite sensible being close to earlier estimates in literature (e.g. Ward & Follows, 2016).

# Contents

1. Introduction

    1.1 General framework

    1.2 Phytoplankton

    1.3 Modeling perspective: the SPLAS model

    1.4Structure of the thesis

2. The 0-D model

    2.1 Formulation

    2.2 Equations

    2.3 Parameterization

    2.4 Code implementation

    2.5 Equilibrium solutions

    2.6 Mechanisms shaping size-spectra

3. Validation and behavior exploration of SPLAS 0-D

    3.1 Summary of the section

    3.2 Ecosystem indicators for 0-D model

        3.2.1 Phytoplankton Limitations

        3.2.2 Size-diversity

    3.3 Default configuration spectrum and importance of zooplankton mortality

        3.3.1 Default size-spectrum

        3.3.2 Importance of zooplankton mortality closure

    3.4 Validation of the 0-D model

        3.4.1 Behavior under changing bottom-up control (N supply)

        3.4.2 Size-diversity dependence on total biomass

        3.4.3 Behavior under changing top-down control (Z mortality)

        3.4.4 Trophic Transfer Efficiency (TTE)

3.5 Behavior Analysis of the 0-D model

3.5.1 Importance of predator selectivity

3.5.2 Impact of phytoplankton sinking and natural mortality

3.5.3 Test on model resolution (number of size-classes)

3.5.4 Importance of assimilation efficiency and half saturation constant of the predator

3.5.5 Time varying N supply

3.6 SPLAS 0-D: Discussion and Summary

3.7 Strengths of the model

3.8 Limits of the model

4.Exploring the vertical dimension: the water column (1-D) model

4.1 Constant vertical diffusion

4.2 Detritus

4.3 Adding Light to phytoplankton growth

4.4 Analysis of vertical phytoplankton size-structure

4.5 Tests on various light profiles

4.5.1 Phytoplankton self-shading

4.6 Testing depth-dependent Eddy Diffusivity

5. Notes on C Export

5.1 A first estimate of C export

5.2 Sensitivity of Carbon Export to Nitrogen Supply

5.3 Limits of C export calculation

5.4 Sensitivity Analysis

6. Conclusion and future directions

6.1 Summary

6.2 Future Improvements

# 1. Introduction

## *1.1 General framework*

A growing attention is being paid to the limits which human activities should not overcome in order not to alter or damage the environment, considered as the boundaries of human sustainable development. Groups of scientists with different expertise from all over the world have recently tried to quantify these limits, defining the "planetary boundaries" that, if not exceeded, allow for sustainable growth and development of humanity (Rockstrom et al., 2009; Steffen et al., 2015). Boundaries have been estimated quantitatively for different human-induced or enforced phenomena happening on Earth (Fig. 1), as land-system change, fresh water use, damages to biosphere integrity, ocean acidification. Once the limits are defined, it is possible to understand if human activities are exceeding these limits or if we are still in a "safe" zone of sustainable development. For some phenomena the quantification of a boundary is still lacking (e.g. atmospheric aerosol loading).

In these studies, a planetary boundary is defined for biogeochemical flows of Phosphorus and Nitrogen (Fig. 1, for details see Rockstrom et al., 2009 and Steffen et al., 2015), showing that these fluxes have already exceeded the sustainable limits for the environment (eutrophication).

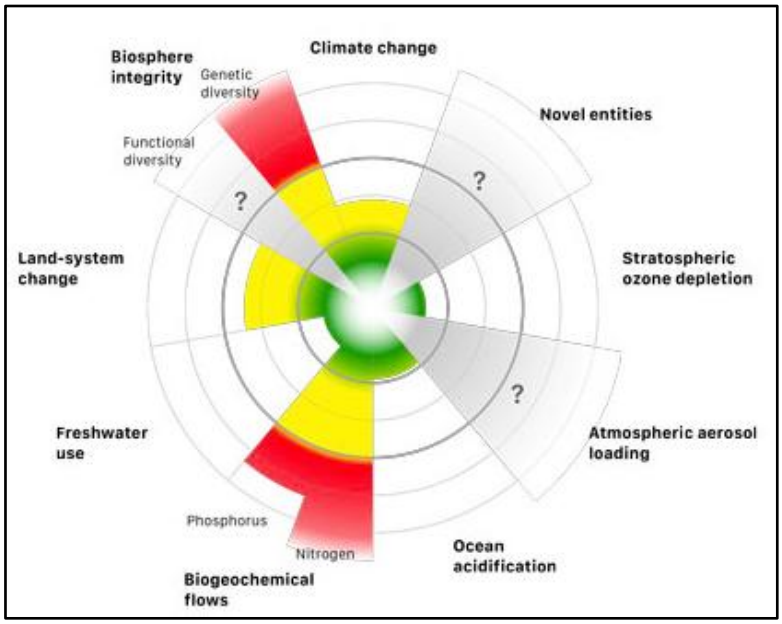


**Figure 1: Planetary boundaries (image from Steffen et al., 2015). Boundaries are defined as ranges (thick gray circle lines). Green: below the limit, safe zone; yellow: inside the range, uncertainty; red: above the safe limit, not sustainable.**

Nitrogen and Phosphorus cycles, being linked to other major elements cycles (e.g. Carbon), have a huge impact on the whole Earth system, as they couple atmosphere, ocean, and biosphere. Moreover, the biogeochemical dynamics of these elements is ultimately linked to climate, with the important participation of marine biota in the nutrient cycles (Fig. 2 for Carbon cycle). Human activities are thus expected to impact the whole Earth system also through the alteration of biogeochemical fluxes (e. g. human induced fertilization).

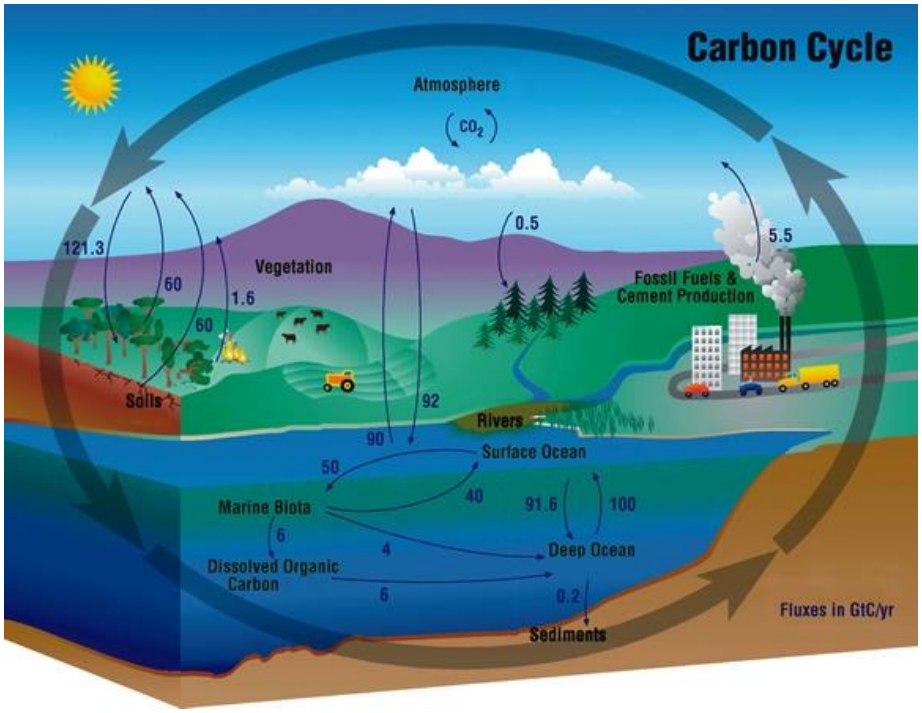


**Figure 2: Sketch of the global Carbon cycle budget. Arrows indicate fluxes, with intensities expressed in GtC/yr. Life in the ocean plays a key role in this cycle and in other major elements cycles as Nitrogen and Phosphorus, connecting many Earth compartments (atmosphere, biosphere, hydrosphere).**

Studying the key players in biogeochemical cycles and trying to estimate related biogeochemical fluxes is of primary importance within the whole Earth framework and related global climate changes.

One of the pivotal players in global biogeochemical cycles is phytoplankton, which impact climate because of their capacity to transport carbon and other elements from the surface ocean, with more light available and in contact with the atmosphere, to the deep ocean and sediments (Falkowski et al., 1998; Sigman and Boyle, 2000; Sarmiento and Gruber, 2006; Williams and Follows, 2011).Phytoplankton are the base of the marine food web: they perform photosynthesis in the upper layers of the ocean where sunlight penetrates most (the euphotic zone), converting inorganic nutrients into organic matter that is then used for

respiration and growth. This growth in turn sustains their predators (zooplankton) and upper trophic levels (fish).

Then, much of the surface "primary productivity" is recycled locally (i.e. returned to inorganic bioavailable forms) through a complex pathway of biological and chemical transformations, while a smaller fraction makes its way into the deep ocean (biological carbon pump). The largest portion of this downward sinking, advected or biologically transported matter is re-mineralized back into inorganic form and ultimately returned to the surface layers, whereas a very small fraction of primary productivity will be buried in marine sediments, where it will stay for a very long time. Meantime, the surface ocean is in contact with the atmosphere, exchanging carbon dioxide depending on the relative concentration.

Enlightening plankton dynamics and mechanisms in these phenomena and understanding how they impact biogeochemistry is crucial to get to more precise estimate of biogeochemical fluxes and in turn to understand how changes in those fluxes can trigger complex feedbacks on the whole Earth system. In this work we focus on the key role of phytoplankton.

### *1.2 Phytoplankton*

Marine phytoplankton (Fig. 3, from Barton, 2011) play a key role in marine ecosystems, global biogeochemical cycles and climate system, being primary producers responsible for nearly half of the global primary production (Field et al., 1998) and constituting the base of the marine food chain. The role of phytoplankton in marine ecosystems depends on their total biomass, biodiversity and size-distribution. Understanding how ecosystems function in relation to species diversity is a key topic in marine ecology, and in ecology more in general (Tilman, 2000; Hooper et al., 2005; Solan et al., 2006).

Taxonomic diversity in marine phytoplankton is often associated with distinct biogeochemical functions (Le Quéré et al., 2005), while size-structure (or size-related diversity) is thought to strongly affect the partitioning of carbon between ocean and atmosphere (Falkowski and Oliver, 2007) and also the abundance and diversity of other organisms in the ocean (Marañon, 2014).Moreover, biogeochemical cycles of major elements, their biologically mediated fluxes and climate processes depend on what size and species of phytoplankton are present and their relative abundance in space and time (Cushing, 1989; Cullen et al., 2002).

In particular, size-related diversity is considered one of the factors in determining ecosystem properties as productivity, stability and nutrient cycling (Hillebrand & Matthiessen, 2009; Wittebolle et al., 2009; Stuart-Smith et al., 2013).For example, most of the biomass produced by small phytoplankton is thought to be quickly recycled within the upper lit layers in the ocean, whereas larger phytoplankton rapidly transport

carbon to the ocean interior, driving the biological carbon pump (Marañon, 2014). Typically, small phytoplankton are dominating in regions of low nutrient concentrations (as tropical and subtropical oceans) while large phytoplankton cells are supported by regions with high nutrient concentrations (Marañon et al., 2001; Hirata et al., 2011).

Phytoplankton cell size ranges over several orders of magnitude, from less than 1 µm up to 200 µm (in equivalent spherical diameter) and affects numerous functional traits and crucial physiological and ecological processes (light absorption, nutrient uptake, sinking, grazing): thus, even if it represents only one component of total functional diversity (others are for example taxonomy, trophic strategy, etc.), it may be considered as one of the most important traits, as some authors recognize (Finkel et al., 2010; Litchman & Klausmeier, 2008; Litchman et al., 2010).

Being size-diversity crucial for ecosystem functioning and ultimately for climate, there is a need for a greater understanding of the community ecology and size-structure of marine phytoplankton: this may contribute to give a better insight on how these factors influence marine biogeochemistry and nutrient cycles.

Also, improving our understanding of how marine systems function at present conditions may contribute to the knowledge of how such systems might respond to future environmental changes.

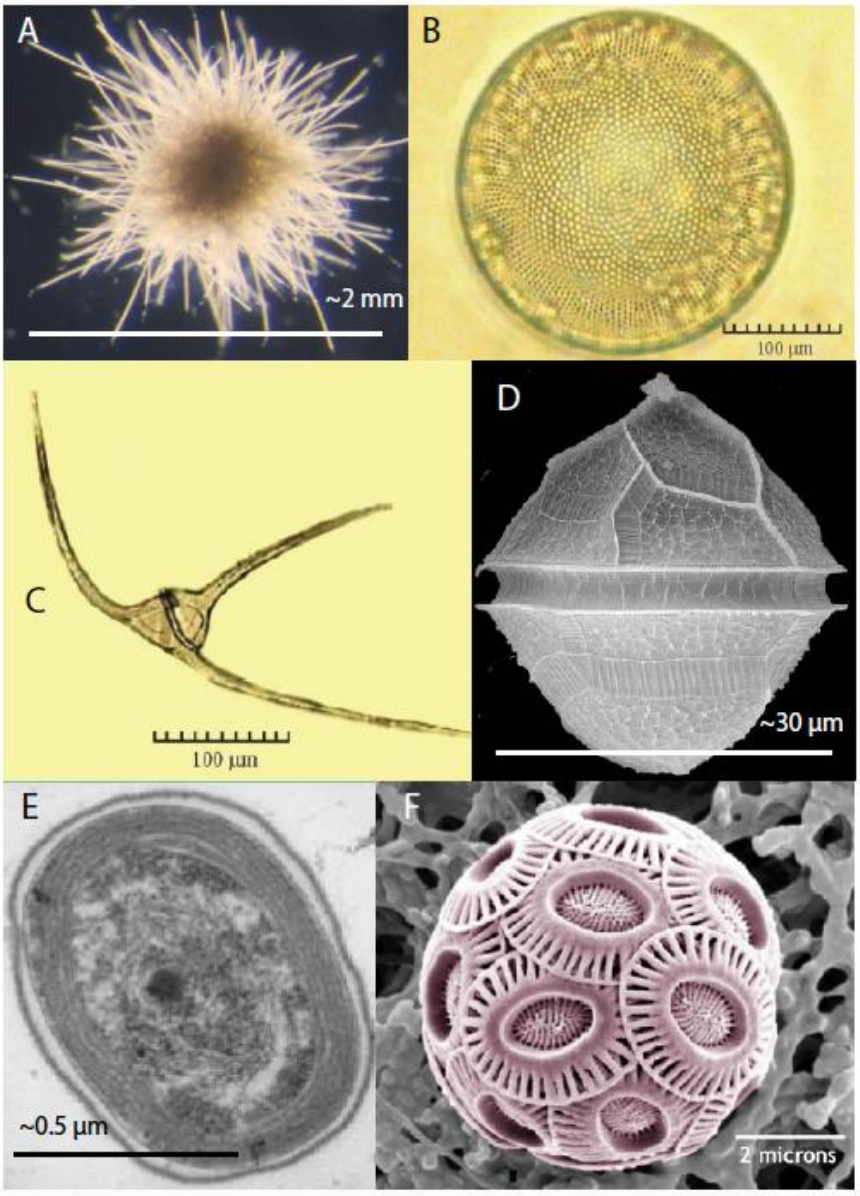


**Figure 3: A range of phytoplankton size/species (images from Barton, 2011). A) Colony of cyanobacteria,*Trichodesmium thibautii*, B) Diatom, *Coscinodiscus oculus iridis*, C) Dinoflagellate, *Ceratium arcticum*, D) Heterotrophic dinoflagellate,*Protoperidinium latistriatum*, E) Cyanobacterium,*Prochlorococcus*, F) Coccolithophore, *Emiliania huxleyi*. For details and full credits of the images see Barton, 2011.**

Note: in SPLAS, the planktonic organism in fig. 3D (heterotrophic dinoflagellate) is considered to be in the zooplankton compartment.

### *1.3 Modeling perspective: the SPLAS model*

From a modeling point of view the inclusion of organism size and diversity in global models of ocean circulation, ecology and biogeochemistry would be a fundamental step ahead. Quantitative relationships between phytoplankton cell size and size-dependent processes listed above can be used to construct mathematical models of plankton community structure.

The rationale behind this thesis work is that we took a simple representation of size-dependent plankton dynamics (inspired to previous works), we tested it in a 0-D framework, and as a further step we extended this view to a one-dimensional view with a more precise dynamics (diffusion and detritus) and highlighted that with simple assumptions we can explain many features observed and get to an estimate of C export. We also show that our estimate is robust, and moreover, that the final version of the model is a step towards real systems representation.

This thesis is meant, from one side, to investigate biogeochemistry with a modeling approach (targeted to obtain biogeochemical fluxes), but also from the other side we want to show the design and development of a new tool, from the background motivations to the construction and achievement of the final version, which may suggest some useful insights on plankton interactions and ecology. In fact, the challenge of building a novel modeling tool for investigating biogeochemistry is a significant part of our approach and here we show, step by step, all the phases.

Keeping this in mind, we developed an idealized, zero-dimensional model to investigate both bottom-up phytoplankton ecological process and top-down processes as zooplankton grazing, as the two perspectives interact to regulate the phytoplankton community (Armstrong, 1994; Ward et al., 2012). The name of the model is SPLAS (Sea PLAnkton Simulator) and its main peculiarity is that it solves plankton size structure, as other models do (e.g. Follows et al., 2007; Ward et al., 2012; Ward & Follows, 2016), but with a simpler approach and with the focus on local (rather than global) dynamics and biogeochemistry.

In this study we put emphasis on a generally underrepresented aspect of planktonic community: structure and allometric variation in zooplankton prey preferences, similarly to the work done by Banas in 2011. There are however a few differences with respect to Banas' work:

- SPLAS uses a larger set of phytoplankton traits, including uptake rate and cellular quota, complicating the trade-offs involved in nutrient affinity. This is a consequence of the use of Droop's model (Droop, 1968). This model tracks the evolution in time of the internal cellular nutrient quota, decoupling the growth (depending on quota) from the nutrient uptake (depending on external nutrient concentration).

- In phytoplankton losses we include a size-dependent sinking term plus a size-independent natural mortality term.
- For zooplankton optimal prey size we used a different allometric relationship, obtained by Wirtz (2012) that accounts for non-isometric scaling.
- Both phytoplankton and zooplankton size-ranges are extended including microphytoplankton and mesozooplankton.

We highlight that SPLAS is a size-spectral model in which plankton diversity is mapped onto body size and allometric power laws are imposed a-priori to set all biological parameters. Therefore all emergent properties of the system (size-abundance/biomass relationships and other ecological features) are a direct consequence of the allometric scaling of vital rates and whatever phenomenon or behavior of plankton community shall result from the simulations, it should be investigated further in a theoretical framework and possibly be accepted as a significant part of the solution.

Similar size-spectral models have been discussed in literature (Moloney and Field, 1991; Gin et al., 1998; Baird and Suthers, 2007; Stock et al., 2008; Poulin and Franks, 2010; Banas, 2011; Ward et al., 2013) with different parameterizations and aims. Some of these and other size-spectral models have treated predation in a relatively simple way, omitting size-based preference or allometric variation of predator's optimal prey size. Inspired to the work of Banas (2011) and Ward et al. (2013), we follow the trend of including complex trophic interactions between zooplankton and phytoplankton, detailing the grazer's prey preference through relationships as those used for other vital rates and physiological parameters. This type of approach is a different perspective with respect to the approach used in another broad class of models, that avoid allometric relationships but instead exploitthe paradigm "Everything is everywhere but environment selects" (Baas Becking, 1934). In such models, parameter values and plankton traits emerge dynamically from the initial configuration through natural-selection principles, rather than being imposed a priori. This is the case of Follows et al.(2007); Bruggeman and Kooijman (2007); Bruggeman (2009); Goebel et al.(2010); Follows and Dutkiewicz(2011); Barton(2011); Mariani and Visser(2010); Mariani et al.(2013).

Also, a current trend in marine biogeochemical modelling is to incorporate Plankton Functional Types (PFTs) inside models, to be able to obtain realistic predictions and represent key processes and feedbacks of the system. Especially plankton seasonal succession provided the motivation for one of the firsts PFT modelling studies (Van den Berg et al., 1996). More complex models were developed soon after this one, like ERSEM (European Regional Seas Ecosystem Model, Baretta-Bekker et al., 1997) including more functional groups (flagellates, dinoflagellates, diatoms) and a couple of modelling studies in the North Sea have provided a good representation of seasonal succession from diatoms to flagellates, putting emphasis also on the physics of the system (Allen et al., 2004; Archer et al., 2004).

In a similar fashion, Merico et al. (2004) developed a model of seasonal succession on the Bering Sea shelf that included also coccolitophores, and their results agreed well with remotely sensed data.

Although results of PFTs are in general good, some concerns have been raised in the past (e.g. Anderson, 2005).

On a broader perspective, our work ranges from the evaluation and study of size-dependent mechanisms in a 0-D framework, to the impact of these mechanisms on biogeochemistry and biogeochemical fluxes in a 1-D framework.

After the validation and results' examination of the 0-D version, SPLAS is applied to a water column model; including vertical turbulent diffusion and compartments for detritus. We are particularly interested in Carbon cycle for its importance to Earth's climate, and at the end of this work we give a qualitative estimate of Carbon export, that is one of the most important properties in marine environments, as it is directly linked to the strength of the Biological Carbon Pump (BCP). Of course, since we only have Nitrogen in our model and our representation is still simplistic, our estimate is dependent on some assumptions, converting Nitrogen into Carbon, and should not be taken as a real estimate ready to be compared to field data. Rather, this is just a starting point towards the main long-term objective of understanding the impact of plankton size-structure in biogeochemistry. In our view, the 1-D model is a natural continuation of the 0-D simple box model, and this complication is also part of the approach: our goal is also to show that SPLAS is a promising tool and with further future developments it may be useful to get reliable results for biogeochemical fluxes, even if now we are starting from simple assumptions and using a minimalistic representation.

In the 1-D experiment we extended the depth-range and added light penetration into the water column, studying the behavior of phytoplankton biomass profile and discussing the implications of considering light for plankton interactions. In particular we will discuss the importance of considering light when shifting from a 0-D view to a water column representation.

Possible future developments are to improve SPLAS representation and eventually validate 1-D SPLAS with many process-studies. As a long-term objective for the future SPLAS might be applied as a module embedded in a more complex biogeochemical model (e.g. the BFM - Biogeochemical Flux Model; Vichi et al., 2007). SPLAS resolution in detail of plankton size-structure could enable to shed more light on plankton role in marine biogeochemistry.

### *1.4 Structure of the thesis*

The present section has introduced the problem and the rationale behind our modeling approach.

- The next section introduces the model equations and parameterizations, gives an overview of the equilibrium solutions and gives also a brief explanation of how size-spectra emerge from size-dependent mechanisms.
- Section 3 discusses the preliminary results obtained, mainly how the size-spectra (size vs biomass) varies under different conditions (different values of parameters influencing bottom-up and top-down control). To demonstrate that the model has a realistic behavior, metrics of ecosystem function are used, in analogy with Banas (2011).In the first part of section 3 we explain how our results agree with theoretical predictions and some observations reported in Ward et al. (2013), whose work gave us great part of the rationale for examining our model's output. In the second part of section 3 we explore model behavior with respect to other parameters. At the end of section 3 we test a time-dependent framework for nutrient input, as a theoretical exercise, and after the validation of this 0-D version of the model we draw some preliminary conclusions on SPLAS.
- In section 4, we consider a 1-D extension of the model with inclusion of turbulent diffusion(constant with depth) and successively a detritus compartment. We discuss the importance of light limitation to phytoplankton growth in a water column model and the implications for biomass depth profile and vertical size-structure. We also discuss what happens to our results when diffusion coefficient varies with depth.
- In chapter 5 we perform estimates of C export and discuss how they compare with previous literature estimates and their variability with nutrient load in our simulations. We also discuss robustness of our results and perform a sensitivity analysis with respect to key parameters of the model.
- We conclude our study with some considerations about SPLAS and point out some of its future improvements (section 6).

## 2. The 0-D Model

### *2.1 Formulation*

The model structure is schematized in fig.4. It is a N-P-Z like model and uses Nitrogen as a currency, quantifying all biomasses in mmolN/$m^3$.Besides Nitrogen pool (N), there is a compartment for phytoplankton (P) and one for Zooplankton (Z), both divided into 70 size-classes. The size range considered here is 1-200 µm for Phytoplankton and 2-1000 µm for Zooplankton.

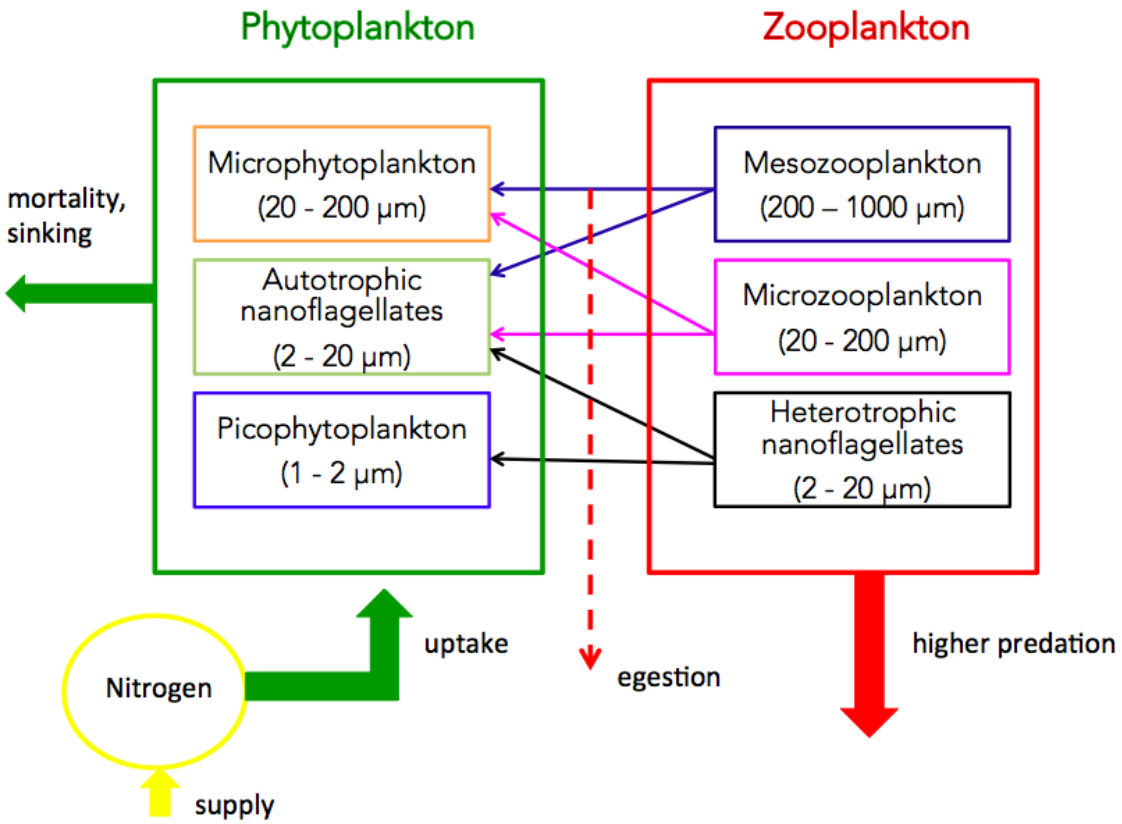


**Figure 4: Scheme of SPLAS model. Nitrogen is the currency: arrows represent nitrogen fluxes. Phytoplankton (green box) and zooplankton (red box) are divided into 70 size-classes that may be associated to functional groups in the smaller boxes. Zooplankton grazing on phytoplankton is size-based and is indicated by thin solid arrows, while the thin dashed arrow represents egestion. Thick arrows represent nitrogen physical supply (yellow), uptake (green) and mortality (green and red for phytoplankton and zooplankton, respectively).**

Phytoplankton cell quota model is used to decouple the rate and timing of growth and the rate and timing of uptake of the limiting nutrient (Caperon, 1968; Droop, 1968) but in the 0-D formulation there is no light and temperature dependence on phytoplankton growth.

The 0-D formulation is kept minimal since we are interested in capturing the essential features of plankton size spectra investigating the dependence of size-structure on some critical parameters as nutrient supply (bottom-up control) or some characteristics of the predation (top-down control). This implies, in first approximation, neglecting light and temperature dependence on P growth, plankton taxonomy, detritus and space dimensions. Some of these features will be included in the 1-D formulation.

Other properties of 0-D SPLAS are:

- Allometric relationships are used for plankton biological parameters, taken from available literature data (growth rate, uptake rate, minimum cell quota, half saturation, sinking for P and ingestion rate, optimal prey size for Z).
- Trophic interactions between P and Z are resolved using size-dependent relationships for optimal prey size and a size-preference feeding kernel is used to couple each zooplankton size-class to phytoplankton size-classes (as formulated by Banas, 2011).
- Plankton mortalities and zooplankton sloppy feeding are lost from the system, and regenerated through an external nutrient supply (S). We chose, similarly to Banas (2011), an "open" formulation, assuming that regeneration of material lost from the system is complex and happens somewhere else; we believe that this formulation in a rather simple model is better than a classic "closed" formulation(e.g. Franks, 2002) assuming an instantaneous and local regeneration of nutrients.
- Since in phytoplankton the taxonomic variation in nutrient utilization traits is largely driven by size variation (Edwards et al., 2012) we expect this model to catch the essential features of the planktonic food web, even with size as a unique trait.

### *2.2 Equations*

The model equations are formulated as follows, using the same notation for parameters as done by Banas (2011):

*Phytoplankton (1)*

$$\frac{dP_i}{dt} = \mu_i P_i - \sum_j graz_{ij} - mP_i - \sigma_i P_i$$

*Zooplankton (2)*

$$\frac{dZ_j}{dt} = \varepsilon \sum_i graz_{ij} - \xi_z Z_j \sum_j Z_j$$

*Nitrogen (3)*

$$\frac{dN}{dt} = S - \sum_i V_i^{max} \frac{N}{k_i + N} \nu_i + \left(1 - \varepsilon - f_{eg}\right) \sum_{i,j} graz_{ij}$$

$P_i$ and $Z_j$ are the i-th and j-th phytoplankton and zooplankton class, represented as biomasses in mmolN/m$^3$. The net growth of each phytoplankton size-class Pi is given by growth $\mu_i$ coming from the uptake of nutrients (according to the quota model), grazing mortality $graz_{ij}$, non-grazing mortality (size-indipendent, estimated as m=0.1 day$^{-1}$, cf. Barton, 2011) and size-dependent sinking $\sigma_i$(inspired to Smayda, 1970).

The equations for phytoplankton growth are:

*(4)*

$$\mu_i = \mu_i^0 \left(1 - \frac{Q_i^{min}}{Q_i}\right)$$

*(5)*

$$\frac{dQ_i}{dt} = V_i^{max} \frac{N}{k_i + N} - \mu_i Q_i$$

And each P size-class biomass is related to the density of cells (cells m$^{-3}$) of that size ($v_i$) via cellular quota:

*(6)*

$$P_i = \nu_i Q_i$$

Eq. 6 is important because it allows to establish the connection between Nitrogen and Carbon in phytoplankton: number of cells per meter cube obtained through this equation will give access to phytoplankton carbon content for a given size-class (see chapter 5 where we introduce the equation for carbon content per cell).

Zooplankton growth (Eq. 2) comes from the assimilation of ingested phytoplankton (with an assumed assimilation efficiency ε=1/3) and a mortality term $\xi_z Z_j \sum_j Z_j$; zooplankton mortality is a closure term according to the formulation of Steele and Henderson (1981,1992) that represents predation by higher trophic levels (fish).It assumes that the mortality of (each) j-th zooplankton type depends on the overall zooplankton biomass rather than on the biomass of the j-th type only. This is biologically justified by the

fact that higher predation is likely to be generalized rather than specialized (Armstrong, 1999). This mortality term represents a continuous loss from the plankton food web (no recycling within the system). It is an important closure term, as usual in this kind of models, but more importantly this particular parameterization of mortality (dependent on total Z biomass) may further act as a stabilizer of the model (Gibson et al., 2005; Oguz et al., 2013; Edwards and Yool, 2000; Record et al., 2013).

Finally, the Nitrogen budget (Eq. 3) is a balance between external nutrient supply (S, in $day^{-1}$), the removal via uptake by phytoplankton and the fraction of total grazing given by zooplankton excreted material (proportional to 1 – assimilation – egestion). As in Banas (2011) assimilation efficiency and egestion fraction (called ε and $f_{eg}$), that control the partitioning of total Z grazing, are assumed to be both 1/3 (equal partitioning between assimilation, egestion and excretion); this is supported by data of Hansen et al. (1997), which report an assimilation efficiency of ε≈0.3 for a wide range of zooplankton, apparently without any allometric dependence.

Grazing by j-th zooplankton class of the i-th phytoplankton class is given by (Banas, 2011):

$$graz_{ij} = I_j \frac{\varphi_{ij} P_i}{K_z + \sum_i \varphi_{ij} P_i} Z_j$$

$I_j$ is maximum ingestion rate, Kz is the prey half saturation level, φis the feeding kernel (or preference function) that represent the size-based preference of $Z_j$ for the prey $P_i$.

The assumed shape of the prey preference function is a log-Gaussian distribution around an optimal prey size, varying allometrically with Z size $x_j$:

$$\varphi_{ij} = exp\left\{-\left(\frac{log_{10}x_i - log_{10}x_j^{opt}}{\Delta x}\right)^2\right\}$$

Where $x_i$ is prey size and $x_j^{opt}$ is the optimal prey size; the breadth of the feeding kernel Δx has unit of log(x) and represents a prey selectivity: the wider the breadth, the greater the "standard deviation" of the function is and the more flattened the function becomes (low selectivity of the predator); on the contrary, the smaller Δx, the narrower the function is (high selectivity of the predator).

Banas (2011) estimated a value Δx=0.25 for ciliates, nauplii, copepodites, using the data from Hansen et al. (1994).

All state variables are reported in Table 2 and all parameters explained in Table 3.

### *2.3 Parameterization*

The allometric equations used for plankton physiological parameters are reported in Table 1, along with the literature from which they are taken or the studies in which they have been used. In this study they are imposed as empirical laws, and their impact on plankton interactions is studied observing the emergent size-spectra (here intended as biomass vs size). Plankton size is specified here as equivalent spherical diameter (ESD) and is expressed in μm.

For what concerns phytoplankton (Eq. 1), one of the most important parameters is growth rate μ; it is observed to decrease with cell size, and we use the equation retrieved by Tang (1995). This law does not consider possible increase of growth rate with size that may happen for some small picophytoplankton (in the range of about 0.2-1 μm; Chisholm, 1992; Raven et al., 2006; Jiang et al., 2005). Furthermore, P taxonomic differences are not considered: those are represented, inside the allometric equation, as different multiplicative constant, while the pure scaling with size (exponent) appears to be the same for a wide range of phytoplankton taxa (Irwin et al., 2006; Ward et al., 2013).

On the contrary, uptake rate ($V_i^{max}$ in eqs 3 and 5) and minimum cell quota ($Q_i^{min}$ in eq. 4) increase with cell size, as the first scales linearly with cell surface, while the second scales with volume for small cells and with surface for larger cells (volume powered to the 2/3), with an average scaling with volume of 0.77, and about 2.3 (7/3) exponent of ESD (Litchman et al., 2007). This behavior is consistent with general cell surface area relationships and enzyme kinetics (Aksnes & Egge 1991).

For the nutrient half saturation ($k_i$ in eqs 3 and 5) we use the simplified relationship of Banas (2011) taken from data reported in Eppley et al. (1969); the linear scaling with cell size is confirmed by other successive studies (Litchman et al., 2007; Irwin et al., 2006) for a wide range of taxa, even if the scaling factor may vary by an order of magnitude.

Finally, a size-dependent sinking ($\sigma_i$ in eq. 1) is included, which may be rather important for a first rough estimate of phytoplankton matter export from the mixed layer. The sinking formula is taken from Smayda (1970), except that the sinking velocity (m/day) multiplying the size scaling is transformed into a sinking rate ($day^{-1}$) dividing by a typical mixed layer depth of 100 m. This aspect will be modified when going into the one-dimensional model, when an actual sinking velocity (m $day^{-1}$) will be included and sinking will be represented a bit more in detail in the water column (section 4). For now, P sinking is just a "rough" size-dependent mortality term in phytoplankton equation.

For zooplankton (eq. 2), the ingestion rate ($I_j$ in $graz_{ij}$) is observed to decrease with organism size (Hansen et al., 1997) and we use the relationship obtained by Banas (2011), that shows a similar falloff as phytoplankton growth rate and is valid for many taxa as flagellates, ciliates, copepods.

Zooplankton half saturation for preys ($K_z$ in $graz_{ij}$) has essentially no allometric scaling, although it may vary by about two order of magnitudes among different functional groups; here we use an average value of 3 mmolN/$m^3$.

We propose here a potential step forward in modeling Z-P interactions, for what concerns the optimal prey size scaling with predator size: contrary to many studies, here we do not consider a constant predator/prey length ratio (Armstrong, 2003; Poulin and Franks, 2010), nor a power law (Banas, 2011). Instead we use a non-isometric scaling proposed by Wirtz (2012) that accounts for intra-body transport limitations for increasingly larger consumers. The non-isometric model considers non-size related features in the optimal prey size $x_j^{opt}$, as variations in structural elements and additional demand(metabolism) as predator volume increases.

$$x_j^{opt} = 0.16 x_j \cdot \exp\{-0.02 \cdot [\log(x_j)]^2\} \qquad [\mu m]$$

In practice, a linear model ($X_j^{opt} = cX_j$) is corrected with an exponential factor depending on a quadratic log-ESD term, so that optimal prey size increases with growing predator size, but with decreasing slope. Since the exponential correction is quadratic in log(ESD) of the predator, the decline in the slope is most apparent in macroscopically large plankton taxa, while the equation for small taxa (in the micro-plankton range) can be approximated by an isometric model (a simple power law, see Wirtz (2012)and fig. 5 for details).

Wirtz (2012) used a huge dataset (mainly Hansen et al., 1994; Fuchs and Franks, 2010) for retrieving the relationship; the equation can be considered to be valid for a wide range of taxa, given that there are no great deviations between data and the empirical estimates, for the whole dataset. The model proposed by Wirtz allows also a quantitative definition of the predator feeding mode, that may possibly be included in the equation above as another factor (intercept of the $\log(x^{opt})$-$\log(x)$ relationship). Including the quantitative feeding mode in the allometric relationship for $x^{opt}$ could make it possible to reach every species-specific optimal prey size, by simply assigning a proper value to such feeding mode (see Wirtz, 2012 for details). This is one of the possible future improvements of the model.

As breadth of the feeding function (selectivity of zooplankton) we chose the empirical estimate of Banas (2011), obtained from data contained in Hansen et al. (1994). The value of 0.25 is fundamentally in agreement with other estimates from Kiorboe (2008), even if slightly narrower.

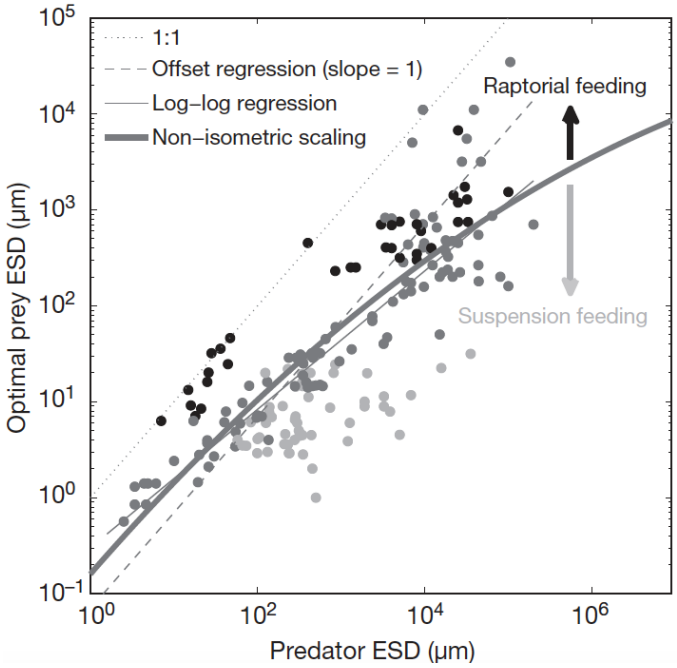


**Figure 5: Optimal prey size vs predator body size plotted for the entire zooplankton. Four statistical model of optimal prey size allometric relationship are displayed for comparisons. (1) The 1:1 line, revealing dinoflagellates, (2) A linear model $x^{opt} = 0.07x_z$, (3) An isometric scaling $x^{opt} = 0.27x_z^{0.75}$,(4) Non isometric model that allows for the definition of a quantitative feeding mode (trait axes defined by the arrows in figure, see future results and Wirts, 2012 for details). Figure from Wirtz (2012).**

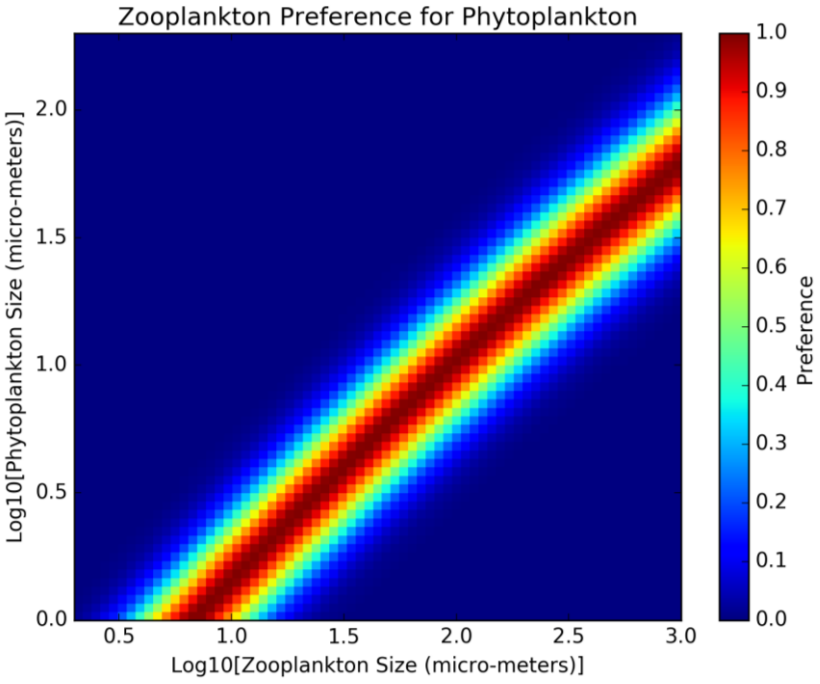


**Figure6: Allometry of optimal prey size vs predator size, according to the model of Wirtz (2012) reproduced by SPLAS 0-D. Color indicates size-preference (calculated using φ with a Δx = 0.25 ). The preference function peaks at the optimal prey size (φ=1) and decreases departing from it, reaching zero asintotically.**

**Table 1**: **Allometric Equations**

(*x* is equivalent spherical diameter - ESD – in µm)

**Phytoplankton**

Growth rate: $\mu_i^0 = 2.6x_i^{-0.45}[day^{-1}]$(Tang, 1995)

Uptake rate: $V_i^{max} = 5.87 \cdot 10^{-12}x_i^2[mmolN\ cell^{-1}day^{-1}]$(Litchman et al., 2007)

Minimum cell quota: $Q_i^{min} = 8.21 \cdot 10^{-13}x_i^{\frac{7}{3}}[mmolN\ cell^{-1}]$(Litchman et al., 2007)

Half saturation constant: $k_i = 0.10\ x_i[mmolN\ m^{-3}]$(Eppley et al., 1969)

Sinking mortality: $\sigma_i = 10^{-4}x_i^{1.17}[day^{-1}]$Adapted from (Smayda, 1970)

**Zooplankton**

Ingestion rate: $I_j = 26x_j^{-0.4}[day^{-1}]$(Hansen et al., 1997; Banas, 2011)

Half saturation constant:$K_z = 3$ $[mmolN\ m^{-3}]$ (Hansen et al., 1997; Banas, 2011)

Optimum prey size: $x_j^{opt} = 0.16x_j \cdot \exp\{-0.02 \cdot [\log(x_j)]^2\}$ $[\mu m]$ (Wirtz, 2012)

Breadth of the feeding preference: $\Delta x = 0.25$ $[log_{10}\mu m]$ (Hansen, 1994; Banas,2011)

**Table 2: State Variables**

| Variable | Units | Definition |
|---|---|---|
| $P_i$ | µMN | Biomass of phytoplankton i-th size-class |
| $Z_j$ | µMN | Biomass of zooplankton j-th size-class |
| $N$ | µMN | Nitrogen concentration |
| $Q_i$ | mmolN cell$^{-1}$ | Cellular quota of phytoplankton i-th size-class |
| $v_i$ | cells m$^{-3}$ | Cells density of phytoplankton i-th size-class |

**Table 3: Parameters**

| Parameter | Units | Definition |
|---|---|---|
| $\mu_i$ | $d^{-1}$ | Growth rate of phytoplankton i-th size-class |
| $graz_{ij}$ | µMN $d^{-1}$ | Grazing of zooplankton j-th class on phytoplankton i-th class |
| $m$ | $d^{-1}$ | Phytoplankton natural mortality |
| $\sigma_i$ | $d^{-1}$ | Sinking rate of phytoplankton i-th size-class |
| $\varepsilon$ | - | Zooplankton assimilation efficiency |
| $\xi_z$ | $(\mu MN)^{-1}d^{-1}$ | Zooplankton mortality rate |
| $S$ | µMN $d^{-1}$ | External nutrient supply |
| $V_i^{max}$ | mmolN $cell^{-1}$ $d^{-1}$ | Maximum uptake rate of phytoplankton i-th size-class |
| $Q_i^{min}$ | mmolN $cell^{-1}$ | Minimum internal quota of phytoplankton i-th size-class |
| $k_i$ | µMN | Nutrient half saturation level for phytoplankton i-th size-class |
| $f_{eg}$ | - | Fraction of grazing egested |
| $\varphi_{ij}$ | - | Preference of grazer $Z_j$ for prey $P_i$ |
| $I_j$ | $d^{-1}$ | Maximum ingestion rate of zooplankton j-th size-class |
| $K_z$ | µMN | Prey half saturation level for zooplankton |
| $x_i$ | µm | Individual size of phytoplankton i-th size-class (ESD) |
| $x_j^{opt}$ | µm | Optimum prey size for zooplankton j-th size-class (ESD) |
| $\Delta x$ | $\log_{10}(\mu m)$ | Zooplankton prey size tolerance (selectivity) |

### *2.4Code implementation*

SPLAS source code is available online at

https://marco_de_pasquale@bitbucket.org/marco_de_pasquale/splas.git.

SPLAS is composed of several "mathematical" core libraries, written in Fortran (2003 standard), for the integration of the equations, with a python3.5 interface to handle input/output and call plotting libraries (Matplotlib 2.0.0). The values of the input parameters are written in a json file, passed to the python interface.

The integration scheme is an explicit 2$^{nd}$ order improved Euler's method (Heun's method) that consists in an intermediate (first-step) evaluation of the variable using Euler's method (predictor term) plus a second step correction using explicit trapezoidal rule (corrector term).

The scheme is stable, provided that the integration time-step is sufficiently small to catch all the characteristic times of the growth of the plankton. Variations in phytoplankton growth rate and zooplankton ingestion rate with size can reach one order of magnitude, and since these parameters represent a time-scale for growth and grazing, it means that each size class has its own characteristic time of growth/assimilation. The time step must be kept smaller than the shortest of such time-scales, in order to capture and sample correctly ecological features and population dynamics.

The time step chosen for our 0-D simulation is 1 minute, which is much smaller than the typical time scale of biogeochemical systems, but it guarantees that every size-class is correctly sampled in time. When extended to a water column model, SPLAS 1-D has been optimized to work with a time-step of 80 minutes, in order to reduce computational cost and allow for the integration of the vertical diffusion term (section 4).

All runs were performed on PICO, an Intel Cluster with IBM NeXtScalearchitecture (Linux Infiniband Cluster) installed at Cineca (Casalecchio di Reno, BO, Italy; for further details https://www.cineca.it/en). PICO has 2 x 20-core login nodes and 51 x 20-core compute nodes each with a memory of 128 GB (Intel Xeon E5 2670 v2 freq. 2.5 Ghz).The Fortran code libraries are compiled with ifort and optimized through the use of MKL libraries for mathematical operations, while the python code is parallelized with the MPI protocol (module mpi4py), in order to perform multiple simulations to study the output with varying parameters.

To optimize performances, profiling with vtune16.3 was conducted on the code.

The code may also be launched in a "GNU environment", loading the corresponding modules and compiling with gfortran, using BLAS libraries instead of MKL. For this reason, and for the choice of interfacing a low level language (Fortran) with a high level language (Python), SPLAS is highly portable.

Anyway for this work the "Intel" version of the model was preferred, as it takes advantage of PICO's hardware.

The default 0-D simulation with 1-minute time-step runs in 40 minutes to cover 10 years. The 1-D version of SPLAS with a time-step of 80 minutes and a vertical grid spacing of 1.5 meters x 15 layers (20 m in total) runs in 6-7 minutes to cover the same amount of time (10 years). The realistic 1-D version with the same time-step of 80 minutes but grid spacing of 5 meters x 41 layers (200 m in total) runs in about 15 minutes.

Now that all technical details are clear, we start discussing the details of plankton dynamics represented inside the model, but before proceeding with the discussion of the output, we briefly examine analytical solutions at the equilibrium.

### *2.5 Equilibrium solutions*

A consistency check for the model equations is to solve the steady state model, that is:

$$\frac{dP_i}{dt} = \frac{dQ_i}{dt} = 0 \quad \forall i$$

$$\frac{dZ_j}{dt} = 0 \quad \forall j$$

$$\frac{dN}{dt} = 0$$

This algebraic system is not easy to solve for what concerns all $P_i$ and $Z_j$ classes, since the equations for phytoplankton and zooplankton are tightly coupled through the grazing matrix: due to the size-based preference $\varphi_{ij}$ there are multiple size-classes of zooplankton eating one fixed size-class of phytoplankton, and vice-versa each class of zooplankton can eat several phytoplankton size-classes.

Nonetheless, from the first equation (derivatives of P biomass and quota equal to zero) using the right hand side of equations 1 and 5 we can find the minimum Nitrogen concentration at which phytoplankton class-size $P_i$ can exist at steady state.

In fact, from $\dot{P}_i = 0$ it follows (eq. 1)that:

$$\mu_i P_i - \sum_j graz_{ij} - mP_i - \sigma_i P_i = 0$$

Let us explicit $\mu_i = \mu_i^0 \left(1 - \frac{Q_i^{min}}{Q_i}\right)$(eq. 4) and write the grazing matrix as:

$$graz_{ij} = g_{ij} P_i Z_j$$

where

$$g_{ij} = I_j \frac{\varphi_{ij}}{K_z + \sum_i \varphi_{ij} P_i}$$

The equation can be now written:

$$\left[\mu_i^0 \left(1 - \frac{Q_i^{min}}{Q_i}\right) - \sum_j g_{ij} Z_j - m - \sigma_i\right] P_i = 0$$

Assuming equilibrium Pi biomass different from zero and simplifying, then multiplying by $Q_i$ one gets:

$$\mu_i^0 (Q_i - Q_i^{min}) - \left(\sum_j g_{ij} Z_j - m - \sigma_i\right) Q_i = 0$$

Which yields the equilibrium cellular quota, (i.e. the cell quota at which phytoplankton size-class i exists at steady state):

$$Q_i^* = \frac{\mu_i^0 Q_i^{min}}{\mu_i^0 - m - \sigma_i - \sum_j g_{ij}^* Z_j^*}$$

Here, * denotes an equilibrium quantity. The minimum internal requirement of phytoplankton $P_i$ for equilibrium is thus a function of its maximum growth rate, minimum cellular quota, combined losses from mortality and sinking, as well as grazing pressure (depending on $P_i$ itself through $g_{ij}$, and on the biomass of each predator $Z_j$).

Setting the total predation on Pi to zero ($\sum_j g_{ij}^* Z_j^* = 0$ ) gives the absolute minimum quota level required for the survival of phytoplankton i-th size-class, in absence of grazing.

$$Q_i^{**} = \frac{\mu_i^0 Q_i^{min}}{\mu_i^0 - m - \sigma_i}$$

This quantity increases with size (Figure 7, obtained for default parameter values in Table1 and Table 4) and considering the grazing term would magnify the values for each size-class (mostly for the smallest, highly predated size-classes).

Note that if there was no mortality at all, the equilibrium quota Q** would coincide with the minimum cell quota $Q^{min}$ (Table 1).

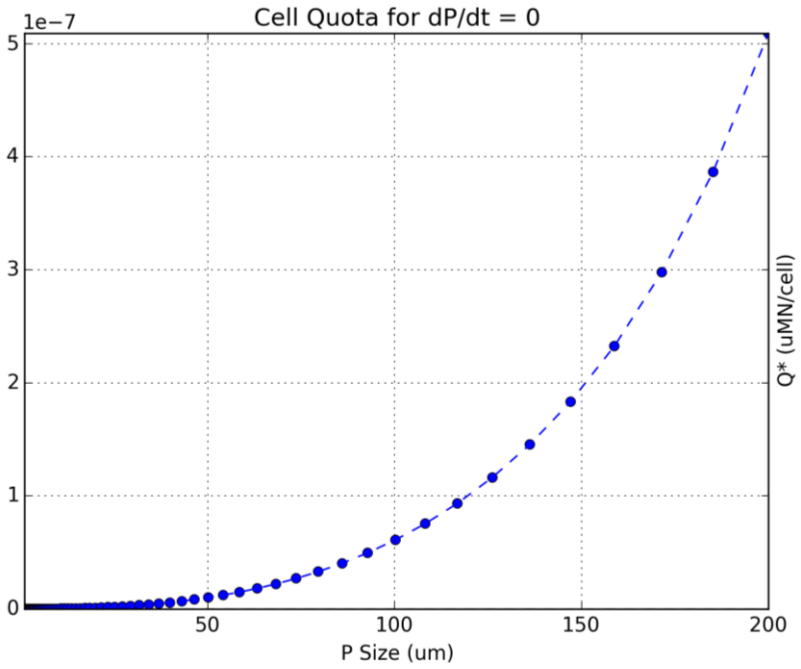


**Figure 7: Phytoplankton Cell Quota for a null derivative (steady state) of the i-th size-class biomass, without grazing term (Q**).**

From quota equation (eq. 5), $\dot{Q}_i = 0$ it follows that:

$$V_i^{max} \frac{N}{k_i + N} = \mu_i^0 \left(Q_i - Q_i^{min}\right)$$

which yields:

$$N_i^* = \frac{\mu_i^0 k_i \left(Q_i - Q_i^{min}\right)}{V_i^{max} - \mu_i^0 \left(Q_i - Q_i^{min}\right)}$$

Substituting $Q_i^*$ for $Q_i$:

$$N_i^* = \frac{\mu_i^0 k_i Q_i^{min} \left(m + \sigma_i + \sum_j g_{ij}^* Z_j^*\right)}{V_i^{max} \mu_i^0 - \left(V_i^{max} + \mu_i^0 Q_i^{min}\right)\left(m + \sigma_i + \sum_j g_{ij}^* Z_j^*\right)}$$

This is the nutrient concentration that allows phytoplankton i-th size-class to survive at steady state (zero derivative of i-th phytoplankton biomass and quota). It depends on all phytoplankton physiological parameters (uptake rate, growth rate, minimum cell quota, half-saturation) and on phytoplankton total mortality (natural, sinking, predation).

Again, setting grazing pressure to zero gives the absolute minimum N required to survive, in absence of predation (full bottom-up limitation):

$$N_i^{**} = \frac{\mu_i^0 k_i Q_i^{min} (m + \sigma_i)}{V_i^{max} \mu_i^0 - \left(V_i^{max} + \mu_i^0 Q_i^{min}\right)(m + \sigma_i)}$$

Also this quantity increases with size, reflecting all trade-offs involved in physiological parameters (Fig. 8, obtained for default parameter values in Table1 and 4).

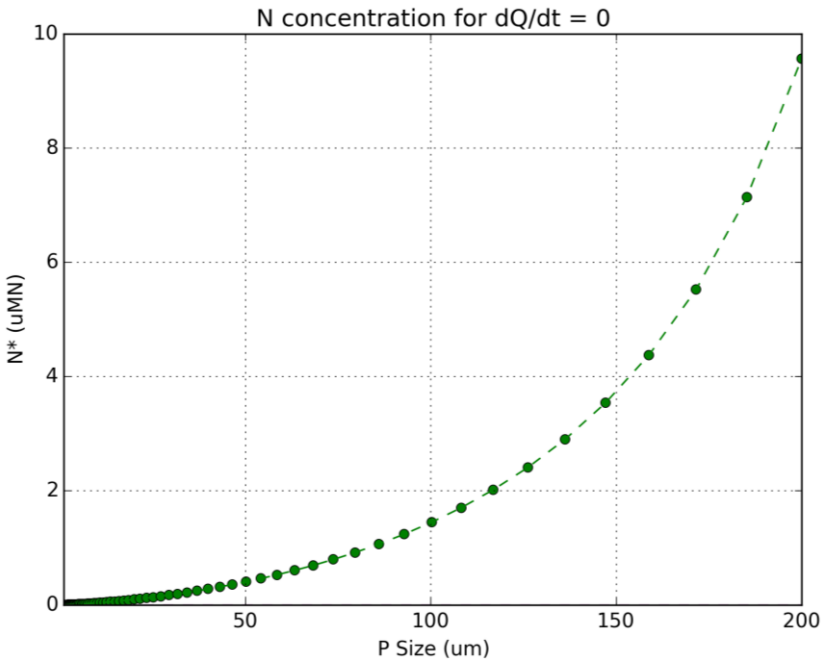


**Figure 8: Nutrient concentration for a null derivative (steady state) of phytoplankton cell quota (N**), calculated for equilibrium cell quota and without grazing term.**

Our analysis in this section is in line with resource competition theory (Tilman, 1982) and aims to show that phytoplankton patterns obtained with SPLAS can be explained in light of this theory. This theoretical framework will be expanded in next section, and will be verified by experiments in section 3.

Increasing the mortality parameters (natural mortality and sinking mortality –m and s respectively-) may lead to discontinuities in Q** and N**, when the denominators in the equations N** and Q** become zero or even negative. In that case, the size-classes falling beyond the discontinuity are suppressed (cannot grow) because they would need a negative quota to have null quota derivative, or a negative N concentration to have a null biomass derivative: in other words this means that, for those size-classes, for any external N concentration $dQ/dt < 0$ and for any cell quota $dP/dt < 0$. Actually, the discontinuity always exists at some point, but in the default case in figure 4 and 5 it falls beyond 200 µm.

The discontinuity point (size) may be different for Q** and N** (and in general it is different), so there may be a "stripe" of size-classes, comprised between the two discontinuities, that can have positive derivative for P but not for Q or vice-versa. These types can survive only for a while, if they have a sufficient initial biomass (or quota), but are "condemned" to die eventually, for a sufficiently long simulation time.

For example, an increased sinking parameter (1 order of magnitude larger with respect to the default case in Table1) moves the discontinuity at around 90 µm for N**(Figure 9): beyond that threshold size-classes cannot survive (cannot have positive Q derivative).

A similar thing happens increasing natural mortality, except that sinking has an allometric dependence for which the effect is magnified at larger size-classes (size to the power 1.17), while natural mortality is the same for all size-classes.

In any case, increasing further the mortality (sinking or natural, or both) moves the discontinuity towards smaller and smaller size classes, excluding more and more sizes from the competition.

This explains why the effect of an increased sinking is to shift phytoplankton size-spectrum towards smaller size-classes: larger phytoplankton is excluded by the excess mortality (see next section). The same happens for an increasing natural mortality.

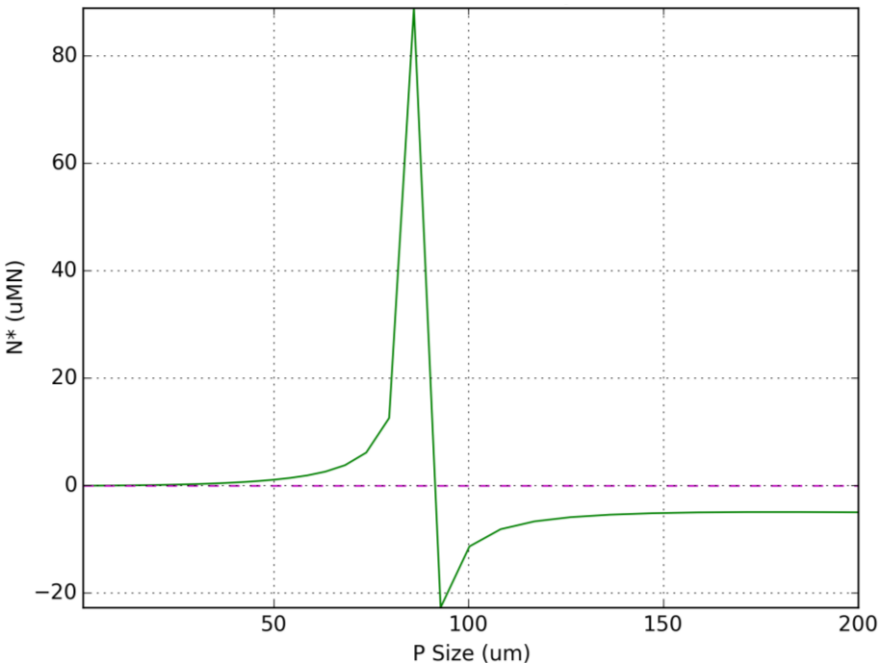


**Figure 9: Effect of increasing mortality on phytoplankton steady state: equilibrium concentration of Nitrogen (N**) in function of phytoplankton size, for an increased sinking (sinking rate of 0.001 day-1 instead of 0.0001 day-1 –default value-). For N > N* a phytoplankton size-class is able to grow at the equilibrium. For sizes larger than about 90 µm, N* is negative, meaning that such large classes cannot reach equilibrium growth (cannot have a positive derivative of P with any value of N).**

### *2.6 Mechanisms shaping size-spectra*

A pivotal step for the consistency-check of the model and for allowing further experiments in the next sections is to understand how phytoplankton and zooplankton community, size-structure and biomass emerge from the dynamics of the model. We want to shed light on how bottom-up and top-down controls interact to give the shape of the size-structure, extending the analysis of the previous section and going more in details.

To study how the size-spectra are formed, starting from the equations, we consider a classical, closed-NPZ system, simpler than ours. In this case the size-spectra would of course look different, but the mechanisms are the same, and in this simplified test case they are easier to understand and describe.

Thus, we implemented a simplified version of SPLAS 0-D, with Monod Uptake kinetics for phytoplankton and with an instantaneous recycle to the nutrient pool of plankton mortality and egested material ($f_{eg} = 0$). Moreover, in this framework we did not consider an external nutrient supply (S = 0) to keep the biomass of the whole system constant. This tool helps us to identify the mechanism underlying the formation of the observed peaks and holes in the size-spectra (see section 3.3 and following for images of size-spectra).

The equations are now:

*Phytoplankton*

$$\frac{dP_i}{dt} = \mu_i^0 \frac{N}{k_i + N} P_i - \sum_j graz_{ij} - mP_i - \sigma_i P_i$$

*Zooplankton*

$$\frac{dZ_j}{dt} = \varepsilon \sum_i graz_{ij} - \xi_z Z_j \sum_j Z_j$$

*Nitrogen*

$$\frac{dN}{dt} = -\sum_i \mu_i^0 \frac{N}{k_i + N} P_i + (1 - \varepsilon) \sum_{i,j} graz_{ij} + \sum_i [(m + \sigma_i) P_i] + \xi_z \left[\sum_j Z_j\right]^2$$

All parameter values and allometric laws are the same as in the full version of SPLAS 0-D (Tables 1 and 4), except for uptake rate ($V_i^{max}$) and minimum quota ($Q_i^{min}$), which are simply not present in this tool model (Monod uptake and growth), and for the N supply that is set to 0.

In this framework the Nitrogen concentration at which phytoplankton i-th class can exist at steady state ($dP_i/dt = 0$) becomes:

$$N_i^* = \frac{k_i\left(m + \sigma_i + \sum_j g_{ij}^* Z_j^*\right)}{\mu_i^0 - \left(m + \sigma_i + \sum_j g_{ij}^* Z_j^*\right)}$$

Therefore without predation:

$$N_i^{**} = \frac{k_i(m + \sigma_i)}{\mu_i^0 - (m + \sigma_i)}$$

Where $k_i$ is the half saturation constant, $\mu^0_i$ is the maximum growth rate and m and $\sigma_i$ are natural mortality and sinking respectively.

We set up an easy experiment to capture how the three compartments (N, P, Z) exchange biomass: we first considered a system with no predators ($Z_j = 0, \ \forall j$) and compute the spectrum of phytoplankton; then we proceed including one predator at a time and each time we compute both spectra of phytoplankton and zooplankton. So we only add biomass to the system by adding one predator, but in every single simulation (with fixed number of predators) the biomass of the system is constant, and therefore it is easier to track where this biomass is flowing at each time step. As in the full simulation of SPLAS 0-D (see section 3.2) we initialize the system to a homogeneous configuration (same initial biomass for all $P_i$, 0.1 µMN, and when there are predators same biomass for all $Z_j$, 0.01 µMN). The Nitrogen pool has an initial content of 1 µMN. Further, the predators are included one at a time in increasing order of size, starting from the smallest (2 µm).

### *2.6.1 System with no predators (N, P system)*

In this simple system, the following equations hold:

*Phytoplankton*

$$\frac{dP_i}{dt} = \mu_i^0 \frac{N}{k_i + N} P_i - mP_i - \sigma_i P_i$$

*Nitrogen*

$$\frac{dN}{dt} = -\sum_i \mu_i^0 \frac{N}{k_i + N} P_i + \sum_i [(m + \sigma_i) P_i]$$

The biomass contained in the system is 8 µMN (70 size classes of phytoplankton initialized at 0.1 µMN, for a total biomass of 7 µMN plus 1 µMN of initial N pool).

In absence of predation, the phytoplankton spectrum is reduced to only one size-class present after the simulation time (10 years as usual). The "winner" size-class is the smallest one, the first class of the interval ($P_1$, ESD = 1 µm, figure 10). This result is predictable from the analysis of the equilibrium solution (N**): in absence of top-down grazer's control, phytoplankton community is fully bottom-up controlled and the size winning is the least N limited, that is the one with the lowest requirement of nutrients (lowest N**), in agreement with the R* rule of ecology for a single resource.

$P_1$ outcompetes all other size-classes by bringing down N concentration to its equilibrium level (that can be calculated to be 0.0042 µMN) and all the excess N becomes biomass of $P_1$. The system reaches steady state after few weeks.

At the end of the simulation $dP_1/dt = 0$, $dN/dt = 0$ (Uptake/growth balances mortality in $P_1$) and almost all biomass is contained in the first size-class (a bit less than 8 µMN) and the small fraction remaining is in the inorganic Nitrogen pool.

This result is robust with respect to initial biomass in the system (results not shown). For example, with a larger initial concentration of Nitrogen (> 1 µMN), the final spectrum is the same, $P_1$ wins (accumulating a higher biomass than in our example) and N sets again to its equilibrium value ($N^{**}_1$).

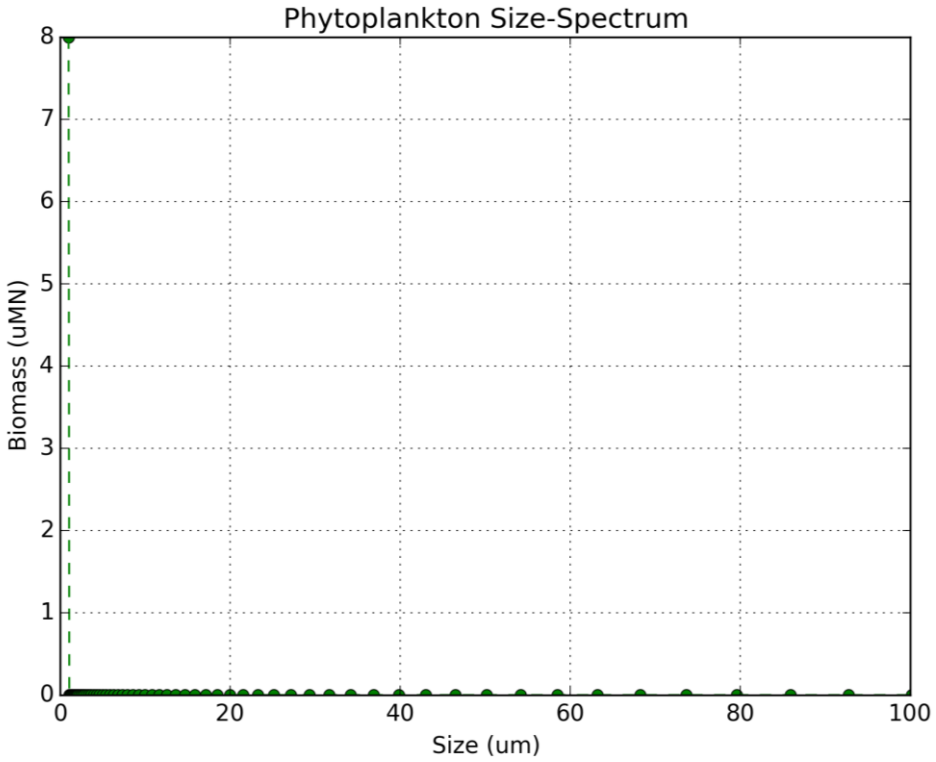


**Figure 10: Phytoplankton final size-spectrum with no predators. The smallest size-class ($P_1$, 1 µm) outcompetes all other classes, having the lowest Nitrogen requirement. This is in agreement with single resource competition theory in ecology.**

### *2.6.2 Introducing the first predator ($Z_1$, 2 µm)*

It is now clear why we introduce predators starting from the smallest: if we introduced as a first predator the right-most one in the zooplankton size interval (the largest, $Z_{70}$, with an ESD of 1000 µm) as a trivial result we would get that after a small time the predator would not be able to feed upon its optimal prey interval (around 60-70 µm) because such preys are too nutrient limited to grow, and the selectivity interval is too small to reach the smallest prey of 1 µm. So we would fall again in a case similar to the previous, and to see substantial differences from that case we would have to introduce a very large number of predators (almost all) and this is not what we want, as we wish to investigate in a straightforward way and with few organisms how size-spectra are emerging.

At the same time it makes no sense for us to start introducing random predators (for example one in the middle, $Z_{35}$, ESD = 42.75 µm) as its effect on the P spectrum would again be transient or not easily traceable.

Introducing $Z_1$seems the easiest way to quantify effect of predation on phytoplankton community.

Total biomass now becomes slightly larger, 8.01 µMN (since we added the initial biomass of $Z_1$ = 0.01 µMN).

The equations become:

*Phytoplankton*

$$\frac{dP_i}{dt} = \mu_i^0 \frac{N}{k_i + N} P_i - graz_{i1} - mP_i - \sigma_i P_i$$

*Zooplankton*

$$\frac{dZ_1}{dt} = \varepsilon \sum_i graz_{i1} - \xi_z Z_j \sum_j Z_j$$

*Nitrogen*

$$\frac{dN}{dt} = -\sum_i \mu_i^0 \frac{N}{k_i + N} P_i + (1 - \varepsilon) \sum_i graz_{i1} + \sum_i [(m + \sigma_i) P_i] + \xi_z [Z_1]^2$$

Predation from $Z_1$ shifts phytoplankton winner towards larger and less predated (less preferred by $Z_1$) size-classes (Fig 11 and comparison with the previous case). This is a simple explanation of how zooplankton grazing (which is also in the general case more intense on smaller phytoplankton) pushes the maximum sustainable phytoplankton towards larger sizes (sustainable in a bottom-up sense, by the resource).

In other words we can say, looking at this simple example, that grazing plays a crucial role in shaping phytoplankton community, by consuming smaller cells and limiting their biomass, creating “space” for less predated and larger ones to grow (otherwise outcompeted by the smaller, more efficient cells).

At the same time, even if its preferred prey is not available (totally consumed in the transient phase), thanks to the finite selectivity (different from zero, bell-shaped preference around the optimal size) the predator could rely on consuming the surviving larger phytoplankton ($P_3$ and $P_4$, ESD of 1.16 µm and 1.25 µm respectively) at a lower rate, due to the lower preference. This allows both the predator and the preys (not overharvested) to survive and coexist. The smallest phytoplankton ($P_1$ and $P_2$) had not enough biomass to sustain the predator, and grazing strongly limited their growth (grazing rate >> growth rate at the beginning, leading to complete extinction). The system reaches a steady state at a higher Nitrogen concentration than the one that would be required by the largest P surviving ($P_4$), in a bottom-up controlled framework (N** of $P_4$ is equal to 0.0056 µMN, the final N concentration sets at about 0.0065 µMN).

Note that the net effect of grazing on phytoplankton dynamics is to increase the concentration of Nitrogen required to grow (have a zero, or larger, derivative in time, in practice shifting from N** to N*): this happens for all predated phytoplankton; in this case $P_1$ and $P_2$ cannot reach the (increased) N* due to very large grazing; on the other hand $P_3$ and $P_4$ experience a lower grazing pressure, and can survive at steady

state with a larger concentration of Nitrogen (Figure 12 for the comparison of the two Nitrogen concentration at steady state, with and without predator). $P_4$ is the least predated, but cannot bring Nitrogen down further than its N*, leaving space for $P_3$ that has a lower N* even if it is more grazed by $Z_1$ (the bottom-up effect is stronger, grazing does not increase $N^*_3$ more than $N^*_4$). This is why they can coexist, and all species larger than $P_4$ simply cannot grow because they are too nutrient limited (requirement larger than $N^*_4$) even if they are less (or not at all) predated.

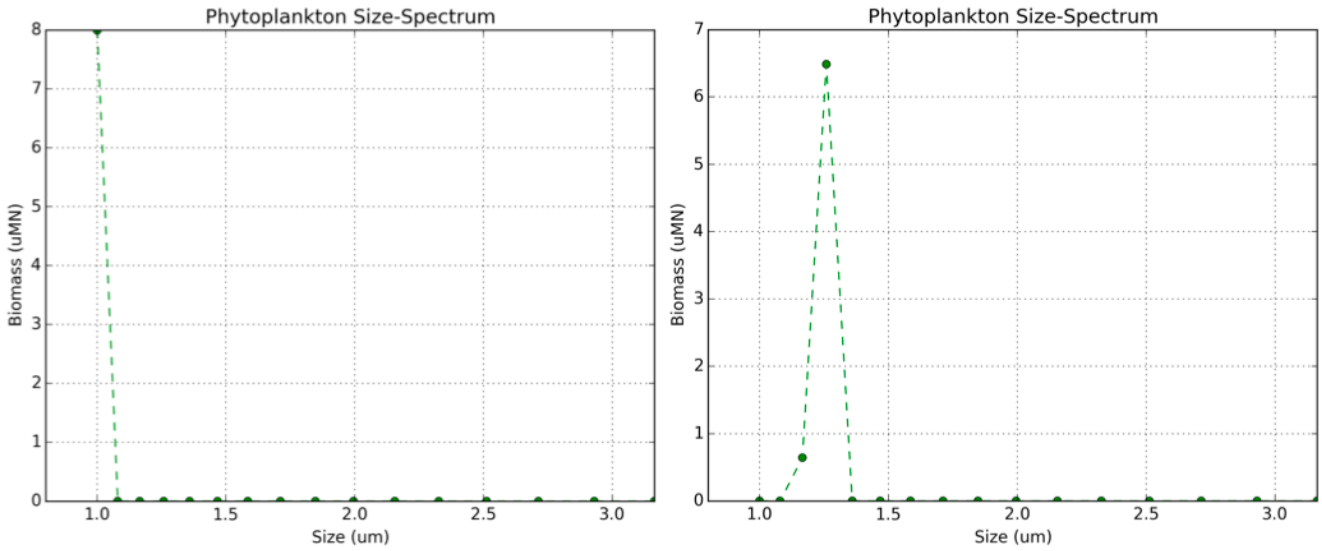


**Figure 11: Left: Phytoplankton size spectrum in absence of predators (detail from fig 10). Right: Phytoplankton size-spectrum with one predator $Z_1$, ESD = 2 µm. Predation shifts the winner towards larger size-classes, consuming totally $P_1$ and $P_2$ and allowing $P_3$ and $P_4$ to take over. The larger size-classes are too nutrient limited to grow, since $P_4$ brings down Nitrogen level to its requirement.**

$P_4$ contains the largest portion of biomass in the system (about 6.5 µMN, Fig. 11, right) and $P_3$ has a biomass of about 0.7 µMN, while the predator has a biomass slightly smaller than 0.9 µMN (figure 13). The remaining smaller part is inorganic Nitrogen (around $N^*_4 = 0.0065$ as stated above).

**With this simple experiment we identified the effect of grazing on phytoplankton: it tends to push the community towards larger sizes, by controlling the biomass of smaller size-classes through the mechanisms explained above, and leaving niches for larger size-classes, that would be more nutrient limited in absence of predation, but are less grazing limited if predators are present**.

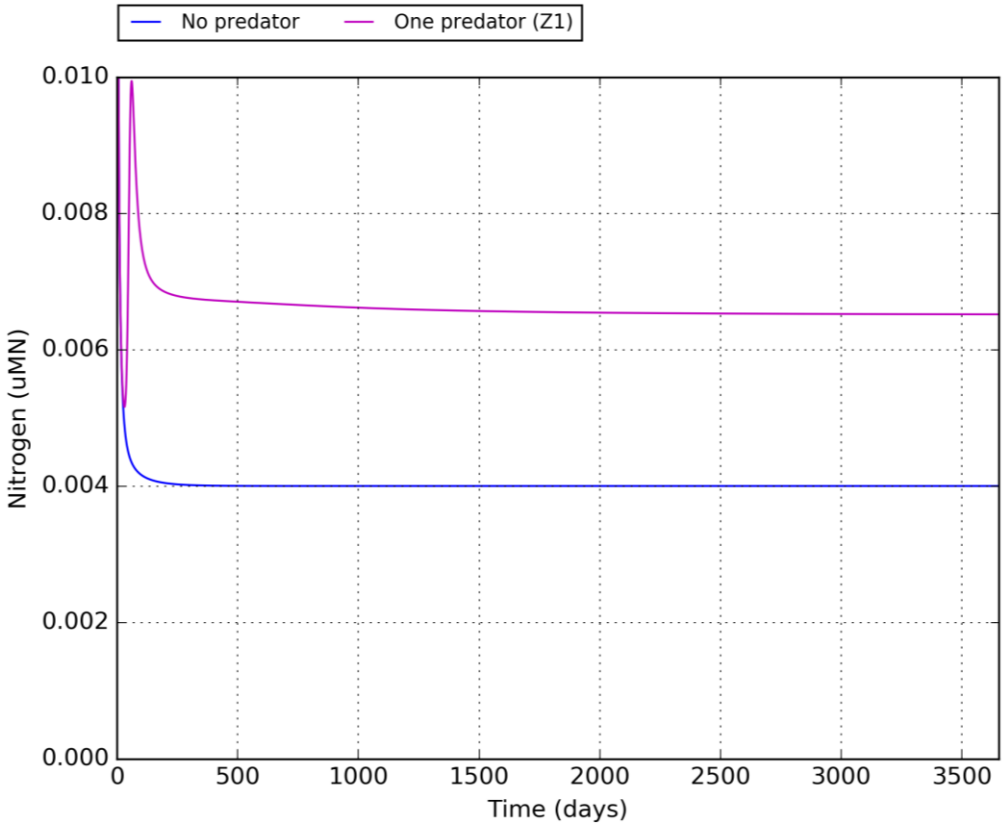


**Figure 12: Nitrogen concentration in time (transient phase is evident, but is not more clearly shown to better visualize the steady state) without predator (blue line) and with predator (purple line). Nitrogen reaches steady state value very quickly in both cases, setting to 0.0042 µMN in the first case and to 0.0065 µMN in the second case. These two values correspond to equilibrium concentration of N for $P_1$ and $P_4$ respectively, the second being increased by grazing pressure ($Z_1$) and leaving a niche for $P_3$.**

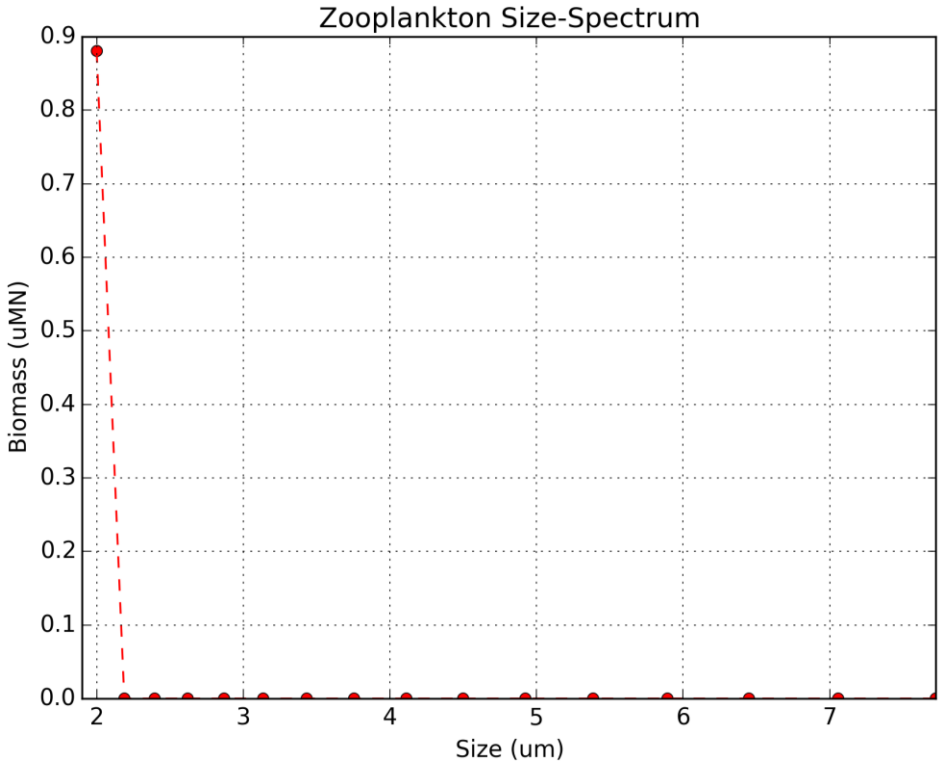


**Figure 13: Zooplankton size spectrum (only one predator, $Z_1$, ESD = 2 µm).**

### *2.6.3 Adding another predator ($Z_2$, 2.19 µm)*

There are now two predators in the system, $Z_1$ and $Z_2$, and the system has one more equation for $Z_2$ and one more grazing term in $P_i$ and N equations ($graz_{i2}$).

Adding a second predator shifts forward (towards increasing sizes) the peaks in both spectra. Phytoplankton winners are now $P_4$ and $P_5$ (figure 14), the latter containing most of the biomass (a bit less than 7 µMN). The system reaches a steady state with a Nitrogen concentration of 0.0073 µMN, that is the equilibrium concentration for $P_5$, accounted for grazing (without grazing it is equal to 0.0063 µMN). Due to the same dynamics as in the previous case, other phytoplankton size-classes are outcompeted because much more consumed by zooplankton ($P_1$, $P_2$, $P_3$) or too nutrient limited (all others from the $6^{th}$ class to the last, largest size). Thus, phytoplankton winner is basically the smallest and at the same time least consumed by predators. It must be as smallest as possible because the N requirement in general increase with size, but at the same time grazing increases N requirement (N*), so the winner should also be the least consumed by zooplankton. The winners ($P_4$ and $P_5$ in this case) set an imaginary boundary between the grazing limited phytoplankton (smaller than $P_4$) and the nutrient limited (larger than $P_5$). Phytoplankton and zooplankton spectra are shown in figure 14.

An interesting phenomenon to notice in predator spectrum (figure 14, left) is that the first predator does not survive, and all zooplankton biomass (again set to less than 0.9 µMN) is accumulated in the second predator ($Z_2$, ESD = 2.19 µm): this is because they consume, with the largest preference, preys very close in size; in particular $Z_1$ eats preferentially $P_1$ with preference $\varphi_{11}$and $Z_2$ eats $P_2$ with $\varphi_{22}$ but at the same time they could consume other preys with preference different from zero and smaller than the two above, and compete for phytoplankton. In other words their grazing pressure is distributed among all phytoplankton size-classes, decreasing and eventually tending to zero for sizes very far to their optimal prey-size.

Since their combined grazing pressure consumes completely some of their preys ($P_1$, $P_2$ and $P_3$) in the transient phase, they eventually rely on eating $P_4$ and $P_5$: these two can survive due to the predation on the first three P classes, and at the same time are not consumed completely because they are eaten with a lower rate due to the lower preference. Feeding on these two “resources” eventually favors the second predator ($Z_2$) because, being slightly larger than the first ($Z_1$), it has a larger preference for the two “available” (surviving) phytoplankton size-classes ($\varphi_{42}>\varphi_{41}$ and $\varphi_{52}>\varphi_{51}$, that means $P_4$ and $P_5$ are closer to the optimal size of $Z_2$ than to the one of $Z_1$). Moreover, since $\varphi_{42}>\varphi_{52}$, $Z_2$consumes more $P_4$ than $P_5$, and this is why $P_5$ has a larger biomass.

Note that the effect of preference takes over the decreasing ingestion rate with increasing size (see Table 1 and $graz_{ij}$ matrix). Therefore, zooplankton population is regulated by phytoplankton community through the preference matrix $\varphi_{ij}$, and in particular by the distance in terms of size between available preys and optimal prey, that sets the competition for resources. The key element that shapes zooplankton community from below is total prey ingestion:

$$I_j \sum_i \varphi_{ij} P_i$$

Where $I_j$ is the ingestion rate of the j-th zooplankton and the other term is the sum of all prey concentration weighted by the preference of that zooplankton for each size of phytoplankton.

On the other hand, predators' community is shaped by mortality that accounts for other intra-specific competition, higher trophic level predation and also cannibalism. This quadratic mortality term (depending on total zooplankton population biomass) plays a crucial role for the stability of the system (Neil Banas, August 2017, personal communication; see section 3.6 for the test on Z mortality). The mortality term becomes more and more important as zooplankton size-classes are added, as it depends on the whole zooplankton community.

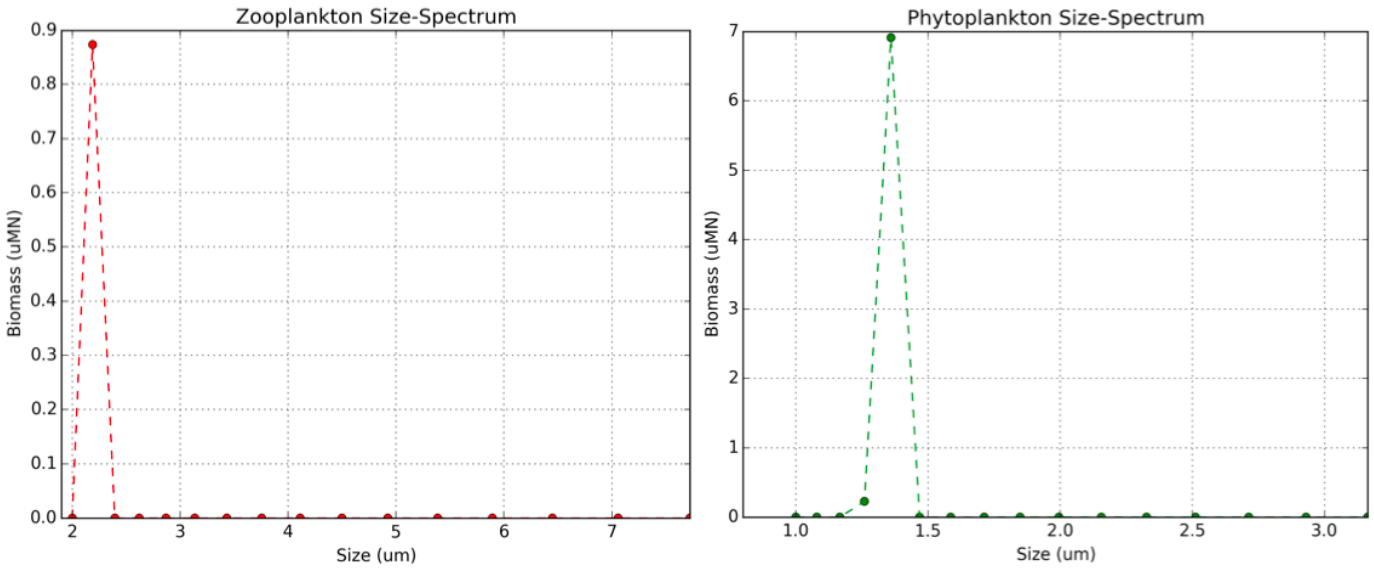


**Figure 14: Zooplankton (left) and Phytoplankton (right) size-spectra with two competing predators ($Z_1$ and $Z_2$, 2 µm and 2.19 µm respectively). Winners are shifted forward with respect to the previous case in fig 11 and 13 ($P_4$ and $P_5$ for phytoplankton, $Z_2$ outcompetes $Z_1$ in zooplankton spectrum).**

### *2.6.4 Adding more predators*

It is now clear the mechanism that shapes phytoplankton community on one size, and zooplankton on the other side. The pattern of shifting the winners towards larger and larger size-classes continues adding more and more predators (increasing the whole biomass of the system by 0.01 µMN at a time).

Each time, P sizes smaller than the winning ones are totally consumed by predators, then all the smaller predators die and the only one surviving is the one that can feed alternatively on the winning phytoplankton sizes, being the one feeding at the maximum rate (at the largest preference for the winners).

In figure 15 we can see the shift in the biomass spectra for both plankton communities, with 14, 15 and 16 predators.

Each time the predator winning is the last included (for the "preference mechanism" explained above) and the phytoplankton winning is the smallest but least predated. The system continues reaching a different steady state at each simulation, with a Nitrogen level equal to the equilibrium concentration of the maximum phytoplankton size. In the new example (figure 15, right) the maximum winning size, contrary to the previous example, has a smaller biomass than the other adjacent winner (see the tail in phytoplankton size spectra – fig. 15, right - cyan, purple and black line). This happens because the preference of the predator is larger for the larger size in this case, and so the biomass of the largest P is more grazing controlled. On the other hand the other winner is less grazing controlled and has a lower N equilibrium level. So the level of nitrogen sets to the equilibrium of the largest, and the two can coexist.

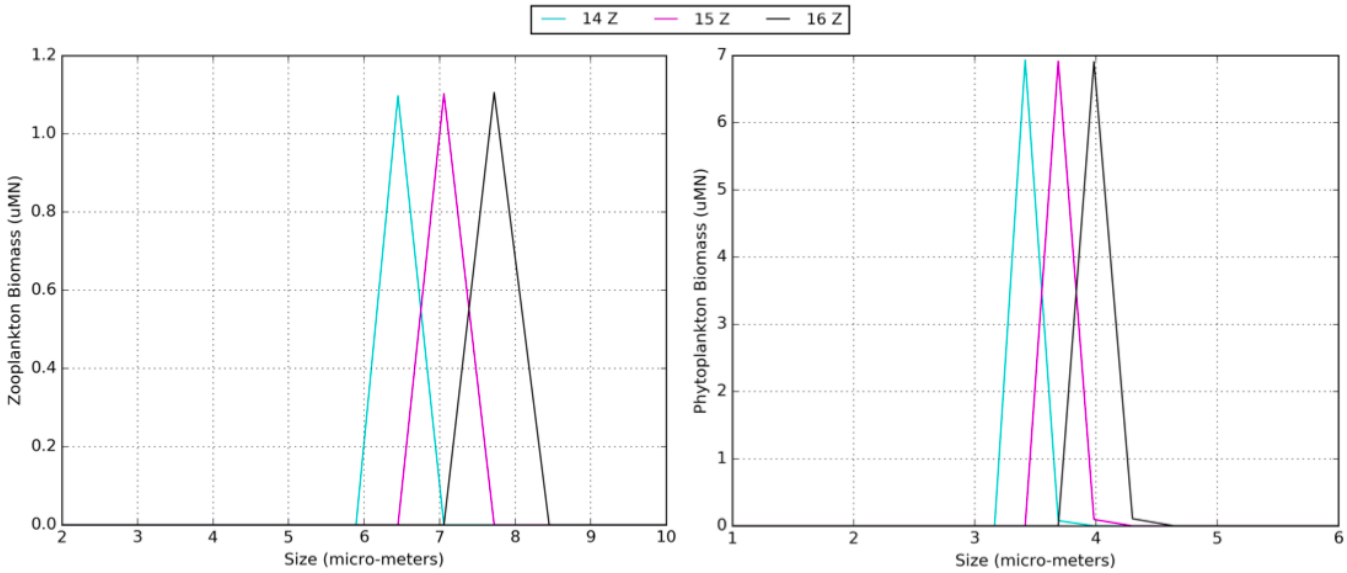


**Figure 15: Zooplankton (left) and Phytoplankton (right) size spectra with 14 predators (cyan line), 15 predators (purple line) and 16 predators (black line). The pattern of increasing winning size continues for the mechanism explained in the text. Each time a predator is included, it outcompetes all smaller predators and shifts phytoplankton winners to larger sizes.**

When inserting the 22nd predator in the system ($Z_{22}$, ESD = 13.26 µm), we start seeing two stripes in the spectra: there are other winning sizes in both zooplankton and phytoplankton community (figure 16). We see in figure 16 three winners for zooplankton ($Z_{14}$, $Z_{15}$ and $Z_{22}$) and three winners for phytoplankton ($P_1$, $P_{25}$ and $P_{26}$); in order to explain this result we start seeing why finally two "stripes" appear in the spectra: including more and more predators in our synthetic "world", at a certain point (in this case with the inclusion of the 22nd predator) the grazing pressure on "small" phytoplankton size-classes (1-10 µm interval) is somehow enough distributed among preys to allow other winners, for which growth rate becomes positive (grazing becomes non-limiting). On one hand other preys are allowed to survive (in particular $P_1$), provided that they are not consumed in excess by predators now, and on the other hand other predators can be sustained by a higher number of surviving preys.

$Z_{14}$, $Z_{15}$ and $Z_{22}$ survive as they are able to sustain themselves with the available preys (winners) more than all other predators, and also thanks to their overall higher preference for many preys that allows them to have a high value of total ingestion ($I_j \sum_i \varphi_{ij} P_i$) during the transient initial phase and to outcompete other predators. In fact, in general, while smaller zooplankton have higher ingestion rates (Table1), they have a somehow narrower bell-shaped preference around their optimal prey-size, making them less favorable to survive, at least when preys are abundant, as they have a smaller number of preys to feed on (Figure 6) while competition among predators is strong and preferences overlap to a certain extent.

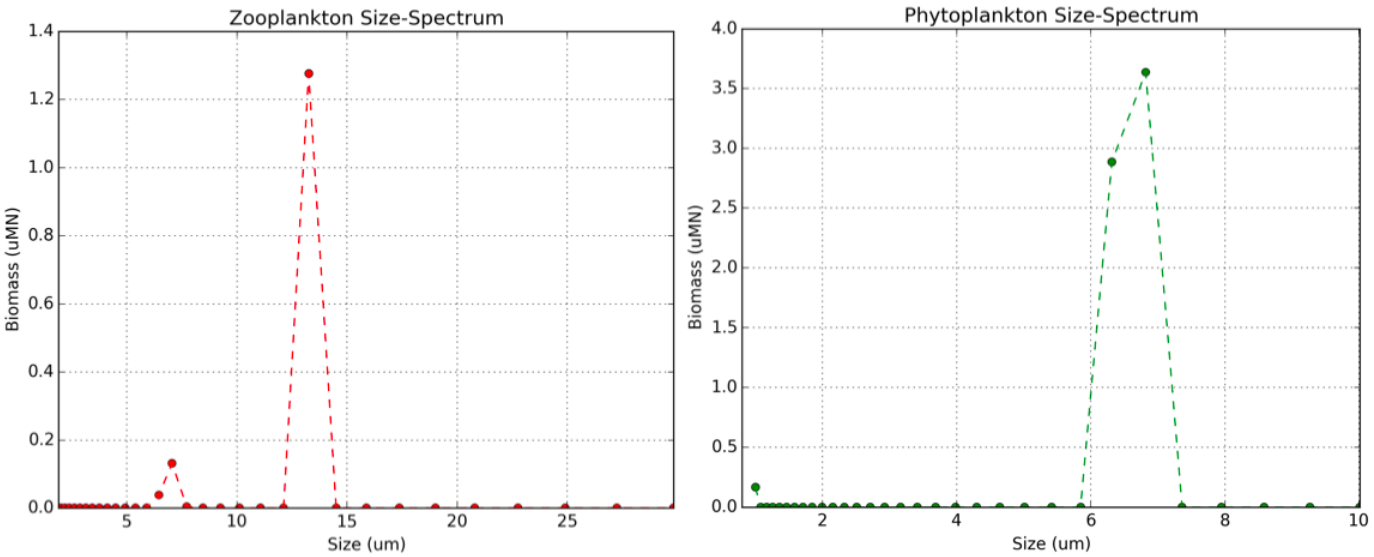


**Figure 16: Zooplankton (left) and Phytoplankton (right) size-spectra with 22 competing predators (from $Z_1$ to $Z_{22}$). Two stripes can be seen in both spectra. Zooplankton winners ($Z_{14}$, $Z_{15}$ and $Z_{22}$) outcompete other predators with their high total ingestion, good combination of ingestion rate and preference for the preys. $P_1$ (left-most peak in phytoplankton spectrum) is able to survive as in this case it is not consumed in excess by predators during the transient phase, and leaves room for other predators to sustain their growth. The other two winners ($P_{25}$ and $P_{26}$) survive for the same mechanism as in previous experiments. In summary, at this point the grazing pressure is enough distributed among preys to allow more than one "stripe" in the spectra.**

It is fair to point out that this result may be also slightly influenced by the absence in the model of picophytoplankton smaller than 1 µm, which are the preferred prey of some of the nanozooplankton (2-4 µm). These zooplankton appear to have a one sided bell-shaped preference in the size-domain, meaning that they have a limited number of preys to feed on with a reduced preference (Figure 17).

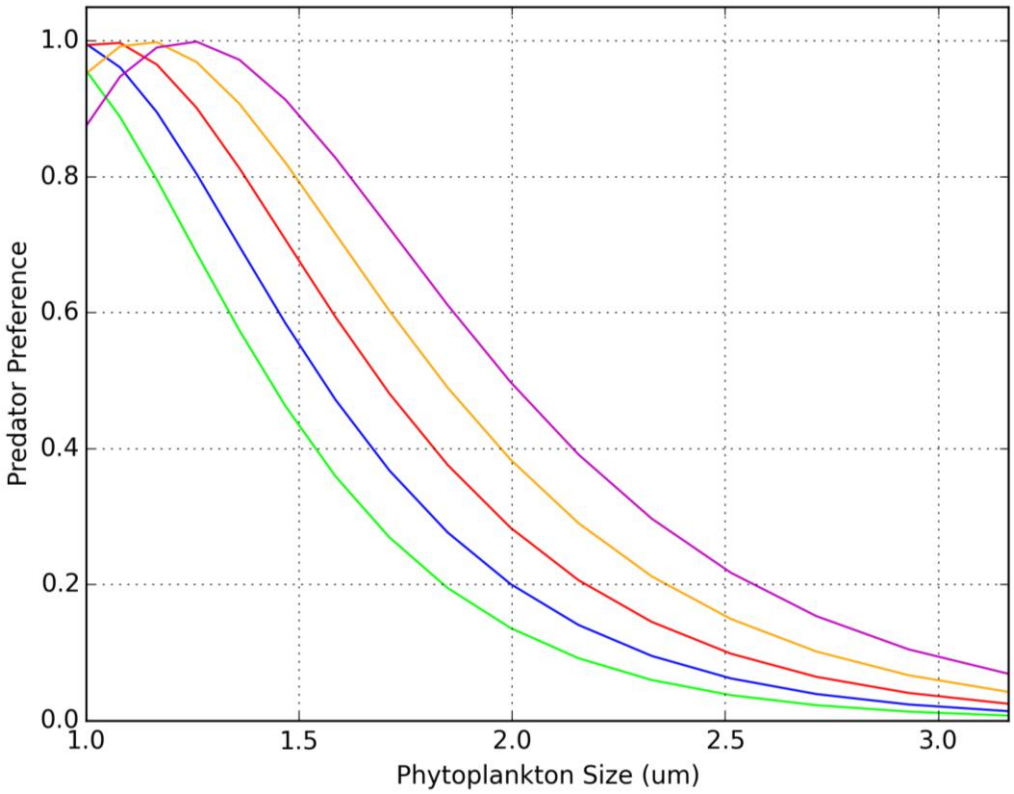


**Figure 17: Preference functions ($\varphi_{ij}$) of some nanozooplankton predators (from left to right, green to purple, 3.14 µm, 3.43 µm, 3.76 µm, 4.11 µm, 4.5 µm). We see that the smaller predators have a one-sided preference (green, blue and red line) while slightly larger predators start having a bell-shaped preference (orange and purple line). This boundary-effect reduces the effective number of available preys in the range >1 µm making these predators less competitive, at least in environments in which preys are abundant and larger predators may happen to eat many preys and have a higher total ingestion.**

We expect this "boundary-effect" to be important when looking in detail at the predation on small picophytoplankton, and of course size-spectra may be a bit altered by the inclusion of smaller organisms, but at the same time we do not expect this effect to compromise our results in the context of our final aim.

As a longer-term future development in order to improve our representation, we aim to include picophytoplankton smaller than 1 µm with a suitable maximum growth rate and also include phytoplankton taxonomy in our system, in a similar way as Ward et al. did in 2013. In this way we hope that eventually we will get to a more complete picture of the role of plankton in size-structured communities and biogeochemistry (see Future Work section).

Adding more predators (23) the size-spectra keep evolving with two "stripes" (figure 18).

Moreover, these results are robust with respect to the biomass in the system (figure 19).

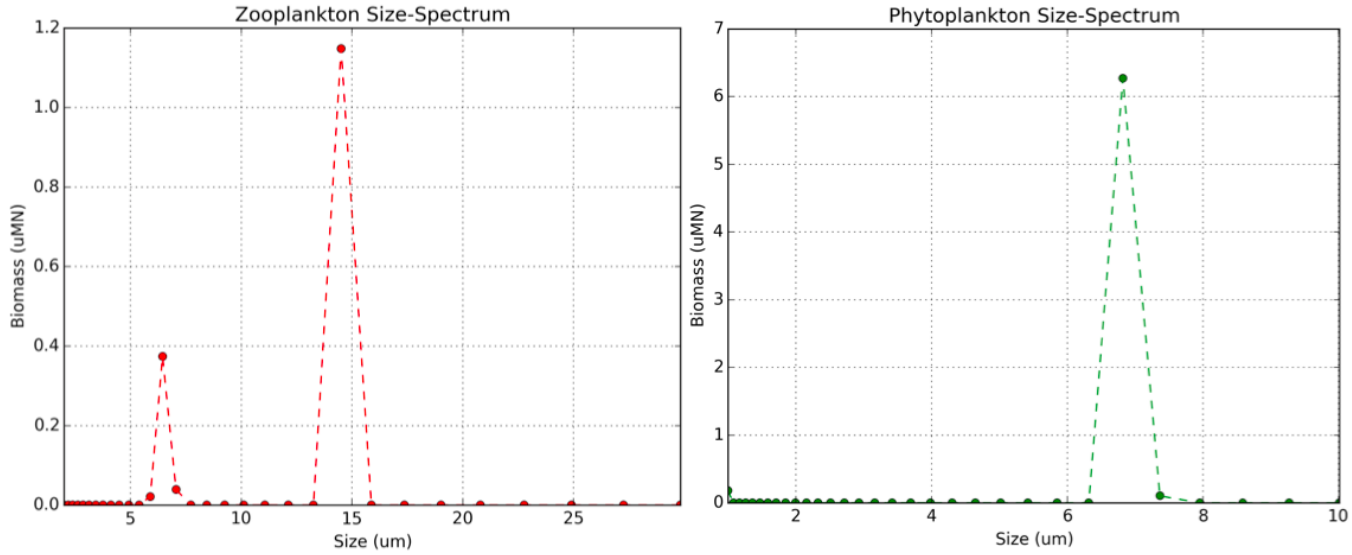


**Figure 18: Zooplankton (left) and Phytoplankton (right) size-spectra with 23 competing predators. As in fig. 21 two stripes can be seen (one very little on the left of phytoplankton spectrum).**

For instance, the system with 23 predators (figure 18) is stable with respect to the initial Nitrogen content (figure 19). Changing the initial pool of Nitrogen we see that the biomass is distributed among the same winners every time. Thus the mechanisms shaping the community size-structure are solid with respect to changes in the biomass inside the system.

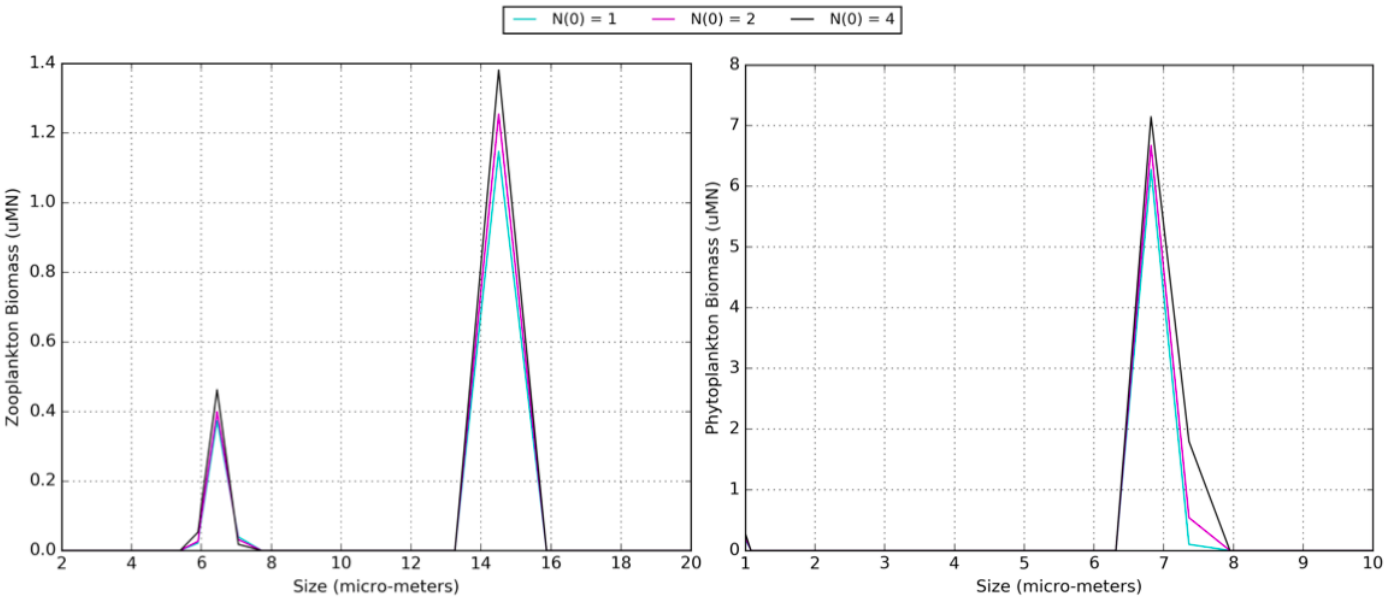


**Figure 19: Zooplankton (left) and Phytoplankton (right) size-spectra with 23 competing predators, for three different initial concentrations of Nitrogen (cyan line 1 µMN, purple line 2 µMN, black line 4 µMN). The spectra are robust with respect to changes in the initial N pool. More biomass does not add new winning size-classes in the system, and is instead accumulated in the same size-classes.**

Summarizing the results of our experiment, we see that in an environment without predators the “winning” phytoplankton is the smallest in size, being the least nutrient limited (the one with the lowest equilibrium N requirement). **The inclusion of predators has the net effect of increasing the equilibrium N concentration and at the same time shifts the phytoplankton winner towards larger size-classes**; the winner becomes the least N limited that is also poorly predated (growth > grazing).

Thus:

- Grazing on small phytoplankton leaves room for larger size-classes to grow.
- Maximum phytoplankton size in the spectrum is a function of grazing.
- Some phytoplankton smaller than the maximum size are able to survive thanks to “holes” in the grazing pressure, whilst others are completely consumed by predators. This generates the peaks (and the holes) in phytoplankton spectrum.
- Zooplankton spectrum (winners) is shaped mainly by the preference for the preys, the key factor being total ingestion (combination of ingestion rate, preference and phytoplankton effective abundance).

**The maximum phytoplankton size surviving is a function of grazing, but also depends on N concentration in the environment, being sensitive to changes in Nitrogen supply**. Figure 20 shows how maximum P size varies with varying supply, and lies close to the intersection of N equilibrium concentration and N final concentration in the environment: in an “ideal” environment without grazing the winner should lie exactly on the intersection (i.e. large sizes would not be able to survive without predators). Predation, while allowing large size-classes to survive, and to a certain extent pushing towards larger sizes the P community, on the other hand pushes the maximum winner to smaller sizes, increasing the value of N equilibrium concentration. For other comments on how plankton communities change with N supply see section 3.4.1.

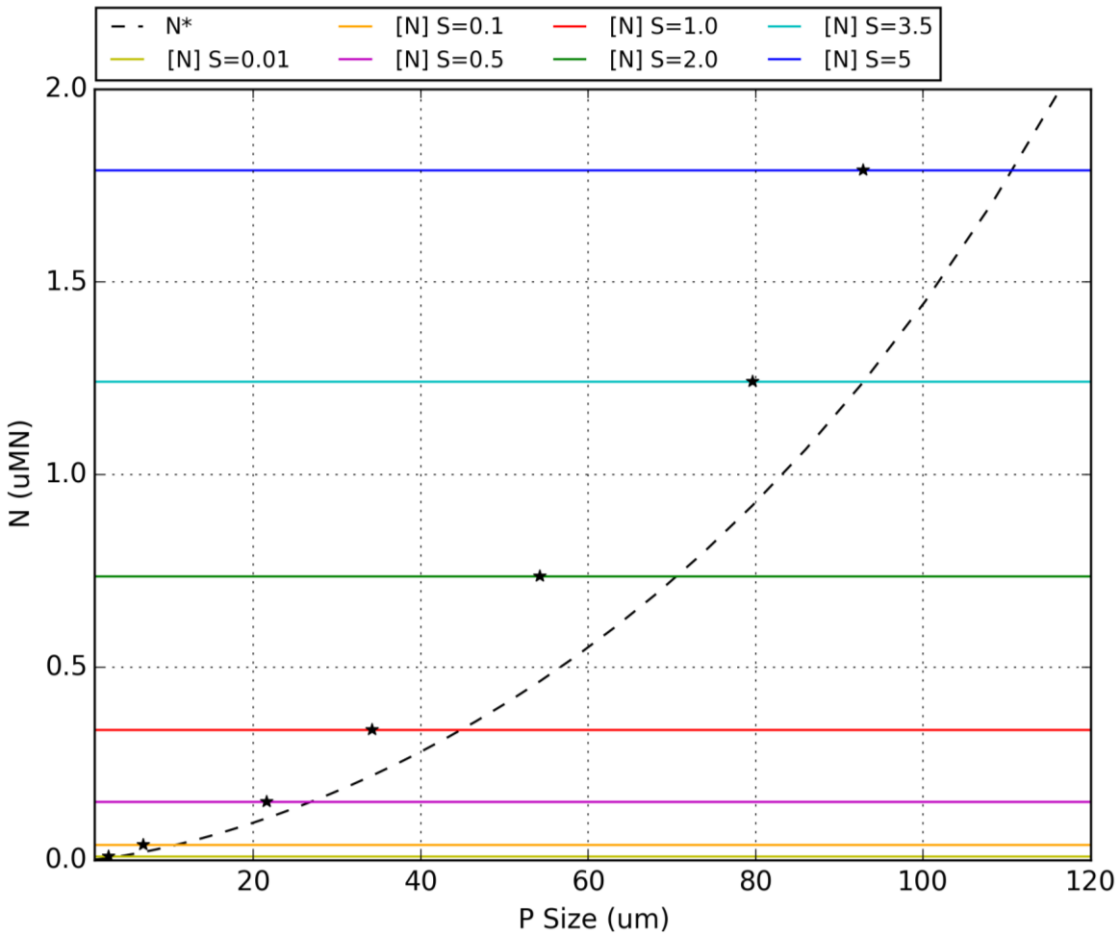


**Figure 20: Maximum phytoplankton size surviving (black stars) plotted against final N concentration (horizontal lines) for simulation with varying N supply in the environment. The graph shows also N equilibrium concentration vs size in absence of grazers (bottom-up control, N**). The winner does not lie exactly on the intersection between final N and N** because grazing increases N equilibrium value, effectively decreasing the size of the winner. The stars lie on an analogous curve next to N**.**

# 3 Validation and behavior exploration of SPLAS 0-D

## *3.1 Summary of the section*

To explore the basic dynamics of SPLAS, we define some Ecosystem indicators, as used by Banas (2011). We will test the model and see if there is enough "lack of pathology" to proceed to a model validation and to a comparison with field data and other more complete test benchmarks. The procedure that we follow is:

1. To introduce the default configuration size-spectrum (default parameters in Table 4), emerging from the interactions analyzed in section 2.6 and discuss the importance of zooplankton mortality closure term.
2. To examine the behavior of the model under different steady nutrient forcing, from 0.01 to 10 milli-moles of N per meter cube (μMN), observing the variation in the size-structure of plankton community, in particular a shift towards larger cell sizes in phytoplankton as N supply increases (co-existence of small and large phytoplankton) and an increasing total biomass, in agreement with theoretical predictions (Ward et al., 2013). Moreover, size-diversity, here represented by Shannon Evenness, shows a parabolic dependence with biomass for both phytoplankton and zooplankton, in agreement with experimental studies (Irigoien et al., 2004).
3. To study the impact of top-down control on the system, varying the mortality parameter of zooplankton population, which represents higher predation losses. This parameter acts as an opposite effect with respect to N supply, removing biomass from the top of the planktonic food-web and causing an opposite shift in the size-structure of the community (towards smaller organisms).
4. It is important to keep in mind that all results are dependent on several grazer's parameters that are assumed constant in this study, as selectivity (prey-size tolerance Δx), assimilation efficiency (ε) and half-saturation for preys (Kz). These parameters do not show allometric dependence, although they may vary somewhat among different zooplankton taxa (Kz may even differ by orders of magnitude); therefore we will see how size-spectra can be impacted by changes in such parameters, as a reminder for future work and other studies.
5. Another parameter influencing the size spectra is phytoplankton sinking, which also regulates carbon export outside of the mixed layer; we will study how the sinking parameter impacts the ecology and the planktonic size-structure.
6. We also examine the behavior of the model varying two poorly constrained parameters: zooplankton half saturation constant for preys and assimilation efficiency.

Recent results (Garcia-Comas et al., 2016) point out how the size-diversity of phytoplankton hinders trophic transfer efficiency (TTE), while zooplankton size-diversity promotes it: we show that SPLAS' output catches this feature, with higher prey size-diversity leading to smaller Zooplankton to Phytoplankton (Z:P) ratios (used as a proxy for TTE), while higher predator size-diversity corresponds to higher Z:P ratios. (Z:P ratio is negatively correlated with phytoplankton diversity and positively correlated with zooplankton diversity).

A result that we want to point out is that all size spectra show peaks and non-monotonic behavior with size, as outlined strikingly by Banas' pioneering work (2011). This is due to the shape of the size-based preference $\varphi_{ij}$. Without this size-based preference (every $\varphi_{ij}$ equal to 1), even keeping all other allometric relationships unchanged, size-diversity collapses to only 1 single P and 1 single Z surviving, that is the least nutrient limited P and the Z with the highest ingestion rate.

Finally, we show how our results do not change qualitatively with increasing resolution (with a larger number of size-classes), demonstrating that the shape of the size-spectra is a consequence of modeled biological interactions and not a mathematical artifact.

## *3.2 Ecosystem indicators for 0-D model*

To test the level of realism inside the model we use quantities that measure the degree of limitation to phytoplankton growth, and indices estimating the diversity (here size-diversity) of both phytoplankton and zooplankton community. We then interpret our results and make some considerations in the light of how SPLAS represents these limitations and the diversity.

### *3.2.1 Phytoplankton Limitations*

We introduce here the bottom-up and the top-down limitation of phytoplankton growth, following Banas (2011). The nutrient (N) limitation of phytoplankton i-th size-class is defined as

$$N_{lim}^{i} = \frac{k_i}{k_i + N}$$

where N is nitrogen concentration and ki is the half saturation constant for the i-th size-class.

This metrics is mathematically bounded between 0 and 1: a value close to 0 means that Nitrogen is not limiting (i-th) phytoplankton growth, while a value close to 1 means that (i-th) phytoplankton is not able to scavenge the nutrient efficiently, or that the nutrient is fully exhausted by that phytoplankton.

The second metrics quantifies phytoplankton limitation due to grazing, and is defined as

$$G^i_{lim} = \frac{1}{\mu_i} \sum_j g_{ij} Z_j$$

where $\mu_i$ is the growth rate of i-th phytoplankton, Zj is j-th zooplankton size-class, and gij is

$$g_{ij} = I_j \frac{\varphi_{ij}}{K_z + \sum_i \varphi_{ij} P_i}$$

such that gij multiplied by phytoplankton and zooplankton biomass gives total grazing (as in section 2.2)

$$graz_{ij} = g_{ij} P_i Z_j$$

In practice $G^i_{lim}$ is the total grazing per unit of prey biomass divided by prey growth rate: a low value means that there is a small grazing pressure (with respect to growth rate) on i-th phytoplankton, thus predation is not limiting its net growth; a high value indicates instead that predators are limiting phytoplankton net growth.

The balance of these two measures gives the limiting factor of i-th phytoplankton growth; as stated before, both depend on size. Typically N limitation increases with size (smallest cells use nutrients more efficiently) while grazing limitation decreases with size (largest cells experience a lower predation).

The behavior of the limitations may vary in time, according to environmental parameters and biomasses; in fig. 21 nutrient and grazing limitation time average (for 10 years of simulation) are shown, with default parameter values (Table 1 and 4).

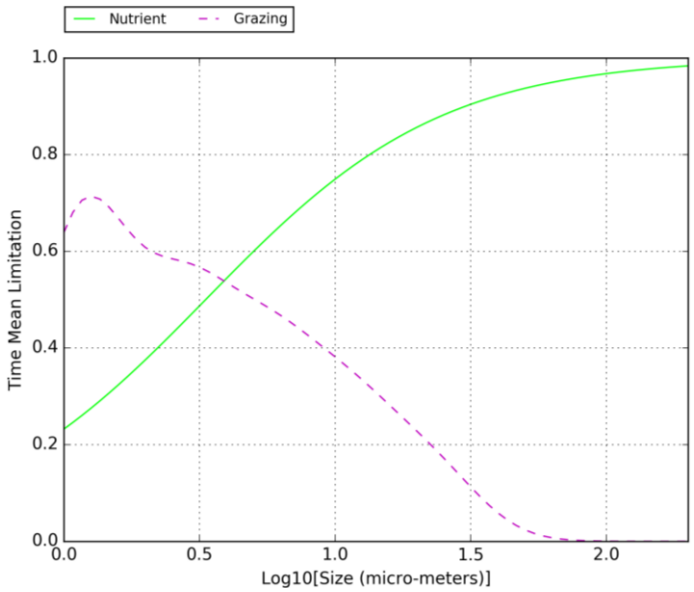


**Figure 21: Nutrient limitation (solid green line) and grazing limitation (dashed violet line) in function of phytoplankton size (time-averaged for 10 years of simulation). The behavior is the expected one: N limitation increases with size and grazing limitation decreases with size, as the smallest size-classes are the least bottom-up limited but suffer a huge grazing pressure, while on the contrary larger cells are the most nutrient limited and least predated.**

### *3.2.2 Size-diversity*

As an index of size-diversity we use Shannon Evenness, which measures how close in abundance each species in an environment is. For phytoplankton it is equal to:

$$SE_P = -\frac{1}{\ln(n)} \sum_{i=1}^{n} \frac{P_i}{P_{TOT}} \ln\left(\frac{P_i}{P_{TOT}}\right)$$

where ln is natural logarithm, n is the number of species (here the number of size-classes), $P_i$ is the biomass of i-th phytoplankton size-class, $P_{tot}$ is phytoplankton total biomass.

Analogously for zooplankton:

$$SE_Z = -\frac{1}{\ln(n)} \sum_{j=1}^{n} \frac{Z_j}{Z_{TOT}} \ln\left(\frac{Z_j}{Z_{TOT}}\right)$$

where $Z_j$ is j-th zooplankton size-class and $Z_{tot}$ is zooplankton total biomass.

Shannon Evenness is bounded between 0 and 1: 0 means that one type (size-class) of plankton makes up all biomass, 1 means that there are equal proportions of each type/species in the environment.

We use the Evenness for consistency with the results of Banas (2011), for an easier comparison. This is good for modeling studies, where one wants to quantify how many types of plankton are present at a given time with respect to all the potentially present types included in the model representation.

In the next section we give an example of phytoplankton and zooplankton size-spectra for the default configuration of the model parameters and 10 years of simulation.

## *3.3 Default configuration spectrum and importance of zooplankton mortality*

### *3.3.1 Default size-spectrum*

Figures 22 and 23 show respectively phytoplankton and zooplankton time mean (10 years) size-spectrum (Biomass in mmolN/$m^3$ against size in μm). These spectra are multi-modal and non-monotonic, showing several peaks at given sizes (default values of the parameters are shown in Table 4).At the default N supply (1 mmolN $m^{-3}$ $day^{-1}$) the maximum phytoplankton size present is below 50 μm, and zooplankton is smaller than 300 μm. We see that increasing the supply leads to shift towards larger phytoplankton size-classes,

while zooplankton spectrum is controlled by the availability of preys and also by their mortality parameter (default value 0.2 $m^3$ $mmolN^{-1}$ $day^{-1}$).

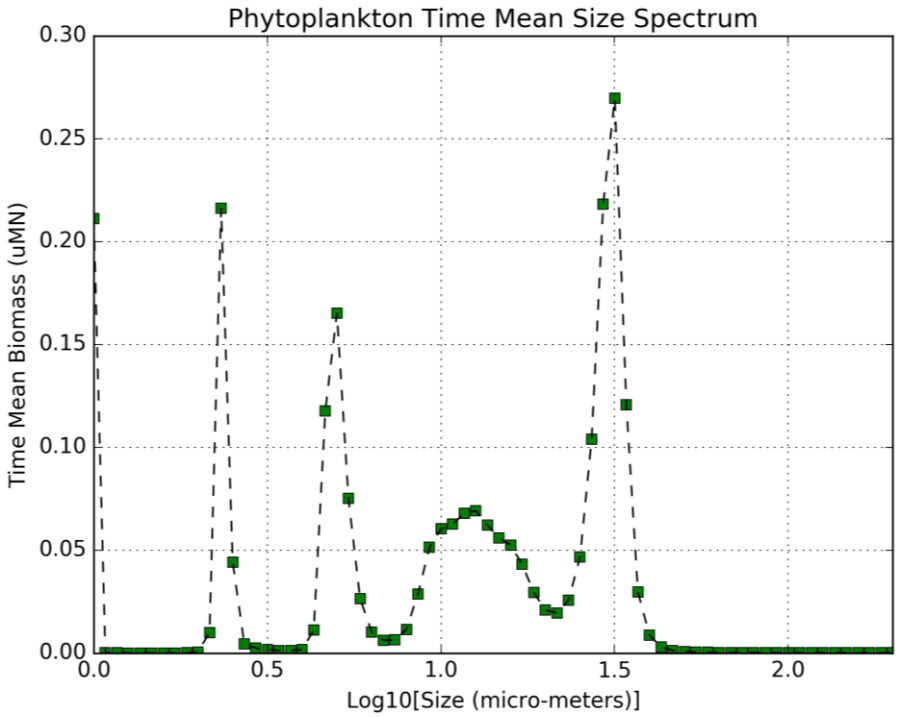


**Figure 22: Phytoplankton time mean size-spectrum for 10 years of simulation, with default parameter values.**

Phytoplankton limitations are shown in figure 21. Larger size-classes (>50 µm) cannot grow in these default conditions, being nutrient limited; at the same time not all the smallest are able to grow since their biomass is reduced by zooplankton predation. Trivially, the size-classes able to grow are those for which net growth (growth – total mortality) is larger than zero.

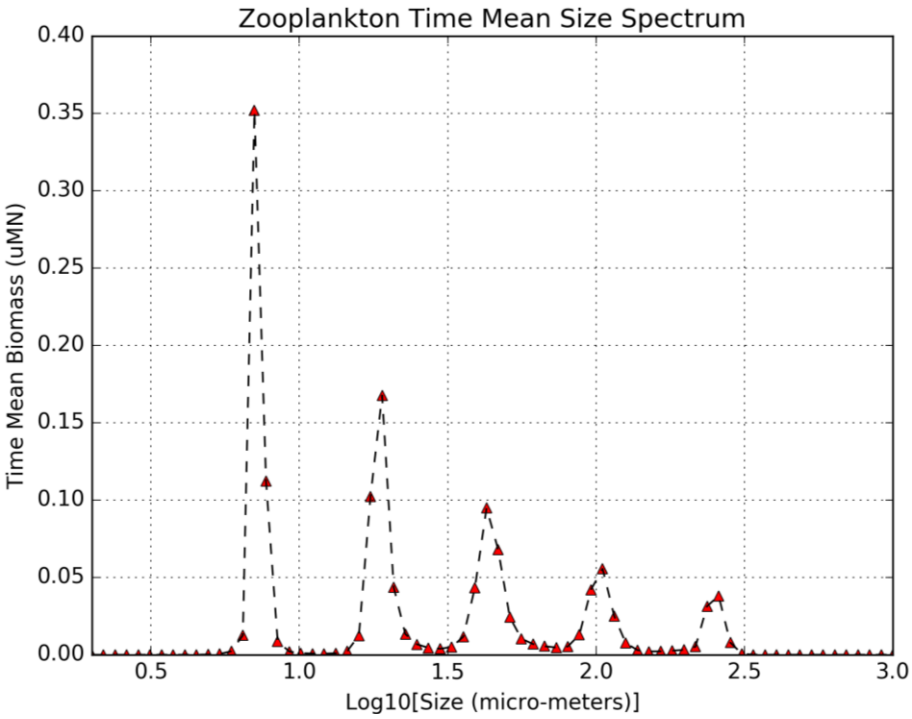


**Figure 23: Zooplankton time mean size-spectrum for 10 years of simulation, with default parameter values.**

The complete spectra (Biomass vs size vs time) can be seen in figures 24 and 25 (phytoplankton and zooplankton respectively). These are used to look at transient dynamics and other details at the beginning of the simulation (e.g. how the system arrives to equilibrium starting from initial conditions, if the final state is steady or oscillating).

Here we mostly consider time average size-spectra, looking at how the mean state of the system varies in different environmental conditions (parameter values as N supply, Z mortality and others).As demonstrated by Ward et al. (2013), in Nitrogen limited systems, the degree of "bottom-up" nutrient limitation dictates the number of size-classes that can coexist, while "top-down" grazers' control limits the amount of biomass within any particular size-class, in turn regulating total biomass in the system. With increasing total phytoplankton biomass (nutrient supply) large phytoplankton do not replace smaller species, but instead coexist alongside them.

We will show in section 3.4.1that SPLAS catches this pattern of increasing phytoplankton biomass through the addition of larger size-classes; this pattern has been explained theoretically by Ward et al. (2013) in terms of the balance between size-dependent nutrient uptake traits and density dependent predation, and has also been confirmed by large-scale field measurements in the Atlantic (Cavender-Bares et al., 2001; Marañon et al., 2001) and through the synthesis of in situ and remote observations (Uitz et al., 2006; Kostadinov et al., 2009; Hirata et al.,2011).

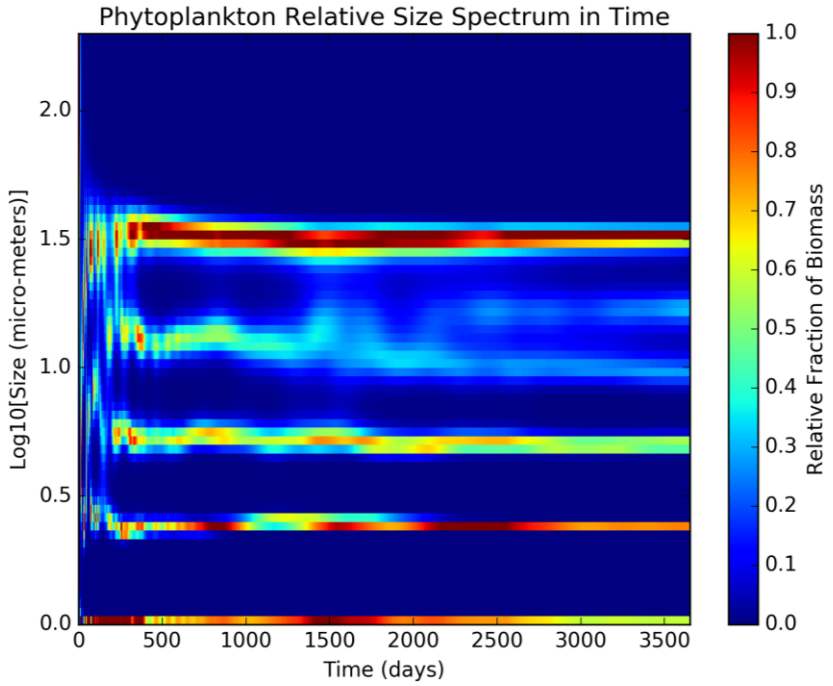


**Figure 24: Phytoplankton size-spectrum in time.**

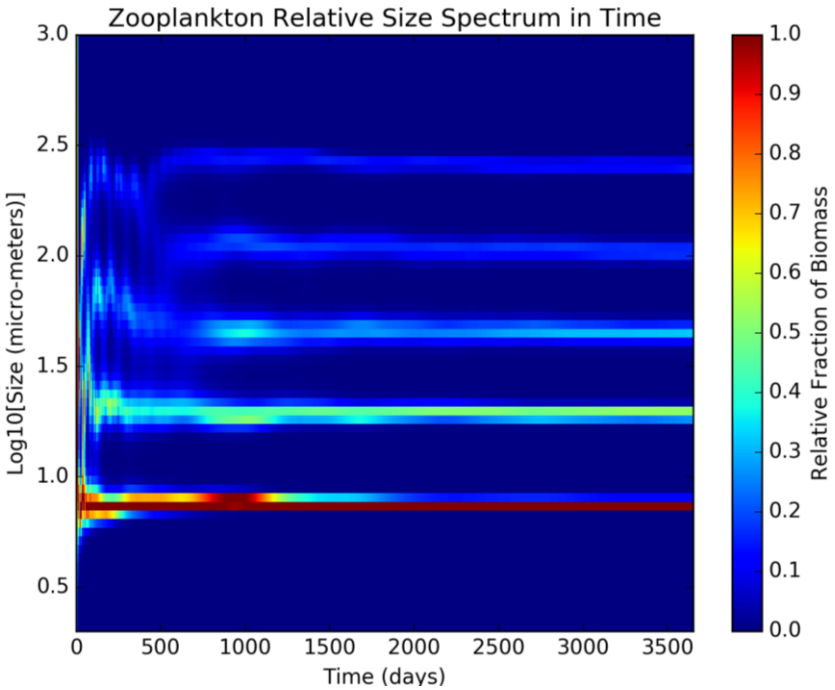


**Figure 25: Zooplankton size-spectrum in time.**

**Table 4: Default value of parameters**

| Parameter | Units | Value |
|---|---|---|
| $m$ | $d^{-1}$ | 0.10 |
| $\varepsilon$ | - | 0.33 |
| $\xi_z$ | $(\mu MN)^{-1}d^{-1}$ | 0.20 |
| $S$ | $\mu MN\ d^{-1}$ | 1.00 |
| $f_{eg}$ | - | 0.33 |
| $K_z$ | µMN | 3.00 |
| $\Delta x$ | $\log_{10}(\mu m)$ | 0.25 |

### *3.3.2 Importance of Zooplankton mortality closure*

In section 2 we outlined the importance of zooplankton mortality closure for our results (size-spectra) and more in general for the stability of the system. Besides the biological justification for our parameterization, in the current section we want to analyze more in depth the effect of this choice and focus on the impact of Z mortality in light of a simple contrast: we compare the results of previous section, where Z mortality contains a series of inter-size coupling, to the results obtained with a simpler intra-size Z coupling. In other words, we compare our default results to results obtained replacing the mortality closure in equation (2) with a simpler quadratic closure ($Z_j^2$).This kind of quadratic closure has been widely used in the past in a lot of NPZ and NPZD models (see literature review in chapter 1). The consequences of the substitution are not straightforward, nor easy to predict at first glance. In the following we try to analyze the differences between the two cases and to point out possible implications of one choice with respect to the other. We also try to explain the reason why our parameterization is so crucial for the system represented in SPLAS.

The simulation we discuss here has the same conditions as the one in the previous section, with the only difference that equation (2) is now modified to be:

$$\frac{dZ_j}{dt} = \varepsilon \sum_i graz_{ij} - \xi_z {Z_j}^2$$

For simplicity, in the following we refer to the modified mortality as "quadratic" mortality (intending quadratic only in $Z_j$), while our choice for mortality (dependent on $Z_{TOT}$) will simply be referred to as "default" mortality.

Figures 26 and 27 show plankton size-spectra obtained with the quadratic mortality, for phytoplankton and zooplankton respectively. We observe that these two size-spectra are very different from the ones in fig. 22-23 obtained with default Z mortality. Phytoplankton spectrum in figure 26 presents a much lower size-diversity with respect to the one in figure 22 and a much larger biomass (see figure 28 for direct comparison): a few very large size-classes accumulate the bulk of phytoplankton biomass. This may be due to a much higher predation pressure on smaller size-classes, which enables such large sizes to grow.

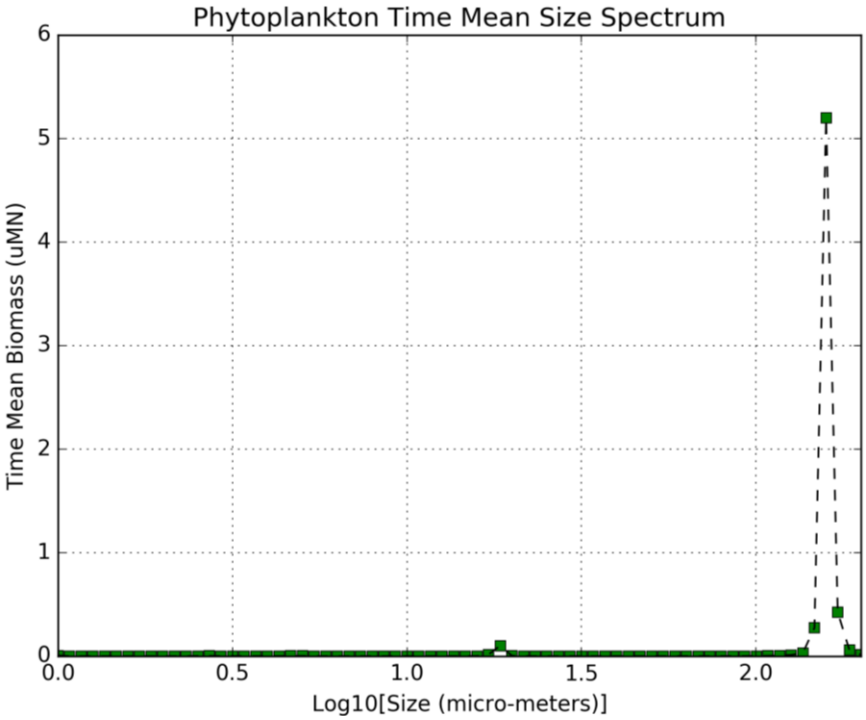


**Figure 26:Phytoplankton time mean size-spectrum for 10 years of simulation, with simpler quadratic Z mortality. Default Z mortality allows a much higher size-diversity.**

In fact, zooplankton spectrum (figure 27) shows a much more continuous distribution and a surprisingly high presence of large size-classes at the right end of the size interval, which is not the case in figure 23 (again, see figure 28 for direct comparison of size-spectra). Both the continuity and the presence of large sizes in Z spectrum may result in a more intense grazing pressure experienced by phytoplankton (figure 29).

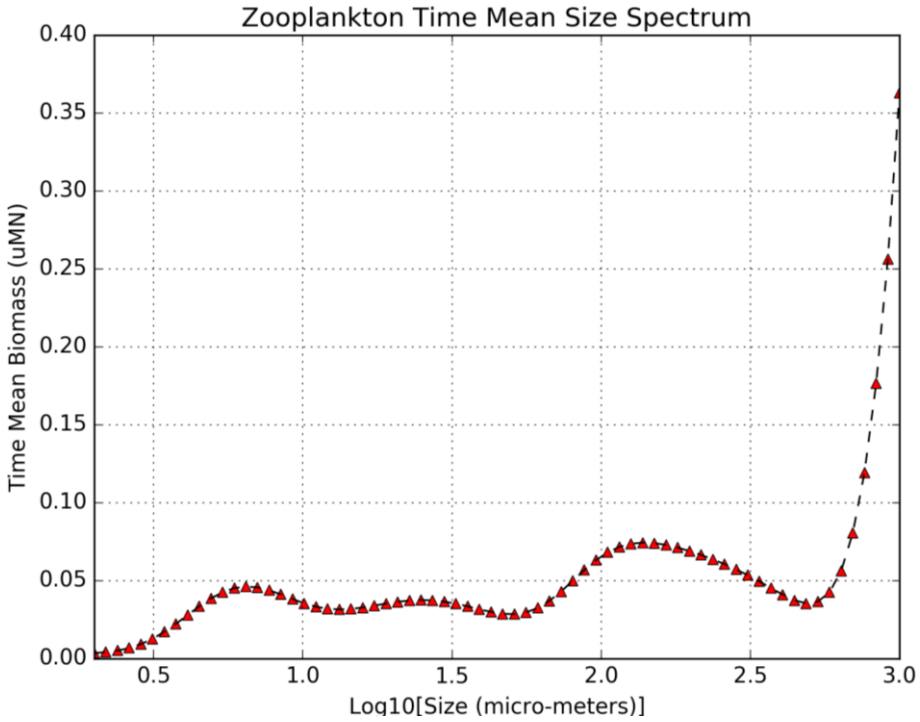


**Figure 27: Zooplankton time mean size-spectrum for 10 years of simulation, with quadratic Z mortality. The spectrum appears much more continuous with respect to the one obtained with default Z mortality.**

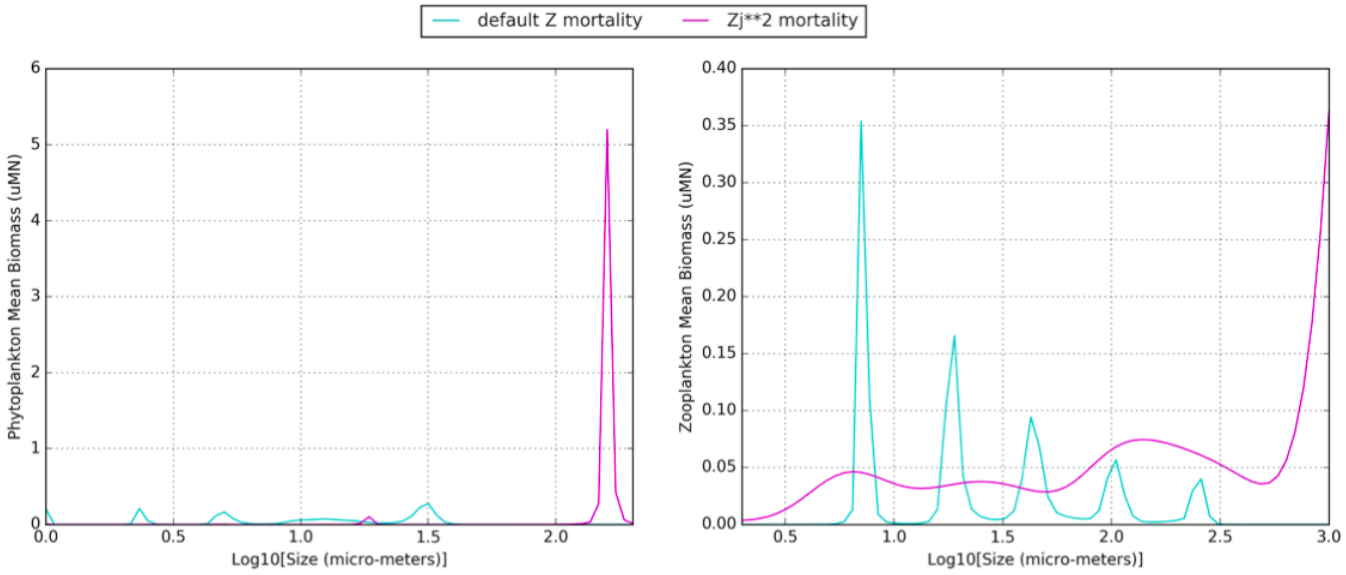


**Figure 28: Direct comparison of plankton size-spectra in the two cases for Z mortality. Left: phytoplankton size-spectra. Right: zooplankton size-spectra. Default Z mortality: cyan line, quadratic Z mortality: purple line.**

As a further confirmation, the limitations metrics in this case (figure 29) have a very different behavior with respect to the ones in figure 21; the N limitation is lower (maximum value = 0.8 against 1 in fig. 21), even if it has the same behavior in the two cases (increasing with P size). Instead, grazing limitation has a completely different behavior in the two cases: in fig. 21 is basically decreasing with size after a small peak at small sizes, in fig. 29 is non-monotonic; moreover, grazing limitation in fig. 29 is in general higher for every phytoplankton size-class and also has a very intense (>1) peak in the interval 35 µm – 100µm which is not present in fig. 21 at all. It is evident that the large sizes (right end) in Z spectrum (figure 27 or 29, right) have an intense predation on this P size-interval. Instead, in both cases sizes larger than 100 µm experience a low grazing pressure.

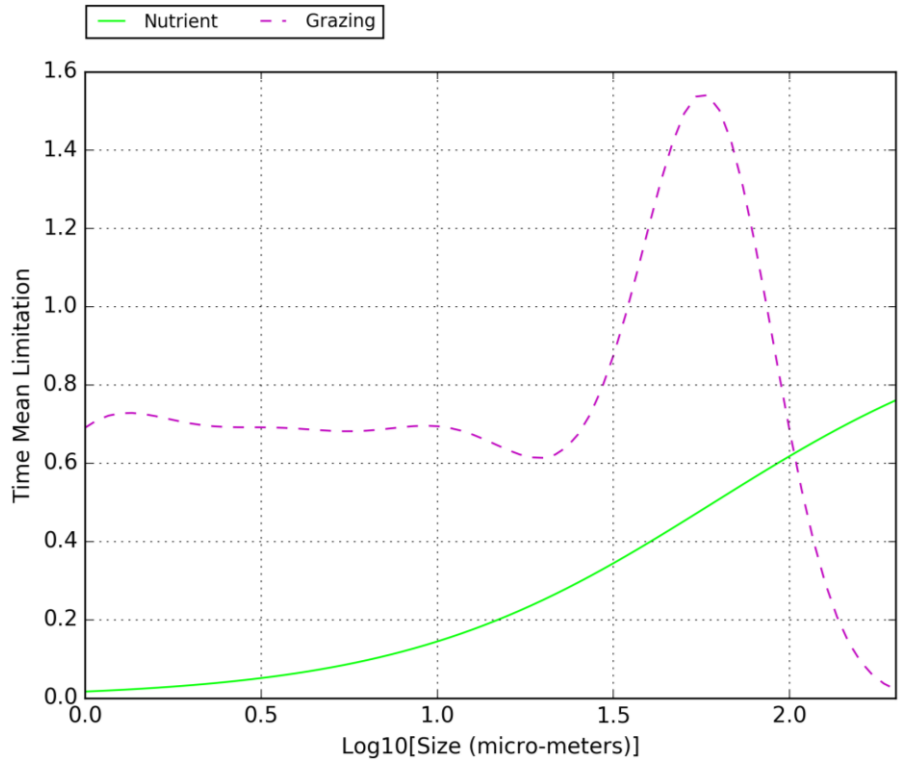


**Figure 29: Nutrient limitation (solid green line) and grazing limitation (dashed violet line) in function of phytoplankton size (time-averaged for 10 years of simulation), with quadratic Z mortality. The behavior is different with respect to the default Z mortality case: N limitation increases with size but is slightly lower, while grazing limitation is non-monotonic. The smallest size-classes are still the least N limited but now suffer an almost constant (independent of size) grazing pressure. Then size-classes larger than 30-35 microns suffer a huge grazing pressure (peak in the figure), which becomes very low at sizes larger than 100 microns.**

In figure 30 and 31 phytoplankton and zooplankton full size-spectrum in time is shown, to highlight differences with respect to figure 24 and 25.

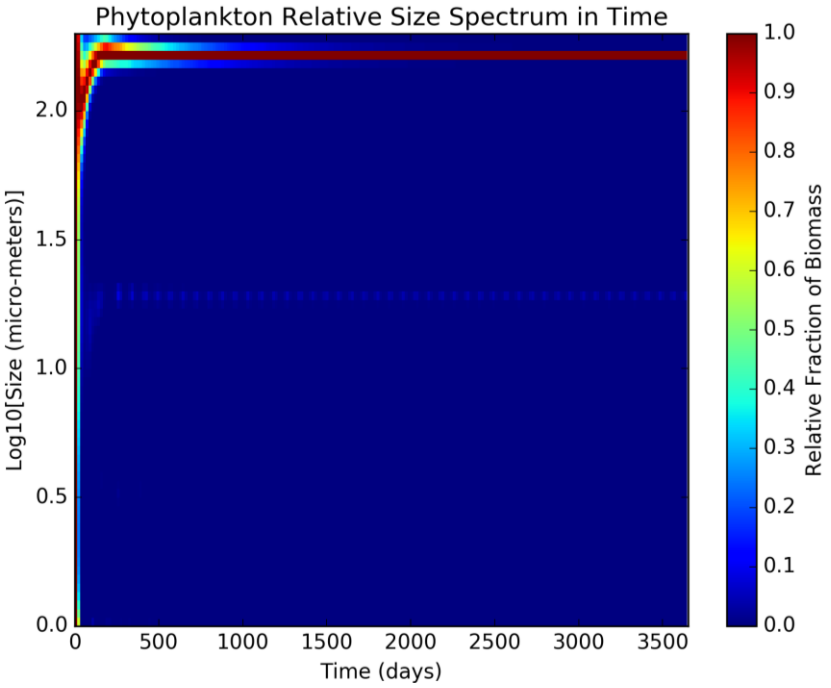


**Figure 30: Phytoplankton size-spectrum in time, with quadratic Z mortality**

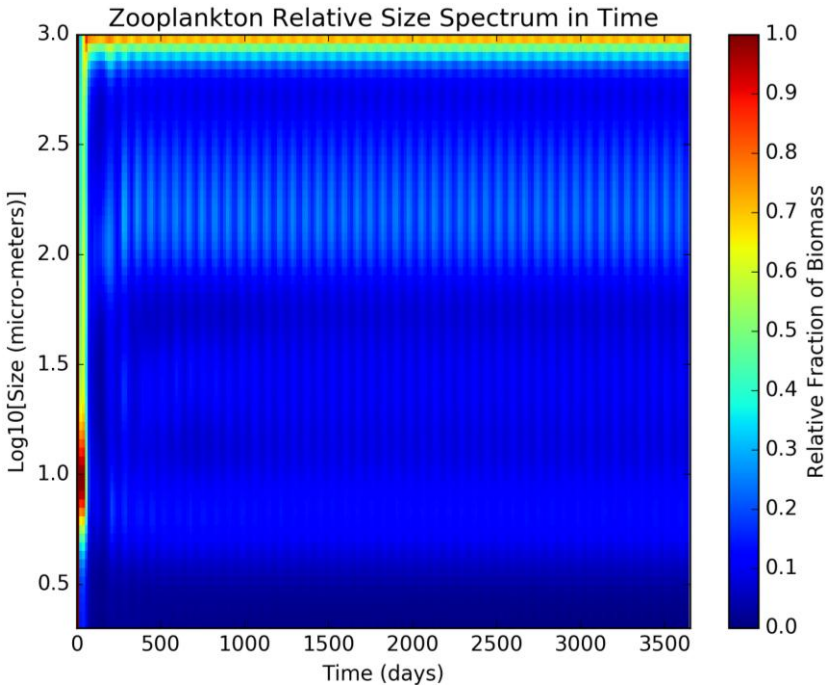


**Figure31: Zooplankton size-spectrum in time, with quadratic Z mortality.**

These results point out the importance of our choice of Z mortality, at least with respect to a simpler and widely used in the past quadratic mortality. In fact, changing our default mortality to a simpler one likely compromises the pattern found in the following (and also in the preceding) sections. Phytoplankton apparently has a much lower size-diversity (and a higher biomass) while zooplankton has a much larger size-diversity (and a higher biomass), with the spectrum appearing continuous and with a peak at the right end. In other words, default mortality (dependent on total Z biomass) helps shaping the "discrete" Z size spectra and also keeps large Z sizes under control, lowering Z diversity and total biomass while also allowing a larger size-diversity for phytoplankton. In this sense of keeping Z population under control and controlling size-diversities, default mortality can be intended as a stabilizer of the system. It is intuitively clear that changing Z mortality messes up our patterns of Z-P interactions.

In figure 32 we plot size-diversities in time for both P and Z: with quadratic mortality phytoplankton size-diversity is much lower and zooplankton size-diversity is consistently higher, in agreement with what we outlined before.

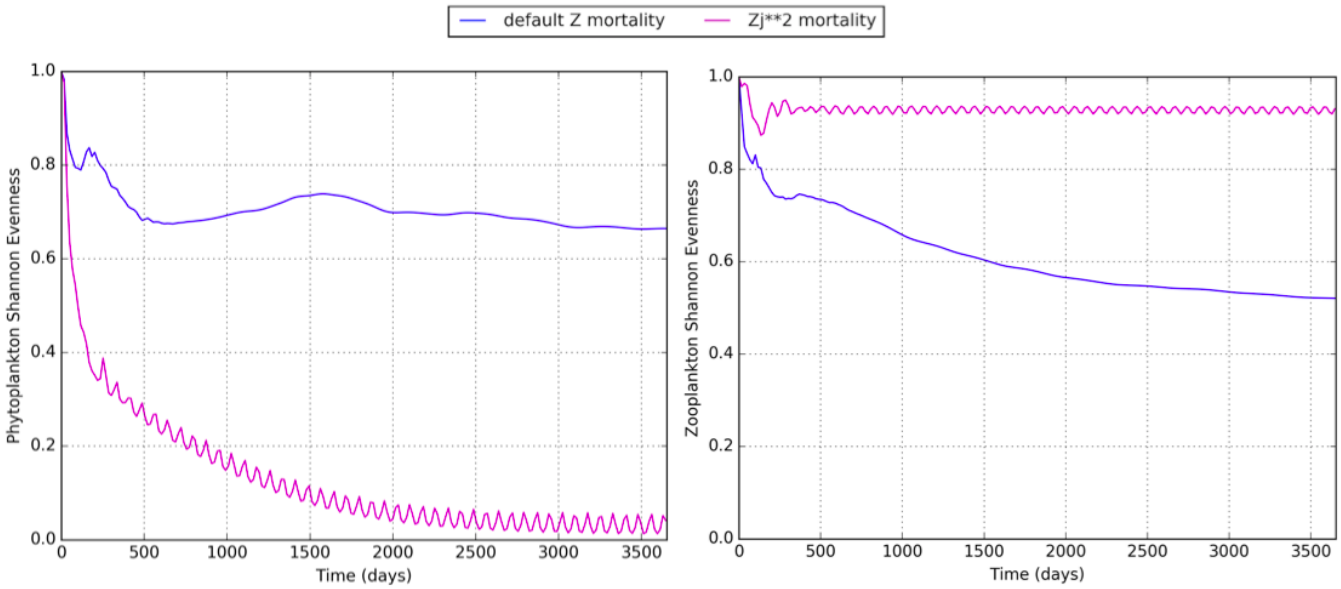


**Figure 32: Plankton size-diversity in time. Left: phytoplankton size-diversity. Right: zooplankton size-diversity. Default Z mortality: blue line, quadratic Z mortality: purple line.**

All our results in the following sections are strictly dependent on the choice of Z mortality: size-spectra are sensitive to the choice of the closure term. If we substitute the default Z mortality with a quadratic one we would not be able to obtain the same patterns of size-diversity vs total biomass and trophic transfer as in sections 3.4.2 and 3.4.4 because the relation between the size-diversity and total biomass is completely different with the two Z mortalities (Table 5). Also our other results on bottom-up and top-down control would be different with a different Z mortality (see next chapter).

| **Quantity** | **Default Z mortality** | **Quadratic Z mortality** | **Relative change** |
|---|---|---|---|
| P biomass (μMN) | 2.41 | 6.21 | + 157 % |
| Z biomass (μMN) | 1.37 | 3.65 | + 166 % |
| Z:P ratio | 0.57 | 0.58 | + 1.75 % |
| P Shannon Evenness | 0.71 | 0.13 | - 82 % |
| Z Shannon Evenness | 0.61 | 0.93 | + 52 % |

**Table 5: Biomasses and Size-diversities with the two different parameterization of Z mortality. Relative change is intended with respect to default mortality value.**

Notice that even if the changes in P and Z biomass compensate giving a comparable Z:P ratio in the two cases, the two scenarios are completely different as size-diversities are upset and so the relationship between size-diversity and total biomass or Z:P and diversity cannot be maintained the same as with the default Z mortality, compromising our results for diversity and trophic transfer patterns. Moreover, we have seen that the size-structure of both phytoplankton and zooplankton are completely different when we switch from default to quadratic Z mortality, probably destroying most of every other result in section 3.

In conclusion, with a quadratic mortality we would not be able to reproduce our results of the following sections and in this sense the choice of parameterization of Z mortality is crucial for the stability of the system but also for its biomass, diversity patterns, size-structure and size-dependent interactions.

## *3.4 Validation of the 0-D model*

For the validation of SPLAS 0-D we performed some tests observing its behavior with respect to variations in the representation, in particular studying:

1. The behavior of phytoplankton size-spectrum changing N supply (section 3.4.1)
2. The representation of size-diversity with respect to total biomass (section 3.4.2)
3. The behavior of plankton size-structure changing Z mortality (section 3.4.3)
4. How the model represents trophic transfer (section 3.4.4)

### *3.4.1 Behavior under changing bottom-up control (N supply)*

We first examine how the system reacts to changes in bottom-up limitation, that is Nitrogen load (S parameter in equation 1, expressed in mmolN $m^{-3}$ $day^{-1}$). Here we assume that Nitrogen is continuously and steadily resupplied into the system. We stress that in our implicit formulation (the same as Banas, 2011) the main assumption is that the biomass lost from the system (phytoplankton natural mortality and sinking, zooplankton mortality and egestion) is regenerated in a complex way elsewhere, and partly returned to the system through the imposed flux of new Nitrogen from below/outside (S). This formulation is alternative to the classic "closed" formulation in which biomass of the system is conserved and regeneration of Nitrogen is local and instantaneous.

We explore a range of Nitrogen loads between 0.01 and 10 mmolN $m^{-3}$ $day^{-1}$. The length of the simulation is 10 years, starting from the same homogeneous initial conditions and letting the size-spectrum emerge.

In figure 33, phytoplankton mean size-spectrum averaged in time is shown, at varying Nitrogen load. Increasing loads allow larger and larger size-classes to coexist alongside the smallest ones. For the default configuration (red line, S = 1.0 mmolN $m^{-3}$ $day^{-1}$) and smaller values (cyan line S = 0.5 mmolN $m^{-3}$ $day^{-1}$, green line S = 0.1 mmolN $m^{-3}$ $day^{-1}$, blue line S = 0.01 mmolN $m^{-3}$ $day^{-1}$) the peaks are low and condensed around smaller sizes (<40 µm). At higher values of supply the peaks increase in value and move towards larger phytoplankton sizes, >100 µm (yellow line S = 5.0 mmolN $m^{-3}$ $day^{-1}$, purple line S = 7.0 mmolN $m^{-3}$ $day^{-1}$, black line S = 10.0 mmolN $m^{-3}$ $day^{-1}$). Notice that biomass in both smaller and larger classes increases, as predicted by Ward et al. (2013).

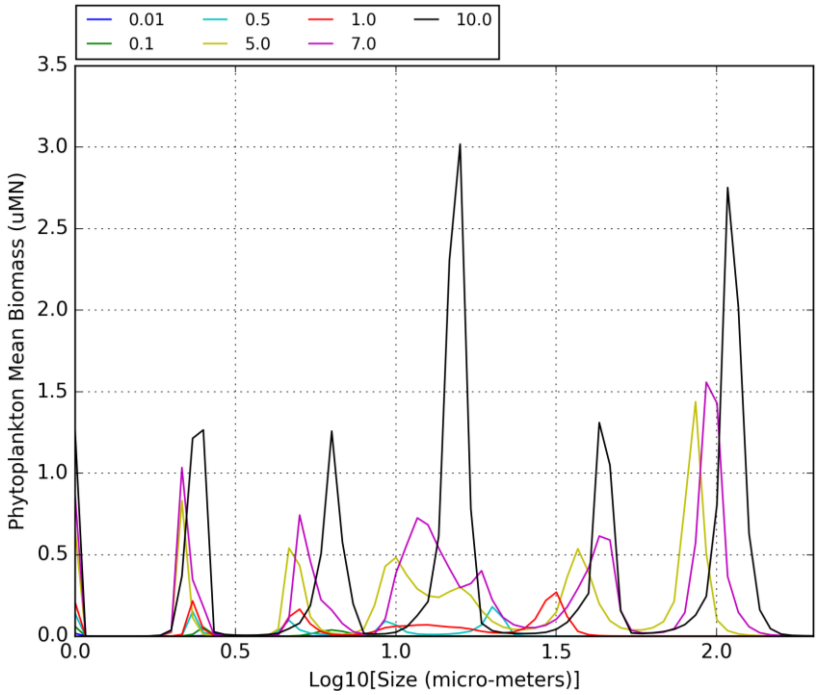


**Figure 33: Phytoplankton time mean size-spectrum at different values of Nitrogen Supply. Default configuration: red line, S = 1.0 mmolN $m^{-3}$ $day^{-1}$. Cyan line, S = 0.5 mmolN $m^{-3}$ $day^{-1}$. Green line, S = 0.1 mmolN $m^{-3}$ $day^{-1}$. Blue line, S = 0.01 mmolN $m^{-3}$ $day^{-1}$.Yellow line,S = 5.0 mmolN $m^{-3}$ $day^{-1}$. Purple line,S = 7.0 mmolN $m^{-3}$ $day^{-1}$. Black line,S = 10.0 mmolN $m^{-3}$ $day^{-1}$.**

At growing N load the mean biomass of the system increases (Figure 34a for both phytoplankton and zooplankton):the larger the load, the higher the biomass in the system (log-log scale in figure 34a).Moreover, for what concerns phytoplankton, as biomass increases the community is dominated by increasingly larger cells (fig 34b): at very low biomasses picophytoplankton make up most of the population, while at intermediate and high biomasses the bulk of the community is composed of nano and micro-phytoplankton respectively.

From phytoplankton size-spectrum (Fig. 33) and composition (Fig. 34b) it is evident that biomass is added in the system through the addition of increasingly larger size-classes. The peaks in the spectrum move towards higher sizes as S is increased, as well as they are increasing in intensity.

The increase in biomass in phytoplankton community triggers an increase in zooplankton biomass (higher food availability). Thus, also zooplankton biomass increases, with smaller organisms more widespread than larger ones (Fig. 35). Zooplankton size-spectrum is influenced by phytoplankton spectrum (prey availability). Anyway the relationship between the two spectra is not straightforward, being complex the dynamics and all size-dependent ecological interactions (basically feeding).

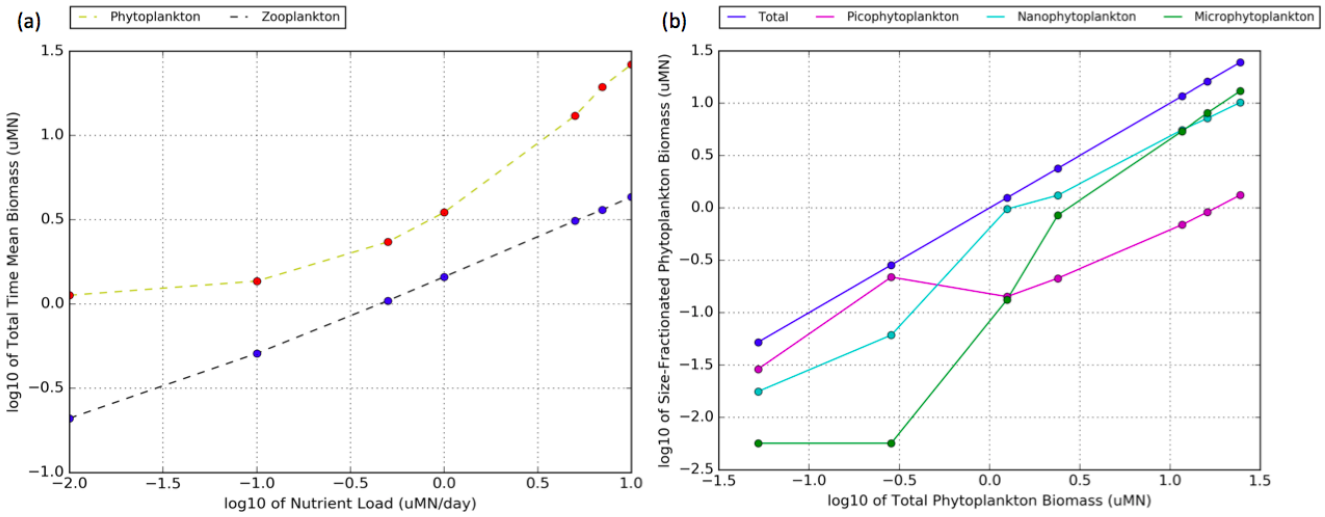


**Figure 34: (a) Biomass of Phytoplankton (red dots, yellow dashed line) and Zooplankton (blue dots, black dashed line) in function of Nutrient Load (values as in fig. 33). (b) Total phytoplankton biomass (blue line) and size-fractionated phytoplankton biomass (pico: purple line, nano: cyan line, micro: green line), in log-log scale.**

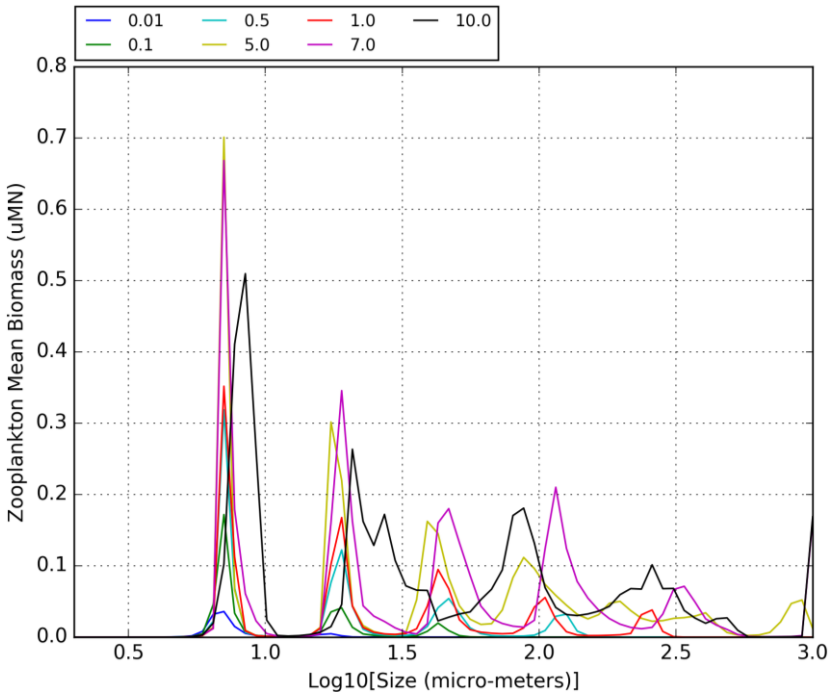


**Figure 35: Zooplankton time mean size-spectrum at different values of Nitrogen Supply (S values as in fig. 33).**

A further confirmation of the agreement between model output and theoretical predictions and field data comes from the observation of the limitation measures defined in section 3.2.1 (Fig. 36).

Biomass shift toward larger size-classes is evident (Fig. 36, left): with increasing total phytoplankton biomass (N load) progressively larger size-classes are established, coexisting with the smaller ones. As S increases overall N limitation decreases while grazing limitation increases (Fig. 36, right), since also zooplankton biomass increases, allowing larger and less predated phytoplankton to survive and grow.

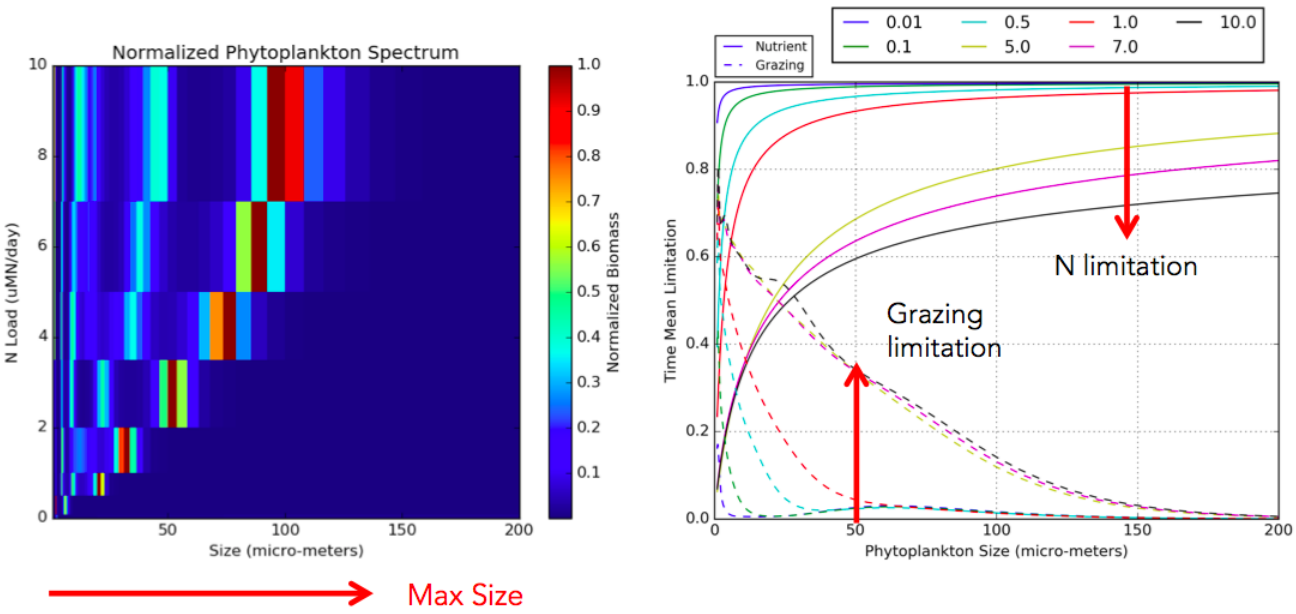


**Figure 36: Phytoplankton time mean size-spectrum vs increasing N load (left) and phytoplankton community limitations (right: solid line N limitation, dashed line grazing limitation for the values of N load –S- as in fig. 33).**

**As Nitrogen load is increased, larger and larger size-classes are established, coexisting alongside smaller ones**: this happens because the size-spectrum of phytoplankton community is shaped through the interaction of grazing limitation and N limitation. At growing N supply the bottom-up limitation is reduced and even if the smallest classes are still the least N limited, the grazing limitation is increased due to an increased zooplankton biomass. This top-down limitation is larger for the smallest size-classes, and so larger classes are allowed to survive and grow (Fig. 33-34-36).

### *3.4.2 Size-diversity dependence on total biomass*

Another benchmark for testing the skills of SPLAS is how it represents plankton diversity. Plankton size-structure and diversity influence the biogeochemical dynamics of marine systems and related biogeochemical fluxes as the C export and the partitioning of $CO_2$ between atmosphere and ocean (Falkowski & Oliver, 2007; Ward et al., 2013).Literature studies (Irigoien et al., 2004; Goebel et al., 2012) suggest that biodiversity has a parabolic dependence on biomass for both phytoplankton and zooplankton community. The diversity is low at both high and very low biomasses, with an optimum in between.

In SPLAS we consider only size-diversity. This is a strong but still reasonable approximation, since taxonomic variation in nutrient utilization traits, and thus in biogeochemical function, is largely driven by size variation (Edwards et al., 2012).We expect size-diversity to be a strong component of biodiversity.

We investigate how SPLAS represents size-diversity, which is an important point for representing part of the biogeochemical function of marine systems. This is a crucial proof of strength of the model, because representing correctly the size-structure (the distribution of biomass among the size-classes) in the different environmental conditions is an important step towards a realistic representation of the biogeochemical function of the system.

As a measure of diversity we use the Shannon Evenness (introduced in section 3.2.2) and we compare our results for size-diversity against total biomass to the results of Banas (2011). Banas obtained a parabolic behavior for phytoplankton size-diversity against total phytoplankton biomass but did not obtain the same result for zooplankton, getting a monotonically increasing function similar to a straight line.

With SPLAS we were able to obtain the parabolic dependence also for zooplankton size-diversity (Fig. 37), in agreement with the experimental study of Irigoien et al. (2004) that found the parabolic dependence for both phytoplankton and zooplankton community. This may be due to the enlarged size-range with respect to Banas' model (2-1000 µm for zooplankton instead of 2.1-460 µm).

Size-diversities and biomasses reported in the graphs of Fig. 37 (left) are calculated from the simulations of previous section (3.4.1, at increasing S): to an increasing N load correspond increasing biomasses of both phytoplankton and zooplankton. Results of Banas (2011) are also shown for comparison (fig. 37, right).

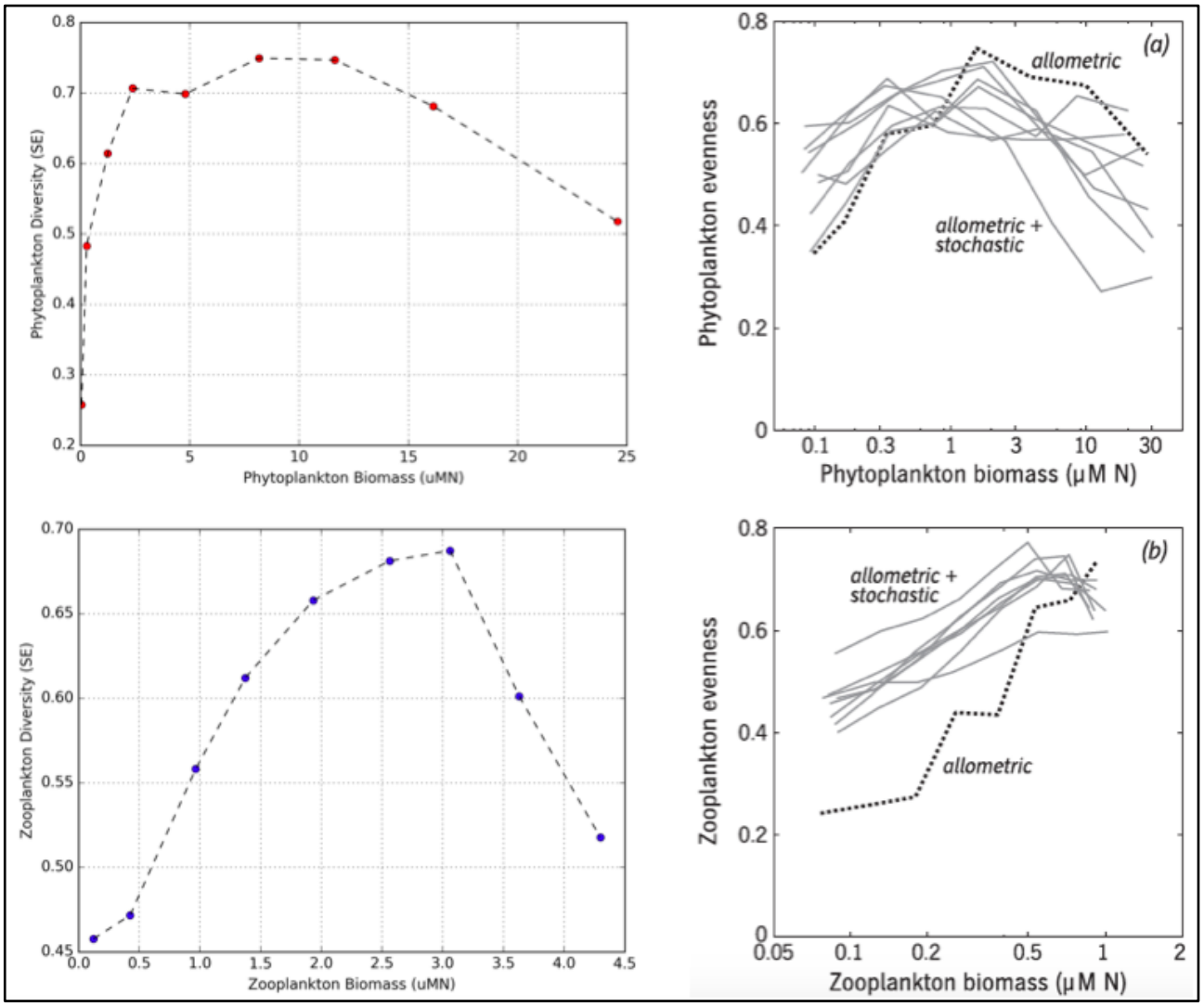


**Figure 37: Left: Phytoplankton Shannon Evenness vs total phytoplankton biomass (top) and Zooplankton Shannon Evenness vs total zooplankton biomass (bottom) for simulations at increasing N supply (S parameter, with values: 0.001, 0.01, 0.1, 1.0, 2.0, 3.5, 5.0, 7.0, 10.0 uMN day-1). Right: Results of Banas (2011) with different runs of his model. Top: phytoplankton evenness vs biomass. Bottom: zooplankton evenness vs biomass.**

Going further, repeating many simulations varying also other parameters (Zooplankton mortality ξ, Zooplankton selectivity Δx, Phytoplankton mortality m, Phytoplankton sinking σ –the coefficient, not the allometric dependence- and more than one parameter at a time) the parabolic behavior is conserved (Fig. 38). Therefore, mimicking different environmental conditions (i.e. varying the parameter values) and collecting the simulation output of size-diversity and biomass, we obtain a parabolic curve: **this proves that the model correctly represents size-diversity because the biomass is well distributed among the different size-classes in the many possible "virtual" environmental conditions**. This result holds for both phytoplankton and zooplankton (Fig. 38).

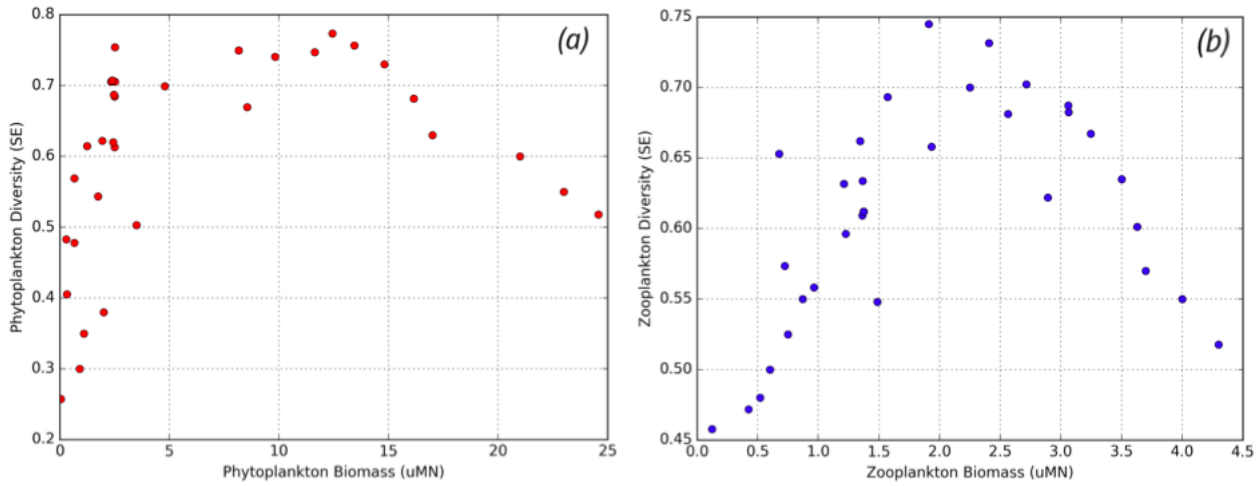


**Figure 38: a) Phytoplankton Shannon Evenness vs total phytoplankton biomass and b) Zooplankton Shannon Evenness vs total zooplankton biomass for simulations varying different parameter values.**

### *3.4.3 Behavior under changing top-down control (Z mortality)*

We explore a range of mortalities (ξ parameter) from 0.05 to 0.25 ($\mu MN^{-1}$ $day^{-1}$) for 10 years of simulation (Fig. 39-40 mean phytoplankton and zooplankton size-spectra respectively).We stress here that the shape of the Z mortality (as in eq. 2) is crucial for obtaining these results.

Increasing the Zooplankton mortality has somewhat an opposite effect with respect to the addition of Nitrogen (increase in N supply) for phytoplankton community. This action of "removal of biomass" from the top of the food-chain is able to shift the regime from a more grazer controlled community (low Z mortality), in which larger, less-predated phytoplankton is favored to a bottom-up limited community (high Z mortality) in which smaller, less N limited phytoplankton outcompete larger species (Fig. 39). In fact, increasing values of ξ shift the size-spectrum towards smaller size-classes. For the default configuration (cyan line, ξ = 0.2 $\mu MN^{-1}$ $day^{-1}$) and the two surrounding values (yellow line ξ = 0.15 $\mu MN^{-1}$ $day^{-1}$ and red line ξ = 0.25 $\mu MN^{-1}$ $day^{-1}$) the peaks in the spectrum are condensed around smaller sizes (<50 μm). At smaller values of mortality the peaks move towards larger phytoplankton sizes, (>50 μm for the green line ξ = 0.1 $\mu MN^{-1}$ $day^{-1}$, >100 μm for the blue line ξ = 0.05 $\mu MN^{-1}$ $day^{-1}$). Thus, at relatively high Z mortality, phytoplankton community is basically N limited, the smallest size-classes being favored. On the contrary, at low Z mortality, smaller phytoplankton are tightly controlled by grazer's population and larger, less predated phytoplankton can grow.

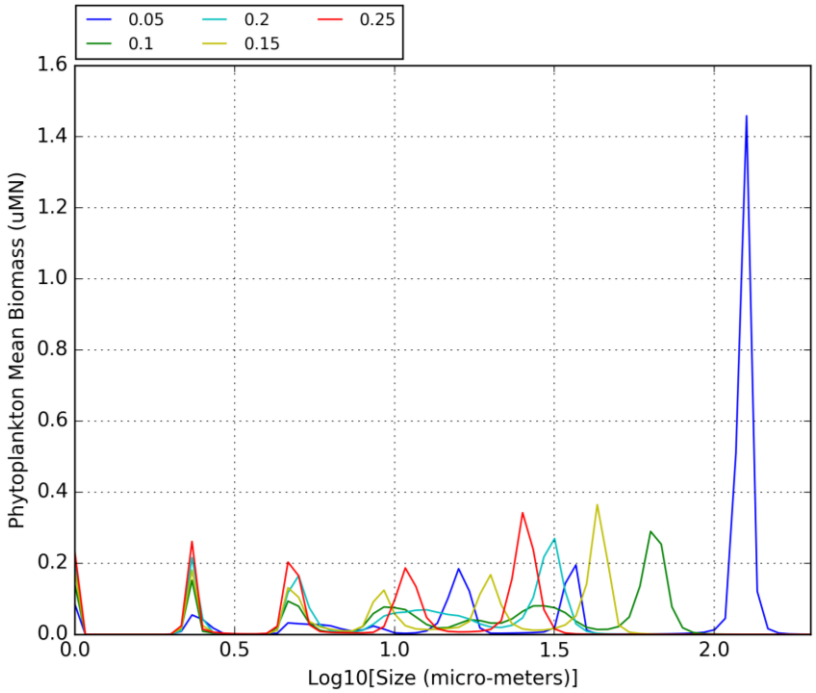


**Figure 39: Phytoplankton time mean size-spectrum at different values of Zooplankton mortality parameter. Default configuration: cyan line, ξ = 0.2µMN$^{-1}$day$^{-1}$.Surrounding values: yellow line,ξ = 0.15 µMN$^{-1}$ day$^{-1}$ and red line,ξ = 0.25µMN$^{-1}$ day$^{-1}$. Smallest values: green line,ξ = 0.1 µMN$^{-1}$ day$^{-1}$ and blue line,ξ = 0.05µMN$^{-1}$ day$^{-1}$.**

For zooplankton size-spectrum a similar thing happens (Fig. 40): the biomass at low mortalities is distributed in the whole size-range, with larger organisms present (blue and green lines in Fig. 40). At high mortalities there is a shift towards smaller organisms, and the biomass is more concentrated at smaller sizes, especially at the very beginning of the size-range (red and yellow lines in Fig. 40).

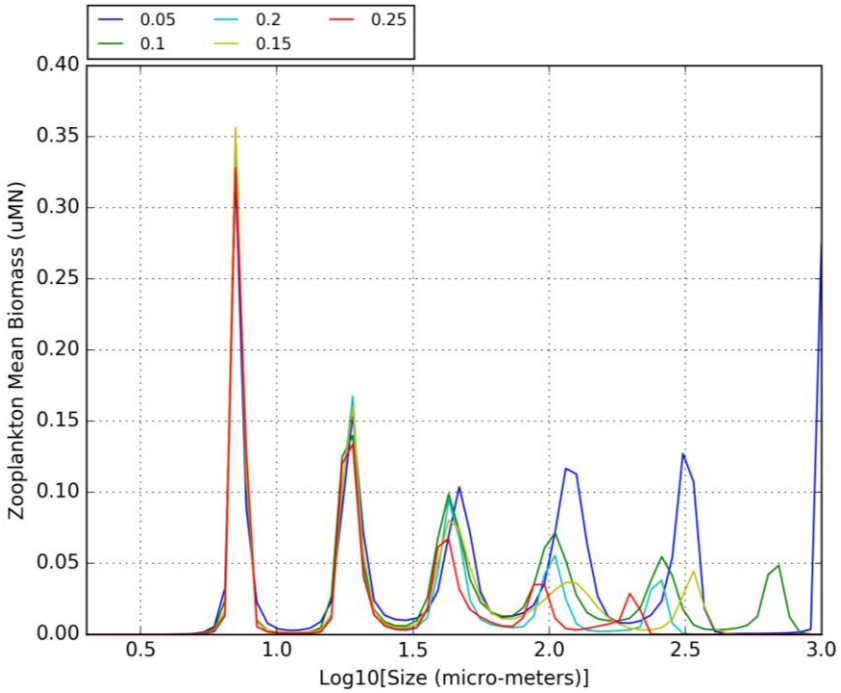


**Figure 40: Zooplankton time mean size-spectrum at different values of mortality (values as in fig. 39).**

Thus, the whole community at low Z mortalities is composed of tightly coupled predator-prey couples, leaving a niche for less predated (larger) phytoplankton size-classes. High Z mortalities instead lead the community to a bottom-up control, in which larger phytoplankton is outcompeted by smaller, less N limited cells, which are consumed by smaller predators.

This pattern is confirmed by the values of the Nutrient and grazing limitations defined in section 3.2.1 for phytoplankton. At increasingly higher Z mortality, grazing limitation decreases while, accordingly, N limitation increases (Fig. 41, right). **Thus, increasing Z mortality shifts the system from a grazing limited to a nutrient limited phytoplankton community: at low Z mortality, phytoplankton is under grazer's control and larger P are favored, while at high Z mortality smallest P are favored (bottom-up control).**

The biomass shift in phytoplankton size-spectrum from larger to smaller size-classes is evident (Fig. 41, left).

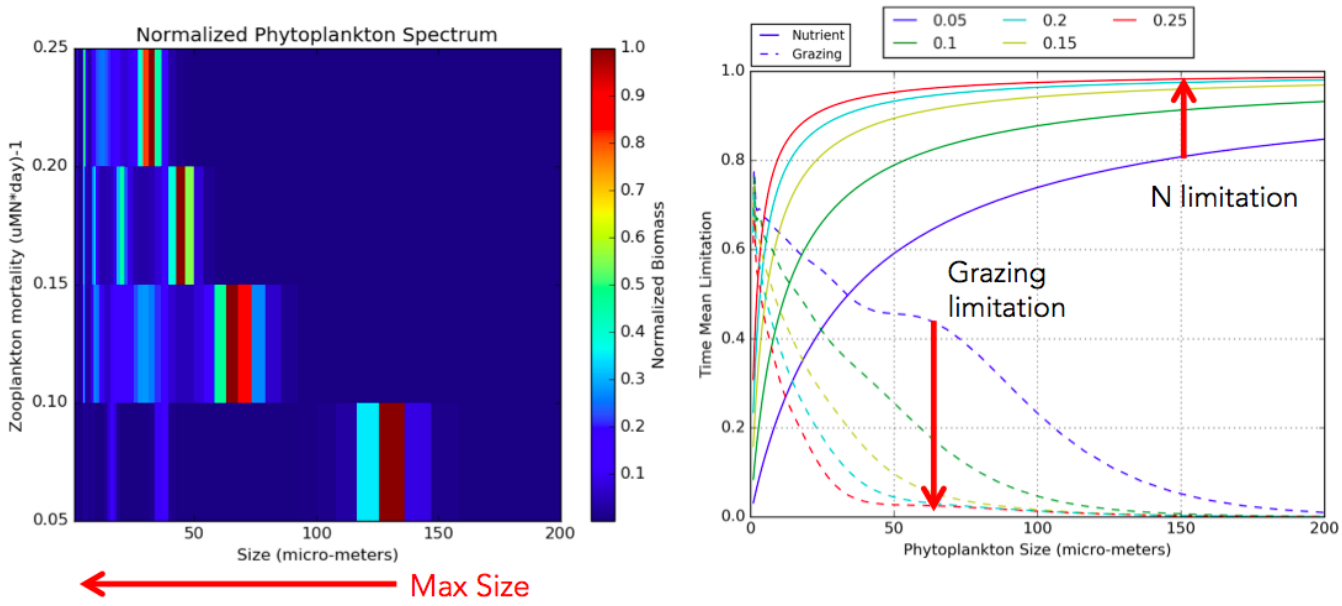


**Figure 41:Phytoplankton time mean size-spectrum vs increasing Z mortality (left) and phytoplankton community limitations (right: solid line N limitation, dashed line grazing limitation for the values of Z mortality –ξ- as in fig. 39).**

The regime shift from grazer's control to bottom-up control (with increasing Z mortality) is further confirmed by the Zooplankton to Phytoplankton average biomass ratio (Fig. 42), that may be considered as an index of the coupling between the two populations (see section 3.4.4).At increasing Z mortality the Z:P ratio decreases, indicating a lower predator's control on the preys.

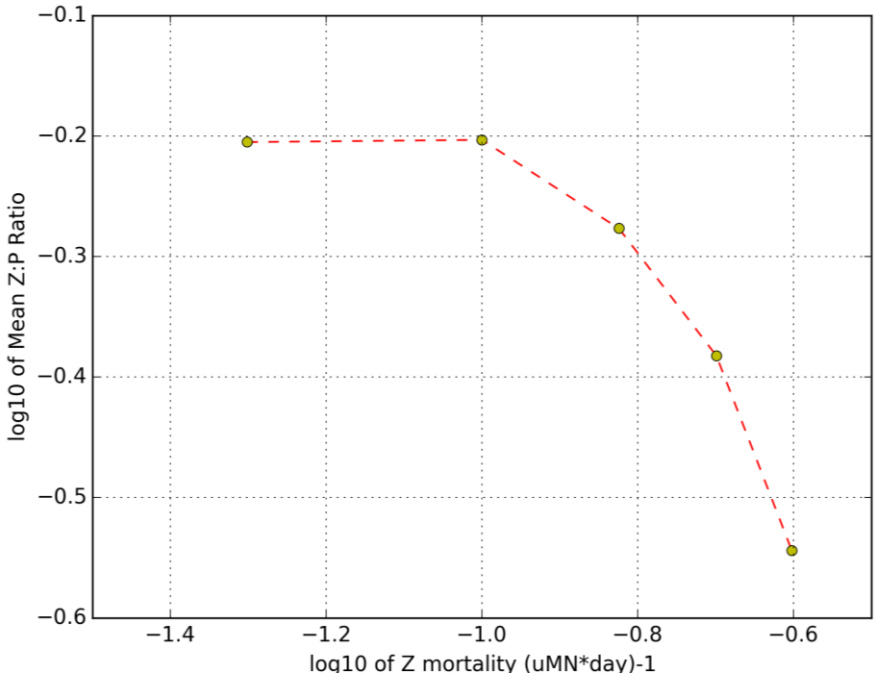


**Figure 42: Time mean Zooplankton to Phytoplankton Biomass Ratio at varying Z mortality (values as in fig. 39).**

### *3.4.4 Trophic Transfer Efficiency (TTE)*

One of the cornerstones of the SPLAS model is the size-based predation that determines zooplankton-phytoplankton interactions. We already saw that zooplankton to phytoplankton biomass ratio can be used to indicate somehow predator's control on the prey (previous section, fig. 42). A recent study from Garcia-Comas et al. (2016) highlighted how predator (zooplankton) and prey (phytoplankton) size-diversity have contrasting effects on this ratio, in particular on trophic transfer and Trophic Transfer Efficiency (TTE).The authors studied a "real" system organized similarly to SPLAS, as they considered only herbivorous zooplankton and the size-range used in their experiment is comparable to SPLAS size-range. They first proved that zooplankton to phytoplankton biomass ratio is a good proxy for trophic transfer and then concluded, via statistical analysis of their data, that prey size-diversity hinders trophic transfer while predator size-diversity promotes it (Figure 43).The mechanisms that lead to these observations are not well established and further investigations are needed; still, this link between size-diversity and trophic transfer seems to be an important feature of plankton ecology. The authors provide several explanations for their findings, bringing into play diet niche partitioning of zooplankton (that would tend to increase trophic transfer) arising with high predator size-diversity, and defense mechanism from predation (working against trophic transfer) with increasing prey size-diversity.

In light of these findings, studying the Z:P ratio and size-diversities obtained from SPLAS simulations in different conditions becomes a good consistency check for the model, in particular for the parameterization we used for predation.

We collected the zooplankton to phytoplankton time-averaged biomass ratio of each simulation, and plotted it against phytoplankton mean size-diversity and zooplankton mean size-diversity during the same simulation. The set of simulations used in figure 44 was made up of the previously examined simulations (varying N supply, Z mortality) plus other simulations obtained from varying other parameters (Z selectivity, P sinking, P mortality) examined in the following sections. This experiment was designed to mimic different environmental conditions, possibly leading to different size-diversities and Z-P coupling. We then calculated Pearson's correlation between biomass ratios and diversities and compared our model results with the experimental results of Garcia-Comas et al. (2016).

Observing Figure 44 we conclude that **SPLAS output behaves similarly to the reference data** (in fig. 43). In particular, we also obtained as well a negative correlation for phytoplankton size-diversity against Z:P ratio, and a positive correlation for zooplankton size-diversity and Z:P ratio. Actually Garcia-Comas et al. (2016) found a stronger effect from prey size-diversity (r = -0.43 against our -0.30) while we obtained a much stronger predator impact (r = 0.53 against their 0.32). The significance level we used is 99%, and we used

Shannon Evenness rather than Shannon index to quantify diversity (see section 3.2.2), but our results do not change using one or the other.

The relationship itself (regression line) is not important as it depends on many environmental variables and may vary geographically. The key point is the connection between size-structure and trophic transfer, in particular the negative trend with prey size-diversity and the positive trend with predator size-diversity. There is no clear causal connection, but the two variables are strikingly linked, as stated by Garcia-Comas et al. (2016).

**The main conclusion from this result is that SPLAS catches the complexity of the ecological interactions between zooplankton and phytoplankton**, even if the mechanisms responsible for this outcome (still unclear anyway) are not explicitly included in the model. This means that, at least, our parameterization of predator-prey interactions is sufficiently realistic to capture a representative Z:P ratio (trophic transfer) with respect to the size-diversity of both predator and prey. The result in figure 44, together with the result of section 3.4.2 (figures 37-38), shows that despite its simplicity SPLAS is able to represent the complexities of real plankton food web, especially size-structure in varying environmental conditions.

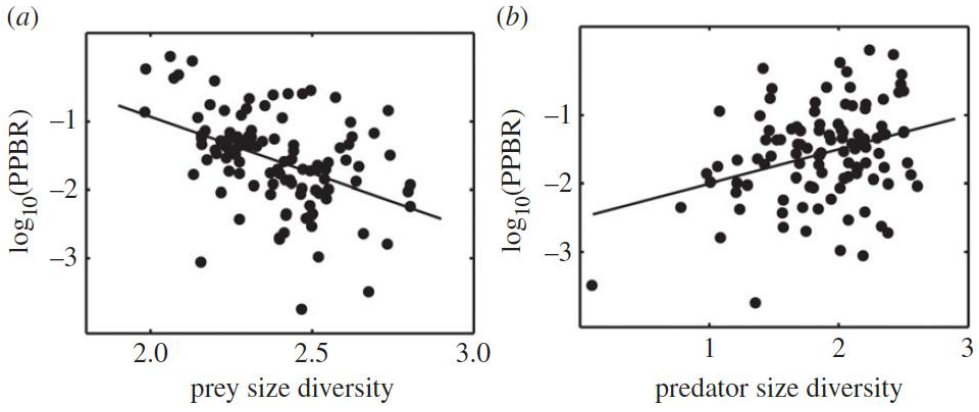


**Figure 43: Effects of (a) prey size-diversity (phytoplankton Shannon index) on biomass transfer efficiency (r=-0.43) and (b) predator size-diversity (zooplankton Shannon index) on biomass transfer efficiency (r=0.32). Image from Garcia-Comas et al. (2016), for details see the publication.**

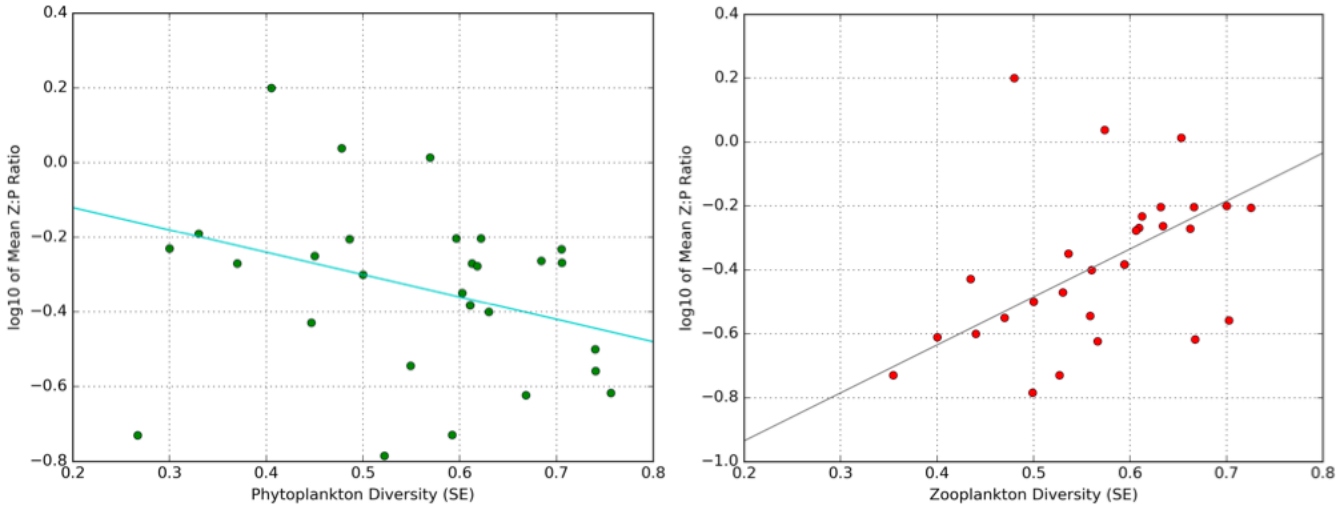


**Figure 44: Zooplankton to Phytoplankton mean biomass ratio against phytoplankton size-diversity (left, r=-0.30) and zooplankton size-diversity (right, r=0.53). Diversity is quantified as Shannon evenness. This is the output from model simulations. The significance level is 99%.**

It is interesting to notice that our ensemble of simulations (fig. 44) is scattered similarly to the field data shown in figure 43. Perhaps investigating the reason why simulations have this scatter around the regression line could point out some speculations about reality; with this in mind we studied four simulations chosen from our wide ensemble: in particular we chose two simulations that have similar output for phytoplankton or zooplankton diversities, and two simulations that have similar Z:P ratio, so to explore the reasons underpinning the spread. The simulations extracted from the ensemble are shown in figure 44bis and details about them are reported in table 6.

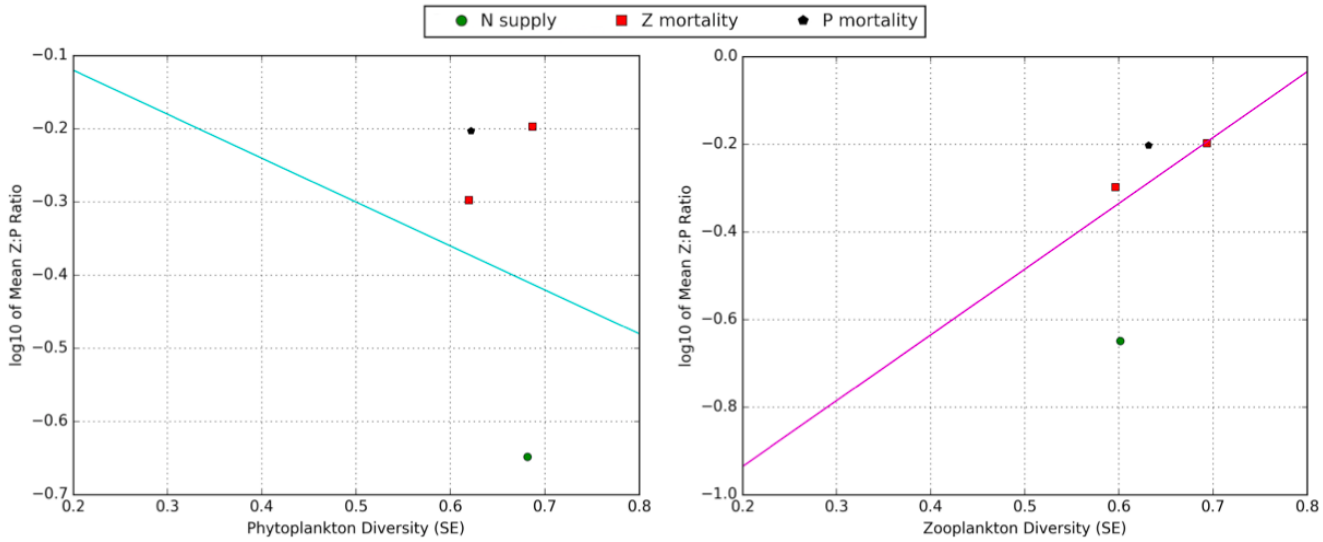


**Figure 44bis: The four simulations chosen from the ensemble of data. One is chosen from the N supply ensemble (green dot) and corresponds to S = 7.0, two are chosen from the Z mortality ensemble (red squares) and have ξ = 0.15 (lying exactly on the regression line on the right, for zooplankton diversity) and ξ = 0.25 while the fourth one is chosen from the P mortality ensemble (black pentagon) and has m = 0.4 and a N supply of 5.**

| **Quantity** (identifier of the simulation) | **N Supply** **(S = 7.0)** (ξ = 0.20) (m = 0.1) | **Z mortality** **(ξ=0.15)** (S = 1.0) (m=0.1) | **Z mortality** **(ξ=0.25)** (S = 1.0) (m=0.1) | **P mortality** **(m=0.4)** (S = 5.0) (ξ=0.20) |
|---|---|---|---|---|
| **P biomass** | 16.15 | 2.47 | 2.43 | 1.93 |
| **Z biomass** | 3.63 | 1.57 | 1.22 | 1.21 |
| **Z:P ratio** | 0.22 | 0.64 | 0.50 | 0.63 |
| **P diversity** | 0.68 | 0.69 | 0.62 | 0.62 |
| **Z diversity** | 0.60 | 0.69 | 0.59 | 0.63 |
| **Zprod:Pprod** | 0.19 | 0.31 | 0.26 | 0.31 |

**Table 6: Details of the four examined simulations. Color codes are explained in the text.**

Interestingly, we notice that:

Case 1. Two of the simulations have similar Z:P ratio but quite different diversity (the one with ξ=0.15 and the one on P mortality, second and last column of table 6, Z:P ratio highlighted in green).

Case 2. The other two simulations (N supply and the one with ξ=0.25, first and third column of table 6) have similar zooplankton diversity (highlighted in cyan) but rather different Z:P ratio.

Case 3. The first two column in table 6 have similar phytoplankton diversity (highlighted in light blue) and rather different Z:P ratio.

Case 4. The last two column have similar phytoplankton diversity (highlighted in grey) and different Z:P ratio.

It would be interesting to know why such simulations have some similar values but yet they are separated points in the Z:P ratio - diversity plan. That might suggest some speculations also on field data (and maybe could help to understand the real world).

Case 1 might be almost self-explanatory, as the relationship between Z and P biomass in each case lead to a Z:P ratio of about 0.63 but the P and Z biomasses are different. The difference in the two points (the "horizontal" scatter between black pentagon and red square in figure 44bis) may be given by the total P and Z biomass which lead to different P and Z diversities in each case (remember section 3.4.2 on diversity vs total biomass), even if in the end they lead to the same net "trophic transfer". A further confirmation can be found by looking at the values of the production rate ratio (Z production over P production), which we quantify as:

$$\frac{Z_{prod}}{P_{prod}} = \frac{\varepsilon \sum_{i,j} graz_{ij}}{\sum_i \mu_i P_i}$$

The values for production ratio that we obtain for the two simulations highlighted in case 1 are similar, equal to about 0.3. Notice that the Z:P production rate ratio is much smaller than the Z:P biomass ratio, but they are similar in the two different simulations. So in this case we have different configurations of P and Z diversities giving rise to the same transfer of biomass from P to Z. That may originate a "horizontal" scatter in figure 44.

Case 2 is more interesting, as the two simulations have similar Z diversities but everything else quite different. In particular the N supply simulation (green dot in fig. 44bis, first column of table 6) has a significant scatter in Z:P ratio with respect to all the other simulations. This is for instance also what happens in case 3, as N supply simulation has similar P diversity to the other simulation with varying Z mortality and again a large scatter in Z:P ratio can be seen. This distance is explained by the large distance in biomass ratio (fig. 44bis),that in turn corresponds to a large distance in production rate ratio: for the supply simulation (first column in table 6, green dot in fig. 44bis) production ratio is equal to 0.19; in particular here we have a very low Z production with respect to phytoplankton production, whereas in the other simulations the production ratio is higher. So the "vertical" scatter might be linked to a much different production ratio and in our very high N load environment (with S=7) P production is relatively large with respect to Z production, more than what happens in all other simulations.

Notice that in the latter simulation production ratio is quite close to biomass ratio, reflecting the much larger P growth with respect to Z growth (look at the biomasses in first column of table 6). Basically here we had similar diversities among simulations but in much different configurations of trophic transfer. That may possibly be the reason for many outliers in figure 44.

The same mechanism of different production could be invoked for explaining the vertical scattering of case 4, where the difference in Z:P ratio (and production ratio) is less pronounced.

In conclusion, the scatter in the simulations in figure 44 may be given by the diversity vs biomass relationship (horizontal scatter, as in case 1) or more importantly by similar diversities but in different conditions of relative Z-P production and thus, trophic transfer (as in case 2, 3, 4): this might be a possible explanation for the many outliers in figure 44 and maybe could lead to speculations about field data in figure 43. Further investigations are needed, of course, but here we can draw one important conclusion: **in each of the four simulations Z:P biomass ratio reflects somehow production ratio**.

## *3.5 Behavior analysis of the 0-D model*

In this section we analyze:

1. The change in size-structure with different predator selectivity (section 3.5.1)
2. The impact of phytoplankton sinking and natural mortality (section 3.5.2)
3. The stability of the results with respect to the model resolution (section 3.5.3)
4. A time varying N supply (section 3.5.4)

### *3.5.1 Importance of predator selectivity*

The results (size-spectra) are sensitive to small changes in the Zooplankton prey-size tolerance (Fig. 45 and 46), that is Δx, defined as the breadth of the log-Gaussian preference function (Fuchs and Franks, 2010; Ward et al., 2013).Δx can be considered as the inverse of predator selectivity: a highly selective predator has a low tolerance, while a generalist grazer has a large tolerance. In fact, increasing the tolerance means that the preference function $\varphi_{ij}$ becomes more spread and less "bell-shaped", while a low tolerance leads to a highly peaked and narrow Gaussian function.

A reasonable value for the width of the size preference in these kinds of model is no larger than 0.5 in log-units (Ward et al., 2013), and we maintained a default value of 0.25 (Table 4) for all other tests (Banas, 2011), in agreement with the data of Hansen et al. (1994). Anyway we tested also a tolerance of 1, to highlight possible limitations of SPLAS and push our model to the limit.

Changing the tolerance of the predators regulates somewhat the distance among the peaks in both prey and predator size-spectra (Fig. 47 and 48), as already stated by Banas (2011): when zooplankton is highly specialized in their prey (Δx small) both biomass spectra are almost continuous and concentrated at low sizes (tight coupling between predator and prey). On the other hand, when zooplankton is generalist (Δx large) the spectra are composed of few (two or three) well-separated peaks (Figures 45, 46, 47, 48).As Δx increases the peaks fade away from each other and the spectrum moves from an almost continuous distribution to two or three isolated peaks.

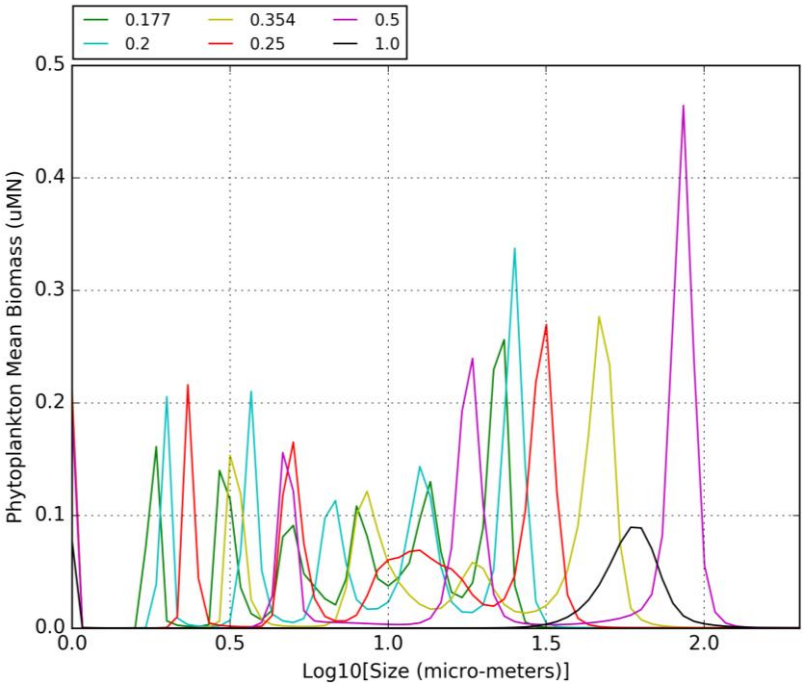


**Figure 45: Phytoplankton time mean size-spectrum at different values of Zooplankton prey size tolerance. Green line Δx = 0.177, cyan line Δx = 0.2, red line Δx = 0.25 (default value), yellow line Δx = 0.354, purple line Δx = 0.5, black line Δx = 1.0. Δx is in log(μm) units.**

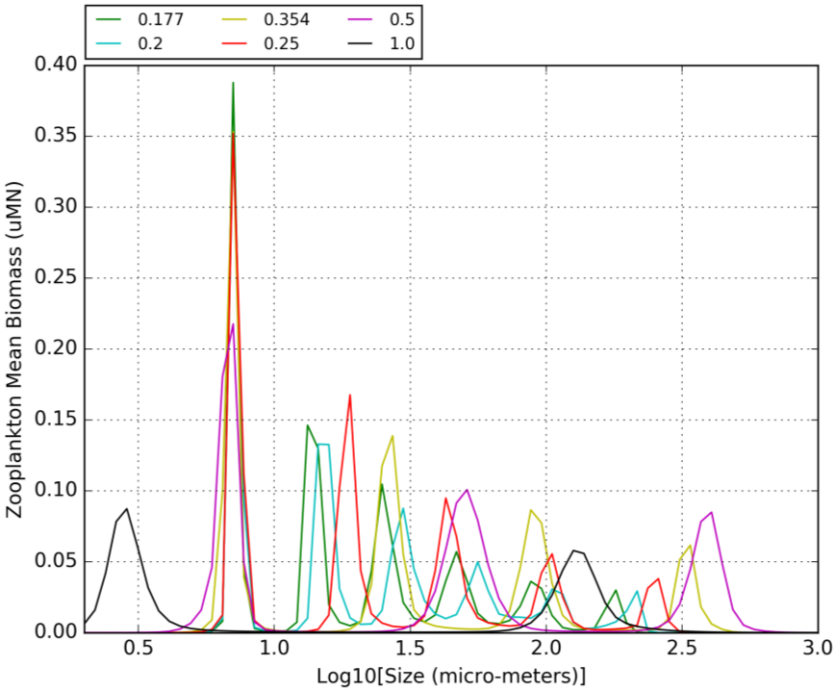


**Figure 46: Zooplankton time mean size-spectrum at different values of Zooplankton prey size tolerance (values as in fig. 45).**

This pattern can be explained by the predation size-law: according to the law of Wirtz (2012) (in Table1), the phytoplankton below about 60-70 µm is the most predated by the whole Zooplankton compartment. Therefore, when zooplankton is very selective, predation is condensed in this size-range, because every predator eats preys that are very close to their optimum size; this leads to a series of tightly connected predator and prey couples in which the predator with the largest preference for the available phytoplankton ($\varphi_{ij}$) is able to feed and survive. The peaks in both predator and prey size-spectra are close in size, being the preference function quite narrow and so the competition among predators reduced (Figures 47 and 48).Notice that the preys are in any case simultaneously limited by nutrient in the environment, so not all preys may be able to grow and be available for grazing.

When instead zooplankton is more generalist, the grazing pressure is more distributed on phytoplankton (because the preference functions $\varphi_{ij}$ are more spread and broadened) and the competition among predators is somehow enhanced by the smaller selectivity, leading to a smaller number of predators surviving and less preys available: these predators are far from each other in terms of size because the width of the preference function is large, and the same happens for preys (Figures 47 and 48).

**In summary: for phytoplankton spectrum, at low tolerances (high predator selectivity) the spectrum is almost continuous and peaks are close in size and concentrated at small size-classes while at high tolerances (low predator selectivity) there are only few well spaced peaks. The zooplankton spectrum follows more or less the same pattern: close peaks concentrated at smaller sizes for low tolerances, well separated peaks for large tolerances.**

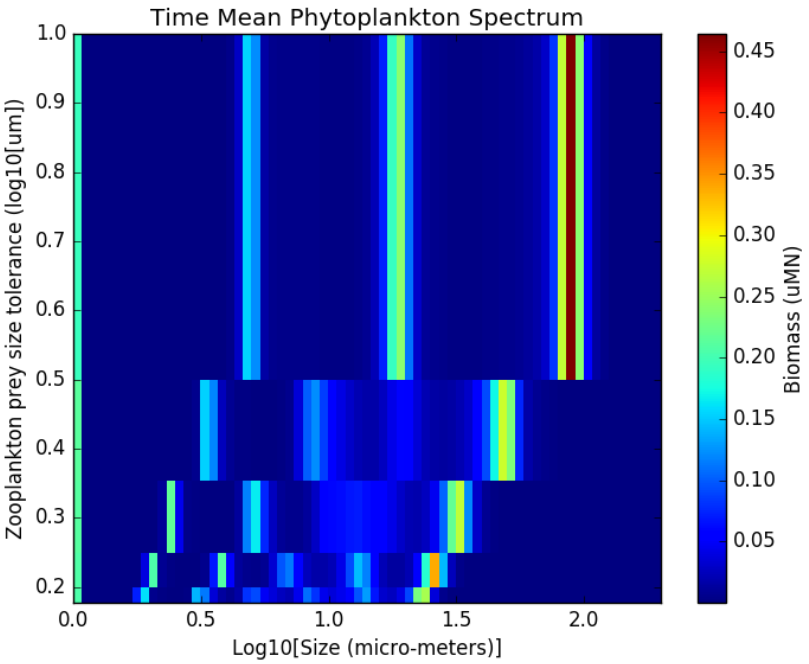


**Figure 47: Phytoplankton time mean size-spectrum vs increasing Z prey size tolerance.**

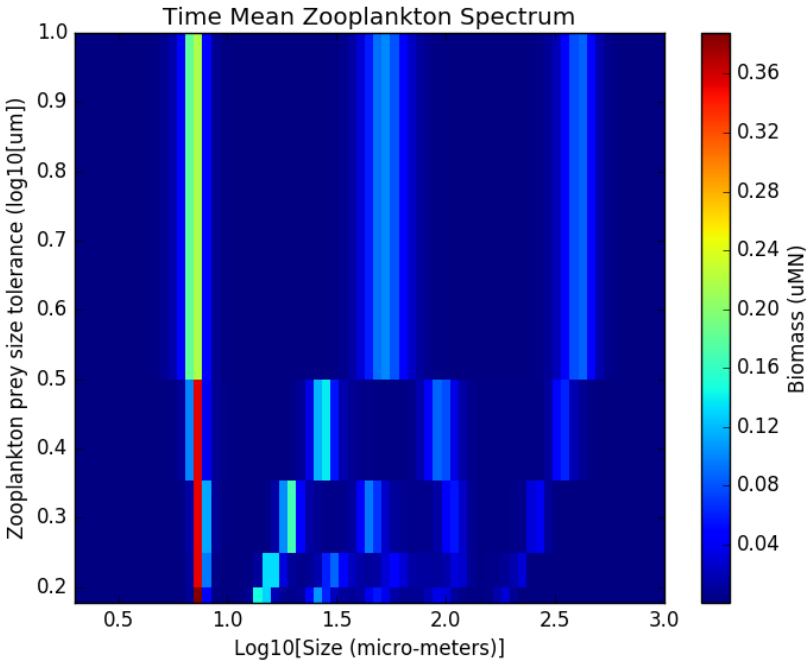


**Figure 48: Zooplankton time mean size-spectrum vs increasing Z prey size tolerance.**

### *3.5.2 Impact of phytoplankton sinking and natural mortality*

We studied here the change in the model output with varying phytoplankton mortality. Total mortality, apart from grazing, is given by the sum of sinking term and natural size-independent death; we varied both terms one at a time, and the results are similar in the two cases (figures 49 and 52):phytoplankton community is pulled towards smaller size-classes with increasing mortalities, and the explanation relies on the equilibrium view discussed in section 2.5. Increasing sinking or natural mortality introduces a discontinuity in the equilibrium concentration of Nitrogen (N*) setting a maximum possible P size in the environment. All size-classes larger than the size of discontinuity cannot have a positive net growth rate.

Sinking is parameterized as a function of size, according to Smayda (1970):

$$\sigma_i = s \cdot x^{1.17}$$

The default value of s is set to 0.0001 $\mu m^{-1.17}$ $day^{-1}$, and we explored what happens for values much larger (0.001 and 0.01 $\mu m^{-1.17}$ $day^{-1}$) and for s = 0, without changing the allometric dependence. The results are shown in figures 49 and 50. The introduction of a sinking term shifts phytoplankton size-spectrum towards smaller cells (as in section 2.5).We can see in Figure 49 that for large values of sinking parameter s (0.001 and 0.01 $\mu m^{-1.17}$ $day^{-1}$, green and blue line respectively) the community is mainly composed of small cells (<70 µm), while without sinking (cyan line) the community is composed of larger sizes with respect to default value (red line).This shift in P community is transmitted to zooplankton community (Figure 50).

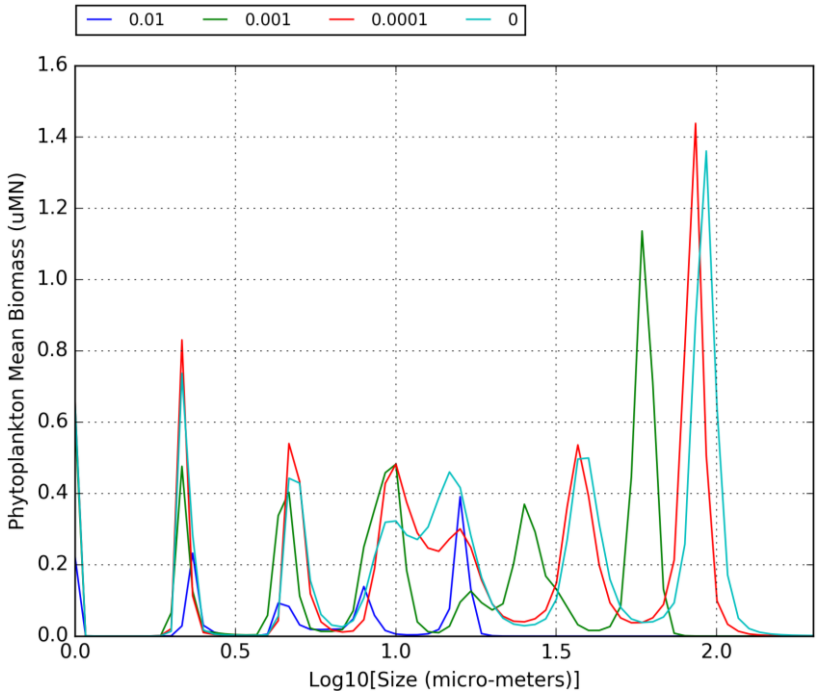


**Figure 49: Phytoplankton time mean size-spectrum for different values of phytoplankton sinking. Large values of sinking parameter s: 0.001 and 0.01 $\mu m^{-1.17}$ $day^{-1}$, green and blue line respectively. No sinking s = 0(cyan line) and default value s = 0.0001 $\mu m^{-1.17}$ $day^{-1}$(red line).**

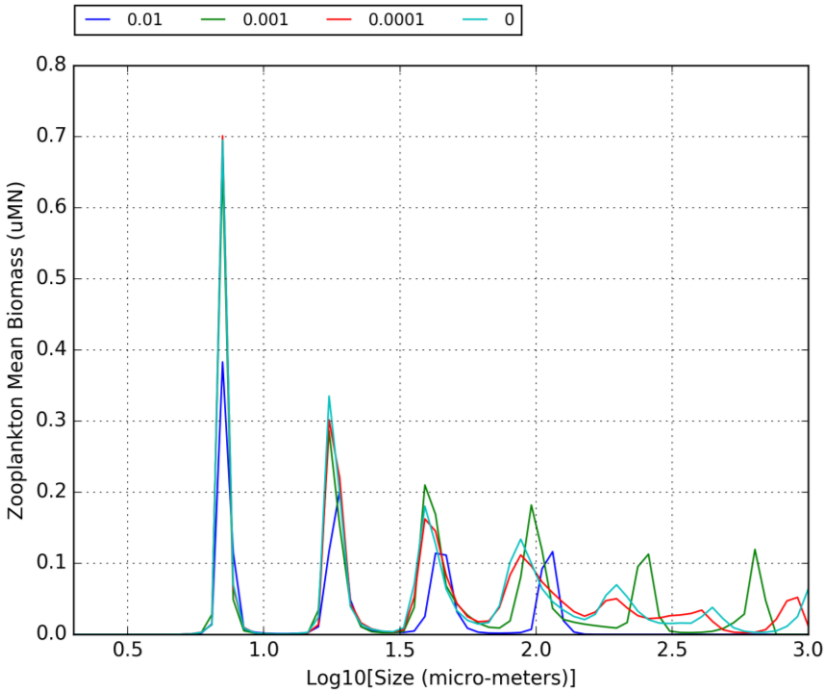


**Figure 50: Zooplankton time mean size-spectrum for different values of phytoplankton sinking. For large values the community is composed of smaller organisms (green and blue lines), which reflects phytoplankton community (prey availability) in fig. 49.**

We could approximately predict the maximum winning size-class in the various cases (for the different values of s) using the theory we developed in section 2.5. In fact, incrementing s changes the N* curve and may possibly introduce discontinuities, preventing from surviving the size-classes larger than a threshold size (figure 51, where the black stars represent maximum winning size-classes). This is the case for s=0.001 $day^{-1}$ and s=0.01 $day^{-1}$(green and blue curve in fig. 51 respectively).In these two cases, sizes at the right of the discontinuity cannot survive, and the maximum winner size is the closest possible to the discontinuity, keeping into account also the grazing pressure (which has the net effect of increasing the N* and shifting the size-spectrum to the left towards smaller sizes).In the other two cases (default case s=0.0001 $day^{-1}$ and s=0.0 $day^{-1}$)no discontinuity is present (at least in the interval 1-200 µm) and the winner is mostly determined by the quantity of Nitrogen in the environment (bottom-up control) as the grazing pressure for large sizes is close to zero: the maximum size is found close to the intersection between N concentration and N*, slightly shifted to the left by grazing pressure (close to zero but not negligible).

The maximum winning sizes in the various cases are (s value in parenthesis): 108.20 µm (s=0.0 $day^{-1}$), 100.21 µm (default s=0.0001 $day^{-1}$), 63.21 µm (s=0.001 $day^{-1}$), 17.13 µm (s=0.01 $day^{-1}$).

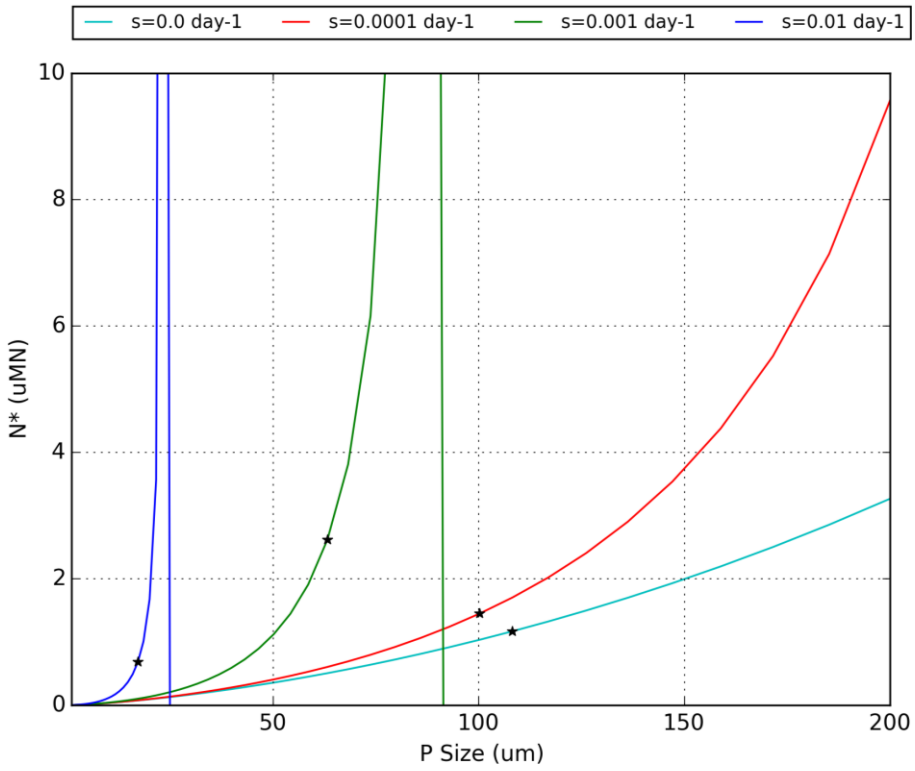


**Figure 51: N* curves and maximum winning sizes (black stars) for the different values of sinking parameter s: 108.20 µm (s=0.0 $day^{-1}$, cyan line), 100.21 µm (default s=0.0001 $day^{-1}$, red line), 63.21 µm (s=0.001 $day^{-1}$, green line), 17.13 µm (s=0.01 $day^{-1}$, blue line).**

Natural phytoplankton mortality m is parameterized as a size-independent phenomenon, with a default mortality rate of m = 0.1 $day^{-1}$ (Table 4). We explored what happens to modeled size-spectra for m = 0.05, 0.2, 0.4, 0.6 and 0.75 $day^{-1}$. Our results show that even if mortality is size-independent, a higher rate affects mostly larger size-classes by increasing equilibrium N concentration of each size-class (N*) possibly introducing a discontinuity (as already seen in section 2.5).

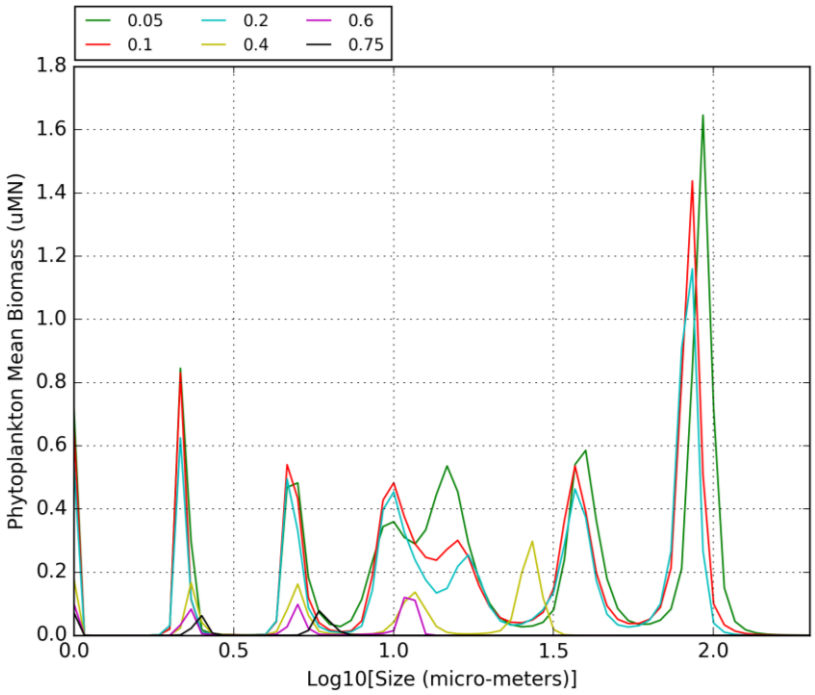


**Figure 52: Phytoplankton time mean size-spectrum for different values of P natural mortality. Higher mortality rates lead to smaller cells in the community, while low rates allow the survival of large cells.**

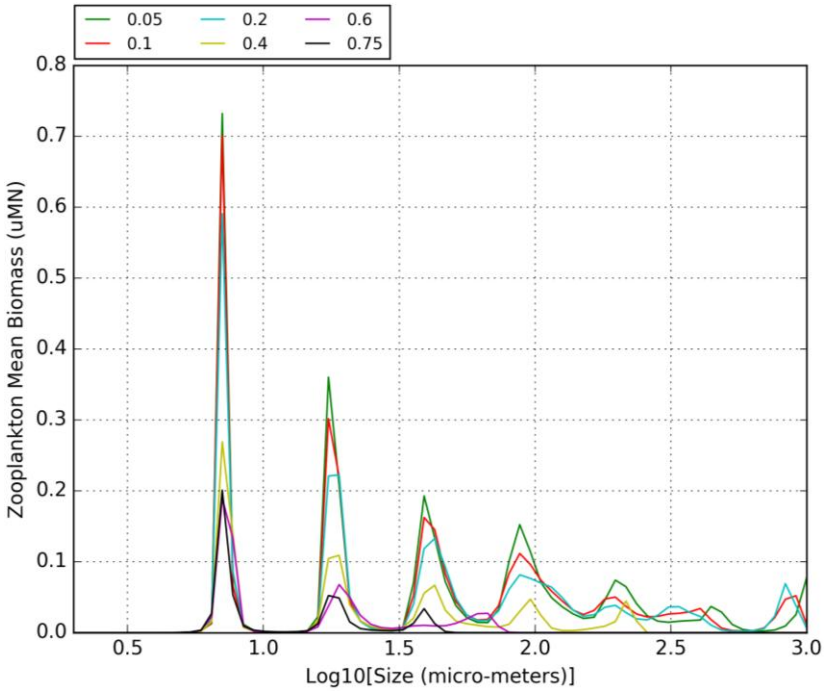


**Figure 53: Zooplankton time mean size-spectrum for different values of P natural mortality. Higher mortality leads to smaller organisms (because of smaller preys, fig. 52).**

Again, we could predict the maximum winning size-class for the different values of mortality using the theory in section 2.5, similarly to what we did above for sinking parameter s (figure 54). Increasing m has the same net effect of increasing s, introducing discontinuities in N* for the largest mortalities in the experiment (m=0.2 $day^{-1}$, m=0.4 $day^{-1}$, m=0.6 $day^{-1}$ and m=0.75$day^{-1}$). The same argument used for sinking applies here for mortality: in the cases with discontinuities, the sizes larger than a certain threshold cannot survive and the maximum winner (black stars in fig. 54) is the closest possible to the "size of discontinuity" given the grazing pressure. In the other cases without discontinuities (m=0.05 $day^{-1}$ and default case m=0.1 $day^{-1}$) the maximum winner (black stars in fig. 54) is decided by almost only Nitrogen in the environment.

The maximum winning sizes in the various cases are (m value in parenthesis): 108.20 µm (m=0.05 $day^{-1}$), 100.21 µm (default m=0.1 $day^{-1}$), 92.80 µm (m=0.2 $day^{-1}$), 29.33 µm (m=0.4 $day^{-1}$), 12.60 µm (m=0.6 $day^{-1}$), 6.31 µm (m=0.75 $day^{-1}$).

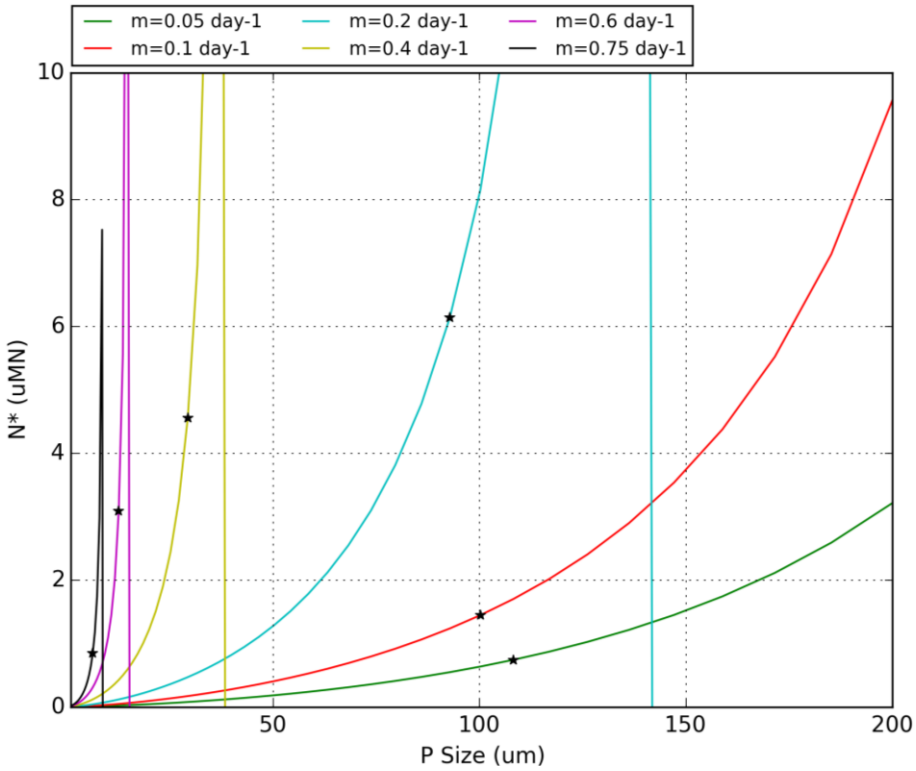


**Figure 54: N* curves and maximum winning sizes (black stars) for the different values of mortality m: 108.20 µm (m=0.05 day$^{-1}$, green line), 100.21 µm (default m=0.1 day$^{-1}$, red line), 92.80 µm (m=0.2 day$^{-1}$, cyan line), 29.33 µm (m=0.4 day$^{-1}$, yellow line), 12.60 µm (m=0.6 day$^{-1}$, purple line), 6.31 µm (m=0.75 day$^{-1}$, black line).**

In conclusion of this section, we would like to point out that section 2.5 gave us a theoretical framework for predicting, at least approximately, the maximum phytoplankton winning size for different values of some key parameters (s and m), using the N* concept already introduced by resource competition theory. **Knowing the value of s (or m) we can already have a guess of the maximum phytoplankton size surviving, especially in cases where N* is discontinuous (for "large" sinking or mortalities).**

### *3.5.3 Test on model resolution (number of size-classes)*

In this section we show that model results do not depend on resolution, i.e. they are robust with respect to the number of phytoplankton and zooplankton size-classes. This is a more technical test for SPLAS, but of course is a key requirement in order to proceed in more complex applications of the model.

We decreased the model resolution and solved for 35 size-classes of both plankton compartments, against the usual 70, using the default parameter values (Table 4).

We observe that varying the resolution, the qualitative size-spectra of both communities are the same (figures 55 and 56), and also the winning sizes are the same. In general the biomass appears slightly "distributed" among winners when resolution is high, because it is unavoidably shared among a larger number of size-classes. Still, the winning size classes remain the same, meaning that the mechanisms that generate such size-spectra are due to internal dynamics/fitness and not to artifices of the size-interval binning. Therefore, results obtained so far, for what concerns size-structure, are robust with respect to the resolution of the model (provided that there is a sufficient number of size-classes).

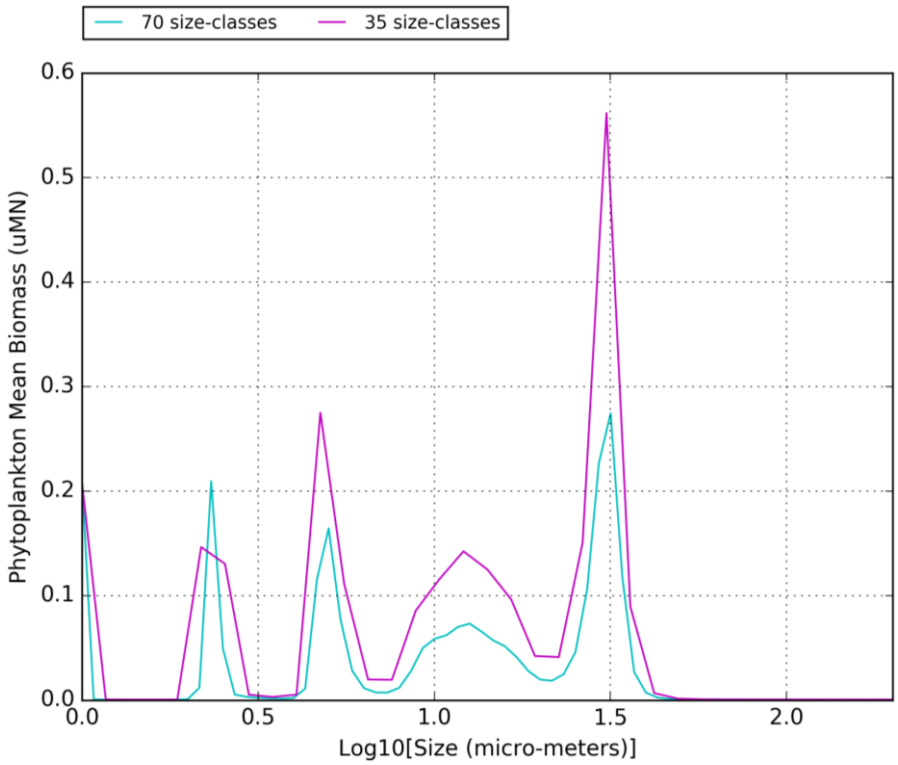


**Figure 55: Phytoplankton time mean size-spectrum with 70 (default, cyan line) and 35 (purple line) size-classes. The peaks (winners) correspond to the same sizes, but with default high resolution (cyan line) they are a bit "smoothed out" by the larger number of size-classes.**

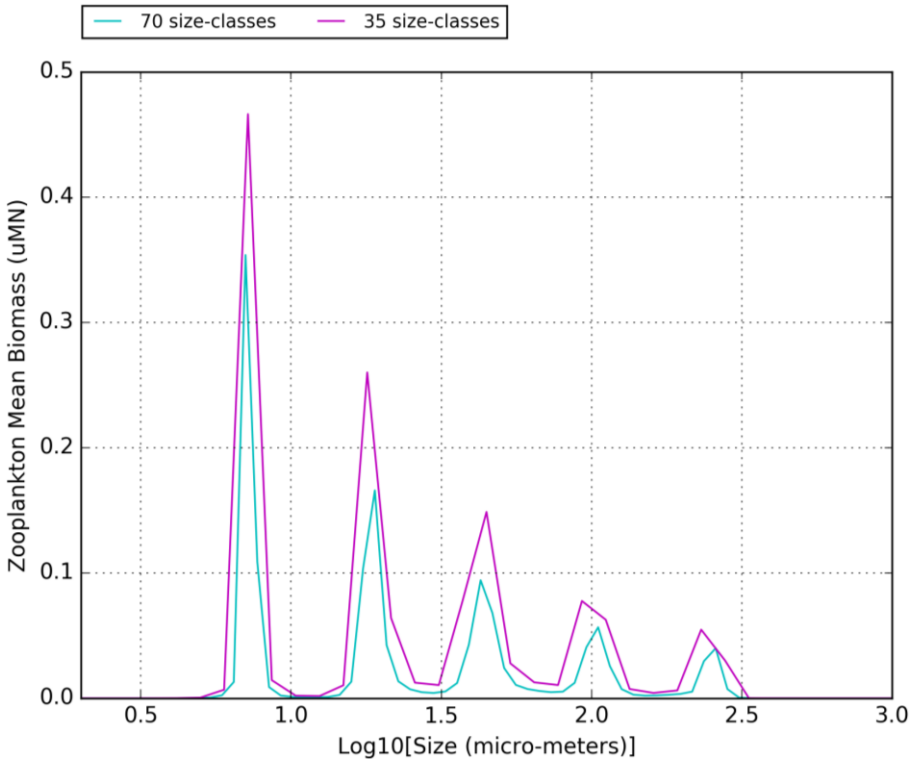


**Figure 56: Zooplankton time mean size-spectrum with 70 (default, cyan line) and 35 (purple line) size-classes. The peaks (winners) are the same, except that with default high resolution (cyan line) they are a bit "smoothed out" by the larger number of size-classes. In Zooplankton spectrum this is a bit less evident than for phytoplankton spectrum.**

Considering the time evolution of total biomasses (Figure 57) and size-diversities (Figure 58) we see that differences are small and results are comparable. In the "low resolution" case phytoplankton mean total biomass is 0.08% higher and zooplankton mean total biomass is 0.01% higher with respect to the default high resolution run. Size-diversity may vary more significantly by varying the number of size-classes. Indeed, differences for diversity are small but appreciable: phytoplankton mean Shannon evenness is 1.52% smaller with "low resolution" and zooplankton mean Shannon evenness is 2.17% smaller.

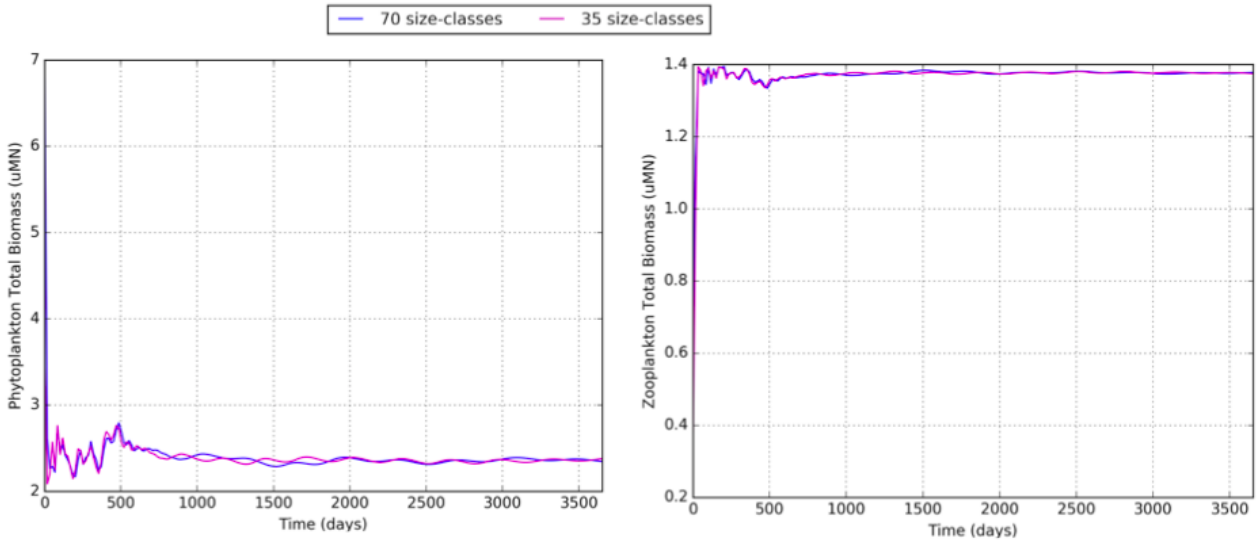


**Figure 57: Phytoplankton total biomass in time (left) and Zooplankton total biomass in time (right) with 70 (blue line) and 35 (purple line) size-classes. No appreciable differences can be seen.**

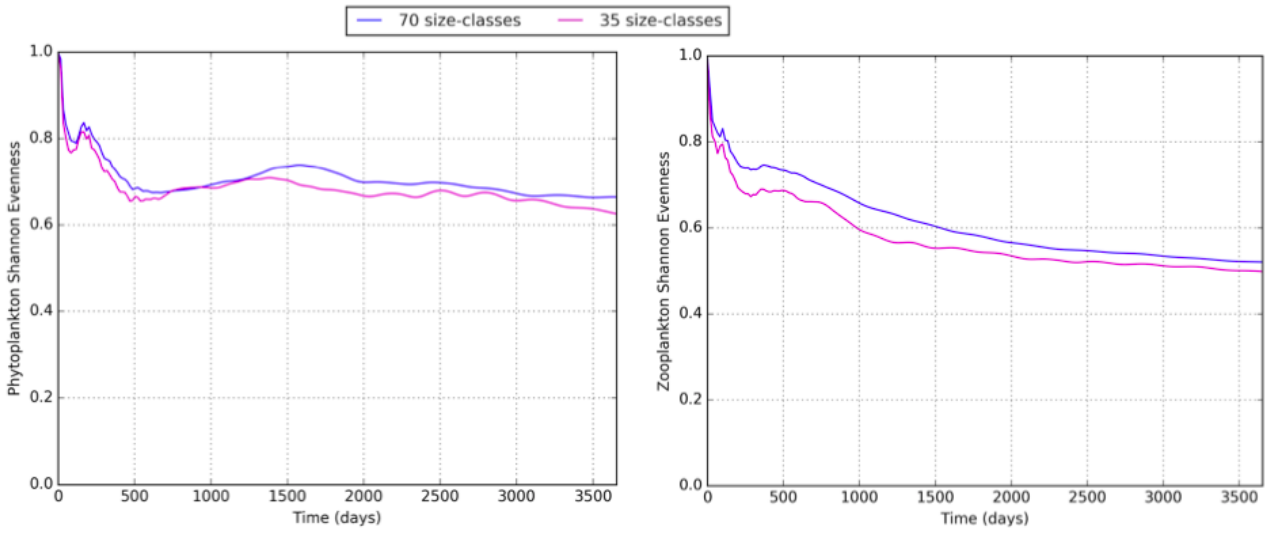


**Figure 58: Phytoplankton size-diversity in time (left) and Zooplankton size-diversity in time (right) with 70 (blue line) and 35 (purple line) size-classes. The two lines are slightly diverging; the low resolution purple line predicts a lowermean size-diversity with respect to the default resolution blue line. Anyway the two results remain comparable.**

These results (Figures 55, 56, 57, 58) show that **SPLAS output is stable with respect to the number of size-classes**, with size-diversity being the most sensitive parameter and size-spectra being a bit "smoothed out" by an high resolution. Instead, with a low resolution peak biomasses appear higher, the spectrum being distributed on a smaller number of size-classes.

### *3.5.4 Importance of assimilation efficiency and half saturation constant of the predator*

We tested the sensitivity of the model to some important yet poorly constrained parameters of zooplankton community, in order to analyze the effect of the uncertainty on planktonic structure in general, and more in detail the effect on our results contained in the previous sections.

We examined the effect of varying the assimilation efficiency of zooplankton (ε parameter) and egested fraction of zooplankton grazing ($f_{eg}$). Then we tested also the effect of zooplankton half saturation constant on the size-spectra.

*Assimilation efficiency and egestion*

The first two parameters (ε and $f_{eg}$) regulate the partitioning of total grazing into assimilation (to Z), excretion/regeneration (to N) and egestion (a loss from the system). Both ε and $f_{eg}$ are assumed to be equal to 1/3 in the default configuration (Table 4), for simplicity. This choice is supported by Hansen et al. (1997) that reported that ε ≈0.3 for a wide range of zooplankton, without any apparent allometric variation. We examined three scenarios: ε = 0.33, $f_{eg}$ = 0.33 (default); ε = 0.6, $f_{eg}$ = 0.3; ε = 0.3, $f_{eg}$ = 0.6. Notice that fixing ε and $f_{eg}$ fixes also N regeneration fraction, equal to 1- ε - $f_{eg}$. The default scenario has equal proportion of assimilation, egestion and regeneration (1/3), while the second and third scenarios have the same regeneration fraction (0.1) but opposite assimilation and egestion fraction (respectively 0.6 and 0.3 the second case, 0.3 and 0.6 the third case). To reduce the effect of N limitation we tested all scenarios with a nutrient supply of 5 µMN/day.

Figures 59 and 60 show respectively phytoplankton and zooplankton size spectra in the three different scenarios: ε and $f_{eg}$ seem to regulate somewhat the distance between the stripes of the winners and also total biomass, every other parameter being fixed. A higher assimilation (ε) means a more efficient transfer of biomass from phytoplankton to zooplankton, indirectly implying a stronger grazer's control which leaves space for large phytoplankton to grow (being poorly predated); on the contrary a higher egestion ($f_{eg}$) means that a large fraction of biomass is lost from the system (somehow "wasted") and this reduces the grazer's control on phytoplankton, which mostly undergoes N limitation.

The spectra are highly dependent on the choice of these two parameters; anyway, even if the winners are different and have different biomass, the results of the previous sections would not change qualitatively under the different assimilation and egestion parameters: the bottom-up and top-down limitations change slightly when ε and $f_{eg}$ are varied, but the patterns observed are conserved under a qualitative point of

view. We would still see an increase in maximum size of phytoplankton with increasing N supply, or a decrease of the maximum size with increasing Z mortality, even with different assimilation and egestion.

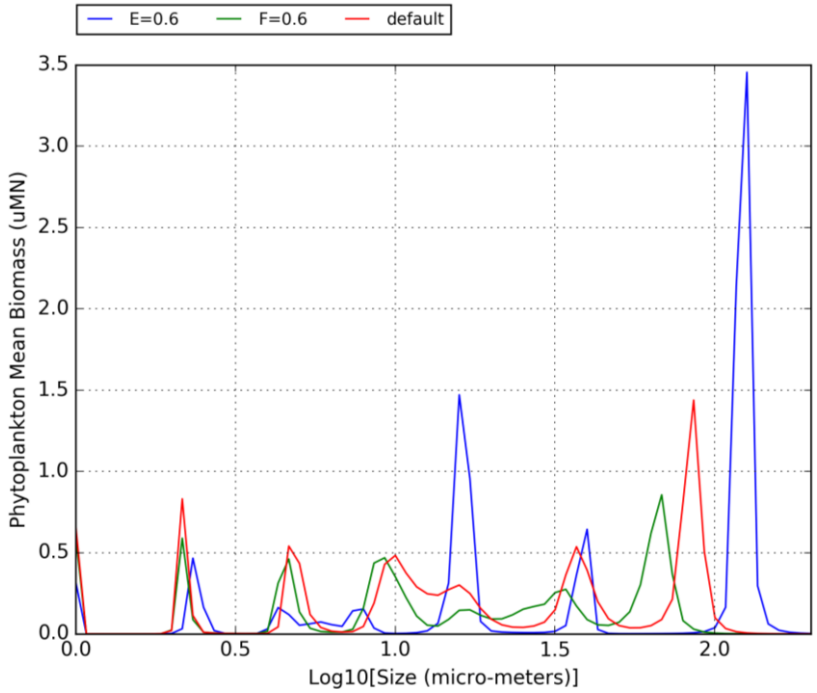


**Figure 59: Phytoplankton time mean size spectrum in the three different scenarios: ε = 0.33, $f_{eg}$ = 0.33 (default, red line); ε = 0.6, $f_{eg}$ = 0.3 (blue line); ε = 0.3, $f_{eg}$ = 0.6 (green line). For all three simulations S = 5 µMN/day.**

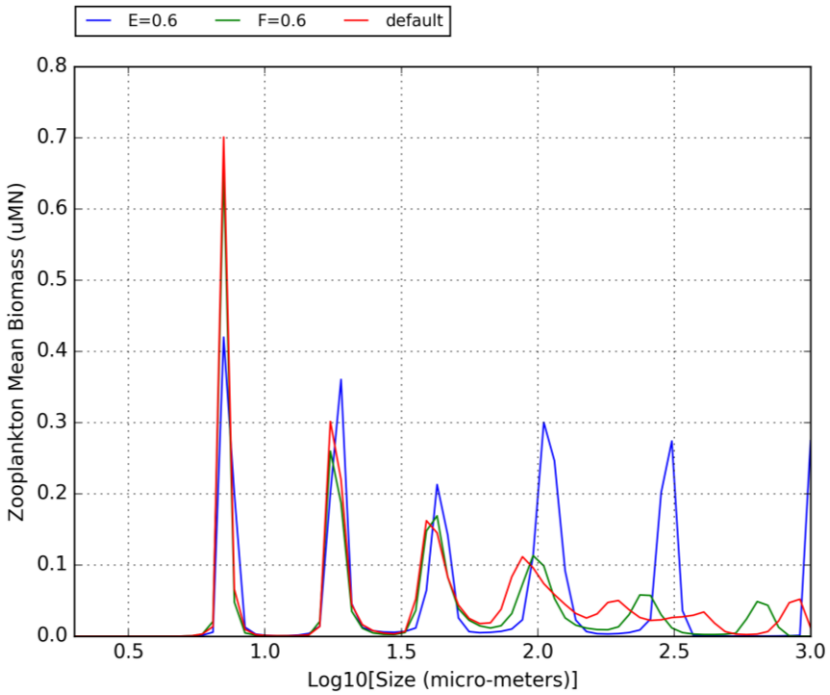


**Figure 60: Zooplankton time mean size spectrum in the three different scenarios: ε = 0.33, $f_{eg}$ = 0.33 (default, red line); ε = 0.6, $f_{eg}$ = 0.3 (blue line); ε = 0.3, $f_{eg}$ = 0.6 (green line). For all three simulations S = 5 µMN/day.**

*Zooplankton Half Saturation*

We studied the effect on size-spectra of different predator half saturation constants. We assumed a default value of 3 µMN according to Hansen et al. (1997). The half saturation does not appear to vary allometrically in zooplankton, although it may vary by one/two orders on magnitude among different functional groups.

We examined five cases, Kz from 1 to 5 µMN in 1 µMN steps, again maintaining a nutrient supply of 5 µMN/day.

Kz has an important effect on the grazing matrix, regulating the top-down control on phytoplankton community; we remind that the grazing function implemented here is a Holling type II functional response

$$graz_{ij} = I_j \frac{\varphi_{ij} P_i}{K_z + \sum_i \varphi_{ij} P_i} Z_j$$

Small values of Kz (1-2 µMN) lead to higher top-down control (higher values of $graz_{ij}$, easier saturation) and on average allow the survival of larger phytoplankton species (less predated), while larger values (4-5 µMN) weaken grazer's control (more difficult saturation of grazing function) and lead to situations in which phytoplankton community is more controlled by nutrients (Figure 61).

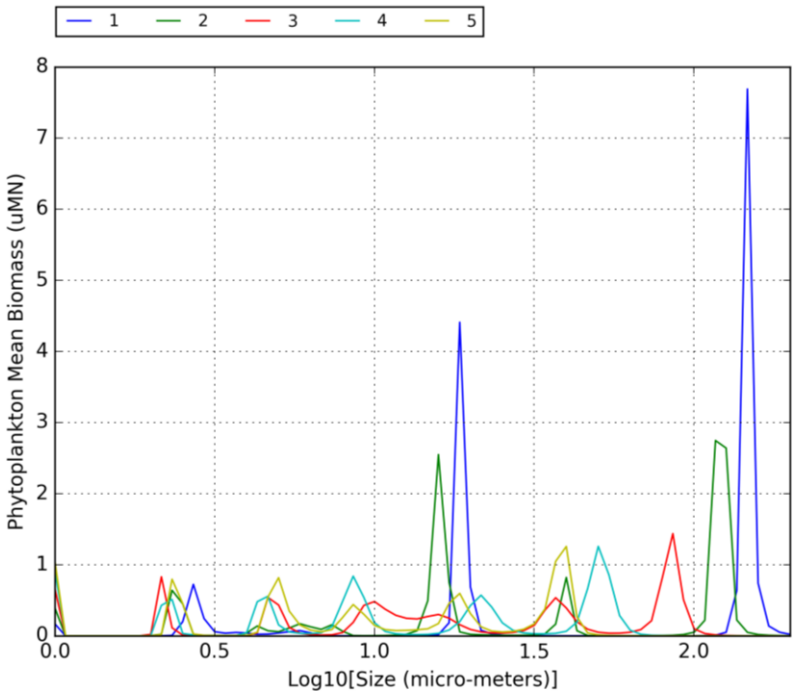


**Figure 61: Phytoplankton time mean size spectrum for different values of zooplankton half saturation constant. Smaller values lead to stronger top-down control on small sizes, allowing large, less predated sizes to grow (blue line Kz = 1 µMN, green line Kz = 2 µMN). Large values lead to situations of N limitation, weakening grazer's control on phytoplankton (cyan line Kz = 4 µMN, yellow line Kz = 5 µMN). Default value Kz = 3 µMN (red line). Nutrient supply is kept at 5 µMN/day.**

For what concerns zooplankton community, a higher half saturation favors small-sized organisms, having a large ingestion rate. On the contrary small values of Kz allow for the survival of larger species (Figure 62).

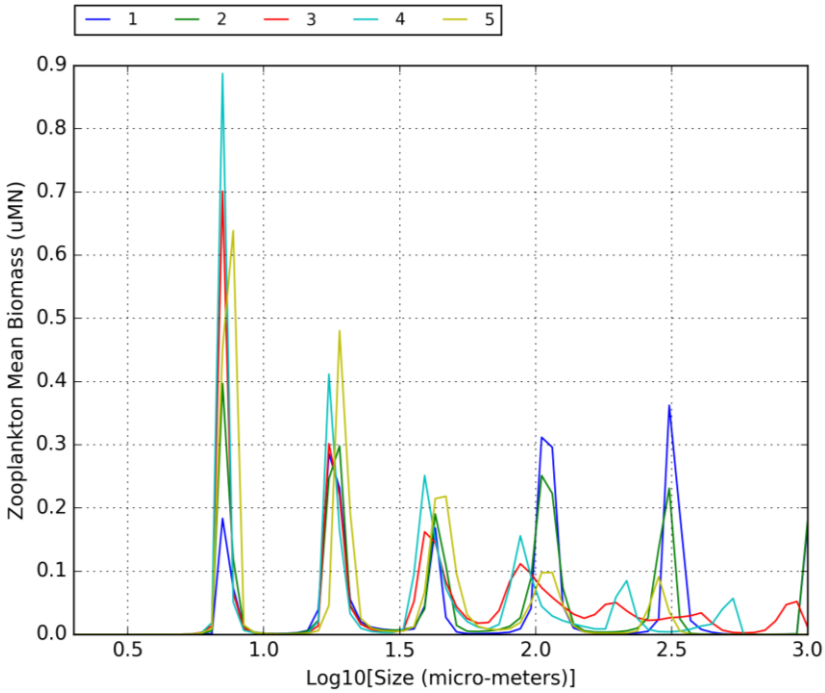


**Figure 62: Zooplankton time mean size spectrum for different half saturation constants. Small values allow for the existence of larger species (blue line Kz = 1 µMN, green line Kz = 2 µMN), while larger values lead to the presence of small-sized organisms (cyan line Kz = 4 µMN, yellow line Kz = 5 µMN). Nutrient supply is kept at 5 µMN/day.**

Kz, similarly to the previous case of assimilation parameter, regulates to some extent the spacing among the different stripes (peaks) in the size-spectra, and thus this parameter is a crucial choice for the model. But, as happened for ε, given a value for Kz, the pattern of the size-spectra do not change qualitatively varying the other parameters (S, Z mortality, selectivity). So, even if the resulting community shapes are different (winning sizes are different), the reaction of the system to top-down and bottom-up control are the same, qualitatively.

We claim that our previous results are robust, at least qualitatively, with respect to changes in these parameters that are the most uncertain.

### *3.5.5 Time varying N supply*

Up to now we examined the behavior of the model in steady environments. Here we briefly examine what happens with a time-varying nutrient forcing rather than a steady one, as a theoretical framework to test the behavior of the model in a variable environment.

In section 3.4.1 we examined the behavior of the model under increasing Nitrogen load, but we considered a steady forcing (i.e. a constant input of nutrients in time). Likely, the steadiness of the supply is the reason why we see many peaks at the same time in the size-spectra of both phytoplankton and zooplankton (fig. 33-35), with the maximum size in the spectrum depending on the intensity of the load. If we consider a time-varying supply(e.g. a sinusoidal input of nutrients) we expect the peak pattern in the spectra to be somehow alternating in time, with peaks in small phytoplankton during low nutrient periods and peaks in larger phytoplankton during high nutrient periods. We also expect zooplankton spectrum to reflect phytoplankton community and the maximum size to depend on the amplitude of the sinusoidal load.

To verify these expectations, we modified nutrient supply in the equation of Nitrogen (eq. 1):

$$S(t) = A \cdot sin^2(\omega t)$$

with A = 1 μMN day$^{-1}$ and ω = π/365 day$^{-1}$ so that the forcing has a period of 2 years (T = 2π/ω = 2x365 days), meaning 1 peak of N each solar year. This forcing is not intended to be realistic, as in natural environments the amplitude may vary in time and the period may be much different than 2 years (depending on the environment) and also the forcing may not be as ideal as a sinusoid; rather this test is meant to verify a reasonable qualitative behavior of the model in time-varying nutrient environment.

We solve the same ODEs (section 2.2) with S(t) instead of S, running the model for 10 years as in all other tests.

*Nitrogen (1) modified*

$$\frac{dN}{dt} = S(t) - \sum_i V_i^{max} \frac{N}{k_i + N} v_i + \left(1 - \varepsilon - f_{eg}\right) \sum_{i,j} graz_{ij}$$

We immediately see that the total phytoplankton and zooplankton biomass reach stable oscillations rather than stabilizing to a nearly constant value, as occurs instead for a fixed supply (comparison in fig. 63-64), with the period of the biomass oscillations resembling the period of the forcing (almost 2 years), which is a reasonable consequence of energizing the system with an oscillating load.

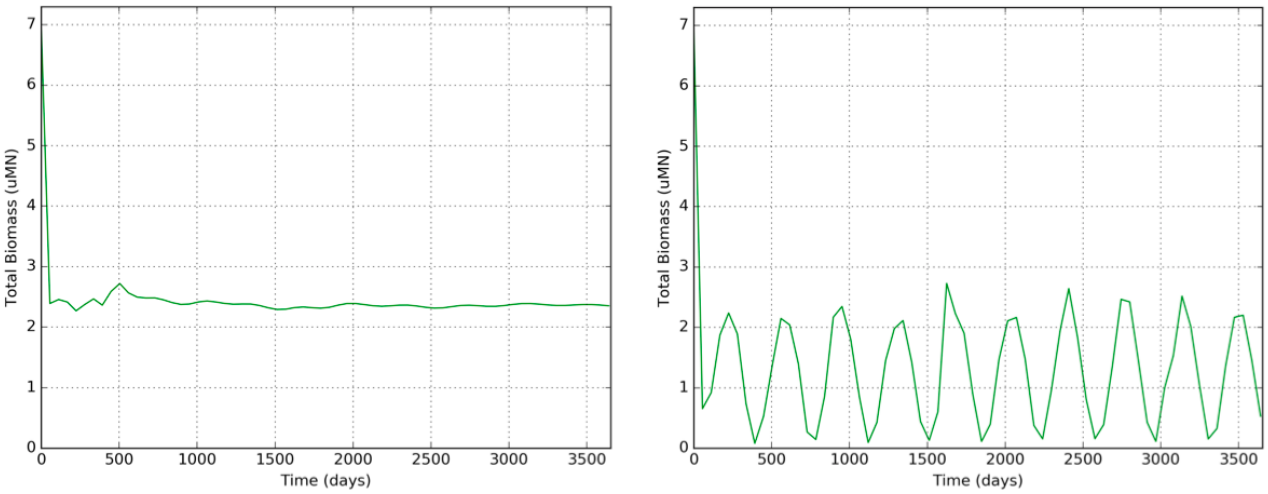


**Figure 63: Phytoplankton total biomass in time. Left: constant N supply (S = 1 µMN day$^{-1}$). Right: sinusoidal N supply (amplitude = 1 µMN day$^{-1}$, frequency = π/365 day$^{-1}$). In the case of steady forcing the biomass reaches a nearly constant value, whereas with a sinusoidal supply the biomass reaches stable oscillations.**

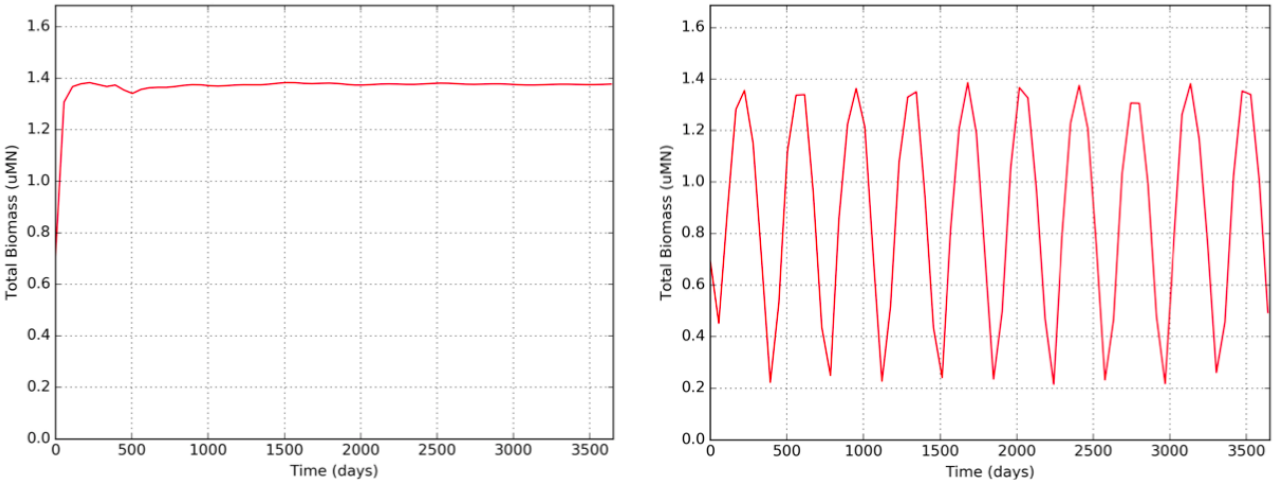


**Figure 64: Zooplankton total biomass in time. Left: constant N supply (S = 1 µMN day$^{-1}$). Right: sinusoidal N supply (amplitude = 1 µMN day$^{-1}$, frequency = π/365 day$^{-1}$). In the case of steady forcing the biomass reaches a nearly constant value, whereas with a sinusoidal supply the biomass reaches stable oscillations.**

The system experiences periods of low biomass and high biomass, in phase with nutrient concentrations (low and high). The size-structures of plankton community in the two periods are different, alternating small organisms and larger ones. Zooplankton community, as a whole, shows a quick response to phytoplankton biomass, as the oscillations of the two communities appear almost in phase (fig. 63-64, right). When nutrients in the environment are low, small phytoplankton cells dominate, grazed by small predators. On the contrary when nutrients are high, larger cells dominate and also grazer's population is composed of larger zooplankton organisms (fig. 65).

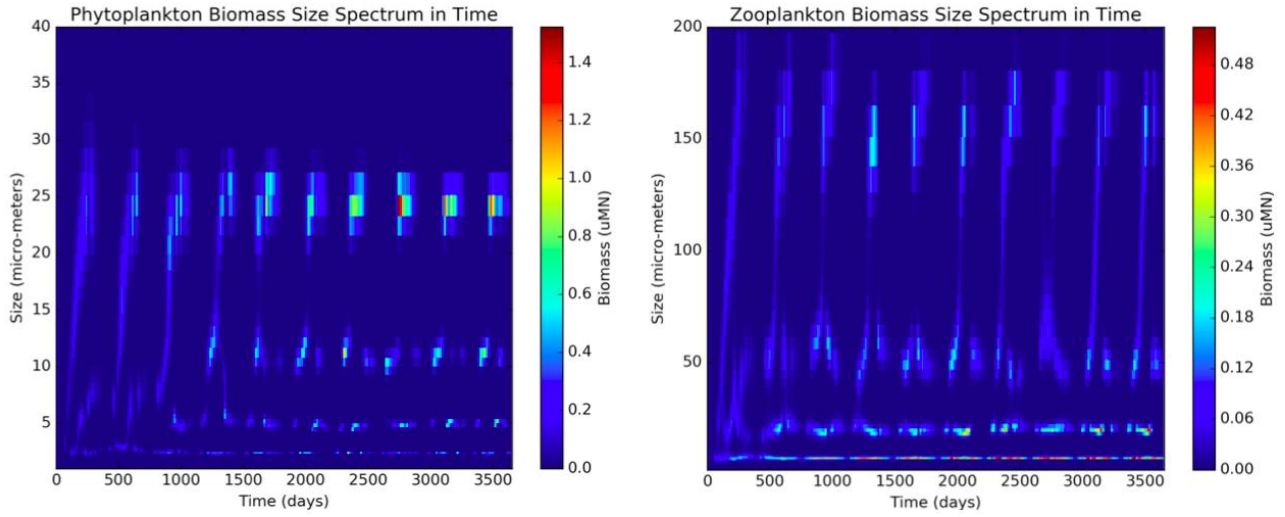


**Figure 65: Phytoplankton (left) and Zooplankton (right) size-spectrum in time, with a sinusoidal N supply (amplitude = 1 µMN day$^{-1}$, frequency = π/365 day$^{-1}$). The alternating peaks in phytoplankton (almost one per year) can be seen for both large (around 25 µm) and small organisms (about 1 µm, 5 µm and 10 µm), with zooplankton spectrum reflecting the spectrum of the preys.**

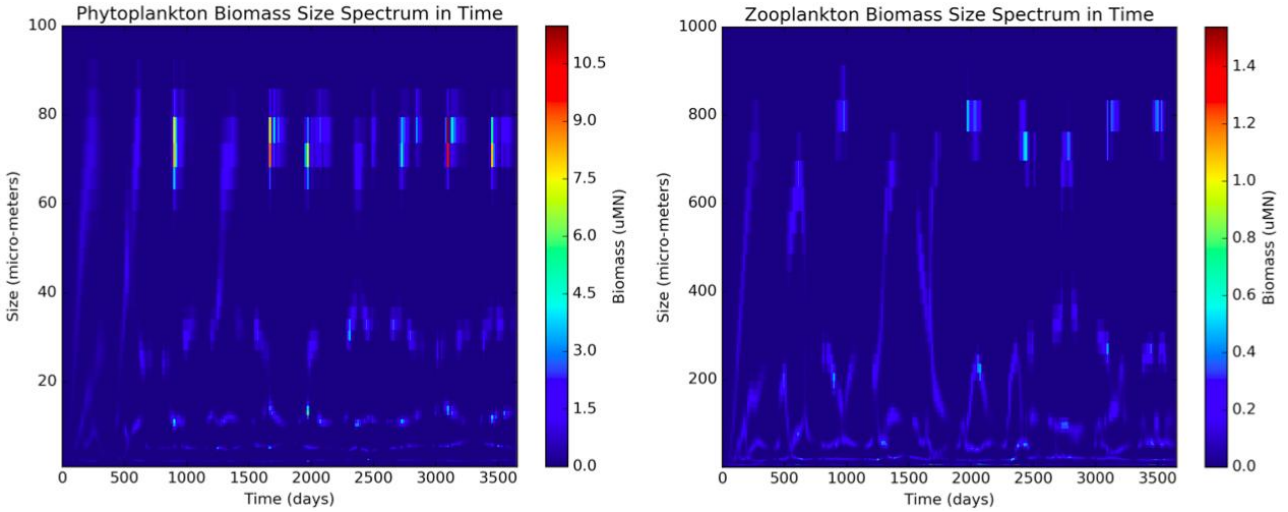


**Figure 66: Phytoplankton (left) and Zooplankton (right) size-spectrum in time, with a sinusoidal N supply (amplitude = 5 µMN day$^{-1}$, frequency = π/365 day$^{-1}$). The alternating peaks are now higher in biomass (see color scales to the right of the graphs) and communities reach much larger sizes than the previous case in fig. 42 (phytoplankton max size around 80 µm, zooplankton max size around 800 µm).**

Increasing the amplitude of the forcing, e.g. from 1 µMN day$^{-1}$ to 5 µMN day$^{-1}$ we notice that the maximum size appearing in plankton community is larger, and that both phytoplankton and zooplankton reach higher peak biomasses (fig. 66).

On the other hand, changing the frequency of the forcing affects the period of the biomass oscillations, and changes the turnover rate between smaller and larger organisms. We considered double (ω = 2π/365 day$^{-1}$, period of 1 year) and half (ω = π/730 day$^{-1}$, period of 4 years) of the default frequency, and results for size-spectra are shown in figures 67 and 68. With a higher frequency (period = 1 year) the alternation between

organisms in the size-structure is more rapid (fig. 67), while with lower frequency (period = 4 years) the turnover is slower (fig. 68). Basically, N load frequency determines the number of cycles per decade for plankton community and establishes the time rate of change of the different size-classes in the populations.

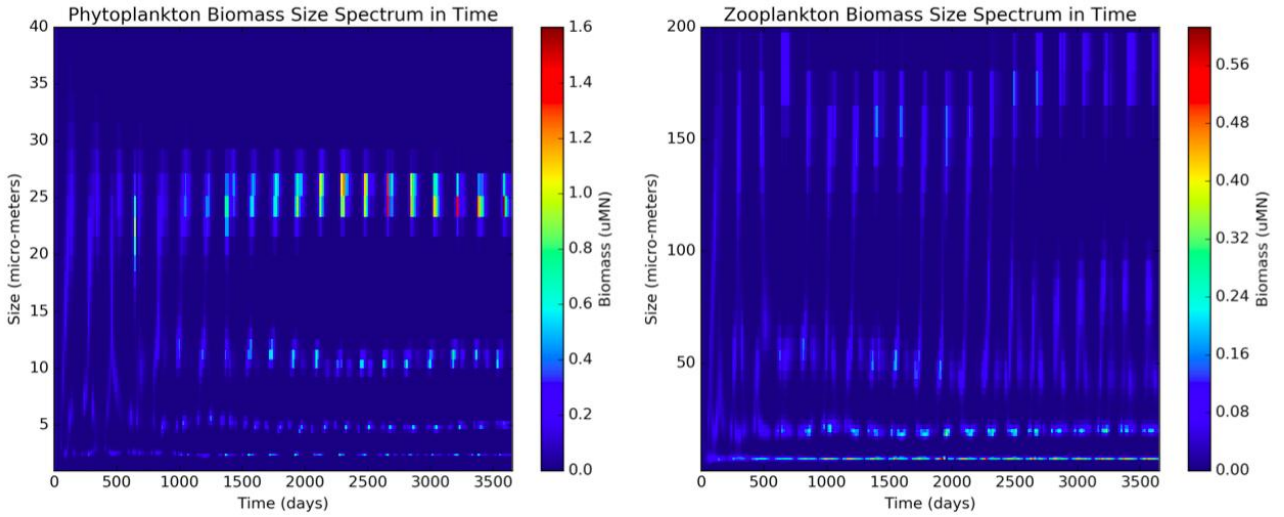


**Figure 67: Phytoplankton (left) and Zooplankton (right) size-spectrum in time, with a sinusoidal N supply (amplitude = 1 µMN day$^{-1}$, frequency = 2π/365 day$^{-1}$). The peaks in biomass of the different size-classes are now alternating more rapidly, following the increased frequency of nutrient load.**

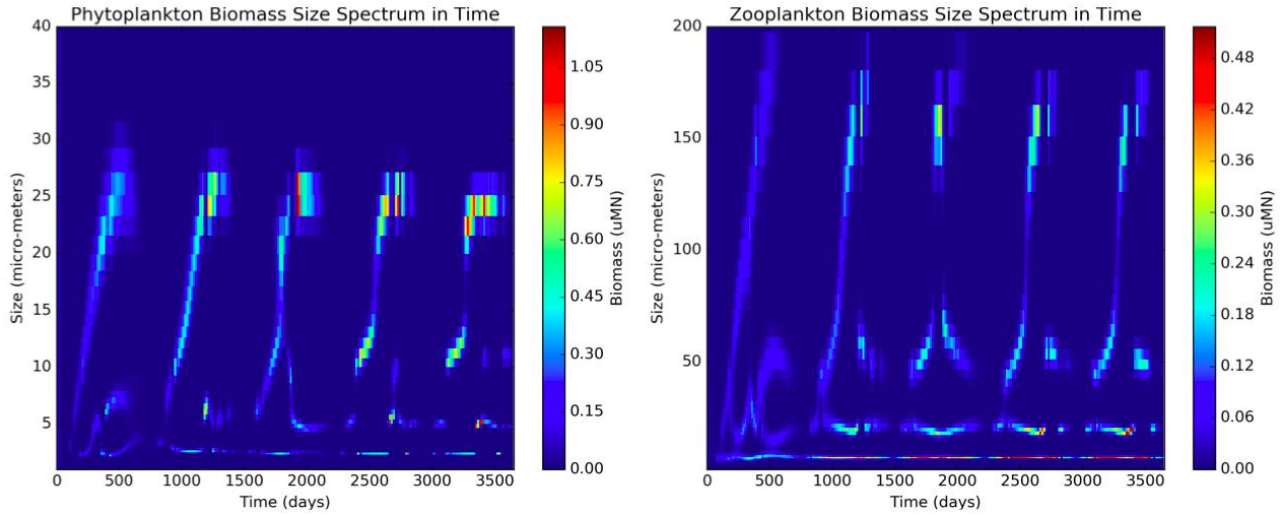


**Figure 68: Phytoplankton (left) and Zooplankton (right) size-spectrum in time, with a sinusoidal N supply (amplitude = 1 µMN day$^{-1}$, frequency = π/730 day$^{-1}$). The peaks in biomass of the different size-classes are now alternating more slowly, following the lower frequency of nutrient load.**

**In conclusion, in presence of an oscillating supply of nutrients the modeled plankton community responds with a similarly oscillating pattern (fig. 63-64). Plankton size-spectra show some sort of "seasonality" (fig. 65), with peaks in small size-classes (low nutrients) alternated in time to peaks in intermediate and large size-classes (medium/high nutrients). On the contrary, a steady forcing led to the coexistence of different peaks (both small and larger size-classes) without alternation (section 3.4.1). The peak biomass and the maximum size in the community depend on the amplitude of the forcing (fig. 65-66) and the frequency (number of cycles per year) resembles the period of the supply (fig. 67-68).**

Notice that also in the steady forcing case (section 3.4.1) total biomass and maximum size in the community depend on the "amplitude" of the forcing (the fixed value of S), but in that case there was no seasonal pattern and alternation. **Thus, the constant supply case can be seen as a limit of the sinusoidal forcing for the period tending to an infinite value (frequency going to zero).** As we get close to the steady limit, oscillations dampen and peaks in the different sizes get closer and closer in time, coexisting in the end. Therefore, the representation of the model is consistent between the two cases.

### *3.6 SPLAS 0-D: discussion and summary*

All the tests concerning validation and sensitivity of the results point out that SPLAS is consistent, gives reasonable output with varying parameters and represents well plankton size-structure to obtain reliable estimates of the biogeochemical fluxes, as C export.

In summary:

1. The model reproduces the phytoplankton community shift towards larger sizes with increasing N load, in agreement with theoretical predictions and experimental observation (e.g. **Ward et al., 2013**) (section 3.4.1).

2. The model catches the (size-)diversity pattern, better than previous studies (**Banas, 2011)**, showing a parabolic dependence on total biomass, as shown in **Irigoien et al., 2004**; **Goebel et al., 2012**(section 3.4.2).

3. The model behaves correctly under variation in top-down control parameters (Z mortality), as Z:P ratio decreases with increasing mortality (regime shift from grazer's control to N control) (section 3.4.3).

4. Tests on trophic transfer efficiency (TTE) in many modeled environmental conditions (parameter values) agree with recent experimental results (**Garcia-Comas et al., 2016**) (section 3.4.4).

5. Size-spectra are strictly dependent on Z prey selectivity as it regulates somewhat the coupling between predators and preys and the space among peaks in the spectra (section 3.5.1).

6. Plankton size-spectra are strongly impacted by a sinking term and natural mortalities, in agreement with equilibrium view of N* (section 3.5.2).

7. Peaks and in general size spectra do not depend on the spacing among size-classes. The spectra look qualitatively the same both with a fine and coarse resolution of the size intervals. The number of size-classes changes, and so the number of "winners", but always around the same size (same peaks of the spectra) (section 3.5.3).

8. Plankton size-spectra are also impacted by other poorly constrained parameter as zooplankton assimilation efficiency and half-saturation constant for preys (3.5.4).

9. The model behaves correctly even when forced by a time-varying N supply, showing predator-prey cycles and oscillating patterns (section 3.5.5).

In virtue of these considerations (the validation and the behavior analysis), the model is able to capture many plankton ecological interactions and size-structure.

### *3.7 Strengths of the model*

SPLAS is able to catch the overall pattern of aquatic plankton food web from a zero-dimensional point of view (see section 3) and seems a promising tool even when included in a 1-D framework with a more complex physical and biogeochemical dynamics (see sections 4 and 5).

The model output includes time-average and time-dependent size spectra of both phytoplankton and zooplankton, therefore size structure of the system and size-dependent interactions are highly resolved and can be used for interpretation and comparison with data.

The model reproduces correctly phytoplankton community shift towards larger size classes when N in the environment increases, and reproduces the relationship between size-diversity and total biomass in different environmental condition. Moreover, SPLAS reproduces the same pattern of Trophic Transfer found in real systems.

Thanks to these results SPLAS is a promising tool for biogeochemical investigations, and when extended to a water column model with vertical turbulent diffusivity it gives useful theoretical insights on phytoplankton ecology. The strength of the 1-D version of SPLAS is that we can reproduce sensible water column features, as the deep biomass maximum, when light is included. Light has also important effects for phytoplankton vertical size-structure.

SPLAS might be able in the future, after significant improvements, to give reasonable estimates of Carbon export flux. In the final chapter of this thesis we perform some rough estimates of C export, that make sense when compared with estimates of more complex and global models (as Ward and Follows, 2016) but still must be taken with caution as they are still poorly significant. They are only useful to give an idea of SPLAS' potential. The main limit of SPLAS now is that the estimates of export are too robust with respect to the key parameters of the model (see the sensitivity analysis). Other limits in the representation are discussed in the following section.

### *3.8 Limits of the model*

The present model omits several phenomena and does not include potentially important features of the plankton food-web.

First, the model excludes large organisms (>1000 μm ESD), zooplankton life cycle and carnivorous grazing (zooplankton predation on other zooplankton) (see Baird and Suthers, 2007).

Second, very small photoautotrophs (<1 μm ESD) are also excluded.

Third, phytoplankton taxonomic differences in growth rate are not considered and the same allometric relationship is used.

Fourth, mixotrophy here is not considered, dividing strictly into phytoplankton (all autotrophic) and zooplankton (all heterotrophic and herbivorous); the importance of mixotrophy in ecosystems and ecosystem related processes has been demonstrated in recent studies (Mitra et al., 2014; Ward and Follows, 2015) and some models that account for mixotrophy have already been proposed (Troost, 2005; Barton, 2011). It is widely accepted in literature studies that not all phytoplankton are autotrophic, nor all zooplankton are heterotrophic: the distinction itself between phytoplankton and zooplankton may be in reality blurred, as mixotrophy is widespread in the marine environment (Sanders et al., 2000; Anderson, 2005; Andersen et al., 2015).

Moreover, it is evident from many studies that heterotrophic dinoflagellates do not follow any of the optimal prey size laws found in literature, as also Banas (2011) stated. This group is composed of relatively large cells (on average about 50-80 µm) that eat phytoplankton of their own size (1:1 predator-prey ratio) or possibly even larger (Hansen, 1992; Jacobson, 1999).

On the other hand, autotrophic dinoflagellates have a far smaller growth rate than the average power law proposed by Tang (1995), and as said before here taxonomic phytoplankton differences are here neglected.

# 4 Exploring the vertical dimension: the water column (1-D) model

In this section we extend the 0-D layout of SPLAS to a water-column1-D model, including very relevant phenomena as vertical diffusion and sinking. It is important to resolve at least the vertical dynamics, as water column phenomena strongly impact carbon export. In this work we modify the model to be a water column model as a natural continuation of our 0-D box model, to include some vertical dynamics in order to have a more realistic base for future development and applications. At this point we are far from realistic applications, but for the future having a 1-D model that solves vertical dynamics is an important starting point. In the long term, solving with this level of detail the size-structure of plankton in the water column could make a difference in shedding new light on how size composition of plankton community impacts biogeochemical fluxes, in particular carbon export. In this framework we stick to a theoretical investigation and discuss some important implications of adding new complexity to the SPLAS model.

The sinking rate of the 0-D version ($day^{-1}$) becomes a velocity (m/day). Suppose we have *M* horizontal layers labeled by k, where k = 1 represents the surface layer and k = *M* is the bottom layer, which is located somewhere at the edge or inside the mixed layer.

The 1-D equations become:

*(7)*

$$\frac{dP_i(k)}{dt} = Growth_i(k) - Grazing_i(k) - Mortality(k) - \frac{\partial}{\partial z}\left(w_i P_i(k)\right) + \frac{\partial}{\partial z}\left(D\frac{\partial P_i(k)}{\partial z}\right)$$

*(8)*

$$\frac{dZ_j(k)}{dt} = Growth_j(k) - Mortality_j(k) + \frac{\partial}{\partial z}\left(D\frac{\partial Z_j(k)}{\partial z}\right)$$

*(9)*

$$\frac{dN(k)}{dt} = Supply(k) - Tot.Uptake(k) + f_{rig} \cdot Tot.Grazing(k) + \frac{\partial}{\partial z}\left(D\frac{\partial N(k)}{\partial z}\right)$$

SPLAS 1-D is designated to solve equations 7, 8 and 9 in different configurations: first we will use a D constant in depth, then we will include a detritus compartment in the dynamics and also light limitation in P growth, and then we will investigate the effects of a depth dependent diffusion D(z).

### *4.1 Constant vertical diffusion*

All *processes* written in words inside the equations have the same parameterization as before, except that now they are layer-dependent. D is the diffusion coefficient ($m^2/s$) and $w_i$ is sinking velocity (m/day).

We start considering a constant diffusion coefficient of $10^{-4}$ $m^2/s$ (vertical eddy diffusivity) throughout the water column. This is a typical value widely found in literature and in community models (e.g. NEMO, https://www.nemo-ocean.eu/wp-content/uploads/NEMO_book.pdf, pp 186-187). We also consider a $w_i$ which is size-dependent and does not vary with depth.

Thus, equations 7-8-9 become simply:

$$\frac{dP_i(k)}{dt} = Growth_i(k) - Grazing_i(k) - Mortality(k) - w_i \frac{\partial P_i(k)}{\partial z} + D \frac{\partial^2 P_i(k)}{\partial z^2}$$

$$\frac{dZ_j(k)}{dt} = Growth_j(k) - Mortality_j(k) + D \frac{\partial^2 Z_j(k)}{\partial z^2}$$

$$\frac{dN(k)}{dt} = Supply(k) - Tot.Uptake(k) + f_{rig} \cdot Tot.Grazing(k) + D \frac{\partial^2 N(k)}{\partial z^2}$$

We solve these equations with a 2nd order central finite difference scheme for diffusion and a backward finite difference scheme for sinking (for stability reasons, since the integration is explicit and forward in time).

As boundary conditions we set:

- For phytoplankton: no exchange other than sinking matter at the bottom
- For zooplankton: no exchange at the top and at the bottom
- For Nutrients: prescribed supply from below

In order to do so we use two external "buffer" layers; in practice we solve the equations in the *M*-2 internal layers, and the two layers at the edges are used for implementing boundary conditions. Each layer is located at the depth

$$z_k = (k - \frac{1}{2}) \cdot \Delta z$$

And the total depth covered by the grid is

$$h = (M - 1) \cdot \Delta z$$

Results of a sample simulation with 10 layers (8 internal layers) can be seen in figures 69 and 70, showing respectively phytoplankton and zooplankton size-spectra in each layer. We used a $\Delta z$ of 1.5 m, covering a total depth of 13.5 m. The first "boundary" layer is found at 0.75 m from the surface and the last at 14.25 m.

These results are obtained setting a very high Nitrogen load in every layer ($Supply(k) = 4.0\ \mu MN\ day^{-1}\ \forall\ k$) to highlight a larger number of stripes in the size-spectra (as seen in SPLAS 0-D, section 3.4.1). The size-spectra are almost homogeneous in depth, except that biomass of some classes of plankton is varying with depth (figures 69 and 70).

The fact that in this first experiment size-spectra are homogeneous in depth (winning size-classes are the same at each depth, except biomass slightly increasing going deeper) is something to keep in mind for when we will include light in P growth.

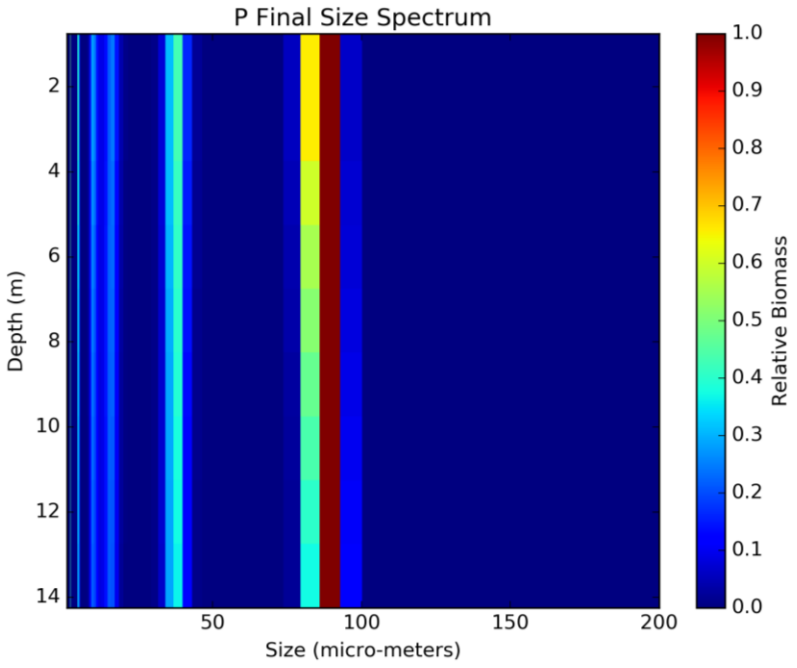


**Figure69: Phytoplankton size-spectrum in each layer. For the vertical grid we used a spacing of Δz = 1.5 m.**

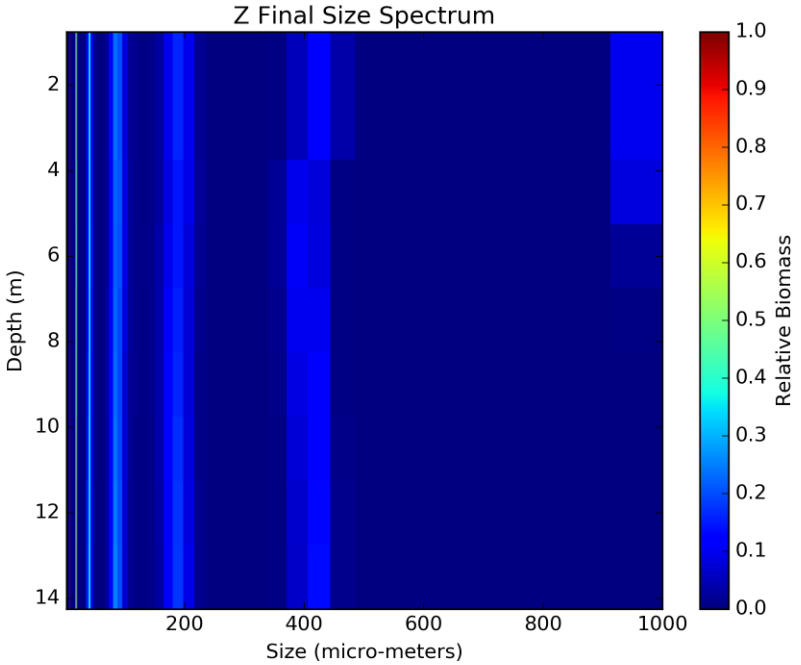


**Figure70: Zooplankton size-spectrum in each layer. For the vertical grid we used a spacing of Δz = 1.5 m.**

### *4.2 Detritus*

We add here a detritus pool containing any organic matter derived from egestion and natural mortality, since organic matter dynamics is not negligible if we want to achieve a reliable assessment of the export in the future. We include detritus since our goal is to have a complete dynamics in SPLAS and for this aim organic matter should be taken into account; secondly, we will perform at the end of the thesis some first order guesses of C export, and for this reason we need to track at minimum a simple detritus compartment. With detritus SPLAS evolves to a full NPZD model. A single detritus pool is included per each layer, in which natural mortality of phytoplankton and zooplankton and the egested fraction of grazing represent sources of detritus, while re-mineralization (organic matter going back to bio-available Nitrogen) represents a sink of detritus. Moreover, detritus physically sinks downward into the successive layer and is diffused throughout the water column. The equation for detritus (OM) in the k-th layer is:

*(10)*

$$\frac{dOM(k)}{dt} = -\psi \cdot OM(k) + m \cdot \sum_i P_i(k) + \gamma \cdot \left[\xi^{1/2} \sum_j Z_j(k)\right]^2 + f_{eg} \cdot \sum_i \sum_j graz_{ij}(k) - w_{OM} \frac{\partial OM(k)}{\partial z} + D \frac{\partial^2 OM(k)}{\partial z^2}$$

We implement for detritus the same boundary condition as for phytoplankton, that is no exchange of matter at the top and no exchange at the bottom other than sinking matter.

The equation for Nitrogen (eq. 9) in the k-th layer is modified accordingly including the term $+\psi \cdot OM(k)$,which represents re-mineralization of organic matter and the re-mineralization rate $\psi$ is set to 0.15 day$^{-1}$as in Oguz et al.(2013). The sinking velocity $w_{OM}$ is set to 8.0 m day$^{-1}$, again as in Oguz et al. (2013; maximum detritus sinking velocity). According to the same paper we adjust also natural phytoplankton mortality (m) to 0.05 day$^{-1}$(instead of 0.1 day$^{-1}$ as earlier in our work) and adapt phytoplankton sinking velocity to $w_i = 0.0041 \cdot {x_i}^{1.17}$ so that maximum velocity is around 2.0 m day$^{-1}$.

The fraction of zooplankton mortality going to detritus ($\gamma$) is set to 0.5 (50% of dead zooplankton goes to detritus and the other is lost or assimilated by higher predators), in agreement with the work of Edwards(2001) where the impact of the inclusion of detritus in an NPZ model is carefully studied in simple terms.

By adding the detritus equation to the system we could perform a guess of the quantity of material (carbon) going out from the *M*-th layer of the water column represented here. We will do this at the end of the thesis and this guess should be seen as an upper bound, rather than a precise estimate, since we are collecting all organic matter in one compartment (without distinction between dissolved and particulate matter) and we are using as a sinking velocity the maximum value of 8.0 m day$^{-1}$ for all detritus (without size-dependence).

Our goal here is to focus on size-structure patterns in plankton, discussing what happens to the 0-D picture when we move it into a dynamic 1-D structure. What happens to size-spectra? We saw that they were homogeneous in depth in section 4.1, so our system for now is almost equivalent to several 0-D boxes in column that communicate among them with a small diffusion term and a sinking matter term. This “communication channel” does not influence the winning size-classes from one layer to another. We will see that this picture changes when we include a player whose role is to break this vertical “symmetry”.

The full set of equations for the generic k-th layer is now:

*(11)*

$$\frac{dP_i(k)}{dt} = \mu_i P_i(k) - \sum_j graz_{ij}(k) - mP_i(k) - w_i \frac{\partial P_i(k)}{\partial z} + D\frac{\partial^2 P_i(k)}{\partial z^2}$$

*(12)*

$$\frac{dZ_j(k)}{dt} = \varepsilon \sum_i graz_{ij}(k) - \xi\, Z_j(k) \sum_j Z_j(k) + D\frac{\partial^2 Z_j(k)}{\partial z^2}$$

*(13)*

$$\frac{dN(k)}{dt} = S(k) - \sum_i Uptake_i\big(N(k)\big) + \big(1 - \varepsilon - f_{eg}\big) \cdot \sum_i \sum_j graz_{ij}(k) + \psi OM(k) + D\frac{\partial^2 N(k)}{\partial z^2}$$

*(14)*

$$\frac{dOM(k)}{dt} = -\psi OM(k) + m\sum_i P_i(k) + \gamma\left[\xi^{1}/_{2}\sum_j Z_j(k)\right]^2 + f_{eg}\sum_i\sum_j graz_{ij}(k) - w_{OM}\frac{\partial OM(k)}{\partial z} + D\frac{\partial^2 OM(k)}{\partial z^2}$$

with boundary conditions:

- For Phytoplankton: no exchange other than sinking matter at the bottom
- For Zooplankton: no exchange at the top and at the bottom
- For Nutrients: no exchange at the top, prescribed supply from below
- For Detritus: no exchange other than sinking matter at the bottom

And with parameter values indicated in Table 7.

The profile of N supply used, S(k) is

$$S(k) = 4.0 \cdot \delta_{kM}$$

where $\delta_{kM}$ is the Kronecker delta, which is 1 for k=M and 0 for all other k. This is equivalent to set a Nutrient supply of 4.0 mmolN $m^{-3}$ $day^{-1}$ at the bottom layer, which is exactly our boundary condition. In the M-2 internal layer the Nitrogen load is null. The value of the supply is chosen in agreement with Banas(2011) and corresponds to a high load in well-mixed turbulent regions.

**Table 7: value of parameters for the SPLAS 1-D model.**

| Parameter | Units | Value |
|---|---|---|
| $m$ | $d^{-1}$ | 0.05 |
| $\varepsilon$ | - | 0.33 |
| $\xi$ | $(\mu MN)^{-1}d^{-1}$ | 0.20 |
| $S(k)$ | $\mu MN\ d^{-1}$ | - |
| $f_{eg}$ | - | 0.33 |
| $\psi$ | $d^{-1}$ | 0.15 |
| $w_{OM}$ | $m\ d^{-1}$ | 8.0 |
| $w_i^{max}$ | $m\ d^{-1}$ | 2.0 |
| $\gamma$ | - | 0.50 |
| $D$ | $m^2\ s^{-1}$ | $10^{-4}$ |

### *4.3 Adding Light to phytoplankton growth*

Let us consider the first 200 m in the water column: we now relax the hypothesis of depth-constant maximum P growth rate and include light (depth) dependence of phytoplankton growth. We will then explore the implications of this change of representation and the consequences of the extended depth range and the inclusion of light; possibly, a condition that we want SPLAS to satisfy is the presence of deep biological maximum (DBM) at a certain depth (Lewis et al., 2017). DBM is one of the most ubiquitous features of the world ocean and mechanisms leading to its formation involve many factors (e.g. nutrients and light, see Cullen, 2015 for a detailed review). We remind that the reproduction of the DBM or any real world pattern is not the main focus of this thesis or SPLAS, but we would like to have a 1-D model that, at minimum, behaves in a reasonable way and is not too distant from reality. We will see in the following that light has some serious implication for 1-D plankton size-structure.

We extend the depth range (41 layers, Δz = 5 m, total thickness = 200m) and include light dependence on phytoplankton growth rate:

*(16)*

$$\mu_i(z) = \mu_i^0 \left(1 - \frac{Q_i^{min}}{Q_i}\right)\left[1 - \exp\left(-\frac{I(z)\cdot\vartheta\cdot\alpha}{\mu_i^0}\right)\right]$$

where we chose a reasonable fixed Chlorophyll a to Carbon ratio ($\vartheta$ = 0.02) and set α = 0.32 $m^2\ W^{-1}$ (Oguz et al., 2013). For what concerns the irradiance I(z) we used a fitted relationship obtained from a light profile measured by a Bio Argo Float in the Mediterranean Sea (float lovbio015c - Central Western Mediterranean - on the 18/03/2015). We used the formula

$$I(z) = I_0 \cdot e^{-k_d z}$$

to fit the data ($R^2$ = 0.85) and obtained $I_0 = 959.83$ W $m^{-2}$ and $k_d = 0.062$ $m^{-1}$(Figure 50).

We still consider here a constant diffusivity with depth (D = $10^{-4}$ $m^2$/s).

Our aim is to verify the behavior of total phytoplankton biomass throughout the water column and check the possible presence of a DBM in some light conditions: we want neither to reproduce the daily cycle nor the seasonality, nor a perfectly realistic profile of Photosynthetically Active Radiation (PAR), as long as it is reasonable (that is why we use the fitted relationship-not the data- and a fixed, but qualitatively correct, $\vartheta$).

Again, we stress that we do this check in order to possibly implement a reasonable behavior for the 1-D model, rather than having a working 1-D model with a completely nonsense biomass pattern. Light adds some sort of rigors to SPLAS representation, even if still far from real oceanic patterns.

We ran the model for 10 years and computed time mean profiles (basically we are running a steady-state simulation). We maintained boundary conditions as earlier in the text (no flux at the top, only P, OM sinking fluxes at the bottom) but in this case a Nitrogen supply from the bottom (at 200m) is not enough to sustain productivity, thus we added a "horizontal" supply in each layer which is the 10% of the supply from below.

In formula

$$S(k) = 0.4\,\mu MN\ day^{-1}\ for\ k = 2, M-1$$

$$S(0) = 0\,, S(M) = 4\,\mu MN\ day^{-1}$$

In this way we obtained the Nitrogen profile in figure 71.

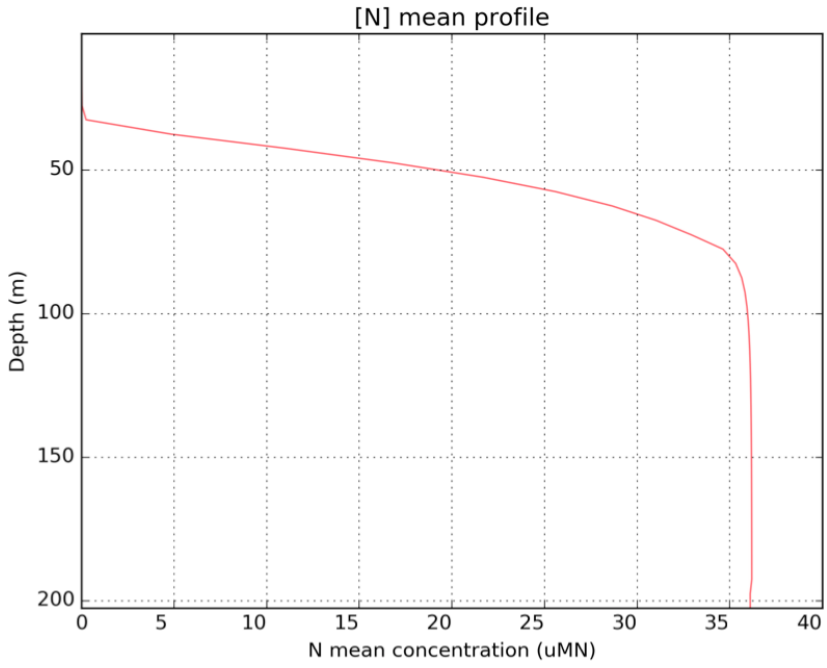


**Figure 71: Nitrogen mean depth profile, obtained with an "extra" horizontal supply in each layer (details in the text).**

This profile of nutrient is well known, with N increasing with depth. It has a nutricline (i.e. region where N concentration gradient starts becoming intense) at about 30 m of depth. This behavior for nutrient profiles is reasonable and makes sense for a water column, as it is generally thought that the largest nutrient concentrations are in the deepest part of the column.

The depth profile we obtain for phytoplankton (fig. 72) shows a “shallow” DBM (about 30 m deep), proving that 1-D SPLAS is able to reproduce this kind of feature when light is included; again, even if our aim is not to reproduce real oceanic patterns, at least we are glad that our model, when extended to a water column model with a light irradiance profile, reproduces a biomass pattern with a deep maximum, rather than having a strange or nonsense behavior that we are not able to explain. Instead, we can simply explain this behavior with the well-known trade-off between nutrient concentration (largest in the deep part of the water column) and light irradiance (largest in the shallow part of the water column).

The bulk of phytoplankton biomass is concentrated above the depth of about 100 m (Figure 72), which is also the point where the total net growth rate of the population becomes zero (not shown). After that point the community has an exponential decay (net growth rate < 0) and we can only see an average population biomass slightly larger than zero (because of the initial transient from the initial value to zero).

This result is somehow in line with our plan towards growing complexity: we started from a simple 0-D box model and validated it, and now we are trying to complicate the picture adding many layers and building a water column model. In this framework we are testing the water column model to see if it gives reasonable results (even if not validated) and we will try to discuss the implications of adding new building blocks to the representation.

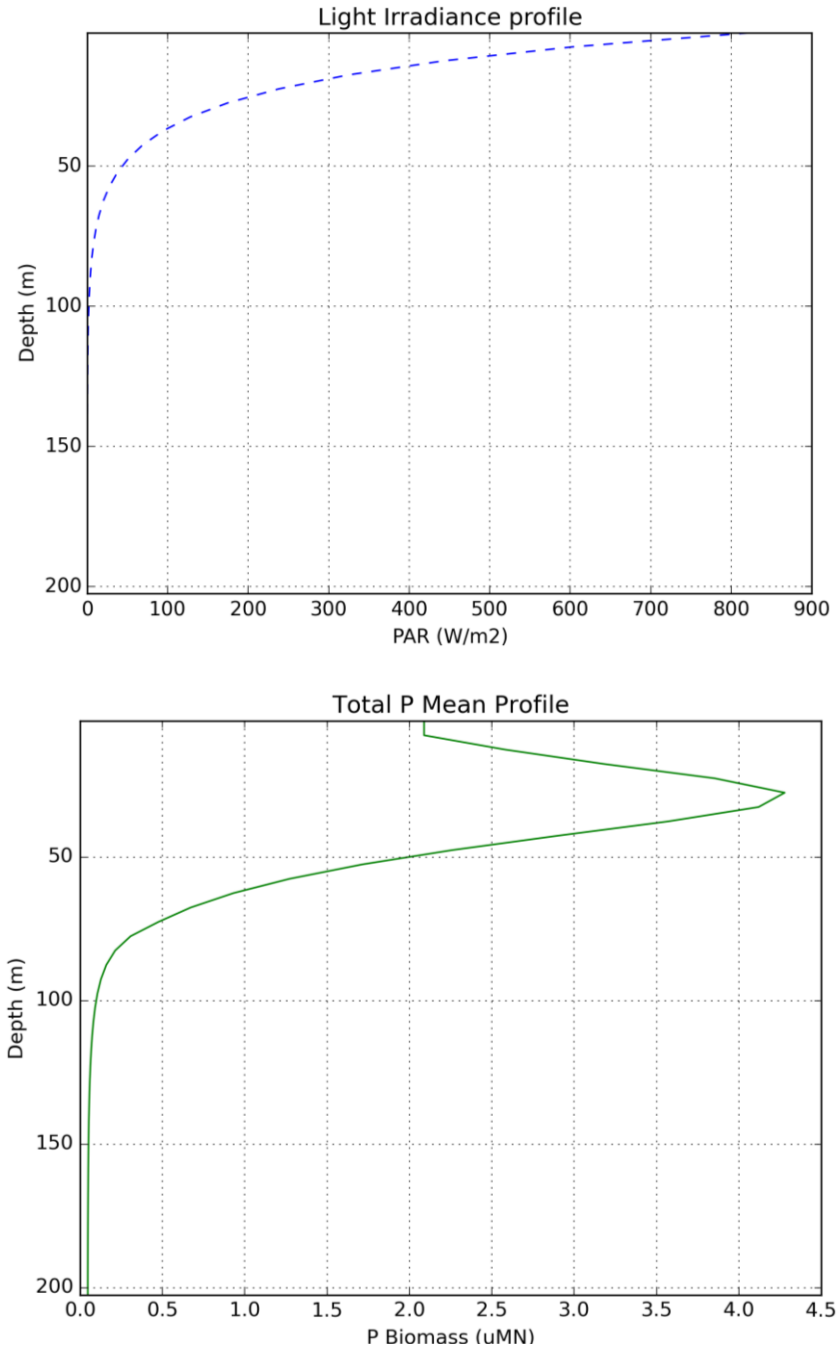


**Figure 72: Top: Light irradiance profile. Bottom: Total Phytoplankton Biomass mean depth profile. The DBM is visible at a depth of about 30 m.**

For what concerns zooplankton population profile, it simply resembles the one of phytoplankton (figure 73, compare to fig. 72): this seems logical, being phytoplankton their only resource. At almost the same depth we can see a deep biomass maximum for the grazers' population (fig. 73) that reflects the DBM in phytoplankton depth profile.

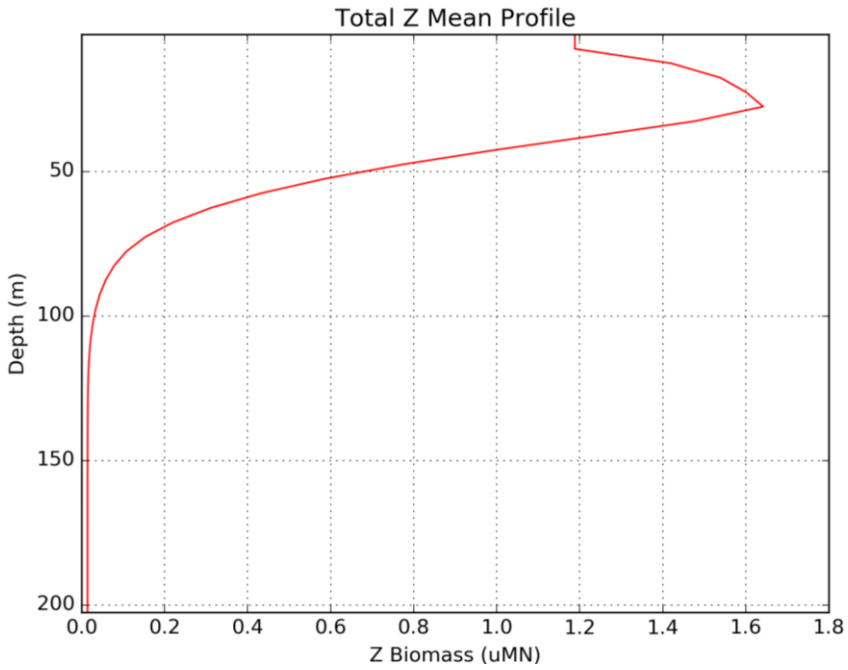


**Figure 73: Total Zooplankton Biomass mean depth profile. This profile resembles phytoplankton depth profile: a deep biomass maximum is visible at the same depth as the DCM in phytoplankton (about 30m, see also fig. 72 for comparison).**

If we were to pursue realism and reproduce real patterns, a necessary successive step would be to consider the effect of temperature on growth, but before two reflections must be outlined: first, if we took the data from the same profile for consistence (lovbio015c, 18/03/2015) we would get an almost constant temperature in the first 300 meters (around 13.5 °C, between 14°C on surface and 13°C deep down in the water column), and thus the effect on growth is only a rescaling of all plankton rates from "optimal" to suboptimal (if we assume an Arrhenius temperature dependence with $T_{ref}$ = 20°C). The qualitative features so far discussed do not change with this rescaling, except a decreased overall growth associated to a lower total biomass.

At the end of this thesis, thanks to the sensitivity analysis we will have an idea of how results vary changing the growth rate (variations of the order 10% in growth rate can mimic variations of few degrees); therefore, in virtue of all these considerations for the moment we do not consider the effect of temperature on P growth, limiting our treatment to how Nitrogen and Light affect growth rates.

Further, the aim is not realism here, rather we want to focus on a more theoretical subject: let us now have a look at the plankton size-structure associated with the profile in figure 72-73, and try to focus on patterns of size-diversity in this virtual environment.

### *4.4 Analysis of vertical phytoplankton size-structure*

Phytoplankton average size-structure (against depth) is shown in figure 74, related to the profile in figure 72. The layers below 100 m are not shown for clarity of the plot, since below that depth biomass is negligible. We immediately see that in this case homogeneity of size-structure with depth is not present, as for instance it occurs without light (in figure 75size-structure in the same configuration but without light dependence, and in figures at the beginning of chapter 4two example plots). So the most important effect of light is to break depth-homogeneity, somehow working against diffusivity. Moreover, we observe that the DBM is made up mostly of phytoplankton in the size-class around 56 µm (see red spots around 30 m depth in figure 74).

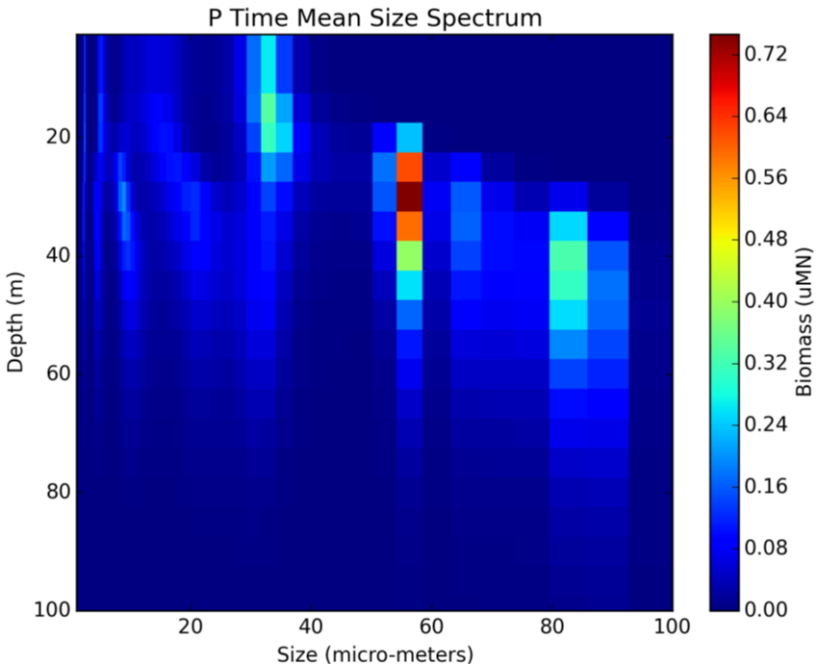


**Figure 74: Phytoplankton time mean size-spectrum against depth. Depth-homogeneity is broken by the inclusion of light dependent phytoplankton growth rate. At 30 m the red spots correspond to the biomass peak (DBM) in figure 72.**

These two results are in contrast: without light we obtained homogeneous size-structures with depth and profiles without DBM, with biomass monotonically increasing with depth. Instead, adding light this homogeneity is broken, and also we do not observe biomass increasing with depth, rather it reaches a maximum and then slowly approaches zero in the deepest layers of the water column.

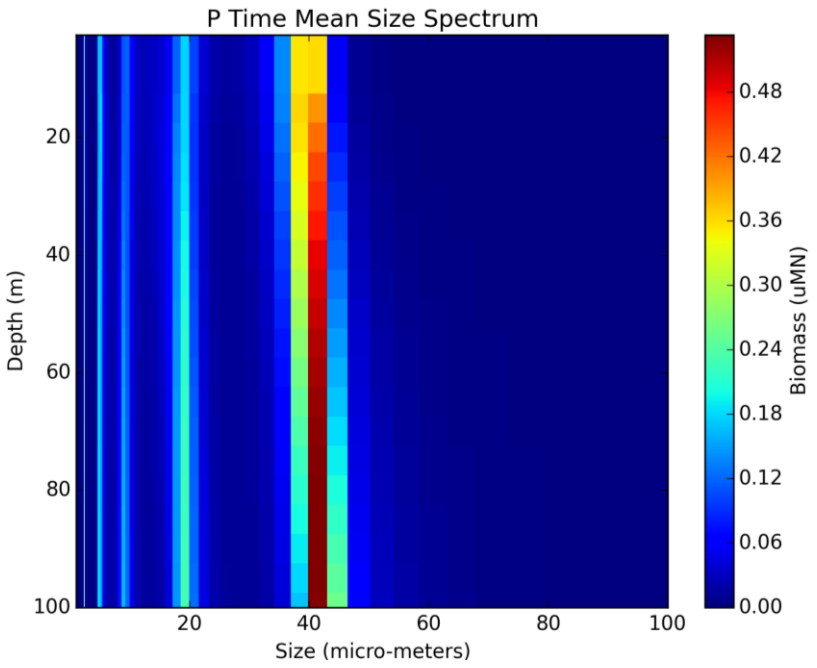


**Figure 75: Phytoplankton time mean size-spectrum against depth, without light dependent phytoplankton growth rate. In this case there is no light limitation to phytoplankton growth, and population can grow without limits also in depth. In this case in fact total biomass increases with depth and no DBM is present.**

Even if the effect of light could be neglected when considering a 0-D model or considering a shallow column, as for example the uppermost 20 meters (in figure 76 a detail of figure 74) we highlight that, when we consider 100-200 m of depth, light effects become important and cannot be neglected. In this case of extended depth the dynamics obtained with and without light is completely different and neglecting light produces huge deviations from a reasonable behavior (in particular unrealistically high biomasses at large depths >100m and no DBM, see also fig. 78).

With the complication of light and extended depth, SPLAS shows coherent results catching the DBM in depth-inhomogeneous size-structure, nonetheless giving reasonable results for N profile as we saw in the earlier section.

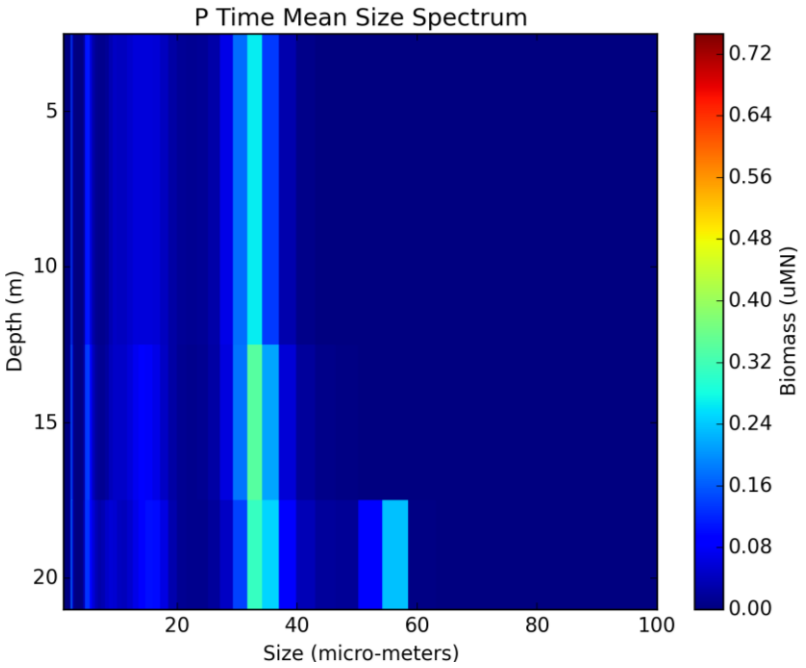


**Figure 76: Detail of figure 74. Size-structure is almost homogeneous except for a peak around 56 µm in the depth range 17-20 m.**

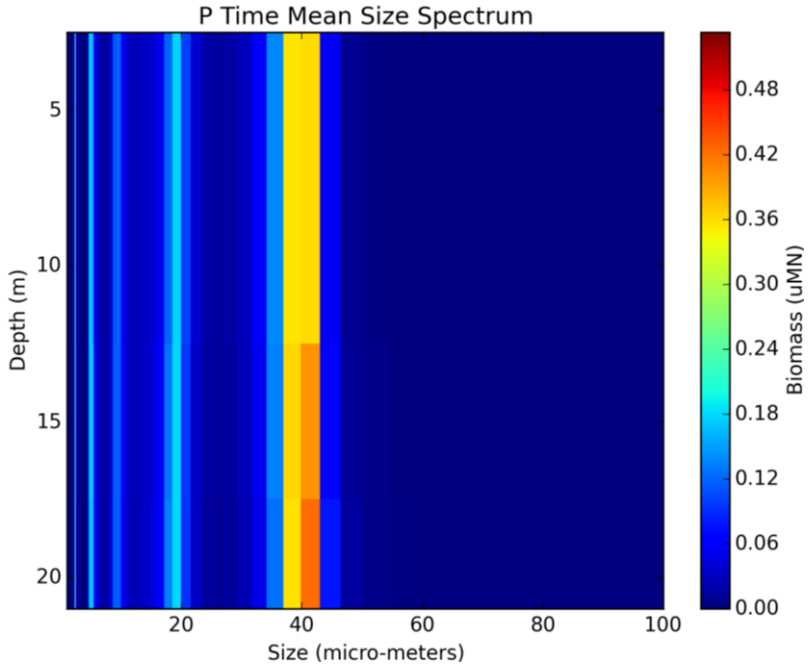


**Figure 77: Size-structure in the upper 20 meters without light in the environment, detail of figure 75. The size-structure differs from previous figure and appears homogeneous. Moreover, biomass increases with depth.**

The size-spectra in the first 20 m look almost similar (fig. 76-77), but the one in figure 76 is not fully homogeneous, unlike the spectrum obtained without light (fig 77). So, *we obtain quite different size-structures with and without light*: for example, in fig. 76 at the depth of almost 20 m there is a peak at 56 microns that is not present in fig.77, and the latter size-spectrum is shifted a bit toward larger size-classes with respect to other stripes in the former plot. The spectra may be considered almost similar, but the fact that in environments deeper than 15-20 m the biomass of the system is increased through the addition of a novel larger size-class, rather than an increase in the already present classes, is a brand new feature for our implementation coming from the depth-dependent growth rate in phytoplankton: this is a fundamental difference from the no-light "homogeneous" case. Moreover, the space among stripes appears fuzzier in fig. 76, while in fig. 77 the stripes appear more delineated.

All of this is to just to say that we could have neglected light if we considered a shallow column, at the cost of committing some sort of "error" but still obtaining a sensible behavior; but if we are to make experiments in a water column of 200 m we shall include light in P growth if we want a reasonable behavior for plankton biomass patterns and size-spectra.

What we want to highlight the most here is that the inclusion of light in the environment determines a water column populated heterogeneously by different size-classes, forming hot spots at various depths, with larger organisms preferring the deepest part of the column and smaller cells living on the surface layers (figure 74); at depths larger than the DBM depth phytoplankton biomass decreases with depth, eventually going close to zero. On the contrary, without light(or depth-dependence in growth) there is no actual factor distinguishing the surface from the deeper layers (except from Nitrogen) and this is why size-spectrum in this case is homogeneous in depth and, in absence of light limitation, biomass follows N concentration and increases with depth (fig. 75 and 78, right).

If we consider only the uppermost layers (up to 10-20 meters) we could still get a reasonable dynamics without light, but as we go deeper and deeper, dynamics changes completely and results are radically different with and without light (comparison in fig. 78).

Trying to summarize this part, as we anticipated ***"light breaks the depth-homogeneity"*** and somehow destroys the vertical isotropy with consequences on the full water column size-spectrum, that becomes an assembly of hot spots at different depths (fig. 74) and on biomass profile, which shows a DBM (fig. 72 and 78). We clearly see the differences enunciated above in fig. 78: without light and considering the whole water column of 200 m we get an unfeasible behavior, as biomass increases with depth.

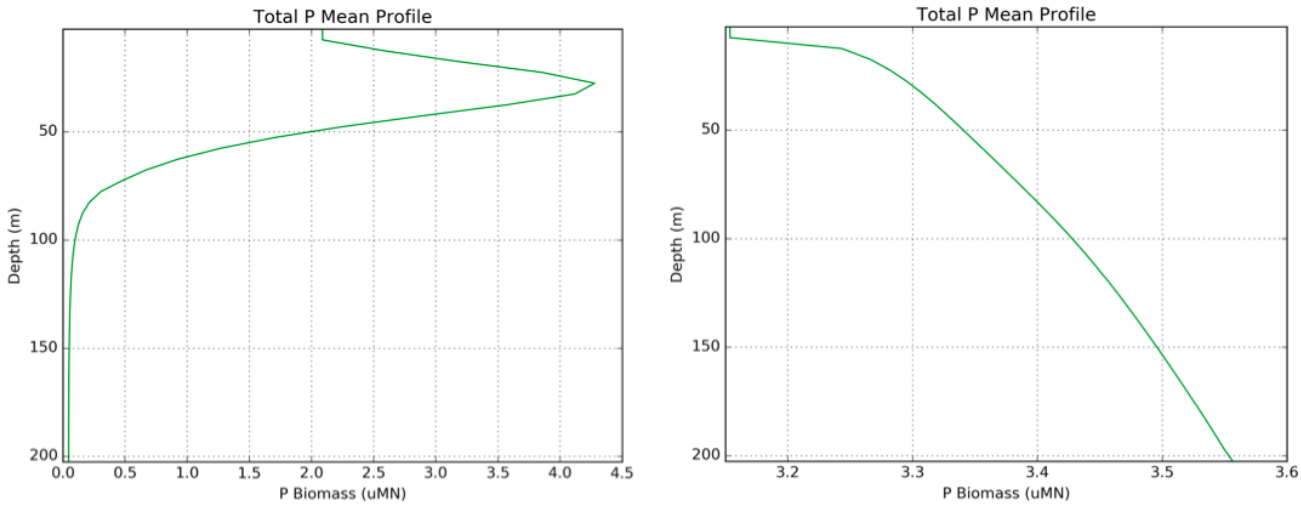


**Figure 78: Total mean phytoplankton biomass depth profile with light (left) and without light (right). The dynamics is completely different between the two cases: biomass is increasing with depth indefinitely in the right panel, while in the left panel a DBM can be seen and an exponential decay at large depths. Phytoplankton biomass at large depths (hundreds meters) in real systems cannot grow like in the right panel, and this is why one must always consider the effect of light in the water column when resolving such large depths.**

We could never have obtained different winning size-classes at different depths without something that gave some kind of "order" to the z-coordinate, differentiating the P growth in each layer. Having a series of communicating layer one above the other without a real z-dependence does not allow for different winners (while the "communication" through sinking and diffusion allows for the exchange of biomass).This is almost equivalent to have several almost identical 0-D boxes (figure 79). Instead, by adding light we could differentiate winners in each layer (figure 80).

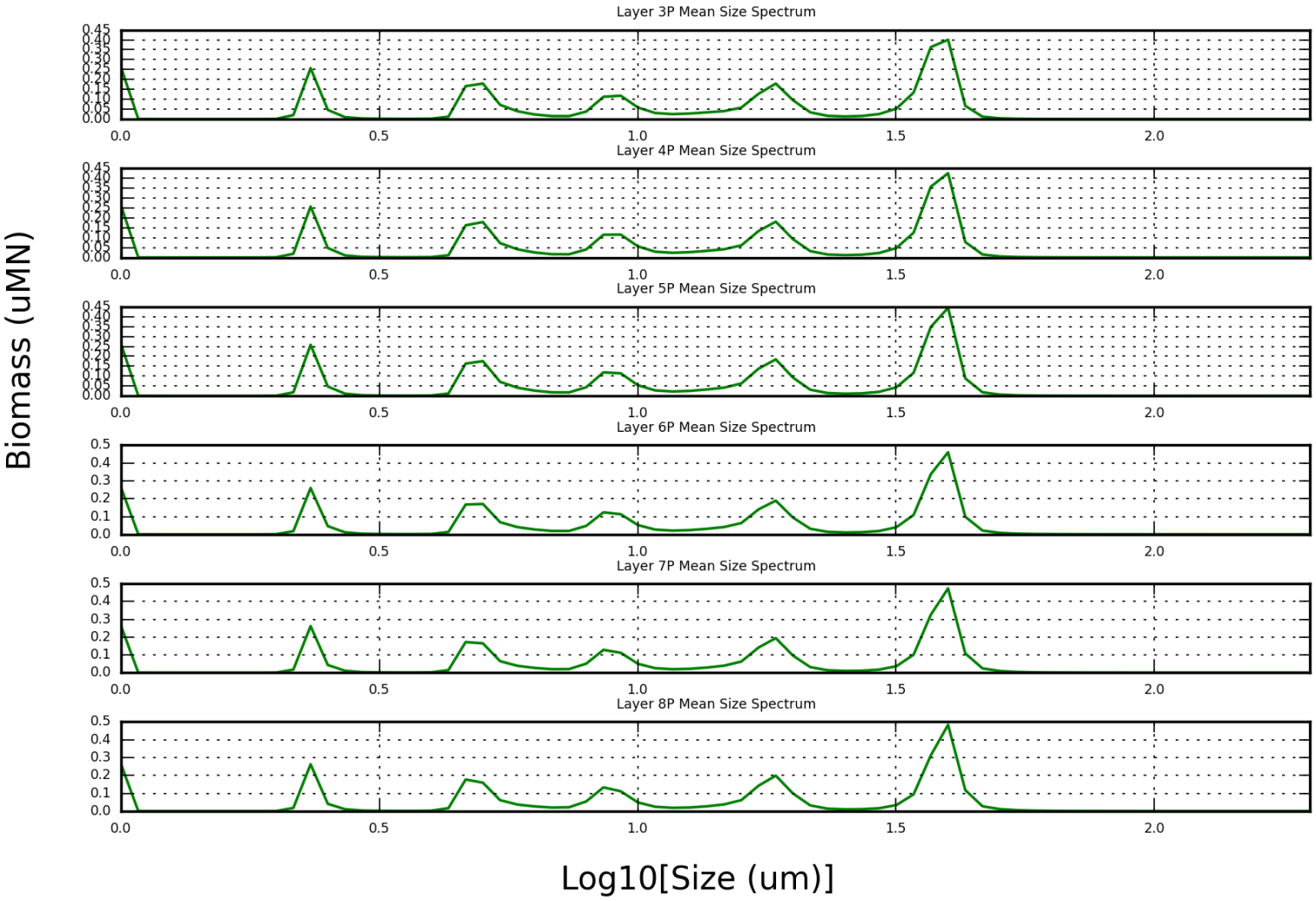


**Figure 79:Phytoplankton size-spectra from the 3rd to the 8th layer (respectively from 12.5 m to 37.5 m depth) obtained without light dependence. Size-spectra are almost identical, except biomass slightly increasing going deeper (notice the scale on y axis).**

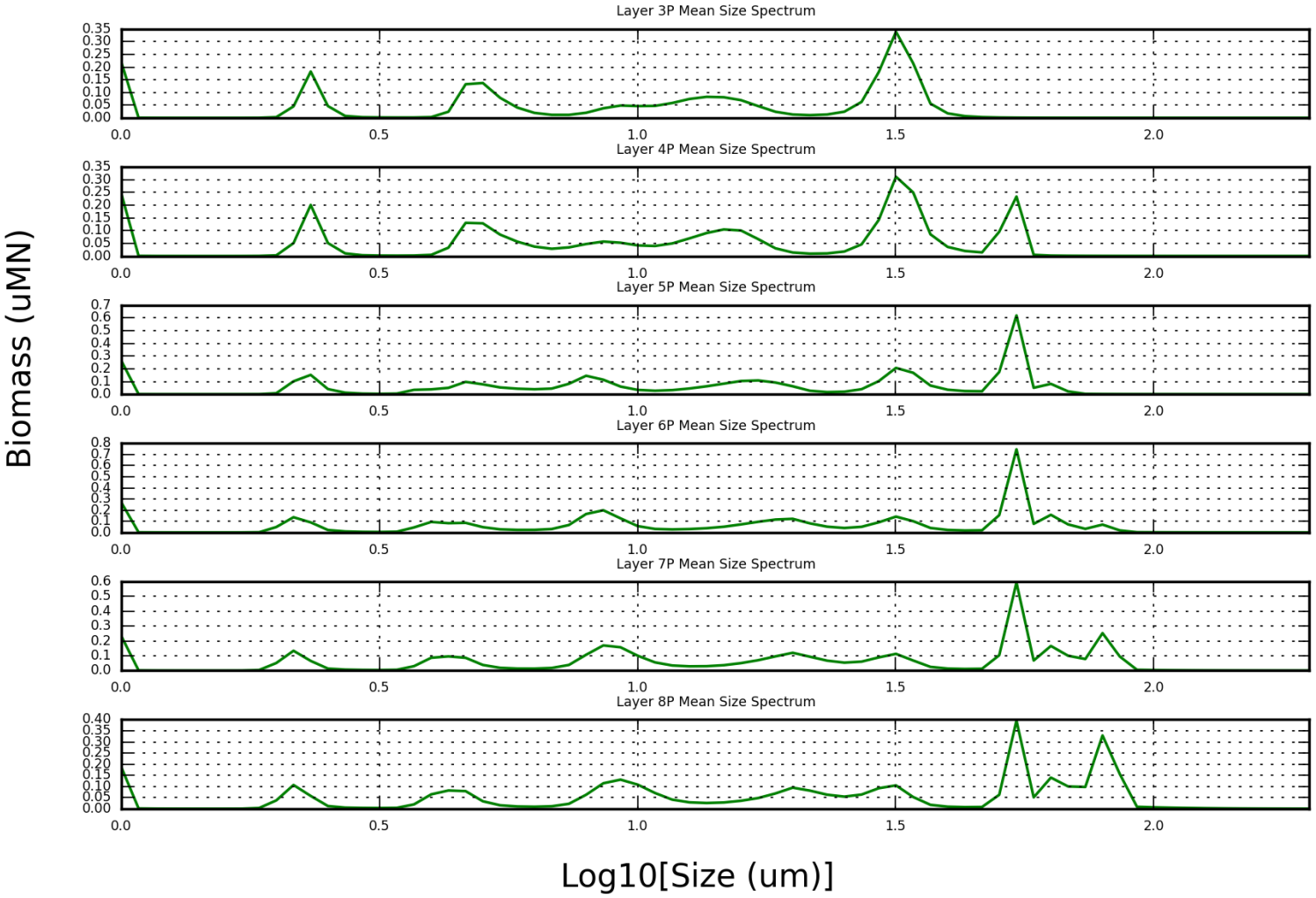


**Figure 80: Phytoplankton size-spectra from the 3rd to the 8th layer (respectively from 12.5 m to 37.5 m depth) obtained including light dependence. Size-spectra look different in each layer, with winners shifting to the right as we go deeper. Notice that also the biomass at the very top layers (3rd, 4th, 5th) is increasing with depth, reaches the maximum in the 6th layer and then decreases again (scale of the y axis). This resembles total biomass profile and the DBM formation (fig. 72).**

### *4.5 Tests on various light profiles*

Considering the role played by light, we chose to modify the light profiles and see how they influence phytoplankton.

In particular, we investigate how the DBM reacts to changes in light parameters, especially extinction constant, and what happens when we use another parameterization of the Photosynthetically Active Radiation (PAR) (I(z) in practice) with the inclusion of self-shading. We will see how DBM depth is regulated by these parameters/processes. This is a further exploration of the 1-D model now that we have set another key feature inside SPLAS (that is light).

As expected, the vertical profile of phytoplankton is sensitive to changes in the light extinction constant, in particular the coefficient $k_d$ regulates the depth of the DBM: when $k_d$ is diminished water becomes more transparent and the depth of the maximum biomass increases, and vice-versa. When the maximum occurs at larger depth it is also increased in "intensity" with respect to shallower DBMs (figure 81). This is reasonable as going deeper in the water column means finding more nutrients (N) available for growth.

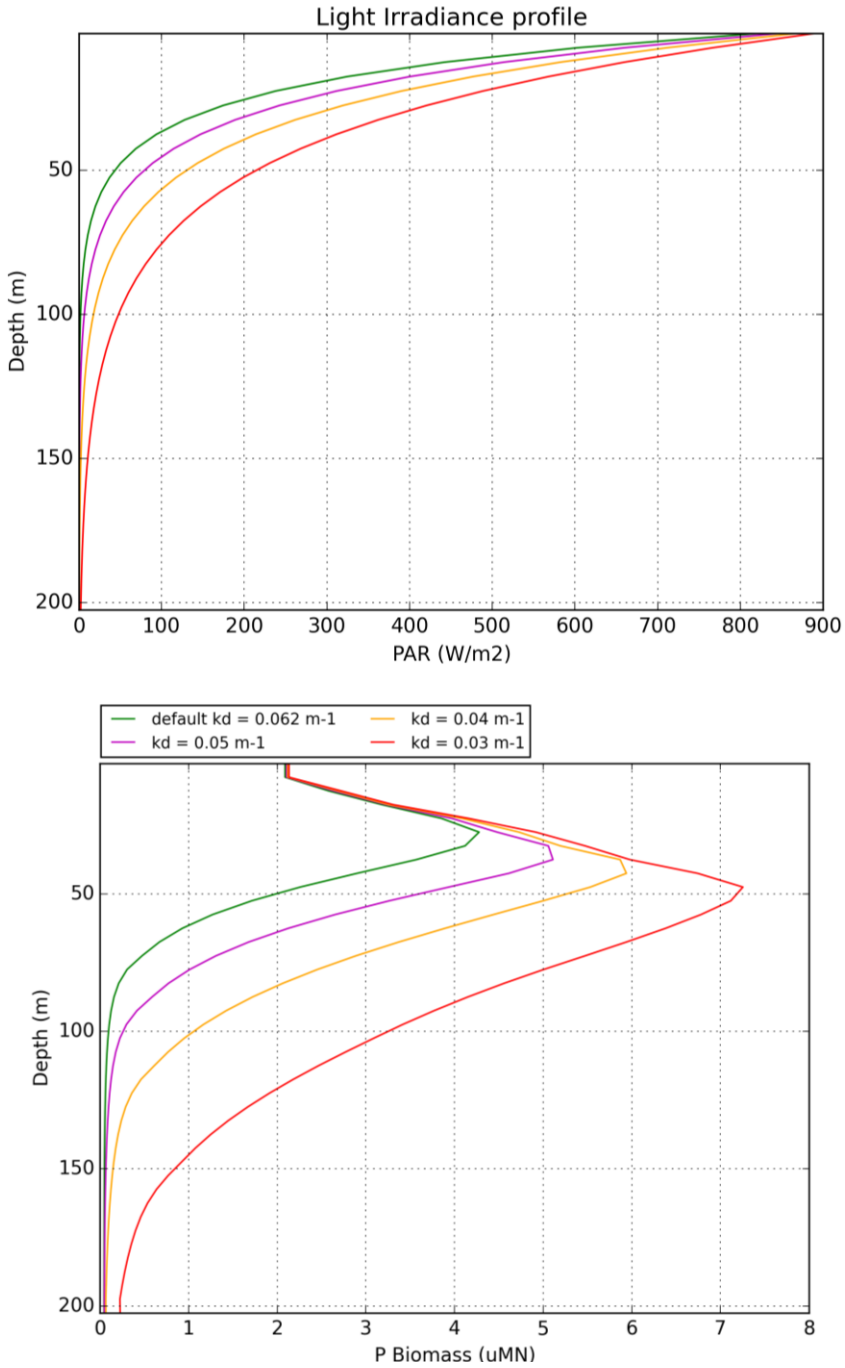


**Figure 81:Top: Light irradiance profile varying extinction constant. Bottom: Total mean phytoplankton biomass depth profile with varying light extinction coefficient $k_d$ (green line default value 0.062 $m^{-1}$, purple line 0.05 $m^{-1}$, orange line 0.04 $m^{-1}$, red line 0.03 $m^{-1}$).**

Accordingly, also Zooplankton biomass maximum is shifted downward and is intensified as $k_d$ is decreased (results not shown). Similarly, Nitrogen vertical profile is shifted downward, i.e. the nutricline is moved at larger depths (figure 82, detail of N profiles) because of consumption by phytoplankton.

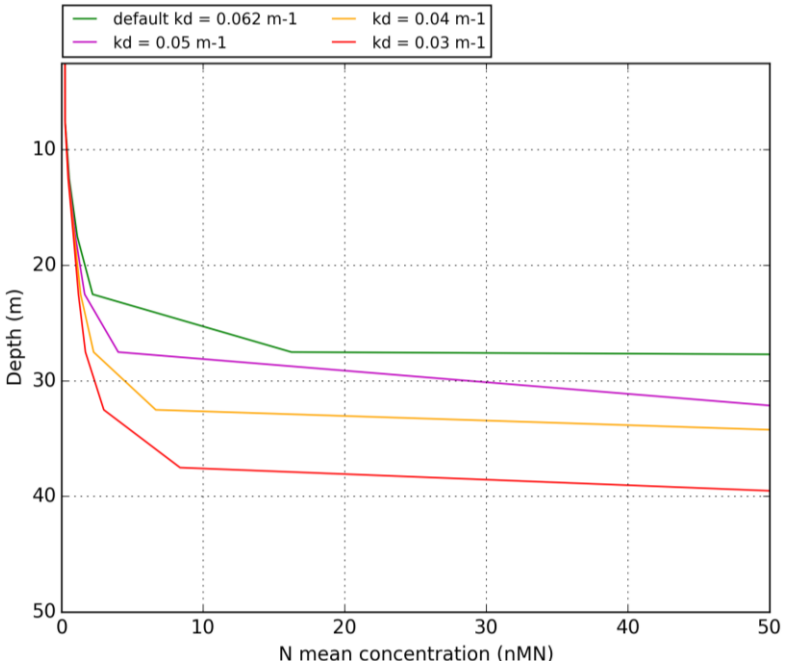


**Figure82: Nitrogen mean depth profile (for the first 50 m) with varying light extinction coefficient $k_d$(as in previous figure). For the first 20 m the N profiles are basically the same, with N concentration almost constant with depth. Then, the depth at which N concentration gradient starts becoming intense (nutricline) varies according to $k_d$: shallower for $k_d$ = 0.062 $m^{-1}$ (around 22 m, green line), diminishes with $k_d$ and becomes about 33 m for kd = 0.03 $m^{-1}$ (red line).**

**With this simple experiment we can conclude that the biomass/concentration profiles represented by the SPLAS 1-D react coherently to changes in the light extinction constant: the depth of the DBM and the nutricline increase with decreasing light extinction, that is with more light penetrating into the water column, deeper environment (with more N) become favorable for growth of phytoplankton and consequently zooplankton.** Thanks to the presence of more nutrients in-depth, the maxima become also more intense but then as phytoplankton shape N profile the nutricline gets deeper.

As light extinction constant is decreased the phytoplankton size-structure pattern is modified accordingly: the biomass blooms are moved deeper in the water column and are more intense (compare figure 83, obtained with $k_d$ = 0.04 $m^{-1}$, with figure 74). This is in line with a deeper DBM formation when light penetrates more into the 1-D structure.

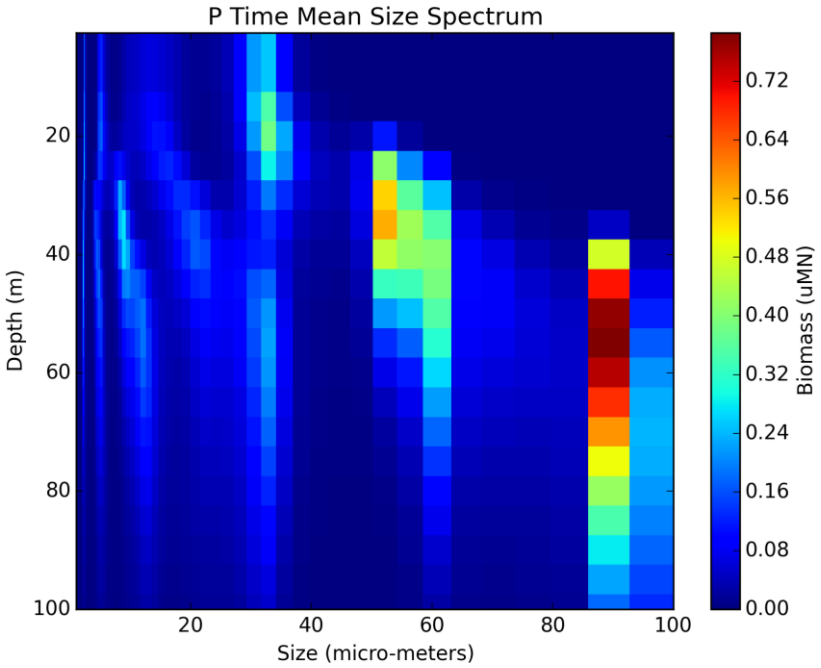


**Figure 83: Phytoplankton time mean size-spectrum against depth for $k_d$ = 0.04 $m^{-1}$. The pattern is the same as in fig. 74, but in this case as a consequence of the reduced $k_d$ the high biomass bloom of large-sizes is more intense and moved slightly deeper in the water column.**

### *4.5.1 Phytoplankton self-shading*

In the following we examine a change in light parameterization as well, introducing phytoplankton self-shading.

The depth profiles represented by SPLAS react coherently also to changes in the parameterization of I(z), for example when phytoplankton self-shading is included.

We substitute I(z) of previous section with:

$$I(z) = I_0 \cdot exp\left[-k_w z - k_p \int_0^z \sum_i P_i(\xi) d\xi\right]$$

maintaining the same value for $I_0$ and considering two values for the background (pure water) extinction constant $k_w$(0.05 and 0.03 $m^{-1}$) and phytoplankton self shading constant $k_p$ (0.02 and 0.01 $m^{-1}$µMN); the first two values of the two constants, respectively, are taken from Oguz et al.(2013) while the other two are obtained via tuning to SPLAS. Results of the two experiments, compared to the default case of previous section, are shown in figure 84.

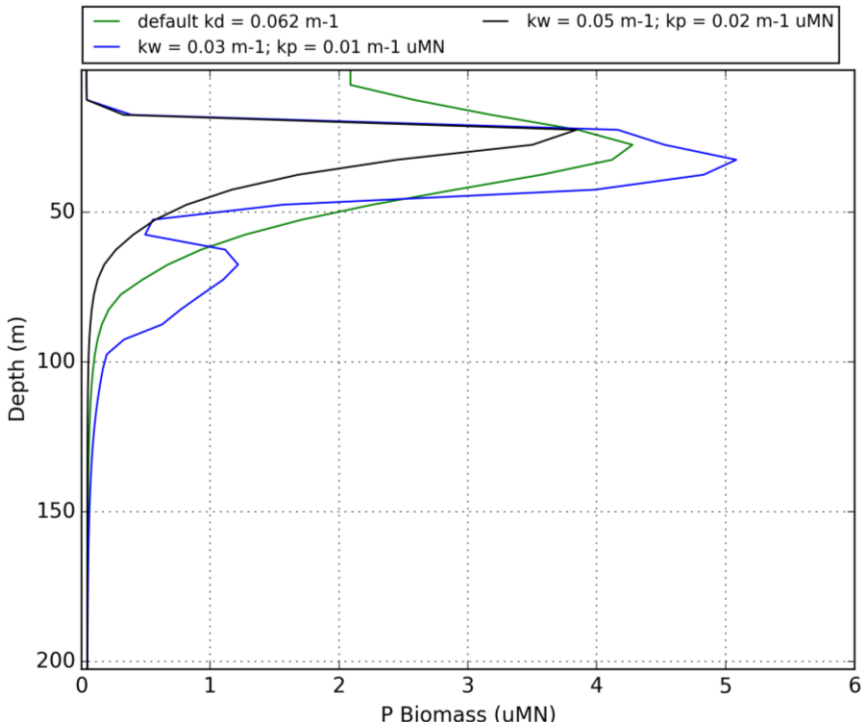


**Figure 84: Total mean phytoplankton biomass depth profile with self-shading (black line kw = 0.05 $m^{-1}$ and kp = 0.02 $m^{-1}$ µMN from Oguz et al., 2013; blue line kw =0.03 $m^{-1}$ and kp = 0.01 $m^{-1}$µMN adaptation to SPLAS) compared to default profile of previous section ($k_d$ = 0.062 $m^{-1}$).**

With the inclusion of a "strong" self-shading (as in Oguz et al., 2013, black line in figure 59) we see that the DBM is shifted higher in the water column and is also reduced in intensity (lower biomass). This is somehow equivalent to increase the $k_d$ of the previous section, except that biomass at the surface is highly reduced with respect to the default case (green line in fig. 84).

If we reduce both background extinction of light and self-shading (blue line in figure 84) we see that the DBM is slightly lowered at 35 meters and increases in intensity (as if we decreased the $k_d$ of the previous section, but again with a strong reduction of biomass in the first meters). Interestingly, after the "shadow" region in the water column right under the DBM, where biomass decreases with depth (down to 50-60 m), at a certain point another biomass peak appears (at about 75 m). We obtain two distinct peaks in the phytoplankton biomass profile, one at a depth of 35 m (the DBM, more intense in biomass) and the second, less intense, at a depth of 75 m. This second peak may be due to the introduction of a self-shading term in I(z) and cannot be obtained with the simpler $k_d$ representation of previous section. In fact, right deeper than the DCM there isa region where phytoplankton cannot grow much because it is shaded by upper and more populated layers (region between 40-60 m of depth). Beyond this oligotrophic layer, phytoplankton living around there (about 70 m) are not excessively shaded by the poorly populated layers above them(and so they are not limited by light), and may be able to moderately grow with the light available at those depths. We hypothesize that this is a phenomenon due to self-shading and is a concentration-

dependent mechanism, which is not achievable by means of the other simplified and aggregated $k_d$-representation of I(z). Anyway other explanations may be possible.

Notice that size-structure with self-shading is quite different from previous cases (see figure 85-86) and varies a lot with the choice of self-shading parameters. In the first case (black line in fig. 84) the bulk of the biomass is concentrated around the DBM depth and almost no biomass is present in the upper layers (fig. 85). The stripes corresponding to the different winner sizes are located at more or less the same depth.

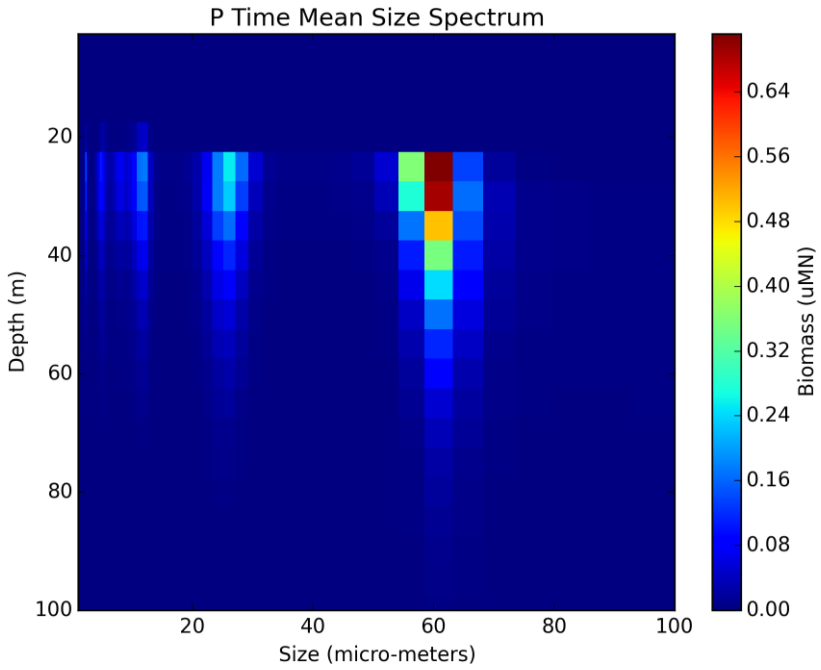


**Figure85: Phytoplankton time mean size-spectrum against depth with inclusion of self-shading (Oguz et al., 2013). The pattern is different from fig. 74. Very low biomass is present at shallow depths, while the largest biomass is concentrated at the DBM depth.**

In the second case (blue line in fig. 84) winners are different from previous case and also from default case in fig. 74, and a second deeper peak can clearly be seen (fig. 86). Again a very low biomass is present at shallow depths.

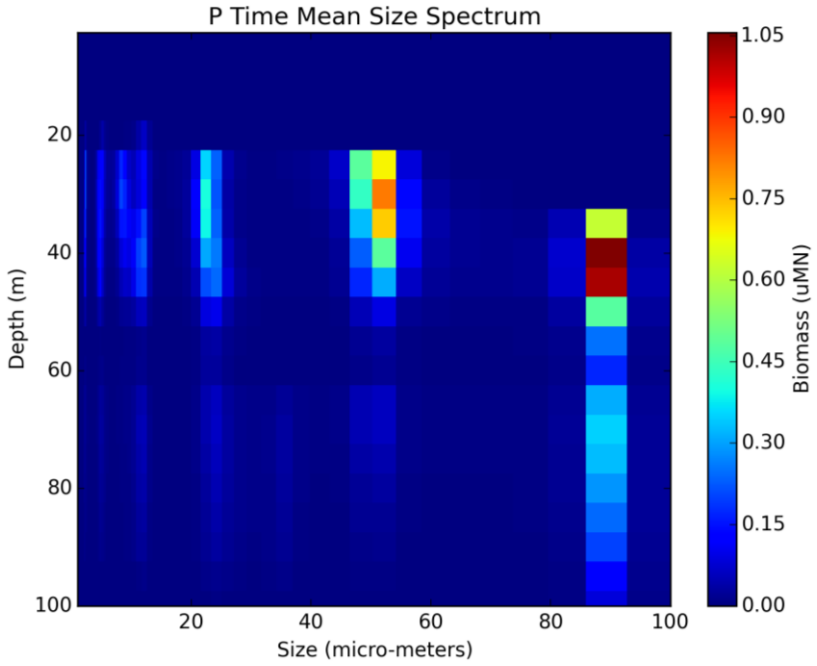


**Figure 86:Phytoplankton time mean size-spectrum against depth with inclusion of self-shading (tuned for SPLAS). The pattern is different from both previous figure (except the small biomass in the top layers) and fig. 74. A second deeper peak can clearly be seen especially at large sizes (90 microns).**

Thus, with the introduction of self-shading the size-spectrum is very sensitive to changes in self-shading parameters: there can be two peaks in total biomass and winner sizes may vary a lot.

In field measurements, multiple peaks are often present in phytoplankton biomass depth-profile, decreasing in intensity as we go deeper (Ryabov & Blasius, 2011); in fact if we analyze chlorophyll data from Bio Argo Float lovbio015c (same profile 18/03/2015), two peaks can be seen in the first 200 m, even more going further down in the water column. Therefore in the future SPLAS may be able to represent multi-modal profiles if a self-shading term with suitable values of the constant is introduced. This is the reason why the blue line profile in fig. 84 may be seen as an important result that further enlightens the potential of SPLAS. Clearly, seen only in this context this result is not particularly significant, but further investigation on this kind of light parameterization may be worth it in the future, especially for understanding the consequences on size-structure.

**With the inclusion of light and phytoplankton self-shading we saw that SPLAS behaves in a sensible and consistent way and gives reasonable results, that may be seen as a starting point to make SPLAS able to reproduce the behavior of real systems(in the long term).** If SPLAS had a non-sense behavior at this point, giving unexplainable and unreasonable outcomes, for sure it would not be worth to try add complexity in the future.

### *4.6 Testing depth-dependent Eddy Diffusivity*

We added light and saw that it has important implications on 1-D phytoplankton size-structure, and also light is a necessary thing to take into account if we wish for a sensible behavior of the model.

To conclude our set of 1-D experiments we relax the hypothesis of constant diffusion coefficient throughout the water column and analyze what happens in SPLAS 1-D (in particular to the DBM of phytoplankton) when diffusion varies with depth: the value $10^{-4}$ $m^2$ $s^{-1}$ is a typical value in the ocean, not representative of any specific case. Up to this section we only considered a unique constant value throughout the water column for all our simulations. We consider now different values of diffusivity at different depths: we start with some tests on how phytoplankton biomass profile varies considering different step-wise functions for vertical diffusivity.

For the moment we neglect in all equations the terms like

$$\frac{\partial D}{\partial z} \cdot \frac{\partial B}{\partial z}$$

where B stays for each of the 4 state variables (P biomass, Z biomass, N concentration, OM concentration). This term arises from the depth variability of diffusion coefficient D. Since D(z) in this test is a stepwise function (fig. 87), its gradient is a “multiple” Dirac-delta centered in the discontinuity points, and zero in all other points in the water column. We now simply do not consider the “jump” in D and consider it as locally constant.

We consider the profiles in figure 87 constant in time. The profile in red in fig.87 is taken from Mukherjee & Tandon (2016) while the others are modulations of this profile, obtained moving up or down the discontinuities and the region of intense mixing (order $10^{-1}$ or $10^{-1.5}$ $m^2$ $s^{-1}$). This test is done in order to see how P biomass profile varies with variations of such intense mixing region.

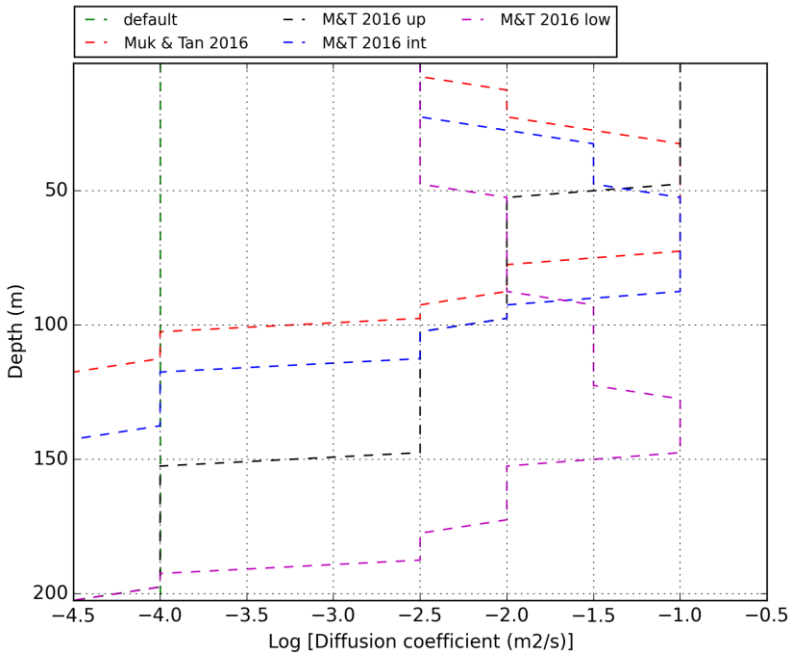


**Figure 87: Depth profiles of diffusion coefficient used in the experiment.**

For simplicity we maintained the formulation of light introduced at the beginning of previous section with the same values for the constants (i.e. simple exponential formulation without self-shading of phytoplankton).

Results for biomass profiles are shown in figure 88.

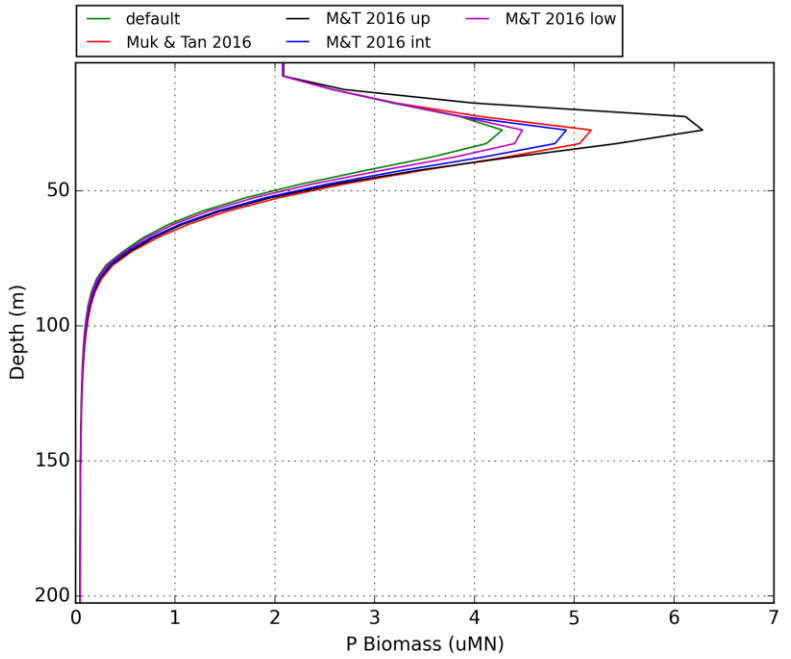


**Figure 88: Phytoplankton biomass profiles in response to diffusion profiles in previous figure (matching colors). The effect of the diffusivity profile depends on where the intense mixing layer is located in the water column.**

The presence of an intense mixing region around 50 m (red line in figure 87) brings more nutrient (N) to phytoplankton in those layers, and the maximum of biomass intensifies (red line in figure 88) with respect to the default constant diffusivity case (green line in figures 87 and 88).Lowering this intense mixing region (blue line in figure 87) has the effect of reducing the DBM with respect to the previous case, bringing less nutrients to phytoplankton at such shallow depths, while mixing in the lower part of the water column produces no net effect since biomass there is too low (due to light absence, blue line in figure 88).Anyway the biomass around the depth of the maximum is still increased with respect to the default case (green line).

Lowering further the mixing profile (purple line in figure 87) reduces even more the intensity of the biomass peak (purple line in figure 88). As we move deeper and deeper this region of intense diffusion, the P profile gets closer and closer to the default case.

On the contrary, raising the more intense mixing layer (black line in figure 87) brings even more N to phytoplankton in the upper layers and the maximum intensifies (black line in figure 88) both with respect to the default case (green line) and the first profile (red line). This is because the mixing layer in this case is all around the DBM (located at about 25 m depth), containing it, and from a phytoplankton reference view this is an optimal condition for growth (more N and enough light).

It is interesting to notice how P profile is pretty insensitive to where the “discontinuity points” are located in the diffusion profiles, but rather responds to where the “intense mixing” region is located in the water column (figure 89 and 90). Probably this occurs because we are neglecting the impact of discontinuities in the diffusion gradient. Anyhow, this *a priori* choice is justified by results at the end of the section.

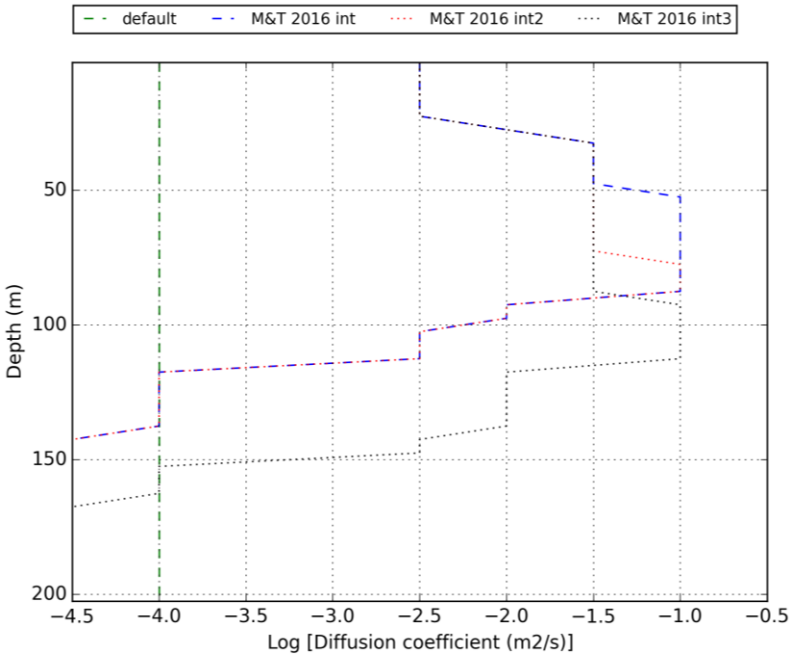


**Figure 89: Diffusion depth profiles with different discontinuity points.**

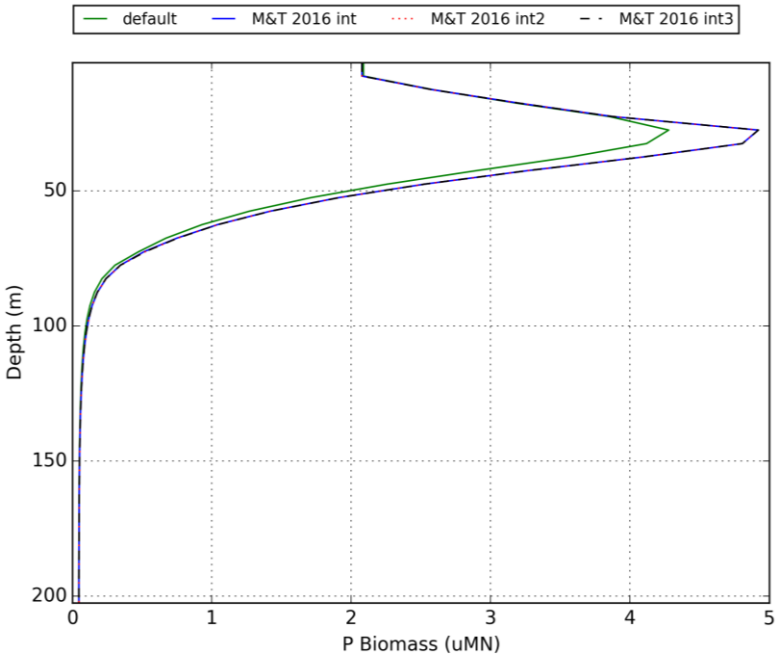


**Figure 90: Phytoplankton biomass profiles in response to diffusion profiles in previous figure (matching colors). The red dotted line and black dashed line cannot be seen clearly since they are overlapped to the blue line. The profiles are insensitive to where discontinuities are, responding instead to where the highest diffusivities are located in the water column.**

In summary, introducing an intense mixing layer in diffusivity profile produces an increase in P biomass in the upper layers (and in the DBM, with respect to the default constant profile) as long as this region is in the part of water column where phytoplankton grows thanks to light presence. Intense mixing in the lower part of the column produces no effects other than bringing less N to phytoplankton in the upper layers. In other words, strong mixing where light is absent and P biomass is very close to zero is useless to biomass profiles. Moreover, the phytoplankton biomass profile is pretty insensitive to where the discontinuities are in the diffusion profile, rather reacting to shift in the whole intense mixing region (at least in this case neglecting diffusion vertical gradients).

These results somewhat depend on the properties of light profile, therefore we perform the same experiment but with a much lower extinction constant: $k_d = 0.03\ m^{-1}$.

The diffusivity profile is the same as earlier (in figure 87) and we obtain almost the same identical results as before (fig. 88) for phytoplankton biomass (see figure 91) except that this time, since the DBM is deeper because of more light penetrating into the water column (and more intense), the "raised" diffusivity profile (black line in figure 87) does not cause an increment of biomass. This happens because -unlike in the previous case (with $k_d = 0.062\ m^{-1}$)- the "intense mixing region" is away from the DBM and phytoplankton at that depth is not taking advantage anymore of the enhanced N. In this case (DBM at a depth of about 50 m) the optimal condition for phytoplankton growth is found with the first profile (red line in fig. 87) for which we see the maximum biomass (fig. 91).

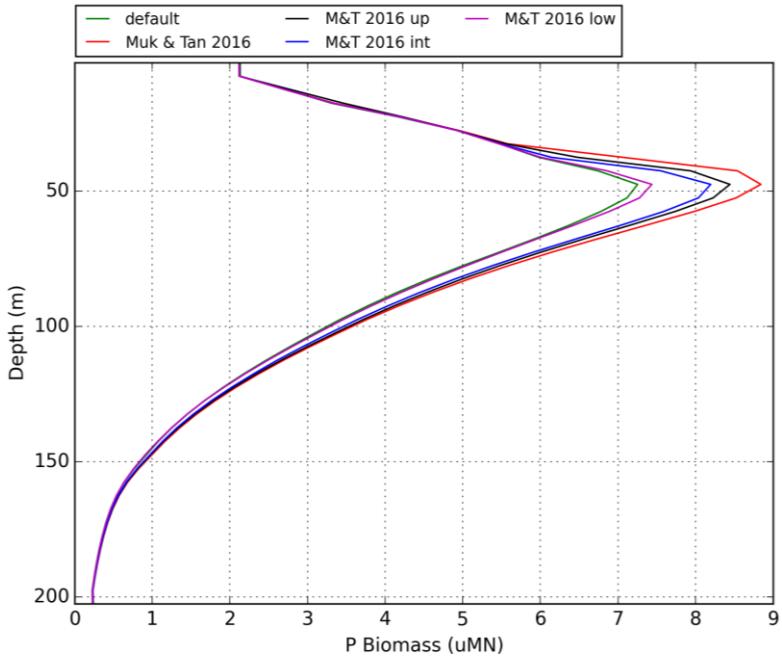


**Figure 91: Phytoplankton biomass profiles in response to diffusion profiles in figure 87 (matching colors). Light extinction constant is reduced to $k_d = 0.03\ m^{-1}$ and the DBM is located at around 50 m. With this $k_d$ diffusion profiles act differently with respect to the previous case.**

**In conclusion, a depth-varying diffusivity modifies to a certain extent phytoplankton biomass profile, in particular a strong mixing increases the intensity of the DBM when the intense mixing region is close to the DBM in depth. We observed that when the strong mixing region is located near the DBM, the peak is much larger in biomass with respect to a constant diffusivity, and larger with respect to the case when strong mixing is far from the DBM (the farther the mixing region, the smaller the peak).** Figure 92resumes these results, plotting phytoplankton biomass profiles in the two different cases of light and for constant diffusion along with depth-varying diffusion (the two cases that maximize DBM biomass in our experiments).The image is shown also for comparison between the cases $k_d$ = 0.062 $m^{-1}$ and $k_d$ = 0.03 $m^{-1}$.

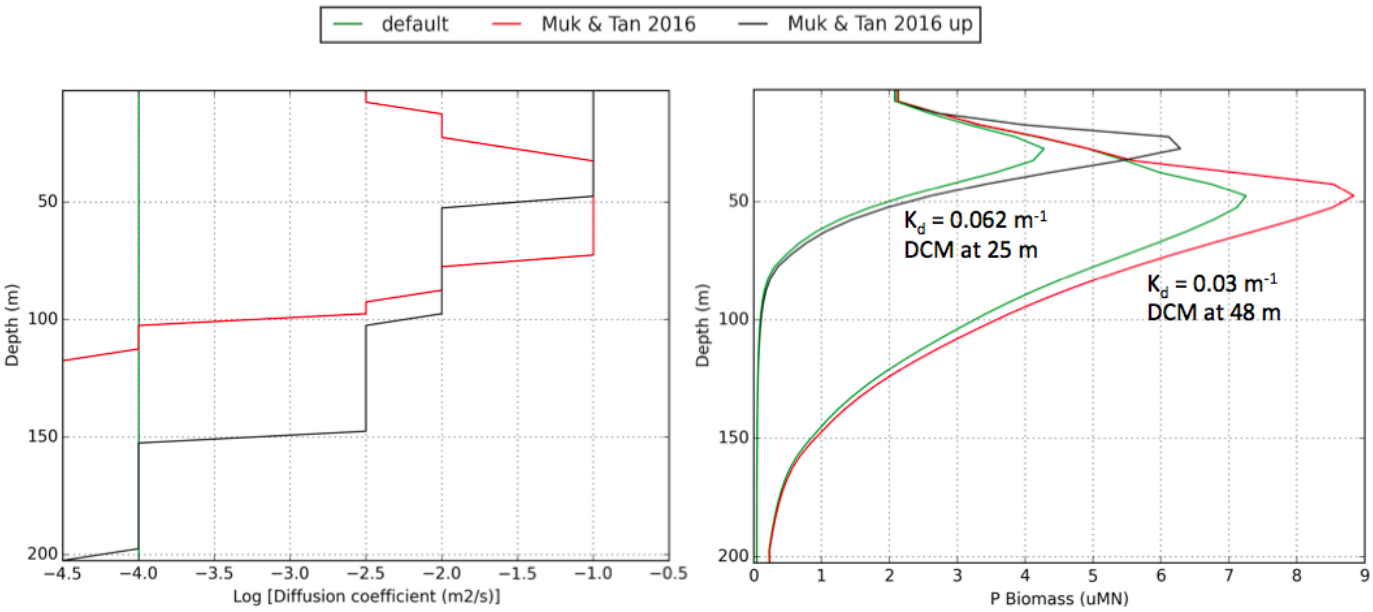


**Figure 92: Right: Phytoplankton biomass depth profile for the two different extinction constant, in the case of constant diffusion and depth-varying diffusion. Left: corresponding diffusion profile used. For each light extinction constant we used the depth-varying diffusion profiles that maximized the biomass peak.**

We did this test in order to quantify how much our phytoplankton biomass profile could change when a z-varying diffusion coefficient is included. It seemed to us a natural step forward after the road we have been travelling so far. It constitutes also a little step towards a more realistic representation.

It seems reasonable to us that intense mixing may change to a certain extent phytoplankton biomass, as diffusion acts concurrently with light to shape the vertical structure.

As a final consideration, we verify the correctness of our assumption of neglecting the diffusion vertical gradient in the equations: thus, we performed two simulations with the same diffusion profile where in one case we included the full diffusion term

$$\frac{\partial}{\partial z}\left(D\frac{\partial B}{\partial z}\right) = \frac{\partial D}{\partial z}\frac{\partial B}{\partial z} + D\frac{\partial^2 B}{\partial z^2}$$

where B stands for each of the state variables (P, Z, N, OM) and in the second case we solved the equations as usual considering only the 2nd z-derivative term.

We chose again a suitable step-wise function (based on Mukherjee & Tandon, 2016) and to account for the diffusivity gradient we interpolate the diffusion profile with a sigmoidal function, to avoid discontinuities and make the step function smoother. The diffusion profiles used are shown in figure 93. We always reference our results with respect to the constant diffusion profile ("default" case) and we quantify the discrepancies by analyzing the differences in P biomasses.

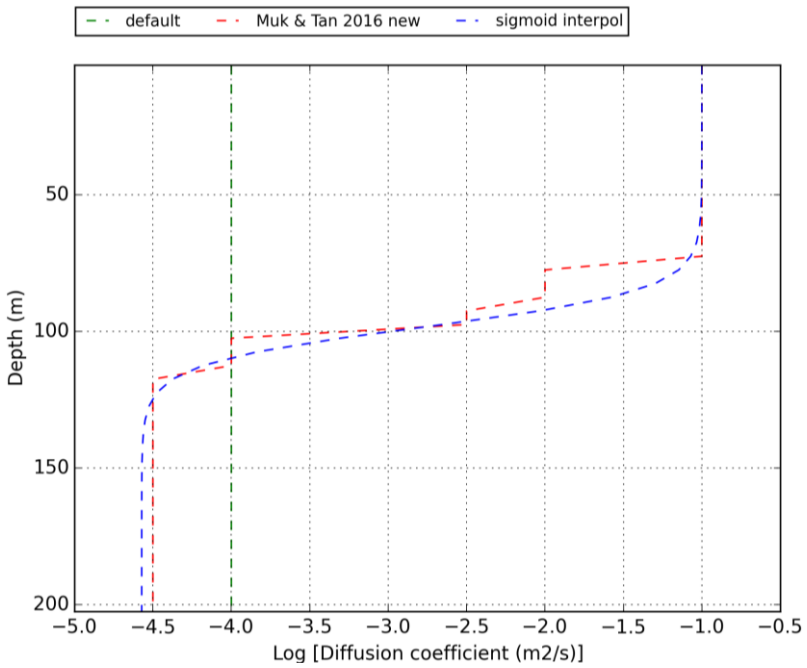


**Figure 93: Diffusion profiles used to test the relative importance of diffusion gradient in the equations. To account for the diffusivity gradient we used an interpolated profile.**

We observe that for the diffusivity profiles in figure 93 the differences in P biomasses are nearly null (fig. 94 red and blue lines) and thus the error committed by neglecting the gradient is almost zero.

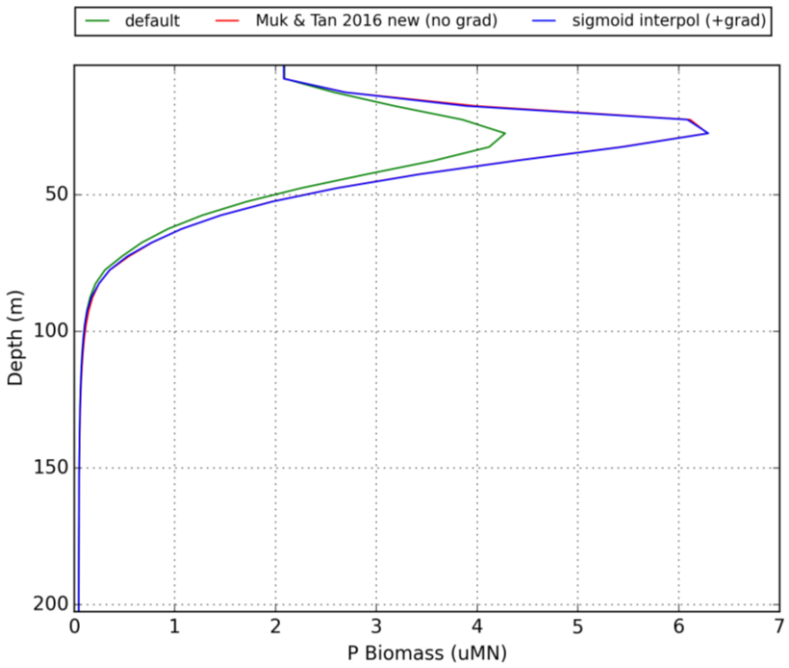


**Figure 94: Phytoplankton biomass profiles in response to diffusion profiles in previous figure (matching colors). The red line is obtained without diffusivity gradient, while the blue line is obtained accounting for that term in the equations. The two are almost totally overlapped, thus the impact of the gradient term in the equations is almost none.**

The diffusivity gradient in this case (fig. 93 and 94) has almost no influence on the dynamics, but that may happen because the region where diffusivity varies most (70-120 meters) is a region with a very small concentration of plankton (and with moderately low biomass derivatives).

To verify this hypothesis, we ran a pair of simulations where the diffusion profile is the first depth-varying profile used at the beginning of the section (Mukherjee & Tandon, 2016) characterized by discontinuities in diffusivity also in the upper layers. As a consequence, in this case the interpolated profile accounts for a gradient significantly larger than zero also at the top of the water column (a “modified” sigmoidal function is used). The two profiles (along with the “constant” case as a reference) are shown in figure 95.

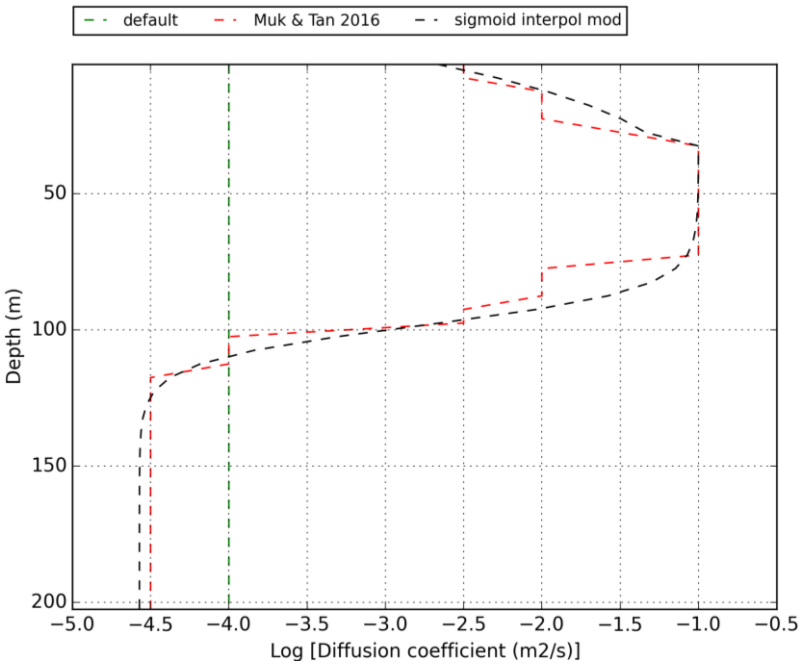


**Figure 95: Diffusion profiles used to test the relative importance of diffusion gradient in the equations. To account for the diffusivity gradient we used an interpolated profile. This time the gradient will be significant also at the top of the water column where phytoplankton is abundant.**

As we expected, neglecting the gradient results in a decrease of the intensity of the DBM (figure 96). So, generally speaking, peak biomass intensity could be enhanced by diffusion gradient (>0 in figure 95) in the upper layers, and similarly reduced if the diffusion gradient is smaller than zero (at least if $\frac{\partial P}{\partial z} > 0$ as usually happens when approaching a DBM as in this case).**Notice that the depth of the P maximum is not changed in any of the experiments in this section, sign of the fact that this maximum is determined uniquely by light and N profiles. The effect of diffusion and/or diffusion gradients is to intensify or reduce this maximum, without shifting its location in the water column.**

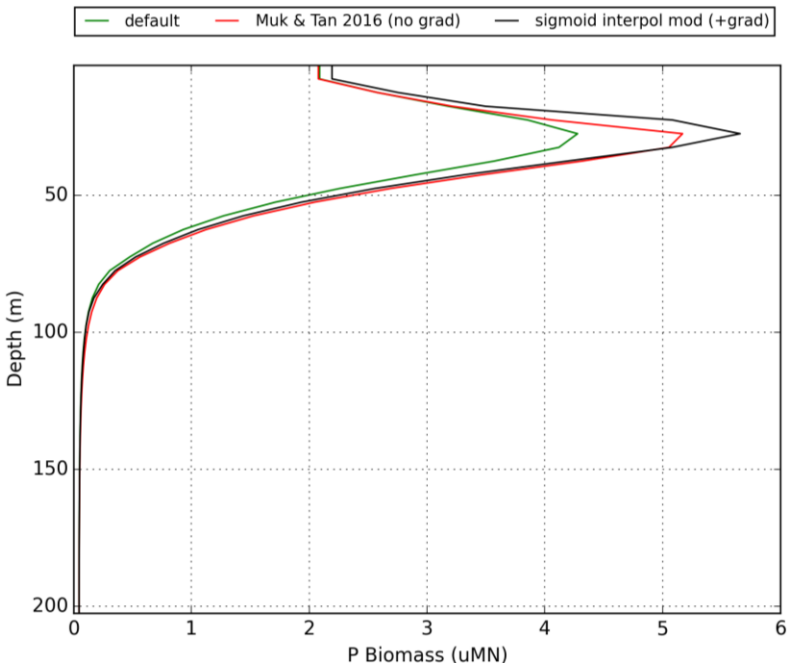


**Figure96:Phytoplankton biomass profiles in response to diffusion profiles in previous figure (matching colors). The red line is obtained without diffusivity gradient, while the black line is obtained accounting for that term in the equations. The two are almost totally overlapped in the lower part, but this time the impact of the gradient term in the equations is appreciable in the upper part of the column, and neglecting it results in an underestimation of phytoplankton biomass (red line with respect to black line).**

The result obtained here somehow further confirms the fact that mixing has effect on phytoplankton profile as long as it is close in depth to the DBM, but this time we get to the same conclusion as before but with respect to the diffusion vertical gradient: the differences in phytoplankton biomass are appreciable only if the gradient is significantly different from zero in the region (depth interval) close to the DCM, otherwise as in the previous examples (figure 93 and 94) it has no effect on the dynamics. Anyway, also looking at figure 96, the error committed in neglecting the gradient is not very large, up to the 10% at the depth of the DBM.

Final considerations:

In chapter 4 we aimed to make a step towards increasing realism inside SPLAS, investigating its sensitivity: we started with the inclusion of the vertical dimension, and then added light limitation of phytoplankton growth and saw that it is necessary when describing vertical dynamics and large depth intervals. We observed how light influences P biomass profile and "breaks" the depth-homogeneity in the size-structure with respect to the "no-light" virtual case. The main result here is that we can obtain a sensible behavior reproducing a DBM in phytoplankton biomass and having different winning size-classes at different depths, rather than having an indefinitely increasing biomass with depth and a depth-homogenous size-spectrum (that are obtained neglecting light). Moreover, the DBM can be "controlled" by the model in depth and intensity by varying the light profile (in particular the extinction constant) with size-structure varying accordingly (size-classes biomass peaks move in depth). If we then add also self-shading of phytoplankton, possibly some concentration dependent mechanisms appear and the model is able to reproduce also "multiple" maxima in P biomass depth-profile (in our example we caught two maxima) while size-structure changes a lot with self-shading parameters.

In the last experiment we tested a few depth-varying diffusivities and saw how this diffusion can enhance or diminish the intensity of our DBM, based on where the most intense mixing is located in the water column. In these experiments we neglected the impact of the term arising from depth-varying diffusivity (diffusivity vertical gradient); anyway we saw that the error committed in doing so is contained, even when the D gradient is significantly different from zero in the sensitive region close to phytoplankton maximum(DBM).

It must be stressed that all experiments in current section are based on a steady-state assumption (no seasonal variation and daily cycle); this is the reason why we use 10 years of simulation: to be sure the system has stably reached a steady state. Nonetheless we saw that some sensible features that are present in real systems can be qualitatively caught and SPLAS has the future potential to give useful insights to plankton dynamics and biogeochemistry.

# 5 Notes on C Export

An important value that SPLAS could support in the future is the Carbon export, calculated from the particular size-structure of plankton. SPLAS has the potential to give important insights on how size-structure contributes to biogeochemical fluxes, although the model needs to be refined and improved with a more realistic representation to give significant results in the future. We think that it may be useful to give a little glimpse of what SPLAS' outcome of export is, to discuss model's limits and link this subject to the general issue discussed in the introduction.

We calculated the export in SPLAS tracking the material going out from the last (*M*-th) layer of the 1-D structure:

*(15)*

$$Export = w_{OM} \frac{\partial OM}{\partial z}\Big]_{k=M} + \sum_i w_i \frac{\partial P_i}{\partial z}\Big]_{k=M}$$

The summation in the second term on the right hand side is intended on size-classes of phytoplankton. With this export formula we are assuming that the diffusive flux outside "our" water column is negligible with respect to the sinking flux and diffusion is important only within our "mixed" structure. This is also the justification for our boundary conditions.

Since all state variables are expressed in terms of Nitrogen (µMN = mmolN $m^{-3}$) the export has to be converted to carbon. For detritus we assume a C:N ratio equal to the Redfield Ratio (106:16; in Redfield, 1934) and convert the concentration to mass multiplying by the molar weight; we will obtain the export flux in gC $m^{-2}$ $day^{-1}$.

Carbon content is size-dependent in phytoplankton, but when considering detritus (in which dead phytoplankton, dead zooplankton and egestion of zooplankton converge) we stick to the Redfield Ratio; this may seem a contradiction, but actually it is coherent within our "coarse" representation of organic matter. When we consider detritus export we "condense" our representation to a unique class, without size-particle distinction. Moreover, we are implicitly assuming that detritus sinking is a more complex phenomenon involving other processes (as aggregation of cells) which we do not solve in details: the latter is also the justification for choosing a much higher sinking velocity (8 m/day) than the one for phytoplankton. Also, we do not track explicitly carbon content of zooplankton and wastes coming from egestion. Therefore, having a higher resolution for phytoplankton inside detritus compartment would be somehow useless, and we assume that on average the whole detritus compartment has a carbon content

coming from a C:N ratio equal to the Redfield Ratio. For the moment we settle for a higher resolution only for phytoplankton compartment.

In fact, for "living" phytoplankton we use the Carbon-Cell volume relationship from Montagnes et al. (1994):

$$C_i = 0.0109 \cdot V_i^{0.991}$$

Where $C_i$ is the carbon contained in a single P cell (pgC cell$^{-1}$) and $V_i$ is cell volume in µm$^3$. As defined in section 2 the label i stands for the size-class and the volume is obtained from the equivalent spherical diameter (ESD, assuming a spherical shape for the cell). In section 2.2 we also introduced equation 6, which links density of phytoplankton cells (cells m$^{-3}$) with biomass (mmolN m$^{-3}$) through cellular quota (mmolN cell$^{-1}$): from this link we can obtain total phytoplankton carbon content (for a given size-class), multiplying $C_i$ by cells density of i-th class. This allows us to consider in SPLAS, although at first order and implicitly, the cellular interplay between carbon and nitrogen quota in phytoplankton and somewhat the variability of C:N quota ratio in response to environmental conditions (light and nutrients).

Of course, with the current state of SPLAS we obtain an estimate of carbon export without an explicit representation of carbon dynamics, rather linking carbon content to the nitrogen cycling within plankton food web.

Again, we stress that this is a rather simplistic approach but still useful, as the computation of plankton size-structure is robust and when we consider saturating light the C:N ratio in phytoplankton is close to the Redfield Ratio and size independent (for saturating N) or slightly higher and increasing with cell size (for limiting N) (Mei et al., 2011).

In fact, our working hypothesis here is non-limiting light (light absorption is not considered in phytoplankton growth rate) so from this point of view the phytoplankton growth in SPLAS is maximized and depends only on N concentration. Moreover in our 1-D version of SPLAS we are considering turbulent diffusion in the upper "mixed" part of the water column and we suppose that in these conditions the N concentration in the environment is sufficient to be considered also non-limiting. Thus, according to Mei et al. (2011), in this situation of saturating light we do not expect our C:N ratio to differ significantly from the Redfield Ratio.

With this, we do not want to say that our estimate is realistic, but rather that it might make sense to analyze carbon export even at this point.

### *5.1 A first estimate of C export*

SPLAS 1-D was ran in the default configuration (Table 7) for 10 years as usual and with the same N supply as before (4 μMN $day^{-1}$ supplied from the bottom) and calculated plankton community size-spectra along with total average carbon export. We used 15 layers (13 internal layers) with a grid spacing ($\Delta z$) of 1.5 m in order to cover a depth of 21 m, which in our opinion is a reasonable thickness for a hypothetical "mixed" layer in our virtual framework.

In this configuration we obtain an average carbon export of about *68.58 mgC* $m^{-2}$ $day^{-1}$ by solving equations 11-14 for 10 years and using equation 15 to obtain such estimate.

As a comparison, Ward and Follows (2016) obtained an average global export of 8.5 GtC $year^{-1}$, calculating a range of estimates between 7.2 and 9.8 GtC $year^{-1}$ depending on absence/presence of plankton mixotrophy; we converted their global yearly value into a daily local (mean) value for comparison (considering the surface of the world oceans equal to about $3.619 \cdot 10^{14}$ $m^2$) and the result is *64.35 mgC* $m^{-2}$ $day^{-1}$ which is pretty close to our earlier estimate.

We must underline that the "converted value" from Ward and Follows (2016) is an average extrapolated from a global estimate and so we do not expect it to be representative of any specific oceanic location in the world. Nonetheless, SPLAS is calibrated on rough evaluations of biological, biogeochemical and physical parameters and these are meant to be mean aggregated values representative of a wide spectrum of real local cases.

This is not to claim SPLAS' success, but just to say that the value obtained for C export is not completely wrong or really far from reasonable. We will see that SPLAS has some limits for export calculation when we will perform sensitivity analysis.

### *5.2 Sensitivity of Carbon Export to Nitrogen Supply*

We tested the response of our system to different Nitrogen loads in terms of carbon export, in order to explore a possible range of variability and examine the sensitivity of the numerical value in function of the Nitrogen input. This is not a test for realism, rather a behavior analysis of 1-D SPLAS.

We maintained the same boundary conditions and the same shape of the supply:

$$S(k) = L \cdot \delta_{kM}$$

but varying the quantity *L* (constant during the simulation, in the default configuration - section 5.1 - *L* = 4.0); all other model's parameters are set to their default values. We performed a simulation of 10 years and calculated average carbon export for *L* equal to 0.0 (no N supply), 1.0, 2.0, 4.0 (default), 5.0, 6.0 and 8.0. We obtained the graph in figure 97, where the average C export is reported against the corresponding value of *L*. It must be specified that in the case *L* = 0.0 there is no additional Nitrogen in the system to sustain phytoplankton life (all growth relies on the initial quantity of N) and so after a very short time with respect to simulation length (between 1 and 2 years) both phytoplankton and zooplankton are completely extinct throughout the water column and detritus concentration (and also export) has eventually gone to zero. The recycling pathway from Detritus to Nitrogen somehow delays this decay, but in the end everything dies. This is the reason why the average export is very low (7.5 mgC $m^{-2}$ $day^{-1}$) with respect to all other cases: after a short transient there is no actual ecosystem dynamics and everything is basically at the equilibrium (N = P = Z = D = 0).

Instead, for *L*> 0 the system stabilizes to a constant value of export, which is usually slightly smaller than the value of the time-average because of an initial peak in the transient phase before the stabilization of plankton size-structure. The stabilization is an effect of the steady Nitrogen load forcing. We decided to include the initial short transient phase in the average as a significant part of the numerical solution.

The average is calculated simply as:

$$< C_{exp} > = \frac{1}{T}\int_0^T C_{\exp}(t)\, dt$$

where T = 10 years. If we took as significant the final export values (at t = 10 years) instead of the time-averages we would get a graph similar to the one in figure 97, except that for a null N load we would get an export value very close to 0 (the export is asymptotically equal to zero, for a sufficiently long time). Another possibility is to consider the average of the "stabilized" phase, excluding the transient: this value is almost equal to the final value, as the transient is really short (between 1 – 2 years for any value of *L*).

In any case, the essence behind the relation between export and Nitrogen load does not change, and we observe that Carbon export increases with increasing values of Nitrogen load. The more nutrient we introduce in the system the more material is lost.

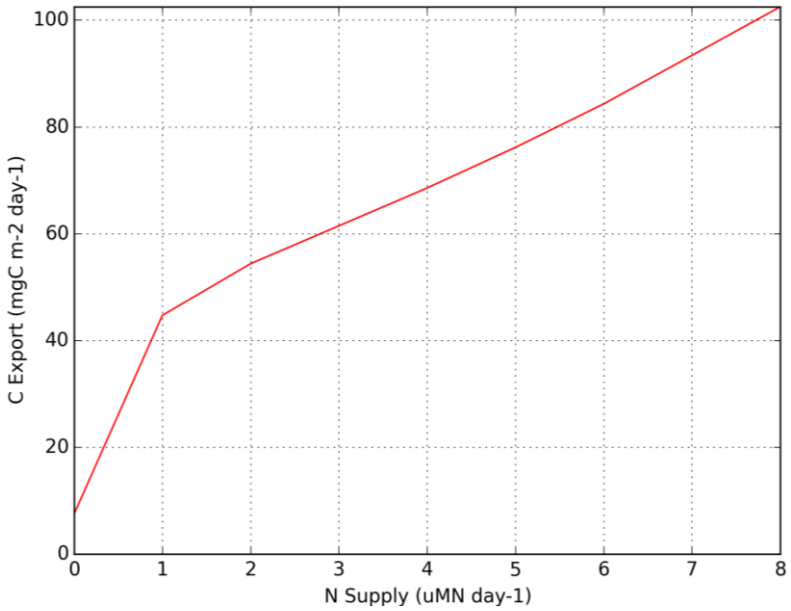


**Figure 97: C export in function of N supply.**

The largest jump in export value occurs between *L* = 0.0 and *L* = 1.0, while for *L*> 1.0 carbon export increases almost linearly with nitrogen supply. The leap from *L* = 0.0 to *L* = 1.0 is a logical result if we consider that between the two simulations there is a large shift in terms of dynamics, plankton size-structure, plankton biomass and detritus concentration. The export is a consequence of the change in dynamical regime, from decay and extinction of life with no supply to sustainability of plankton life in the water column with the introduction of new nitrogen. The successive increases of N supply do not determine such abrupt changes but only shift the size-structure (as in section 3.4) and enhance biomasses and export.

Export values obtained in this experiment range from 7.5 to about 102 mgC $m^{-2}$ $day^{-1}$ and excluding the simulation in extreme conditions we got a reduced range (44.7 - 102 mgC $m^{-2}$ $day^{-1}$). This range, when mapped on a global scale, implies an interval of export from 5.9 to 13.5 GtC $year^{-1}$ if we consider as local averages the value indicated by 1-D SPLAS. Although rough estimates, the values obtained make sense and agree with other more precise estimates in literature (Ward & Follows, 2016; US JGOFS).

### *5.3 Limits of C export calculation*

The comparison with Ward & Follows (2016) is just intended to give an idea of what are the results of another more complex model and to explain the potential that SPLAS has. It is evident that the approach of SPLAS has limits: the main two limits of our approach consist in the single organic matter compartment with all material sinking at a unique velocity and in the assumption of a C:N ratio equal to the Redfield Ratio (106:16) for detritus, which is often not the case in real systems (Finkel et al., 2010; Klausmeier et al., 2008; Kiørboe, 2013).

It must be also underlined that we are neglecting vertical dial migration of zooplankton, which can be an important vehicle for carbon export. In the future this feature could be included in the model to refine our estimate, along with the features explained in the following section.

Anyway, more in general, inside 1-D SPLAS we are far from the realism necessary to give a better insight into biogeochemical fluxes, and within our analysis we stick to a merely theoretical point of view. In this whole section we are just trying to give a taste of how we could extract information about carbon export and on the values that we obtain now. These values are currently not 100% significant, for the limits discussed above and in general for the current state of the model.

Another limit, maybe the most important, is discussed in the following section.

### *5.4 Sensitivity analysis*

We will see in this section that our C export estimates are robust with respect to some selected key parameters, in particular the two involved in the calculation of carbon export: sinking velocity of phytoplankton and detritus. This robustness may be good if representing a particular geographic location, but from the other side it could be seen as SPLAS not being able to reproduce natural variability in the ocean.

We performed sensitivity analyses with respect to diffusion coefficient (D), phytoplankton sinking velocity ($w_p$), detritus sinking velocity ($w_{OM}$), re-mineralization rate ($\psi$) and phytoplankton maximum growth rate ($\mu_0$). We increased and decreased the value of these parameters by 10% and studied the response (i.e. the corresponding % variation with respect to the default value – table 7) of Carbon export and other properties like plankton biomasses and size-diversities, N and OM concentration, in the same conditions as at the beginning of this section (15 layers, grid spacing ($\Delta z$) of 1.5 m, max depth 21 m, N Load = 4 $\mu$MN $day^{-1}$). All results of the analyses (% variations) are summarized in Table 8. The % variations reported for depth

dependent quantities (biomasses, concentrations and size-diversity indices) refer to the variation of the depth-average.

The details of the analysis are summarized in the following:

- Diffusion coefficient (D): defaultvalue $10^{-4}$ $m^2$ $s^{-1}$
- P sinking velocity ($w_P$): default value (size-dependent) in the range [0.0041 - 2.0] m/day
- Detritus (OM) sinking velocity ($w_{OM}$): default value 8 m/day
- Re-mineralization rate ($\psi$): default value 0.15 $day^{-1}$
- P growth rate ($\mu_0$): default value (size-dependent) in the range [2.6 - 0.23] $day^{-1}$

Further in this section we explored also larger variations of these parameters, since 10% may be considered a too small variation for some of them (e.g. eddy diffusivity).

Referring to table 8, for what concerns carbon export the estimate has the largest sensitivity to the detritus sinking velocity, order 7%, with respect to a 10% variation of the velocity. The sensitivity to phytoplankton sinking velocity is appreciable but much lower, order 1-2%. In both cases carbon export increases with increased sinking velocity, as one would expect from the formula at the beginning of section.

The export is also slightly affected by phytoplankton growth rate (about 1% variation), while is very poorly affected by variations in diffusion coefficient and in re-mineralization rate (variation less than 0.01%). We can fairly conclude that in any case the estimate, ranging from a minimum of 63.86 to a maximum of 73.48 mgC $m^{-2}$ $day^{-1}$, is pretty stable and does not change abruptly due to variations in these key parameters, especially the two sinking velocities.

The other state variables (biomasses, concentrations and size-diversities) are almost insensitive to variations in diffusion coefficient, detritus sinking velocity and re-mineralization rate. Thus, the whole output of the simulation (including also export) is robust with respect to such variables. We must highlight that in the case of organic matter concentration depth profile, the variations with detritus sinking velocity are actually intense but opposite in the upper layers and the bottom layers (matter tends to sink more/less with increased/decreased $w_{OM}$) and this is why the variations of the average concentration are “smoothed out” in table 8.

We also notice the stability of the values of the variables with respect to phytoplankton sinking, as variations are appreciable but always of the order of 1-2%. In general, we can say that the theoretical framework designed by SPLAS is not “destroyed” by 10% variations in all the mentioned parameters. In conclusion, all our results are robust with respect to diffusivity, sinking velocities and re-mineralization rate and show contained overall variations, with the peak variation in carbon export with respect to detritus sinking velocity.

This aspect is positive if we are interested in representing a particular location (with small variability) and reproduce given values, but in general is a limit of the model, reducing the spectrum of applications of the model and what the model could be able to represent. In particular the very small sensitivity of carbon export with respect to diffusion is a crucial limit of our representation. Even if our earlier estimate of section 5.1 can be seen as reasonable, it may result rigid with respect to configuration changes, thus representing a drawback of SPLAS.

For what concerns phytoplankton growth rate variations, results are not as stable as earlier results. In particular, N concentration (order 10% variations), P biomass (order 3%) and Z size-diversity (5-7% variations) appear to vary significantly with variation in growth rate. This means that P growth rate is a crucial parameter for our output and for realistic applications we must very carefully choose a suitable parameterization of light (depth) dependent limitations in phytoplankton growth. In this sense natural variability of growth could be reproduced. But again, our estimate of carbon export is not highly sensitive to growth rate, even if apparently biomasses and size-diversity are, and so this confirms a stability of export estimate even with different configurations of biomass and size-structure. This might be further investigated and changed in the future.

We must also notice a peculiarity of our simulations' output: apparently phytoplankton Shannon evenness has a local maximum in the default values of $w_P$ (phytoplankton sinking velocity) and $\mu_0$ (phytoplankton growth rate), as moving away from these default values in both directions (± 10%) results in a decrease of the evenness. Further investigations are required to understand this point.

In conclusion, summarizing our sensitivity analysis:

- Simulation output is highly stable with respect to diffusivity (D) and re-mineralization rate ($\psi$) showing very low % variations (less than 0.05%). This is a good thing apart from the small variability of C export.
- Simulation output is robust with respect to phytoplankton sinking velocity ($w_P$), showing significant but contained variations (1-2%).
- Simulation output is pretty robust with respect to detritus sinking velocity ($w_{OM}$), as there are no appreciable variations in all variables apart from C export and OM concentration, which anyway show reasonably contained variations (C export 7%, [OM] 0.5%). We are happy that export does not depend too much directly on our choice for this parameter, but also this fact will need further investigations. Maybe a more realistic parameterization will be a solution in the future.
- All quantities (export, biomasses, concentrations, diversities) are pretty much robust with respect to ± 10% variations in D, $\psi$, $w_P$, $w_{OM}$.

- Our estimate of C export is generally robust, having the largest variation with respect to $w_{OM}$ (order 7%), $w_P$ (order 1-2%) and $\mu_0$(order 1%) and showing almost no variation with respect to D and $\psi$. This may be seen as the main limit of the model at its current state.
- Variations in phytoplankton maximum growth rate ($\mu_0$) trigger significant variations in the output, especially in Nitrogen concentration and zooplankton size-diversity;$\mu_0$is a crucial parameter for our simulations and we must be very careful in future applications.
- Likely, phytoplankton size-diversity may have a local maximum close to our default values of $w_P$ and $\mu_0$ (further investigation is required).

**Table 8: Sensitivity analysis**

| Parameter | C export | P mass | Z mass | [N] | [OM] | PSE | ZSE |
|---|---|---|---|---|---|---|---|
| $D$ +10% | -0.001% | -0.003% | <0.001% | <0.001% | <0.001% | +0.003% | +0.006 |
| $D$ -10% | +0.001% | +0.002% | <0.001% | <0.001% | <0.001% | -0.003% | -0.006 |
| $w_P$+10% | +1.28% | -1.82% | +0.12% | +1.54% | -1.13% | -0.77% | -1.84% |
| $w_P$-10% | -1.76% | +1.83% | -0.11% | -1.45% | +0.71% | -0.71% | +2.42% |
| $w_{OM}$+10% | +7.14% | <0.001% | <0.001% | <0.001% | -0.50% | <0.001% | <0.001% |
| $w_{OM}$-10% | -6.87% | <0.001% | <0.001% | <0.001% | +0.34% | <0.001% | <0.001% |
| $\psi$ +10% | -0.007% | +0.02% | +0.02% | +0.03% | -0.02% | -0.003% | +0.02% |
| $\psi$-10% | +0.007% | -0.03% | -0.02% | -0.03% | +0.03% | +0.003% | -0.02% |
| $\mu_0$+10% | +0.75% | -3.13% | +0.28% | -9.78% | +0.20% | -0.31% | -4.55% |
| $\mu_0$-10% | -1.10% | +3.57% | -0.33% | +10.64% | -0.31% | -1.56% | +7.60% |

Orange/red = largest sensitivity (>3%)

Green = smallest sensitivity (<0.1%)

Yellow = appreciable sensitivity (> 0.1% and <3%)

Variations for P and Z mass, N and OM concentrations, P and Z Shannon Evenness (PSE and ZSE) are intended for depth-averaged quantities.

# 6 Conclusions and future directions

## *6.1 Summary*

The goal of this thesis was to set the way towards a reliable view of biogeochemistry in marine ecosystems, remaining in a theoretical framework. We tried, as a final step in the preceding chapter, to perform estimates of biogeochemical fluxes (in particular carbon export), for the importance that the latter has to the whole earth system, starting from climate. Our estimates must be considered as a starting hint for future development and a representation of the potential of SPLAS, rather than a valid estimate ready to be compared to experimental data or other modeling studies.

Aligned with the aim of biogeochemical investigation, the rationale behind the development of SPLAS was that the size-structure of plankton communities determines to a certain extent the biogeochemical features of a particular marine ecosystem. We developed the model based on this cornerstone, solving the size-spectrum (abundance versus biomass) of both phytoplankton and zooplankton populations with a huge level of detail, taking inspiration from the work of Banas (2011).

We validated the 0-D version against patterns found in real systems, taken from literature studies (section 3), demonstrating that SPLAS in the future can be a useful tool for the investigation of biogeochemistry. We also tested the behavior of the model with respect to different parameters (in the last part of section 3) and those tests are not validated against any data but we thought they are worth including in order to give an overview of the model representation. At the very end of section 3 we also tested the behavior of our representation in a time varying environment(N supply).

In section 4we used SPLAS in a more complicated framework, trying to add complexity to our picture and adopting a one-dimensional column with physical diffusion,1-D sinking, and light limitation. We already saw the behavior of the model in 0-D and wanted to test its behavior in a brand new 1-D representation. This seemed to us a natural continuation for SPLAS. At this point we also included a detritus pool in the representation and we needed this to eventually obtain a numerical estimate of carbon export (in section 5). Chapter 4 is focused on the analysis of the impact of light in 1-D: light is necessary to obtain a sensible behavior of phytoplankton biomass in the water column, whereas at the end of chapter 4 we investigated on the diffusion profiles.

Our approach shows that even starting from simple hypotheses and with a basic formulation, it is possible to get to a rough representation of biogeochemistry.

Section 4 showed the presence of a Deep Biological Maximum (DBM) in phytoplankton profile, which is a feature we obtained with the inclusion of light limitation in phytoplankton growth. We are interested in this result not because we wanted to reproduce it from the beginning, but rather because it is a sensible behavior for the model. Neglecting light in the 1-D model we would not obtain a reasonable behavior for the biomass profile and investigating size-structure and biogeochemistry with a non-sense phytoplankton biomass profile is meaningless.

Another interesting feature obtained including light is that the size-structure becomes non homogeneous with depth.

As we extended the depth range to 200 m we could not neglect anymore co-interactions of Nitrogen and light in phytoplankton growth: we obtained a sensible phytoplankton profile with the presence of a DBM at about 25 m and this maximum is strongly dependent on the value of the extinction coefficient ($k_d$). We reproduced the maximum at different depths with varying $k_d$ and the behavior we obtained seems coherent with the physics (and the biogeochemistry): as $k_d$ decreases, the maximum (and the nutricline) gets deeper in the water column and also more intense.

We also tried experimenting the self-shading of phytoplankton and with suitable values of the constants we were able to reproduce a two-peak behavior in phytoplankton biomass profile, with a DBM at 35 m and then a second less intense peak 75 m deep; this may be due to a concentration-dependent mechanism and for sure it cannot be obtained without the inclusion of a self-shading term. This multi-modal depth profile is in perspective an interesting result, as it is a feature often present in real systems (for example analyzing chlorophyll data from Bio Argo Floats two peaks can be seen in the first 200 meters). For now we simply accept this as a result.

We also tested depth-varying diffusivities and evaluated how they influence phytoplankton biomass profiles, with notable effects only when an intense mixing region is located close to phytoplankton maximum. In our experiments the diffusivity is not able to vary the depth of the DBM, mainly controlled by light and Nitrogen profiles. We also examined the error made by neglecting the diffusion gradient (mixed term $\frac{\partial D}{\partial z}\frac{\partial P}{\partial z}$) in the equations, and observed that it is relatively small; thus, assuming that it is negligible is a reasonable assumption in most cases.

Chapter 5 concludes this work by estimating Carbon export, to close the circle linking directly to the introduction of this thesis. Here we also performed a sensitivity analysis on these results.

The value we obtained for C export resulted reasonable, and close to previous estimates (Ward and Follows, 2016). Of course, we must consider the intrinsic uncertainties, the many limits of SPLAS and the extrapolation from a global context of Ward's estimate. Possibly with a specific choice of parameter values and with future improvements and validation, SPLAS could be used everywhere to give useful insight onto the biogeochemistry of a specific region. Currently, we are in between a theoretical framework and realism: a lot of work still needs to be done to pursue valid export estimates.

Our study of carbon export was only meant to give a taste of what the model is capable of, but the estimate is rather rough and in the future it must be refined and improved to be strictly linked to the biogeochemistry and to environmental variability. At this point this link is not so strong, and in fact our results are robust with respect to variations in key parameters: this may be good for some quantities, but not for carbon export which is stable with respect to variations in sinking velocities of phytoplankton and detritus, and shows little variations with other parameters as diffusivity, re-mineralization rate and P growth rate.

Notice also that in SPLAS, C export increases with increasing nitrogen supply, which is somewhat the "master" parameter of our simulations. This might be a sensible behavior, but must be further investigated in the future.

To summarize, we are confident that in the future 1-D SPLAS, after several improvements, could be applied to real test cases, e.g. it could be included in a complex model as the BFM. All the results obtained so far enlighten the potential of SPLAS, so we are confident that when applied to real frameworks it will give good results and shed light on biogeochemical properties and size-dependent mechanisms. Of course, before that many steps forward must be done in order to accomplish a realistic representation: the development is not over and several improvements will be applied and other tests on the model performances will be done (e.g. more experiments in time-varying frameworks).

### *6.2 Future Improvements*

1-D SPLAS is a promising tool for the resolution of local biogeochemical fluxes and in the future we aim to include it as a module in more complex biogeochemical models, online or offline coupled to circulation models.1-D SPLAS could for instance be used as a module of the BFM (Biogeochemical Flux Model, model details in Vichi et al., 2007a; Vichi et al., 2007b; Vichi et al., 2015), solving more in detail the size-structure of plankton food web, giving better insight into the biogeochemistry and performing more precise estimates of nutrient fluxes. In fact, the BFM has only few plankton functional groups and could benefit from the inclusion of detailed plankton size-classes. On the other side, the BFM represents more precisely other biogeochemical features (bacterioplankton, more nutrients, etc.) and 1-D SPLAS could improve the representation of pre-existing biogeochemical models being included as a module, and this coupling can exploit the strength of both models to give excellent results, also with the "full" model coupled to a physical circulation model.

But before that, many future improvements to the model representation could be done, as for example:

- To add pico-phytoplankton smaller than 1 micron (hopefully we can introduce at least pico-phytoplankton starting from 0.6/0.7 μm).
- To add a separate omnivorous Mesozooplankton compartment, eating both phytoplankton and smaller zooplankton, to account for the impact of carnivorous grazing (now we only account for some cannibalism with the Z mortality term).
- To consider trophic strategy (auto-, hetero- or mixo-trophy) and the inclusion of dinoflagellates, having important roles in the biological carbon pump (Mitra et al., 2014; Ward and Follows, 2015).
- To represent time-varying dynamics (time-dependent mixing, light and N supply) and reproduce seasonality and daily cycles.
- To add new traits other than size, like zooplankton feeding mode (as in Wirtz, 2012) or phytoplankton defense from predation and phytoplankton taxonomy (different intercepts of the growth rate relationship, as in Ward et al., 2013).
- To validate the 1-D model against data, similarly to what has been done with the 0-D model.

This thesis ends here, but a lot of work still has to be done.

**Acknowledgements:**

The research reported in this work was supported by OGS and CINECA under HPC-TRES program – Line A2 (award grant 2014-01). Many thanks to the whole ECHO (Ecology and Computational Hydrodynamics in Oceanography) group of the OGS for the scientific and human support. The author would also like to thank Øyvind Fiksen and all the organizers of the 3rd International Workshop on Trait-based Approaches to Ocean Life (20-23 August 2017, Bergen and Øs, Norway) for the precious feedbacks and the illuminating experience. Thanks also to Neil S. Banas (Department of Mathematics and Statistics, University of Strathclyde, Glasgow, UK) for the helpful discussion and useful suggestions during the above workshop.

**References:**


Aksnes, D. L. & Egge, J. K. (1991). A theoretical model for nutrient uptake in phytoplankton. *Mar. Ecol. Prog. Ser.*, 70, 65–72.

Allen, J. I., Siddorn, J. R., Blackford, J. C. *et al*. (2004) Turbulence as a control on the microbial loop in a temperate seasonally stratified marine systems model. *J. Sea Res.* , 52, 1–20.

Andersen, K. H., Aksnes, D. L., Berge, T., Fiksen, Ø., & Visser, A. (2015). Modelling emergent trophic strategies in plankton. *Journal of Plankton Research*, *37*(5), 862–868. http://doi.org/10.1093/plankt/fbv054

Anderson, T. R. (2005). Plankton functional type modelling: Running before we can walk? *Journal of Plankton Research*, *27*(11), 1073–1081. http://doi.org/10.1093/plankt/fbi076

Archer, S. D., Gilbert, F. J., Allen, J. I. *et al*. (2004) Modelling of the seasonal patterns of dimethylsulphide production and fate during 1989 at a site in the North Sea. *Can. J. Fish. Aquat. Sci.* , 61, 765–787.

Armstrong, R.A. (1994). Grazing limitation and nutrient limitation in marine ecosystems: Steady state solutions of an ecosystem model with multiple food chains. *Limnology and Oceanography*, 39(3), 597-608. http://doi.org/10.4319/lo.1994.39.3.0597

Armstrong, R. A. (1999). Stable model structures for representing biogeochemical diversity and size spectra in plankton communities. *Journal of Plankton Research*, *21*(3), 445–464. http://doi.org/10.1093/plankt/21.3.445

Armstrong, R. A. (2003). A hybrid spectral representation of phytoplankton growth and zooplankton response: the 'control rod' model of plankton interaction. *Deep-Sea Res. II* , 50, 2895–2916.

Azaele, S., Pigolotti, S., Banavar, J. R., & Maritan, A. (2006). Dynamical evolution of ecosystems. *Nature*, *444*(7121), 926–928. http://doi.org/Doi 10.1038/Nature05320

Baas Becking, L.G.M. (1934) Geobiologie of Inleiding Tot De Milieukunde. W.P. Van Stockum & Zoon, The Hague.

Baird, Mark E., Emsley, Steve M., McGlade, Jacqueline M. (2001). Modelling the interacting effects of nutrient uptake, light capture and temperature on phytoplankton growth. *Journal of Plankton Research*, *23*(8), 829–840. http://doi.org/DOI 10.1093/plankt/23.8.829

Baird, M. E., & Suthers, I. M. (2007). A size-resolved pelagic ecosystem model. *Ecological Modelling*, *203*(3-4), 185–203. http://doi.org/10.1016/j.ecolmodel.2006.11.025

Banas, N. S. (2011). Adding complex trophic interactions to a size-spectral plankton model: Emergent diversity patterns and limits on predictability. *Ecological Modelling*, *222*(15), 2663–2675. http://doi.org/10.1016/j.ecolmodel.2011.05.018

Baretta-Bekker, J. G., Baretta, J. W. and Ebenhöh, W. (1997) Microbial dynamics in the marine ecosystem model ERSEM II with decoupled carbon assimilation and nutrient uptake. *J. Sea Res.* , 38, 195–211.

Barton, A. D., Dutkiewicz, S., Flierl, G., Bragg, J., & Follows, M. J. (2010). Response to Comment on "Patterns of Diversity in Marine Phytoplankton." *Science*, *329*(5991), 512–512. http://doi.org/10.1126/science.1190048

Barton, A. D., Dutkiewicz, S., Flierl, G., Bragg, J., & Follows, M. J. (2010). Patterns of diversity in marine phytoplankton. *Science*, *327*(5972), 1509–1511. http://doi.org/10.1126/science.1184961

Barton, A. D., Finkel, Z. V, Ward, B. a, Johns, D. G., & Follows, M. J. (2013). On the roles of cell size and trophic strategy in North Atlantic diatom and dinoflagellate communities. *Limnology and Oceanography*, *58*(1), 254–266. http://doi.org/10.4319/lo.2013.58.1.0254

Barton, A. D., Pershing, A. J., Litchman, E., Record, N. R., Edwards, K. F., Finkel, Z. V., … Ward, B. A. (2013). The biogeography of marine plankton traits. *Ecology Letters*, *16*(4), 522–534. http://doi.org/10.1111/ele.12063

Barton, A. D. (2011). Trait-based Approaches to Marine Microbial Ecology. *Department of Earth, Atmospheric, and Planetary Science, Massachussetts Institute of Technology (MIT), Cambridge.*

Bruggeman, J. (2009). Succession in plankton communities - A trait-based perspective. *Department of Theoretical Biology, Vrije Universiteit Amsterdam*.

Bruggeman, J., & Kooijman, S. a L. M. (2007). A biodiversity-inspired approach to aquatic ecosystem modeling. *Limnology And Oceanography*, *52*(4), 1533–1544. http://doi.org/10.4319/lo.2007.52.4.1533

Cabrini, M., Fornasaro, D., Cossarini, G., Lipizer, M., & Virgilio, D. (2012). Phytoplankton temporal changes in a coastal northern Adriatic site during the last 25 years. *Estuarine, Coastal and Shelf Science*, *115*, 113–124. http://doi.org/10.1016/j.ecss.2012.07.007

Caperon, J. (1968). Population growth response of Iscochrysis galbana to nitrate variation at limiting concentrations. *Ecology*, 49, 866–872.

Cavender-Bares, K. K., Rinaldo, A. and Chisholm, S. W. (2001) Microbial size spectra from natural and nutrient enriched ecosystems. Limnol. Oceanogr., 46, 778–789.

Cermeño, P., Marañón, E., Harbour, D., Figueiras, F. G., Crespo, B. G., Huete-Ortega, M., Harris, R. P. (2008). Resource levels, allometric scaling of population abundance, and marine phytoplankton diversity. *Limnology and Oceanography*, *53*(1), 312–318. http://doi.org/10.4319/lo.2008.53.1.0312

Chisholm, S.W. (1992). Phytoplankton size. *In* P. G. Falkowski and A. D. Woodhead [eds.]. Primary productivity and biogeochemical cycles in the sea. Plenum Press, New York, pp. 213–237.

Cullen, J.J., P.J.S. Franks, D.M. Karl and A. Longhurst. (2002). Physical influences on marine ecosystem dynamics. In: A.R. Robinson, J.J. McCarthy and B.J. Rothchild (eds.), *The Sea - Volume 12*. pp. 297-336. Wiley, New York.

Cullen, J. J. (2015). Subsurface chlorophyll maximum layers: Enduring enigma or mystery solved? Ann. Rev. Mar. Sci. 7: 207–239. doi:10.1146/annurev-marine-010213-135111

Cushing, D.H. (1989). A difference in structure between ecosystems in strongly stratified waters and those that are only weakly stratified. *J. Plankton Res.*, 11, 1-13.

Droop, M.R. (1968). Vitamin B12 and marine ecology. IV. The kinetics of uptake, growth and inhibition in Monochrysis lutheri. *J. Mar. Biol.Assoc. UK*, 48, 689−733.

Dutkiewicz, S., Follows, M. J., & Bragg, J. G. (2009). Modeling the coupling of ocean ecology and biogeochemistry. *Global Biogeochemical Cycles*, *23*(4), 1–15. http://doi.org/10.1029/2008GB003405

Dutkiewicz, S., Scott, J. R., & Follows, M. J. (2013). Winners and losers: Ecological and biogeochemical changes in a warming ocean. *Global Biogeochemical Cycles*, *27*(2), 463–477. http://doi.org/10.1002/gbc.20042

Dutkiewicz, S., & Follows, M. (n.d.). *Trait trade offs and cell size for ocean ecosystem modeling*.

Edwards, A. M. (2001). Adding detritus to a nutrient-phytoplankton-zooplankton model: a dynamical-system approach. *Journal of Plankton Research*, 23 (4), 389-413.

Edwards, A.M., Yool, A., 2000. The role of higher predation in plankton populationmodels. Journal of Plankton Research 22, 1085–1112.

Edwards, K. F., Thomas, M. K., Klausmeier, C. A., & Litchman, E. (2012). Allometric scaling and taxonomic variation in nutrient utilization traits and maximum growth rate of phytoplankton. *Limnology and Oceanography*, *57*(2), 554–566. http://doi.org/10.4319/lo.2012.57.2.0554

Edwards, K. F., Thomas, M. K., Klausmeier, C. A., & Litchman, E. (2015). Light and growth in marine phytoplankton: Allometric, taxonomic, and environmental variation. *Limnology and Oceanography*, *60*(2), 540–552. http://doi.org/10.1002/lno.10033

Eppley, R. W., Rogers, J. N., & Mccarthy, J. J. (1969). half saturation constants for uptake of nitrate and ammonium.

Falkowski, P.G., Barber, R.T. & Smetacek, V. (1998) Biogeochemical Controls and Feedbacks on Ocean Primary Production. Science, 281(5374), 200-206.

Falkowski, P. G. and Oliver, M. J. (2007) Mix and match: how climate selects phytoplankton. *Nat. Rev. Microbiol.*, 5, 813–819.

Field, C.B., Behrenfeld, M., Randerson, J. & Falkowski, P.G. (1998). Primary production of the biosphere: integrating terrestrial and oceanic components. *Science*, 281, 237-240.

Finkel, Z. V., Beardall, J., Flynn, K. J., Quigg, A., Rees, T. A. V, & Raven, J. A. (2010). Phytoplankton in a changing world: Cell size and elemental stoichiometry. *Journal of Plankton Research*, *32*(1), 119–137. http://doi.org/10.1093/plankt/fbp098

Flynn, K. J., & Mitra, A. (2016). Why Plankton Modelers Should Reconsider Using Rectangular Hyperbolic (Michaelis-Menten, Monod) Descriptions of Predator-Prey Interactions. *Frontiers in Marine Science*, *3*(September). http://doi.org/10.3389/fmars.2016.00165

Follows, M. J., & Dutkiewicz, S. (2011). Modeling diverse communities of marine microbes. *Annual Review of Marine Science*, *3*, 427–451. http://doi.org/10.1146/annurev-marine-120709-142848

Follows, M. J., Dutkiewicz, S., Grant, S., & Chisholm, S. W. (2007). Emergent biogeography of microbial communities in a model ocean. *Science (New York, N.Y.)*, *315*(5820), 1843–6. http://doi.org/10.1126/science.1138544

Franks, P.J.S. (2002). NPZ Models of Plankton Dynamics: Their Construction, Coupling to Physics, and Application. *Journal of Oceanography*, 58(2), 379-387. https://doi.org/10.1023/A:1015874028196

Fuchs, H. & Franks, P. (2010). Plankton community properties determined by nutrients and size-selective feeding. *Mar. Ecol. Prog. Ser.*, 413, 1–15.

García-Comas, C., Sastri, A. R., Ye, L., Chang, C.-Y., Lin, F.-S., Su, M.-S., … Hsieh, C.-H. (2016). Prey size diversity hinders biomass trophic transfer and predator size diversity promotes it in planktonic communities. *Proceedings of the Royal Society B: Biological Sciences*, *283*(1824), 20152129. http://doi.org/10.1098/rspb.2015.2129

Gentleman, W., Leising, A., Frost, B., Strom, S., & Murray, J. (2003). Functional responses for zooplankton feeding on multiple resources: A review of assumptions and biological dynamics. *Deep-Sea Research Part II: Topical Studies in Oceanography*, *50*(22-26), 2847–2875. http://doi.org/10.1016/j.dsr2.2003.07.001

Gibson, G. A., Musgrave, D. L., Hinckley, S. (2005). Non-linear dynamics of a pelagic ecosystem model with multiple predator and prey types. *Journal of Plankton Research*, 27 (5), 427–447.

Gin, K. Y. H., Guo, J., Cheong, H.F. (1998). A size-based ecosystem model for pelagic waters. *Ecol. Model.*, 112, 53–72.

Goebel, N.L., Edwards, C.A., Zehr, J.P. & Follows, M.J. (2010). An emergent community ecosystem model applied to the California Current System. *Journal of Marine Systems*, 83, 221–241.

Goebel, N.L. et al. (2012). Modeled phytoplankton diversity and productivity in the California Current System. *Ecol. Model.*, 264, 37-47.http://dx.doi.org/10.1016/j.ecolmodel.2012.11.008

Guidi, L., Chaffron, S., Bittner, L., Eveillard, D., Larhlimi, A., Roux, S., … Gorsky, G. (2015). Plankton networks driving carbon export in the oligotrophic ocean. *Nature*, *532*(7600), in review. http://doi.org/10.1038/nature16942

Hansen, P.J. (1992). Prey size selection, feeding rates and growth dynamics of heterotrophic dinoflagellates with special emphasis on Gyrodinium spirale. *Mar. Biol.*, 114, 327–334.

Hansen, B., Bjørnsen, P. K., & Hansen, P. J. (1994). The size ratio between planktonic predators and their prey. *Limnology and Oceanography*, *39*(2), 395–403. http://doi.org/10.4319/lo.1994.39.2.0395

Hansen, P. J., Koefoed, P., & Winding, B. (1997). Zooplankton grazing and growth: scaling within the 2-2,000-micrometer body size range. *Limnology and Oceanography*, *42*(4), 687–704.

Hillebrand, H. & Matthiessen, B. (2009). Biodiversity in a complex world: consolidation and progress in functional biodiversity research. *Ecol. Lett.*,12, 1405-1419.

Hirata, T., Hardman-Mountford, N. J., Brewin, R. J. W. et al. (2011) Synoptic relationships between surface chlorophyll-a and diagnostic pigments specific to phytoplankton functional types. *Biogeosciences*, 8, 311–327.

Hooper, D. et al. (2005). Effects of biodiversity on ecosystem functioning a consensus of current knowledge. *Ecol. Monogr.*, 75, 3-35.

Irigoien, X., Huisman, J. and Harris, R.P. (2004) Global biodiversity patterns of marine phytoplankton and zooplankton, *Nature***429**, 863-867. http://doi:10.1038/nature02593

Irwin, A. J., Finkel, Z. V., Schofield, O. M. E., & Falkowski, P. G. (2006). Scaling-up from nutrient physiology to the size-structure of phytoplankton communities. *Journal of Plankton Research*, *28*(5), 459–471. http://doi.org/10.1093/plankt/fbi148

Jacobson, D.M. (1999). A brief history of dinoflagellate feeding research. *J. Eukaryot. Microbiol.*, 46, 376–381.

Jiang, L., Schofield, O. M. E., & Falkowski, P. G. (2005). Adaptive evolution of phytoplankton cell size. *The American Naturalist*, *166*(4), 496–505. http://doi.org/10.1086/444442

Kiørboe, T. (2013). Zooplankton body composition. *Limnology and Oceanography*, *58*(5), 1843–1850. http://doi.org/10.4319/lo.2013.58.5.1843

Kiørboe, T. (2011). How zooplankton feed: Mechanisms, traits and trade-offs. *Biological Reviews*, *86*(2), 311–339. http://doi.org/10.1111/j.1469-185X.2010.00148.x

Kiørboe, T. (2008). A Mechanistic Approach to Plankton Ecology. *Princeton University Press, Princeton, NJ*.

Klausmeier, C. A., Litchman, E., Daufresne, T., & Levin, S. A. (2008). Phytoplankton stoichiometry. *Ecological Research*, *23*(3), 479–485. http://doi.org/10.1007/s11284-008-0470-8

Kostadinov, T. S., Siegel, D. A. and Maritorena, S. (2009) Retrieval of the particle size distribution from satellite ocean color observations. J. Geophys. Res., 114, C09015.

Le Quere, C., Harrison, S. P., Colin Prentice, I., Buitenhuis, E. T., Aumont, O., Bopp, L., … Wolf-Gladrow, D. (2005). Ecosystem dynamics based on plankton functional types for global ocean biogeochemistry

models\rdoi:10.1111/j.1365-2486.2005.1004.x. *Global Change Biology*, *11*(11), 2016–2040. http://doi.org/10.1111/j.1365-2486.2005.01004.x

Legendre, L., & Rassoulzadegan, F. (1995). Plankton and nutrient dynamics in marine waters. *Ophelia*, *41*(August 2013), 153–172. http://doi.org/10.1080/00785236.1995.10422042

Legović, T., & Cruzado, A. (1997). A model of phytoplankton growth on multiple nutrients based on the Michaelis-Menten-Monod uptake, Droop's growth and Liebig's law. *Ecological Modelling*, *99*(1), 19–31. http://doi.org/10.1016/S0304-3800(96)01919-9

Lewis, D. M., Brereton, A., & Siddons, J. T. (2017). A large eddy simulation study of the formation of deep chlorophyll/biological maxima in un-stratified mixed layers: The roles of turbulent mixing and predation pressure. *Limnology and Oceanography*, *62*(5), 2277–2307. http://doi.org/10.1002/lno.10566

Litchman, E., & Klausmeier, C. A. (2008). Trait-Based Community Ecology of Phytoplankton. *Annual Review of Ecology, Evolution, and Systematics*, *39*(1), 615–639. http://doi.org/10.1146/annurev.ecolsys.39.110707.173549

Litchman, E., Klausmeier, C. A., Schofield, O. M., & Falkowski, P. G. (2007). The role of functional traits and trade-offs in structuring phytoplankton communities: Scaling from cellular to ecosystem level. *Ecology Letters*, *10*(12), 1170–1181. http://doi.org/10.1111/j.1461-0248.2007.01117.x

Litchman, E., Ohman, M. D., & Kiørboe, T. (2013). Trait-based approaches to zooplankton communities. *Journal of Plankton Research*, *35*(3), 473–484. http://doi.org/10.1093/plankt/fbt019

Litchman, E., de Tezanos Pinto, P., Klausmeier, C.A., Thomas, M.K. & Yoshiyama, K. (2010). Linking traits to species diversity and community structure in phytoplankton. *Hydrobiologia*, 653, 15-28.

Marañón, E., Holligan, P. M., Barciela, R. et al. (2001) Patterns of phytoplankton size structure and productivity in contrasting open-ocean environments. *Mar. Ecol. Prog. Ser.*, 216, 43–56.

Marañón, E. (2008). Inter-specific scaling of phytoplankton production and cell size in the field. *Journal of Plankton Research*, *30*(2), 157–163. http://doi.org/10.1093/plankt/fbm087

Marañón, E., Cermeno, P., Lopez-Sandoval, D. C., Rodriguez-Ramos, T., Sobrino, C., Huete-Ortega, M., … Rodriguez, J. (2013). Unimodal size scaling of phytoplankton growth and the size dependence of nutrient uptake and use. *Ecology Letters*, *16*(3), 371–379. http://doi.org/10.1111/ele.12052

Marañón, E. (2014). Cell size as a key determinant of phytoplankton metabolism and community structure. *Ann. Rev. Mar. Sci.*,7, 1-24.

Mariani, P. & Visser, A. W. (2010). Optimisation and emergence in marine ecosystem models. *Prog. Oceanogr.*, 84, 89-92.https://doi.org/10.1016/j.pocean.2009.09.010

Mariani, P.; Andersen, Ken H.; Visser, André W.; Barton, Andrew D.; Kiorboe, T. (2013). Control of plankton seasonal succession by adaptive grazing. *Limnol. Oceanogr*, *58*(1), 1–11. http://doi.org/10.4319/lo.2013.58.1.0000

Mei, Z. P., Finkel, Z. V., & Irwin, A. J. (2011). Phytoplankton growth allometry and size-dependent C:N stoichiometry revealed by a variable quota model. *Marine Ecology Progress Series*, *434*, 29–43. http://doi.org/10.3354/meps09149

Merico, A., Tyrrell, T., Lessard, E. J. *et al*. (2004) Modelling phytoplankton succession on the Bering Sea shelf: role of climate influences and trophic interactions in generating *Emiliania huxleyi* blooms 1997–2000. *Deep-Sea Res. I* , 51, 1803–1826.

Merico, A., Brandt, G., Smith, S. L., & Oliver, M. (2014). Sustaining diversity in trait-based models of phytoplankton communities. *Frontiers in Ecology and Evolution*, *2*(October), 1–8. http://doi.org/10.3389/fevo.2014.00059

Merico, A., Bruggeman, J., & Wirtz, K. (2009). A trait-based approach for downscaling complexity in plankton ecosystem models. *Ecological Modelling*, *220*(21), 3001–3010. http://doi.org/10.1016/j.ecolmodel.2009.05.005

Mitra, A., et al. (2014). The role of mixotrophic protists in the biological carbon pump. *Biogeosciences*, 11(4), 995-1005.

Moloney, C.L. & Field, J.G. (1991). The size-based dynamics of plankton food webs. I. A simulation model of carbon and nitrogen flows. *Journal of Plankton Research*, 13(5), 1003-1038. https://doi.org/10.1093/plankt/13.5.1003

Montagnes, D. J., Berges, J. A., Harrison, P. J. and Taylor, F. (1994). Estimating carbon, nitrogen, protein, andchlorophyll a from volume in marine phytoplankton, Limnol. Oceanogr., 39, 1044–1060.

Mukherjee, S., & Tandon, A. (2016). Comparison of the simulated upper-ocean vertical structure using 1-dimensional mixed-layer models, (July), Ocean Science Discussion. http://doi.org/10.5194/os-2016-45

Neuer, S., Davenport, R., Freudenthal, T., Wefer, G., Llinás, O., Rueda, M.-J., … Karl, D. M. (2002). Differences in the biological carbon pump at three subtropical ocean sites. *Geophysical Research Letters*, *29*(18), 32-1-32–4. http://doi.org/10.1029/2002GL015393

Oguz, T., Macias, D., Renault, L., Ruiz, J., Tintore, J. (2013). Controls of plankton pro-duction by pelagic fish predation and resource availability in the Alboran andBalearic Seas. *Progress in Oceanography*, 112–113, 1–14.

Pollard, R. T., Salter, I., Sanders, R. J., Lucas, M. I., Moore, C. M., Mills, R. A., … Zubkov, M. V. (2009). Southern Ocean deep-water carbon export enhanced by natural iron fertilization. *Nature*, *457*(7229), 577–580. http://doi.org/10.1038/nature07716

Poulin, F.J. & Franks, P.J.S. (2010). Size-structured planktonic ecosystems: constraints, controls and assembly instructions. *Journal of Plankton Research*, 32(8), 1121–1130.http://doi.org/10.1093/plankt/fbp145

Raven, J. A., Finkel, Z. V. & Irwin, A. J. (2006). Picophytoplankton: bottom-up and top-down controls on ecology and evolution. *Vie et Milieu*, 55, 209–215.

Record N. R., Pershing A. J., Maps F.. The paradox of "the paradox of the plankton", *ICES Journal of Marine Science* , 2013, vol. 70 (pg. 1-5)

Redfield, A.C. (1934). On the proportions of organic derivations in sea water and their relation to the composition of plankton. *James Johnstone Memorial Volume*. (ed. R.J. Daniel). University Press of Liverpool, 176–192.

Reynolds, C. (1983). A physiological interpretation of the dynamic responses of populations of a planktonic diatom to physical variability of the environment. *New Phytologist*, 41–53. http://doi.org/10.1111/j.1469-8137.1983.tb03467.x

Rockström, J., Steffen, W., Noone, K., Persson, Å., Chapin, F. S., III, Lambin, E., Lenton, T. M., Scheffer, M., Folke, C., Schellnhuber, H., Nykvist, B., De Wit, C. A., Hughes, T., van der Leeuw, S., Rodhe, H., Sörlin, S., Snyder, P. K., Costanza, R., Svedin, U., Falkenmark, M., Karlberg, L., Corell, R. W., Fabry, V. J., Hansen, J., Walker, B., Liverman, D., Richardson, K., Crutzen, P. & Foley, J. (2009). Planetary boundaries:exploring the safe operating space for humanity. *Ecology and Society*, 14(2), 32.http://www.ecologyandsociety.org/vol14/iss2/art32/

Ryabov, A. B., & Blasius, B. (2011). A graphical theory of competition on spatial resource gradients. *Ecology Letters*, *14*(3), 220–228. http://doi.org/10.1111/j.1461-0248.2010.01574.x

Sanders, R. W., Berninger, U. G., Lim, E. L., Kemp, P. F. & Caron, D. A. (2000). Heterotrophic and mixotrophic nanoplankton predation on picoplankton in the Sargasso Sea and Georges Bank. *Mar. Ecol. Prog. Ser.*, 192, 103–118.

Sarmiento, J.L.S & Gruber, N. (2006). Ocean biogeochemical dynamics. Princeton University Press, Princeton, NJ, USA.

Sigman, D.M & Boyle, E.A. (2000). Glacial/interglacial variations in atmospheric carbon dioxide. Nature, 407, 859-869.

Smayda, T.J. (1970). The suspension and sinking of phytoplankton in the sea. *Oceanog. Mar. Biol.*, 8, 353–414.

Solan, M., Raffaelli, D.G., Paterson, D.M., White, P.C.L. & Pierce, G.J. (2006). Marine biodiversity and ecosystem function: empirical approaches and future challenges. Introduction. *Mar. Ecol. Prog. Ser*., 311, 175-178.

Stec, K. F. (2015). Role of life strategies in diatom biodiversity: a modelling approach. *Department of Life and Biomolecular Sciences, Open university of London, London.*

Steele, J. H., & Henderson, E. W. (1981). A Simple Plankton Model. *Source: The American Naturalist*, *117*(5), 676–691. http://doi.org/10.1086/283752

Steele, J. H. & Henderson, E. W. (1992). The role of predation in plankton models. *J. Plank. Res.*, 14, 157-172.

Steffen, W., Richardson, K., Rockström, J., Cornell, S. E., Fetzer, I., Bennett, E. M., Biggs, R., Carpenter, S. R., de Vries, W., de Wit, C. A., Folke, C., Gerten, D., Heinke, J., Mace, G. M., Persson, L. M., Ramanathan, V., Reyers, B. & Sörlin, S. (2015). Planetary boundaries: guiding human development on a changing planet, *Science*, **347**(6223), 736. doi:10.1126/science.1259855

Stock, C. A., Powell, T. M. & Levin, S. A. (2008). Bottom-up and top-down forcing in a simple size-structured plankton dynamics model. *J. Mar. Syst.*, 74, 134–152. http://doi.org/10.1016/j.jmarsys.2007.12.004

Stuart-Smith, R.D. et al. (2013). Integrating abundance and functional traits reveals new global hotspots of fish diversity. *Nature*, 501, 539-542.

Tang, E. P. Y. (1995). The allometry of algal growth rates. *Journal of Plankton Research*, *17*(6), 1325–1335. http://doi.org/10.1093/plankt/17.6.1325

Tilman, D. (1982). Resource competition and community structure. Princeton Monographs in Population Biology 17. Princeton University Press, Princeton, NJ

Tilman, D. (2000). Causes, consequences and ethics of biodiversity. *Nature*, 405, 208-211.

Troost, T. A., Kooi, B. W. & Kooijman, S. A. L. M. (2005). Ecological specialization of mixotrophic plankton in a mixed water column. *Am. Nat.* , 166, E45–E61.

Uitz, J., Claustre, H., Morel, A. et al. (2006) Vertical distribution of phytoplankton communities in open ocean: an assessment based on surface chlorophyll. J. Geophys. Res., 111, C08005. doi:10.1029/ 2005JC003207.

Umani, S. F., Malfatti, F., & Del Negro, P. (2012). Carbon fluxes in the pelagic ecosystem of the Gulf of Trieste (Northern Adriatic Sea). *Estuarine, Coastal and Shelf Science*, *115*, 170–185. http://doi.org/10.1016/j.ecss.2012.04.006

Van den Berg, A. J., Ridderinkhof, H., Riegman, R. *et al*. (1996) Influence of variability in water transport on phytoplankton biomass and composition in the southern North Sea: a modelling approach (FYFY). *Cont. Shelf Res.* , 16, 907–931.

Vichi, M., Cossarini, G., Gutierrez, Mlot, E., Lazzari, P., Lovato, T., Mattia, G., Masina, S., McKiver, W., Pinardi, N., Solidoro, C., Zavatarelli, M. (2015).The Biogeochemical Flux Model (BFM): Equation Description and User Manual. BFM version 5.1. BFM Report series N. 1. March 2015, Bologna, Italy, pp. 89.

Vichi, M., Masina, S., and Navarra, A., (2007a).A generalized model of pelagic biogeochemistry for the global ocean ecosystem. Part II: numerical simulations. Journal of Marine Systems, 64, 110-134.

Vichi, M., Pinardi, N., and Masina, S., (2007b). A generalized model of pelagic biogeochemistry for the global ocean ecosystem. Part I: theory. Journal of Marine Systems, 64, 89-109.

Volkov, I., Banavar, J. R., Hubbell, S. P., & Maritan, A. (2007). Patterns of relative species abundance in rainforests and coral reefs. *Nature*, *450*(7166), 45–9. http://doi.org/10.1038/nature06197

Ward, B. A., Dutkiewicz, S., Jahn, O., & Follows, M. J. (2012). A size-structured food-web model for the global ocean. *Limnology and Oceanography*, *57*(6), 1877–1891. http://doi.org/10.4319/lo.2012.57.6.1877

Ward, B. A., Dutkiewicz, S., & Follows, M. J. (2013). Modelling spatial and temporal patterns in size-structured marine plankton communities: Top-down and bottom-up controls. *Journal of Plankton Research*, *36*(1), 31–47. http://doi.org/10.1093/plankt/fbt097

Ward, B.A. & Follows, M.J. (2015). Marine mixotrophy increases trophic transfer efficiency, mean organism size, and vertical carbon flux. *PNAS*, 113, 2958-2963. http://doi.org/10.1073/pnas.1517118113

Williams, R. & Follows, M.J. (2011). Ocean Dynamics and the Carbon Cycle,Cambridgue University Press, Cambridge, U.K.

Wirtz, K. W. (2012). Who is eating whom? Morphology and feeding type determine the size relation between planktonic predators and their ideal prey. *Marine Ecology Progress Series*, *445*, 1–12. http://doi.org/10.3354/meps09502

Wittebolle, L. et al. (2009). Initial community evenness favours functionality under selective stress. *Nature*, 458, 623-626.

Ye, L., C. Y. Chang, C. García-Comas, G. C. Gong, and C. H. Hsieh (2013). Increasing zooplankton size diversity enhances the strength of top-down control on phytoplankton through diet niche partitioning. *Journal of Animal Ecology*. doi: 10.1111/1365-2656.12067